THE DYNAMIC BEHAVIOUR OF OIL LUBRICATED JOURNAL BEARINGS

by

Mark Thomas Gardner

Submitted in fulfilment of the requirements for the

degree of Doctor of Philosophy

Department of Applied Mathematical Studies,

The University of Leeds.

October, 1983

Abstract

This thesis is concerned with the dynamic behaviour of oil lubricated journal bearings and particularly with the small vibrations about the equilibrium position known as 'oil whirl'. The importance of shaft flexibility and oil film cavitation to this phenomena are investigated.

Several authors have shown that by the use of linear techniques it is possible to derive a stability borderline which can be used for design purposes to ascertain whether or not a bearing is stable. These linear techniques are used to examine journal bearings with flexible shafts operating under a range of cavitation boundary conditions. It is demonstrated that these boundary conditions, particularly the behaviour of a lubricant during a vibration, play a crucial role in determining the predicted stability of the bearing. The effect of shaft flexibility is to make the bearing less stable, but the extent of this change is also governed by the oil film behaviour.

Nonlinear analytical techniques are used to carry out an investigation into the behaviour of a journal bearing operating with a rigid shaft close to the stability borderline for a particular set of cavitation boundary conditions. It is found that two types of behaviour are possible: (i) supercritical, in which small stable whirl orbits are possible at speeds just above the threshold speed (the speed above which the bearing is unstable according to linear theory). (ii) subcritical, in which small unstable orbits exist at speeds just below the threshold speed. The parameter space is split into two regions, one subcritical and the other supercritical. Several methods are used in the investigation; it is shown that the methods give identical results, but only if they are applied correctly. These results are subsequently confirmed by a numerical integration of the equations of motion. The thesis concludes with an investigation of the application of nonlinear techniques to a variety of cavitation boundary conditions.

Acknowledgements

I would like to express my sincere thanks to Dr. M. Savage and Dr. C. Taylor for their supervision, help, guidance and enthusiasm throughout this work. I would also like to thank Mr. D. Knapp and Dr. C. Myers for many helpful discussions over the last three years. Thanks are also due to the Science and Engineering Research Council for their financial support.

Contents

Nomenclature

A	shaft centre
B_{XX}, B_{YY} etc	nondimensional damping coefficients
D	diameter of bush
F	bearing load
F	nondimensional bearing load
K_{XX}, B_{YY} etc	nondimensional stiffness coefficients
F_r, F_t	radial and tangential hydrodynamic forces
$\bar{F}_r, \bar{F}_t$	nondimensional forces
F_X, F_Y	cartesian force components
$\bar{F}_X, \bar{F}_Y$	nondimensional forces
L	axial bearing length
O	centre of bush
R	radius of bush
S	Sommerfeld number ($R^3 L\omega\mu/Fc^2$)
S_m	modified Sommerfeld number ($RL^3\omega\mu/(Fc^2)$)
X,Y	nondimensional co-ordinates
a, amp	ratio of whirl amplitude to a perturbation of the rotor speed
a_e	whirl amplitude ratio (stable whirl)
$a_1, a_2 \ldots a_{34}$	Taylor expansion coefficients
$b_1, b_2 \ldots b_{34}$	Taylor expansion coefficients
$\bar{a}_1, \bar{a}_2 \ldots \bar{a}_{34}$	$a_1/\bar{\omega}_s^2$ etc.
$\bar{b}_1, \bar{b}_2 \ldots \bar{b}_{34}$	$b_1/\bar{\omega}_s^2$ etc.
c	bearing radial clearance
e	journal eccentricity
h	fluid film thickness
2m	mass of shaft plus rotor
p	hydrodynamic pressure
r	shaft radius

t	time
x^1, y^1	rotor centre coordinates
x, y	nondimensional coordinates ($x=x^1/c$, etc.)
z	axial co-ordinate
$\bar{\alpha}$	real part of the eigenvalue $\bar{\lambda}$ of the Jacobian matrix
ϵ	eccentricity ratio (e/c)
ϵ_s^*	value of ϵ_s above which the system is always stable
θ	angular co-ordinate
$\bar{\lambda}$	non-dimensional eigenvalue
μ	lubricant viscosity
ν	stability parameter ($F/mc\omega^2$)
ν_1	stiffness term ($F/mc\omega_1{}^2$)
σ	system parameter ($S_m/\bar{\omega}$) or ($S/\bar{\omega}$)
τ	nondimensional time (ωt)
φ	attitude angle
ω	rotational speed
$\bar{\omega}$	nondimensional speed ($(mc/F)^{1/2}\omega$)
ω_1	first critical speed in bending of the shaft
Ω	whirl frequency
$\bar{\Omega}$	whirl frequency ratio (Ω/ω)

<u>subscripts</u>

s	refers to steady state conditions
$\cdot$	time derivative (d/dt)
$'$	nondimensional time derivative ($d/d\tau$)

<u>note</u>

There are several sections in this thesis where the use of a symbol is particular to that section. Where this is the case the symbol is defined where it is introduced.

INTRODUCTION

In a plain journal bearing, a circular shaft rotates in a bush of circular cross-section. The load on the shaft causes its centre to take an eccentric position within the bush, thus forcing fluid into a converging/diverging space and creating a pressure distribution, which in turn supports the load. Instability in a journal bearing often manifests itself in the form of oil whirl, in which the journal, as well as rotating about its own axis, performs a secondary orbit around the bush. This can have disastrous consequences, particularly as in practice the inner diameter of the bush is only one or two parts per thousand greater than that of the shaft.

An important factor affecting the stability or otherwise of a journal bearing is the existence of air cavities within the fluid film. In fact both the stability and the dynamic behaviour of a journal bearing are very sensitive to the cavitation boundary conditions; an apparently small and subtle change in the position of the cavity can have a dramatic effect on the vibrational characteristics of the bearing.

Oil whirl can manifest itself in two different forms: cylindrical whirl and conical whirl. In cylindrical whirl the two ends of the shaft are in phase; in conical whirl they are 180° out of phase (see Figure 1). However, for all but the shortest shafts the lowest natural mode of vibration is the cylindrical one and therefore this investigation will ignore conical whirl.

Another important influence on stability is shaft stiffness. Much of the analytical work on journal bearings has assumed a rigid shaft, but in practice this is not the case. Intuitively one might suppose that the lower the first critical speed in bending of the shaft, then the greater the likelihood of the motion being unstable, since fluid film instabilities might interact with other vibrations. It is possible, however, to find a quantitative relationship between shaft stiffness and stability.

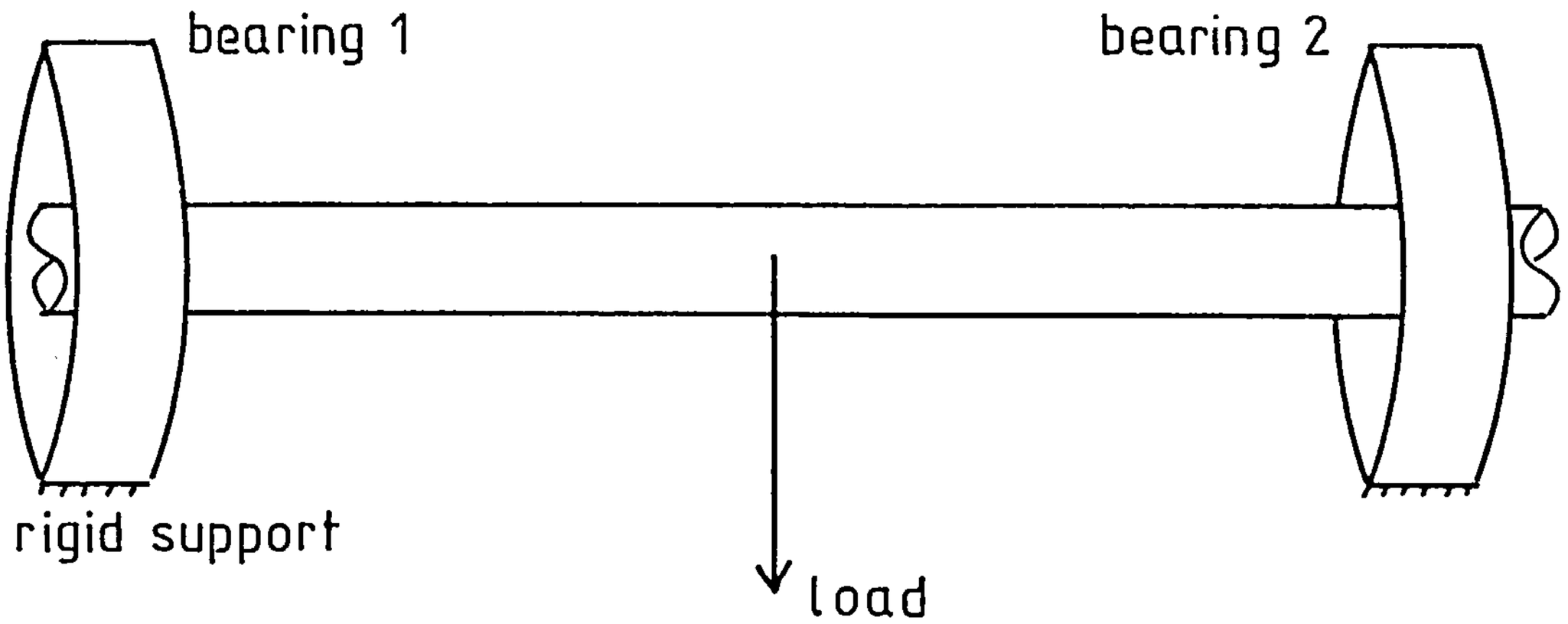

Figure 1a A rigid shaft supported in fluid film bearings

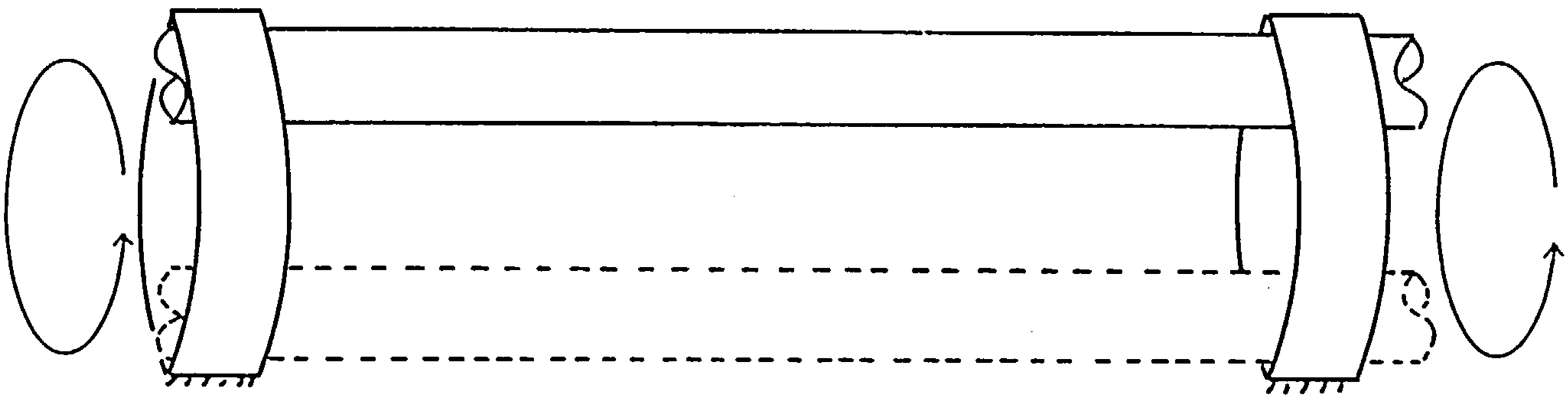

Figure 1b Cylindrical whirling

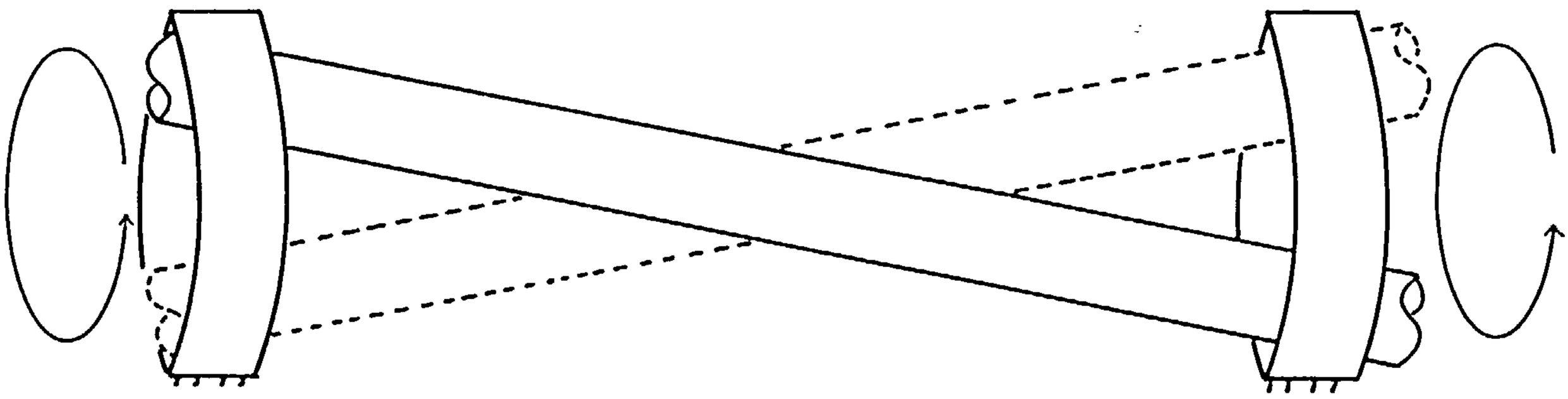

Figure 1c Conical whirling

Journal bearing instability can result in several types of oil whirl (these are discussed in more detail in Chapter 1), which are characterised by particular frequencies and amplitudes. It may well be the case that although a bearing is unstable in the conventional sense, the resulting whirl is stable and of small amplitude. Frequently this represents an acceptable mode of operation for the bearing and consequently the determination of criteria for this kind of motion constitutes a valuable exercise.

The objectives of this thesis are:

(1) To examine the effects of cavitation and oil supply position on the onset of bearing instability; in particular, to quantify the role played by shaft flexibility.

(2) To use analytical and numerical methods to consider the motion outside the region of stability and in particular to investigate the existence of any small, closed whirl orbits (limit cycles).

(3) To contrast the use of different nonlinear techniques for the investigation of oil whirl.

(4) To extend the use of nonlinear analytical techniques beyond their application to the simplest bearing models in order to find realistic criteria for the existence of small, stable whirl orbits.

The model used in this investigation is as follows. A horizontal, flexible, massless shaft supports at its midpoint a rotor of mass 2m. The shaft is mounted between two identical journal bearings; consequently we need only examine one bearing supporting a load m (Figure 2). In addition it is assumed that:

(1) The rotor is symmetric and perfectly balanced and is in perfect alignment to the bearing axis.

(2) The shaft spins with constant angular velocity about its axis.

(3) The load carried by the rotor is due solely to gravity.

(4) The bearing mountings are fixed and rigid.

(5) The viscosity of the lubricant is constant.

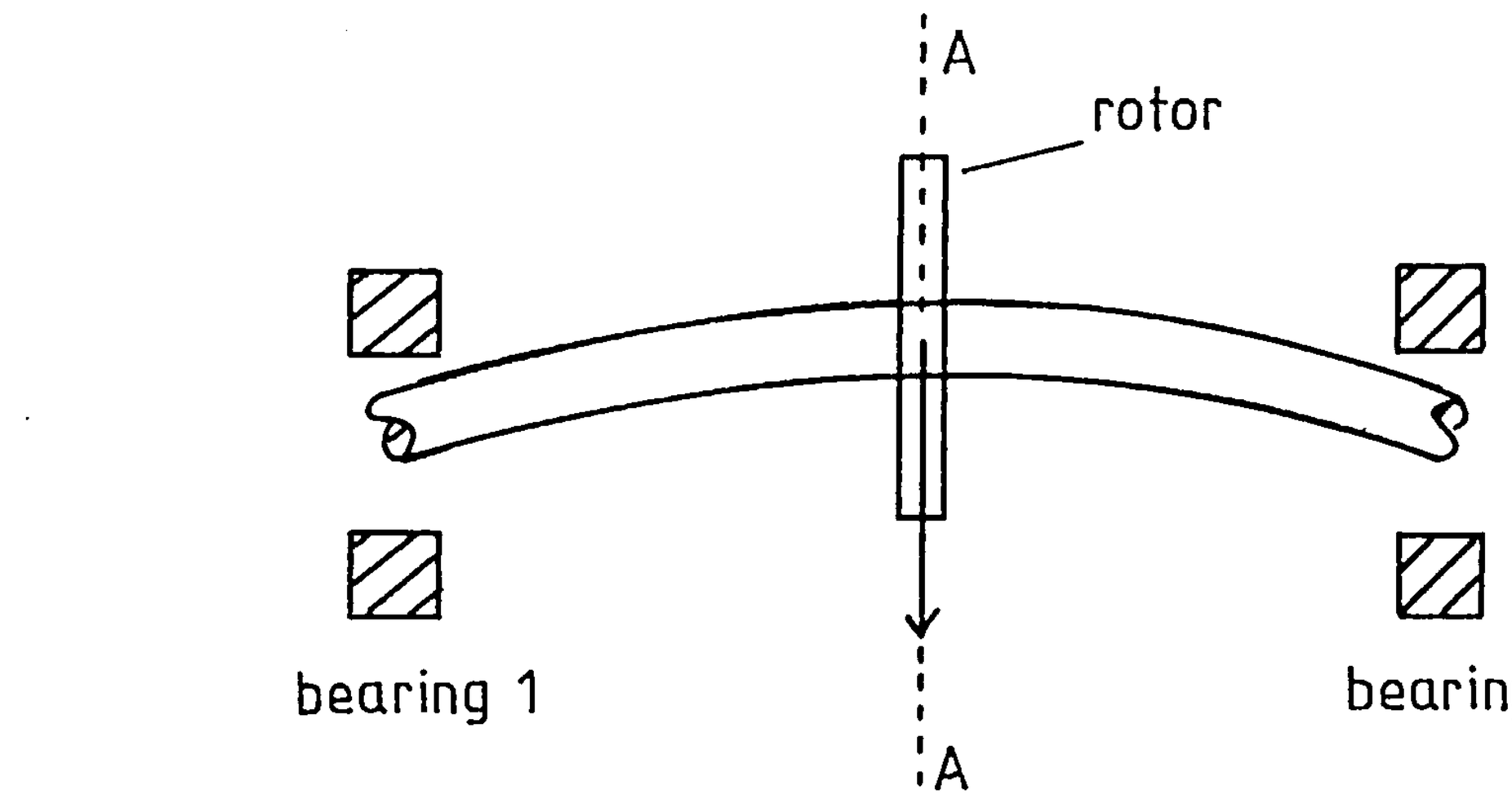

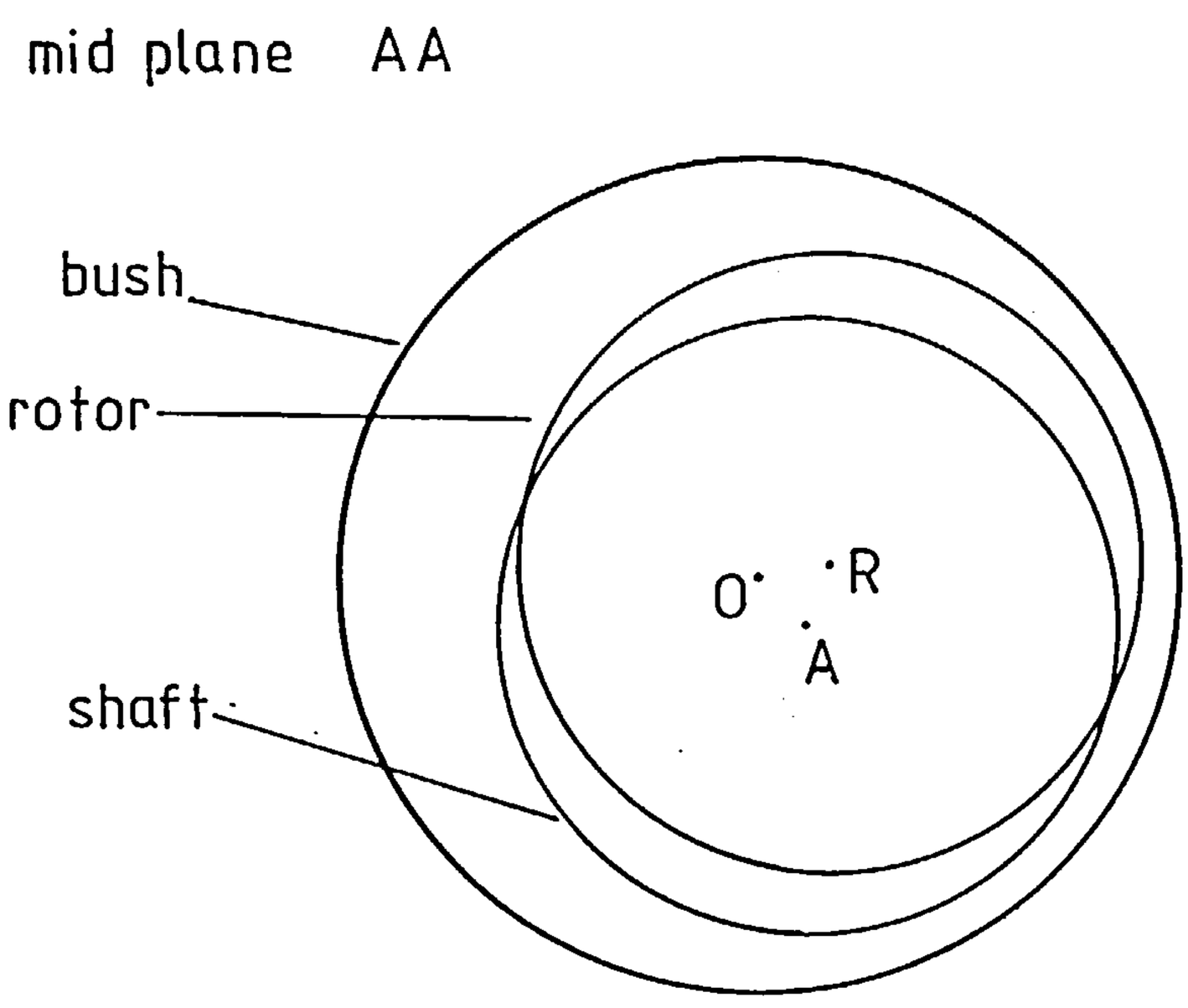

Figure 2 A flexible shaft supported in fluid film bearings

CHAPTER 1

BASIC CONCEPTS AND HISTORICAL REVIEW

1.1 Reynolds' equation

The differential equation describing the pressure distribution in a fluid being used to lubricate two surfaces was first defined by Osborne Reynolds (1886). It can be deduced from the Navier-Stokes equation using the following assumptions:

(1) The lubricant is a Newtonian fluid.

(2) Inertia and body force terms are small compared with pressure and viscous terms.

(3) The flow is laminar.

(4) No-slip boundary conditions exist between the lubricant and the bearing solids.

(5) The lubricant properties (e.g. density, viscosity) remain constant across the film thickness.

(6) Pressure variation across the film thickness is negligible.

(7) The velocity derivatives with respect to the film thickness are large compared to all other derivatives.

(8) Effects due to the curvature of the bearing surfaces can be ignored.

The full Reynolds' equation is not only very cumbersome, but also contains many terms that would only arise in the most general of lubrication situations. Cameron (1970) has pointed out that although it might be possible to construct a mental picture of a bearing for which the full equation was required, it would certainly not be possible to conceive of a use for such a bearing. Consequently, although many analytical derivations are available (e.g. Pinkus and Sternlicht (1961)), it is more useful to derive from first principles a specialised equation, applicable to the particular lubrication circumstances under consideration. In particular, the situation shown in Figure 1.1 is analogous to that of the journal bearing with a stationary bush. A cartesian co-ordinate system is assumed, such that (u,v,w) correspond

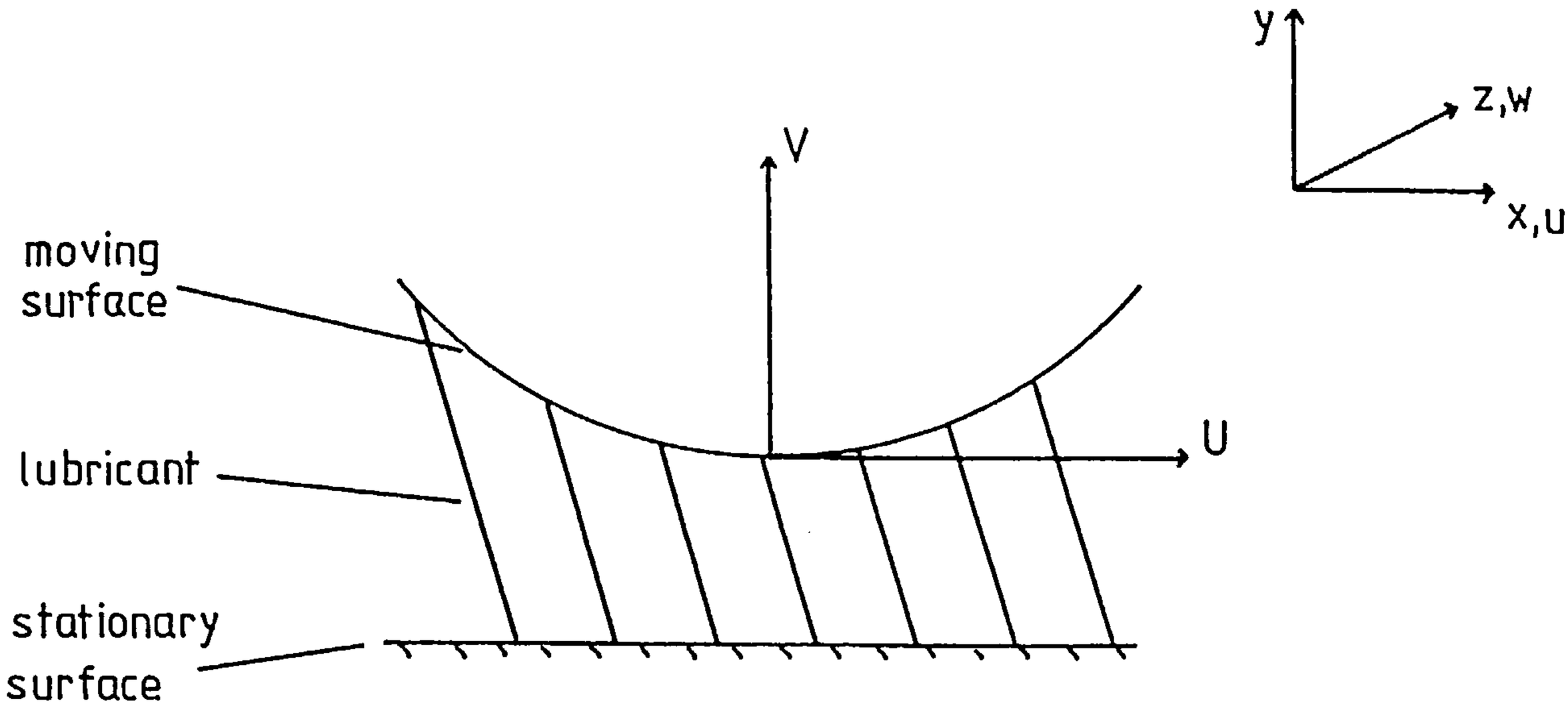

Figure 1.1 A typical lubrication situation

---

x-y plane

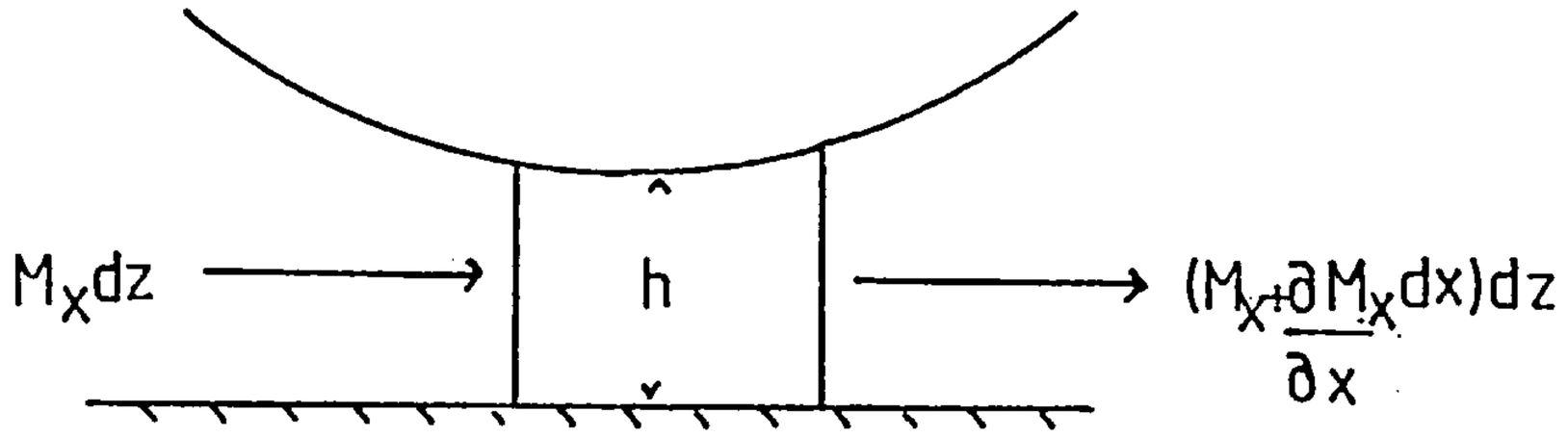

M_x = rate of mass flow in x-direction per unit width

Figure 1.2

Figure 1.3

to the movement of the shaft in the (x,y,z) directions respectively. In order to derive Reynolds' equation for this situation, first consider a column of fluid as shown in Figure 1.2. The net mass flow into the column of fluid is given by the difference between the flow in and the flow out. Therefore:

$$\text{Net mass flow} = M_x dz - (M_x + \frac{\partial M}{\partial x}_x dx)dz$$

$$= - \frac{\partial M}{\partial x}_x dxdz$$

Similarly, if we consider a column of fluid in the z-y plane, it can be seen that the net mass flow into the column is given by:

$$- \frac{\partial M}{\partial z}_x dzdx$$

The mass of the control column shown in Figure 1.2 is given by:

$$M_c = \rho h dzdx$$

Conditions of continuity demand that the rate of increase of the mass of the control column is equal to the net mass flow into the column. This leads to the relationship:

$$\frac{d}{dt}(\rho h dzdx) = - \frac{\partial M}{\partial x}_x dxdz - \frac{\partial M}{\partial z}_z dzdx$$

$$\frac{d(\rho h)}{dt} = - \frac{\partial M}{\partial x}_x - \frac{\partial M}{\partial z}_z \qquad (1.1)$$

It is now necessary to find an expression for the flow rates M_x and M_z.

Consider an element of fluid of sides dx,dy,dz (as shown in Figure 1.3). The equilibrium of this element requires that the pressure and stress terms cancel each other out. First consider the x-direction:

$$p dydz + (\tau_x + \frac{\partial \tau}{\partial y}_x dy)dxdz = \tau_x dxdz + (p + \frac{\partial p}{\partial x} dx)dydz$$

$$\rightarrow \quad \frac{\partial \tau}{\partial y}_x = \frac{\partial p}{\partial x}$$

Under assumption (1), the fluid is Newtonian, and so the stress/strain rate relationship is given by:

$$\tau_x = \mu \frac{\partial u}{\partial y}$$

$$\frac{\partial \tau_x}{\partial y} = \frac{\partial}{\partial y}\left(\mu \frac{\partial u}{\partial y}\right)$$

$$\rightarrow \quad \frac{\partial p}{\partial x} = \frac{\partial}{\partial y}\left(\mu \frac{\partial u}{\partial y}\right) \qquad (1.2)$$

Similarly, by considering the equilibrium of the fluid in the z-direction, we can obtain the relationship:

$$\frac{\partial p}{\partial z} = \frac{\partial}{\partial y}\left(\mu \frac{\partial w}{\partial y}\right)$$

In order to find the flow rate, consider equation (1.2). Since the pressure is independent of y (under assumption (6)), we can integrate to obtain:

$$\mu \frac{\partial u}{\partial y} = \frac{\partial p}{\partial x} y + C_1$$

Since the viscosity is independent of y (under assumption (5)), we can integrate a second time to obtain:

$$\mu u = \frac{\partial p}{\partial x} \frac{y^2}{2} + C_1 y + C_2$$

From the boundary conditions in Figure 1.1, this leads to:

$$u = \left(\frac{y^2 - hy}{2\mu}\right) \frac{\partial p}{\partial x} + \frac{Uy}{h}$$

The mass flow rate per unit width in the x-direction is given by:

$$M_x = \int_0^h \rho u \, dy$$

$$M_x = -\frac{h^3 \rho}{12\mu} \frac{\partial p}{\partial x} + \frac{\rho U h}{2} \qquad (1.3)$$

Similarly, the mass flow rate per unit width in the z-direction is given by:

$$M_z = - \frac{h^3 \rho}{12\mu} \frac{\partial p}{\partial z} \qquad (1.4)$$

There is no Couette term analogous to $\rho Uh/2$ in (1.4) since the upper surface does not move along the z-axis. Equations (1.3) and (1.4) can now be substituted into (1.1) to obtain the following relationship:

$$- \frac{\partial}{\partial x}\left\{ \frac{-h^3 \rho}{12\mu} \frac{\partial p}{\partial x} + \frac{\rho U h}{2} \right\} - \frac{\partial}{\partial z}\left\{ \frac{-h^3 \rho}{12\mu} \frac{\partial p}{\partial z} \right\} = \frac{d(\rho h)}{dt} \qquad (1.5)$$

In many engineering situations the lubricant density and viscosity are assumed to be constant, so ρ and μ can be taken outside the derivatives in (1.5). In this case the moving surface is rigid, so U is independent of x. Hence (1.5) becomes:

$$\frac{\partial}{\partial x}\left\{ -h^3 \frac{\partial p}{\partial x} \right\} + \frac{\partial}{\partial z}\left\{ -h^3 \frac{\partial p}{\partial z} \right\} = 6\mu U \frac{\partial h}{\partial x} + 12\mu V \qquad (1.6)$$

This is one form of Reynolds' equation appropriate to the analysis of a journal bearing. The terms on the right hand side indicate the way in which the pressure is built up.

(1) The first term corresponds to the physical wedge, since the variation of film thickness with respect to height leads to an increase in pressure as the lubricant is swept into a converging region.

(2) The second term represents the squeezing of the fluid film with respect to time (due to the vertical movement of the upper surface), and is known as the squeeze-film term.

1.2 The journal bearing

In a journal bearing under normal operating conditions, the shaft adopts an eccentric position within the surrounding bush. The two co-ordinates which are required to fix its position with respect to the bush are the eccentricity e (this represents the distance between the centres of the bush and the shaft) and the attitude angle φ (this is given by the angle between the line of centres and the downwards vertical). The eccentricity ratio is defined by $\epsilon=e/c$. The parameters which are required to specify the bearing geometry are:

R = radius of the bearing L = bearing length

r = shaft radius c = radial clearance (=R-r)

An angular co-ordinate θ is also defined in order to locate positions within the bearing relative to the line of centres (see Figure 1.4).

In order to facilitate the application of Reynolds' equation to the journal bearing, it is more convenient to express it in polar co-ordinates. This can be achieved by the use of the following substitutions:

$$x = R\theta \tag{1.7}$$

$$h = c(1+\epsilon\cos\theta) \tag{1.8}$$

The expression for the film thickness (1.8) is an approximation based on the fact that $c/R \ll 1$. Its derivation is straightforward and can be found in several texts (e.g. Cameron (1970)). The shaft has instantaneous radial and tangential velocity components:

$$\frac{de}{dt} \text{ and } e\frac{d\varphi}{dt}$$

These expressions permit the calculation of the velocity components for any general point M on the bearing surface:

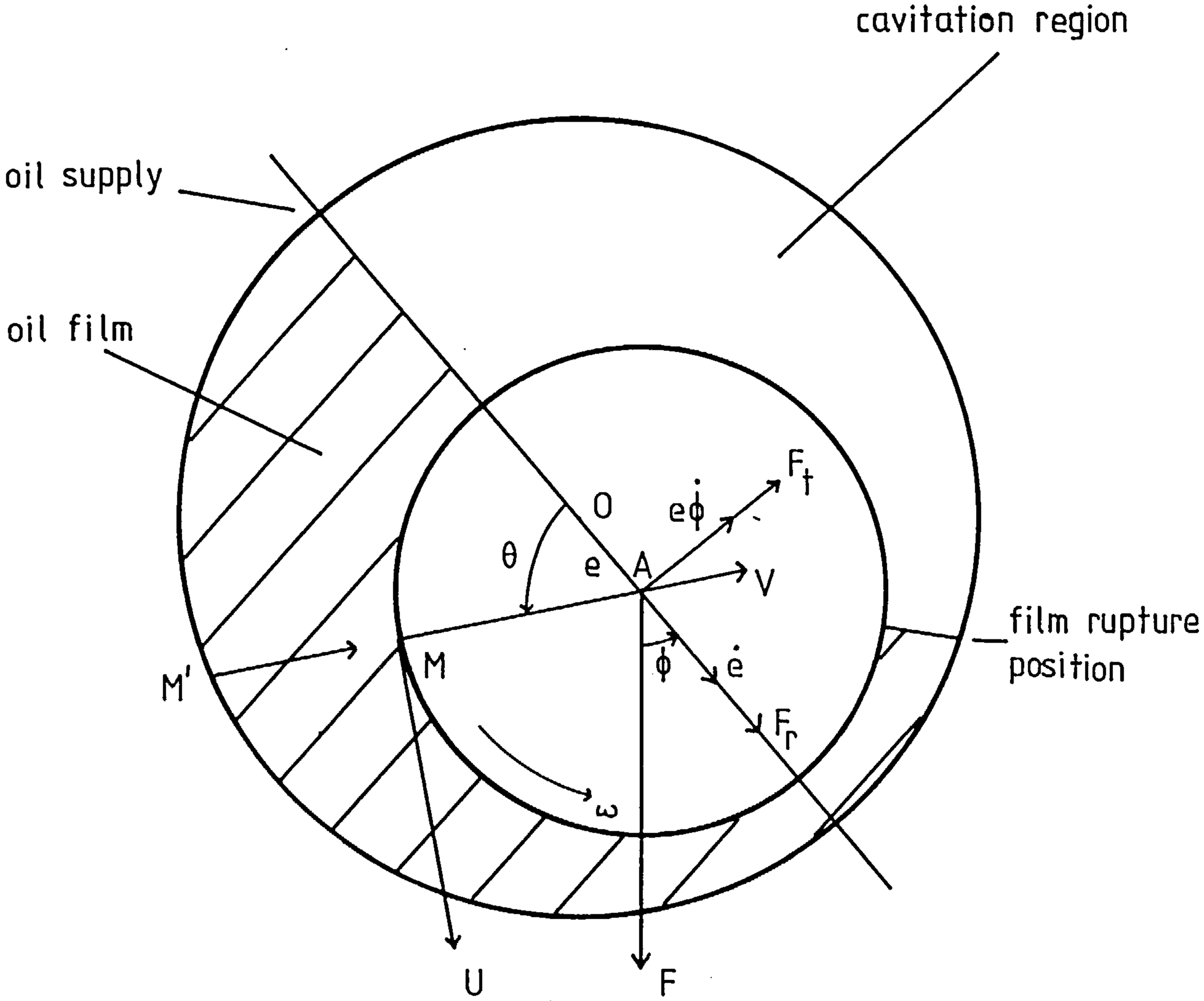

O - bearing centre
A - shaft centre
ω - rotational speed
θ - angular co-ordinate
e - shaft eccentricity
φ - attitude angle
F - load
F_r, F_t { hydrodynamic force components

Figure 1.4 The Journal Bearing

$$U = R\omega + \dot{e}\sin\theta - e\dot{\varphi}\cos\theta \tag{1.9}$$

$$V = \dot{e}\cos\theta + e\dot{\varphi}\sin\theta \tag{1.10}$$

Substituting (1.7)-(1.10) into (1.6) yields:

$$\frac{\partial}{\partial\theta}\left[\left(\frac{1+\epsilon\cos\theta}{12}\right)^3 \frac{\partial p}{\partial\theta} \right] + R^2\frac{\partial}{\partial z}\left[\left(\frac{1+\epsilon\cos\theta}{12}\right)^3 \frac{\partial p}{\partial z} \right]$$

$$= 6\mu\frac{R^2}{c^2}\left[-\epsilon(\omega-2\dot{\varphi})\sin\theta + 2\dot{\epsilon}\cos\theta + O(c/R) \right] \tag{1.11}$$

Since the terms $O(c/R)$ are small compared to the rest of the right hand side of (1.11), they can be neglected. Equation (1.11) represents a second order partial differential equation for the pressure distribution within a journal bearing under operating conditions. Unfortunately, despite the many simplifying assumptions already made during its derivation, it cannot, in general, be solved analytically. It is, however, possible to make a number of simplifying approximations, two of which are as follows:

The long bearing approximation

This approximation assumes that the bearing is sufficiently long for there to be no pressure variation along its axial length. In this case:

$$\frac{\partial p}{\partial z} \propto 0$$

Hence (1.11) reduces to:

$$\frac{\partial}{\partial\theta}\left[\left(\frac{1+\epsilon\cos\theta}{12}\right)^3 \frac{\partial p}{\partial x} \right]$$

$$= 6\mu\frac{R^2}{c^2}\left[-\epsilon(\omega-2\dot{\varphi})\sin\theta + 2\dot{\epsilon}\cos\theta \right] \tag{1.12}$$

An equivalent assumption is that side leakage (loss of lubricant at the

bearing ends) is neglected.

The short bearing approximation

Ocvirk (1952) assumed that the bearing was very short. This assumption is based on the fact that in many applications L/D < 3/4, so that the pressure gradient with respect to z is much greater than that with respect to θ. In this case:

$$\frac{\partial p}{\partial \theta} \ll \frac{\partial p}{\partial z}$$

Hence (1.11) reduces to:

$$\frac{\partial}{\partial z}\left[\frac{(1+\epsilon\cos\theta)^3}{12\mu} \frac{\partial p}{\partial z} \right]$$

$$= \frac{6\mu}{c^2} \left[-\epsilon(\omega-2\varphi)\dot{}\sin\theta + 2\epsilon\dot{}\cos\theta \right] \qquad (1.13)$$

Although the pressure distributions obtained by the use of these approximations are by no means quantitatively accurate, they do enable analytical techniques to be used to investigate the static and dynamic behaviour of the journal bearing. It is possible to combine the two approximations to develop a more sophisticated bearing model, which gives a more realistic pressure distribution in a finite bearing e.g. Warner (1963). However, since all the qualitative features of the dynamic behaviour of the journal bearing are present in the long and short approximations, this thesis will not examine finite bearing models.

1.3 Cavitation

One of the main features of the solution of Reynolds' equation common to both long and short bearing approximations is the existence of subambient pressures in the diverging part of the gap between the bush and the shaft. A typical pressure distribution is shown in Figure 1.5. It is assumed that the lubricant pressure is ambient as it is fed into the bearing (this assumption can be modified later). The presence of subambient pressures in the diverging part of the film causes the single phase flow of the lubricant to break down as the film ruptures or cavitates. The tendency of liquids to cavitate in the presence of subambient pressures is well known (Batchelor (1967)). The phenomenon occurs in three forms:

(1) Gaseous cavitation - which can be caused by the growth of suspended bubbles of gas (usually air), or the release of dissolved gases within the lubricant.

(2) Ventilated Cavitation - wherever subambient pressures occur, air from the surrounding atmosphere is sucked into the low pressure region.

(3) Vaporous Cavitation - as the pressure in the lubricant falls below its vapour pressure, the lubricant boils and cavities of its own vapour form.

For a journal bearing the contribution from ventilated cavitation by far outweighs the contribution from the other two forms, although vaporous cavitation can be important in dynamic situations. It is important to understand the crucial role played by cavitation in the dynamic behaviour of the bearing if a realistic analysis is to be undertaken.

For small loads which generate pressures whose order of magnitude is small compared to atmospheric pressure, the space between the bush and the shaft may be filled completely with oil (Figure 1.6). This situation has been shown to be inherently unstable (Holmes (1963), Myers (1981)) for all eccentricities and speeds. The shaft does not assume an equilibrium position,

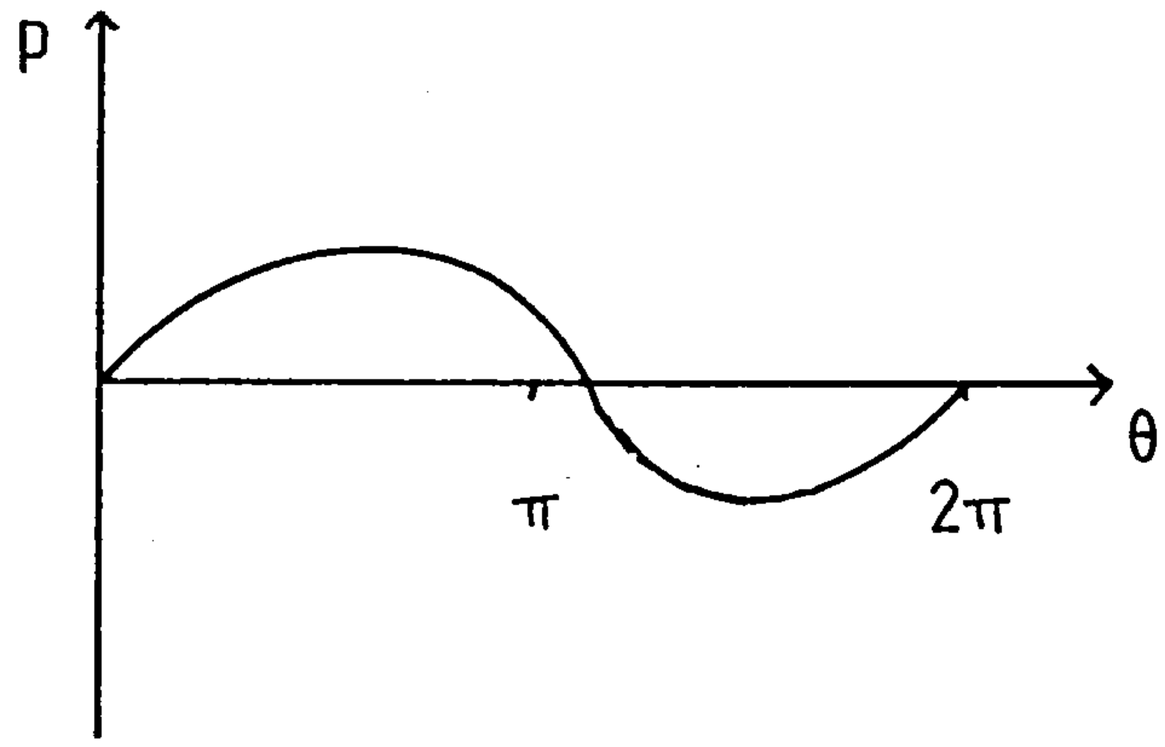

Figure 1.5 A typical pressure distribution

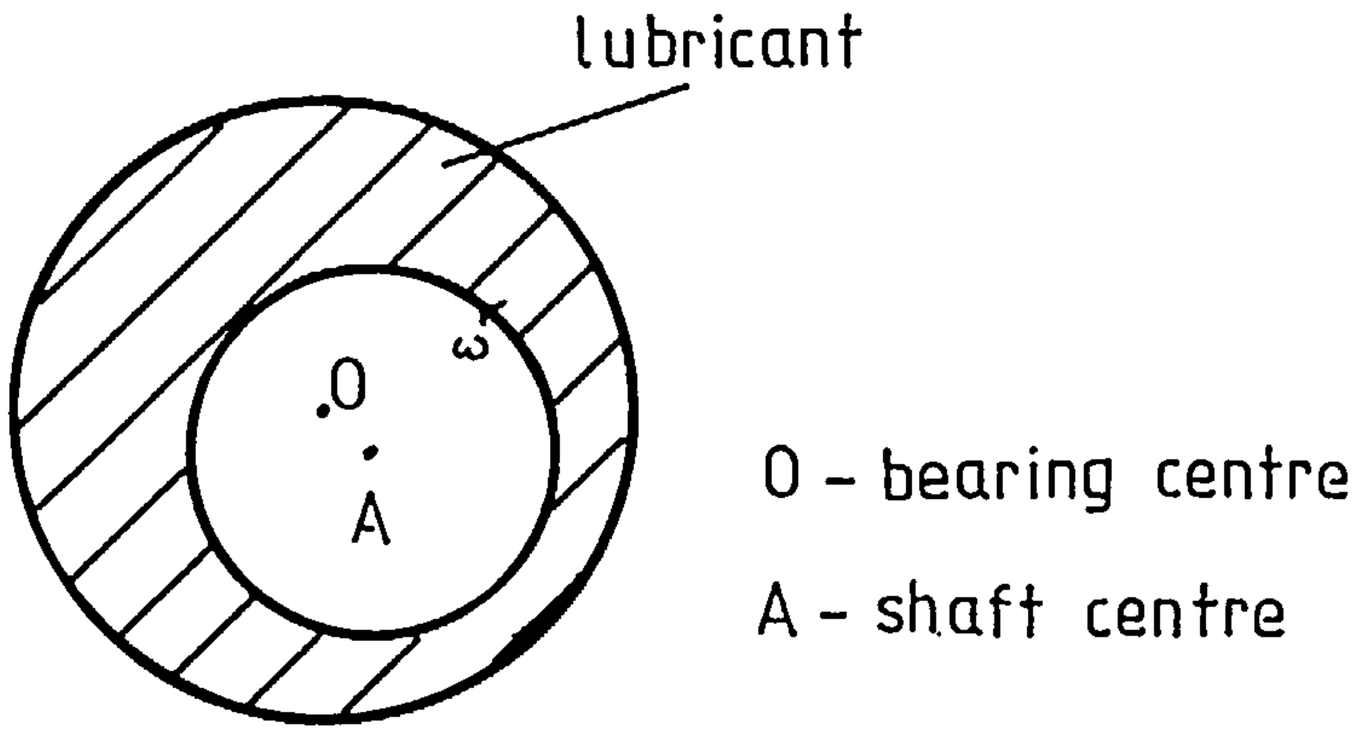

Figure 1.6 A journal bearing with a full film

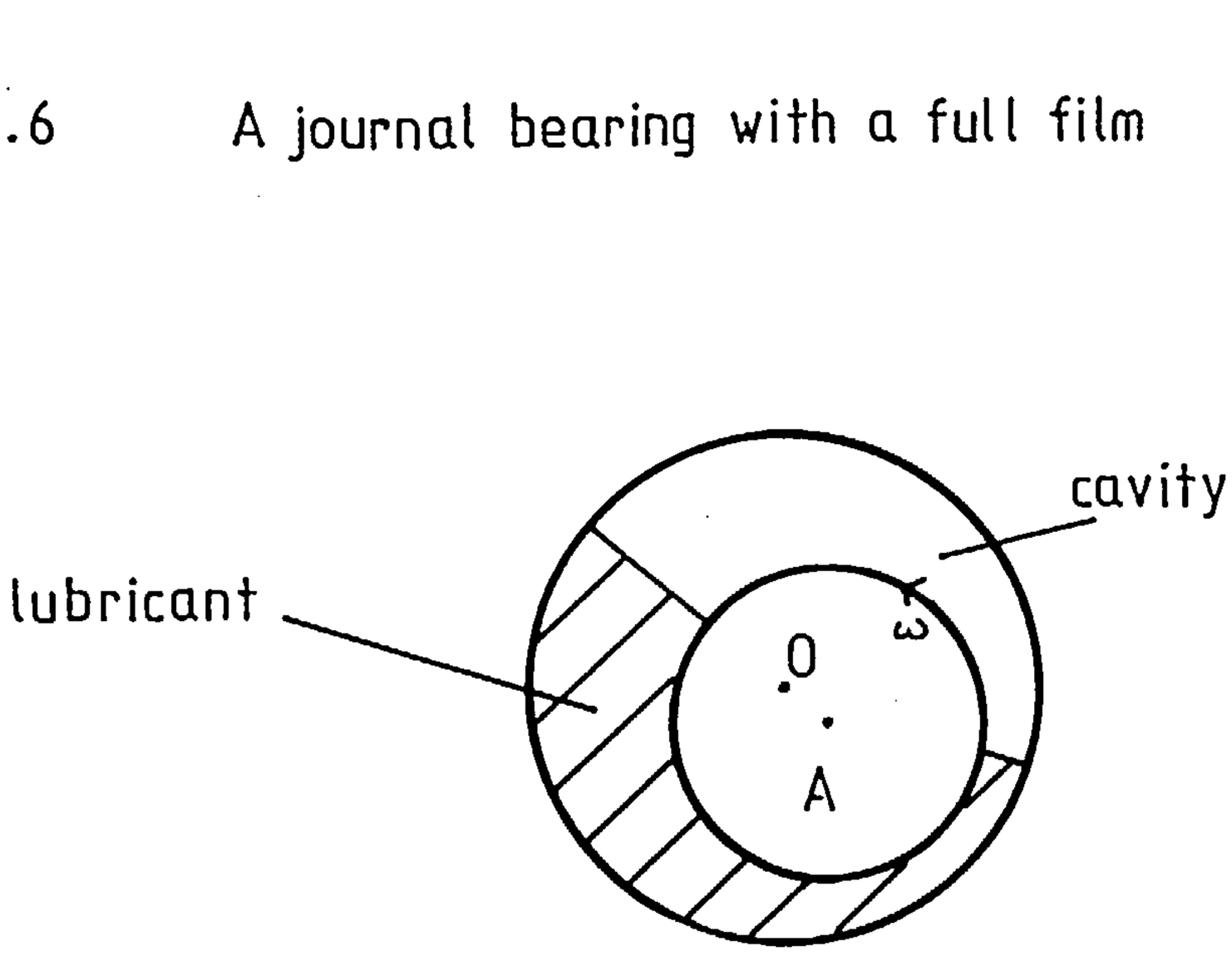

Figure 1.7 A journal bearing with a cavitated film

but orbits outwards towards the bearing casing i.e. $\epsilon \rightarrow 1$. For higher loads with generated superambient pressures well in excess of atmospheric, the oil film ruptures close to the position of minimum film thickness (Figure 1.7), creating a cavity, or series of cavities, in the divergent section. Work by several authors (e.g. Poritsky (1953), Holmes (1960)) has confirmed that the presence of this air cavity stabilises the journal bearing, thus permitting, under certain conditions, the centre of the shaft to take up an equilibrium position. This investigation will be concerned with bearings operating with an air cavity distributed over some section of the gap between bush and shaft. It is possible to feed the lubricant into the bearing at a superambient pressure, thus ensuring that the pressure is greater than atmospheric everywhere in the bearing; however, due to the destabilising effect of a noncavitated film, this thesis will not consider such a situation.

The present understanding of the phenomenon of cavitation is by no means complete. Previous attempts to determine the position of the cavity and its behaviour under dynamic conditions will be discussed in Chapter 2. It will be shown that the vibrational/stability characteristics are very sensitive to the location and extent of the cavity. This in turn illustrates the need to model the cavitation phenomena as accurately as possible.

1.4 Different types of rotor instability

Before proceeding to the main part of this thesis, it is necessary to specify exactly which type of dynamic behaviour is under consideration. This clarification is necessary because of the confusion that has built up over the years in the terminology of the subject. This will be considered in greater depth in Section 1.6. Essentially there are two different types of

fluid film instability:

(1) Oil Whirl - this is a phenomenon determined by the properties of the bearing film. It is typically a small amplitude motion with a frequency close to that of half shaft speed.

(2) Resonant Whip - this is a large amplitude motion occuring with a frequency close to that of the first critical speed in bending of the shaft. It is commonly encountered when the shaft speed exceeds twice this critical speed.

This thesis is concerned with Oil Whirl.

1.5 The hydrodynamic forces

Once a particular version of Reynolds' equation has been solved, the hydrodynamic forces on the shaft are found by integrating the pressure distribution over the oil film - A_r. Traditionally, these forces are resolved into two mutually perpendicular components (see Figure 1.4).

(1) A radial component - F_r - acting outward along the line of centres.

(2) A tangential component - F_t - acting in an anticlockwise direction perpendicular to the line of centres.

$$F_r = \iint_{A_r} p\cos\theta \; d(A_r) \quad ; \quad F_t = \iint_{A_r} p\sin\theta \; d(A_r) \qquad (1.14)$$

For the long bearing (1.14) becomes:

$$F_r = LR\int_{\theta_1}^{\theta_2} p(\theta)\cos\theta d\theta \quad ; \quad F_t = LR\int_{\theta_1}^{\theta_2} p(\theta)\sin(\theta)d\theta \qquad (1.15)$$

For the short bearing:

$$F_r = R\int_0^L\int_{\theta_1}^{\theta_2} p(\theta,z)\cos(\theta)d\theta dz \;;\; F_t = R\int_0^L\int_{\theta_1}^{\theta_2} p(\theta,z)\sin(\theta)d\theta dz \quad (1.16)$$

θ_1 and θ_2 refer to the beginning and end of the fluid film, where we assume that a cavity exists in the region $\theta_1<\theta<\theta_2$. The values of θ_1 and θ_2 will depend on the particular film rupture model under consideration; they will be dealt with in Chapter 2. The forces can be nondimensionalised as shown below. First, note that the bearing load is given by:

$$F = (F_r^2 + F_t^2)^{1/2}$$

Define:

$$\bar{F}_r = \frac{F_r}{SF} \quad ; \quad \bar{F}_t = \frac{F_t}{SF} \quad (1.17a)$$

$$\bar{F}_r = \frac{F_r}{S_m F} \quad ; \quad \bar{F}_t = \frac{F_t}{S_m F} \quad (1.17b)$$

$$\tau = \omega t \quad \rightarrow \quad \frac{d}{dt} = \omega\frac{d}{d\tau} \quad (1.18)$$

(1.17a) applies for the long bearing and (1.17b) for the short bearing. S and S_m are nondimensional quantities, known as the Sommerfeld number and modified Sommerfeld number, respectively; they are defined by:

$$S = \frac{R^3 L\omega\mu}{Fc^2} \quad ; \quad S_m = \frac{RL^3\omega\mu}{Fc^2}$$

Evaluation of F_r and F_t for both long and short bearing models, yields, for given geometry and viscosity:

$$\bar{F}_r = \bar{F}_r(\epsilon,\dot{\epsilon},\varphi,\dot{\varphi}) \quad ; \quad \bar{F}_t = \bar{F}_t(\epsilon,\dot{\epsilon},\varphi,\dot{\varphi}) \quad (1.19)$$

The nature of the functions $\bar{F}_r$ and $\bar{F}_t$ reflects the cavitation boundary

conditions and bearing geometry. The steady state (equilibrium) position of the journal is easily found by putting:

$$\dot{\epsilon} = \dot{\varphi} = 0$$

the steady state force components (see Figure 1.8) are denoted by:

$$\bar{F}_{rs} = \bar{F}_{rs}(\epsilon_s) \quad ; \quad \bar{F}_{ts} = \bar{F}_{ts}(\epsilon_s) \tag{1.20}$$

and the steady state value of the attitude angle is given by:

$$\varphi_s = \tan^{-1}\left\{ \frac{-\bar{F}_{ts}}{\bar{F}_{rs}} \right\}$$

In practice the relationship between ϵ_s and φ_s is almost semicircular. Figure 1.9 shows the possible steady state positions for a number of typical fluid film models. The nondimensional load capacity is given by:

$$\bar{F} = \sqrt{(\bar{F}_{rs}^2 + \bar{F}_{ts}^2)} = \bar{F}(\epsilon_s) = \frac{1}{\bar{S}} \text{ or } \frac{1}{\bar{S}_m} \tag{1.21}$$

So it can be seen that the value of the Sommerfeld number (modified Sommerfeld number) represents the inverse of the nondimensional load capacity.

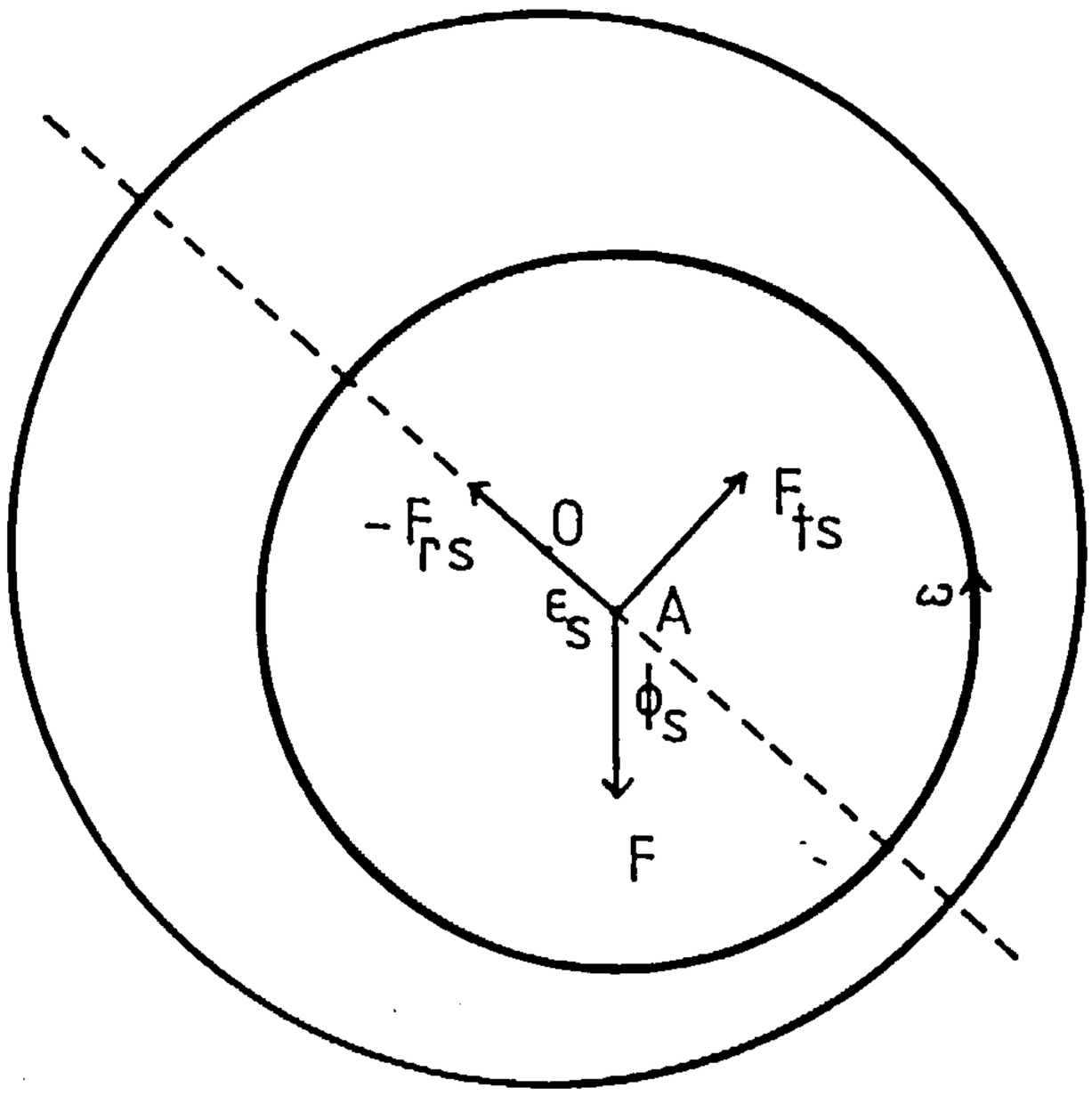

Figure 1.8 A journal bearing under steady state conditions

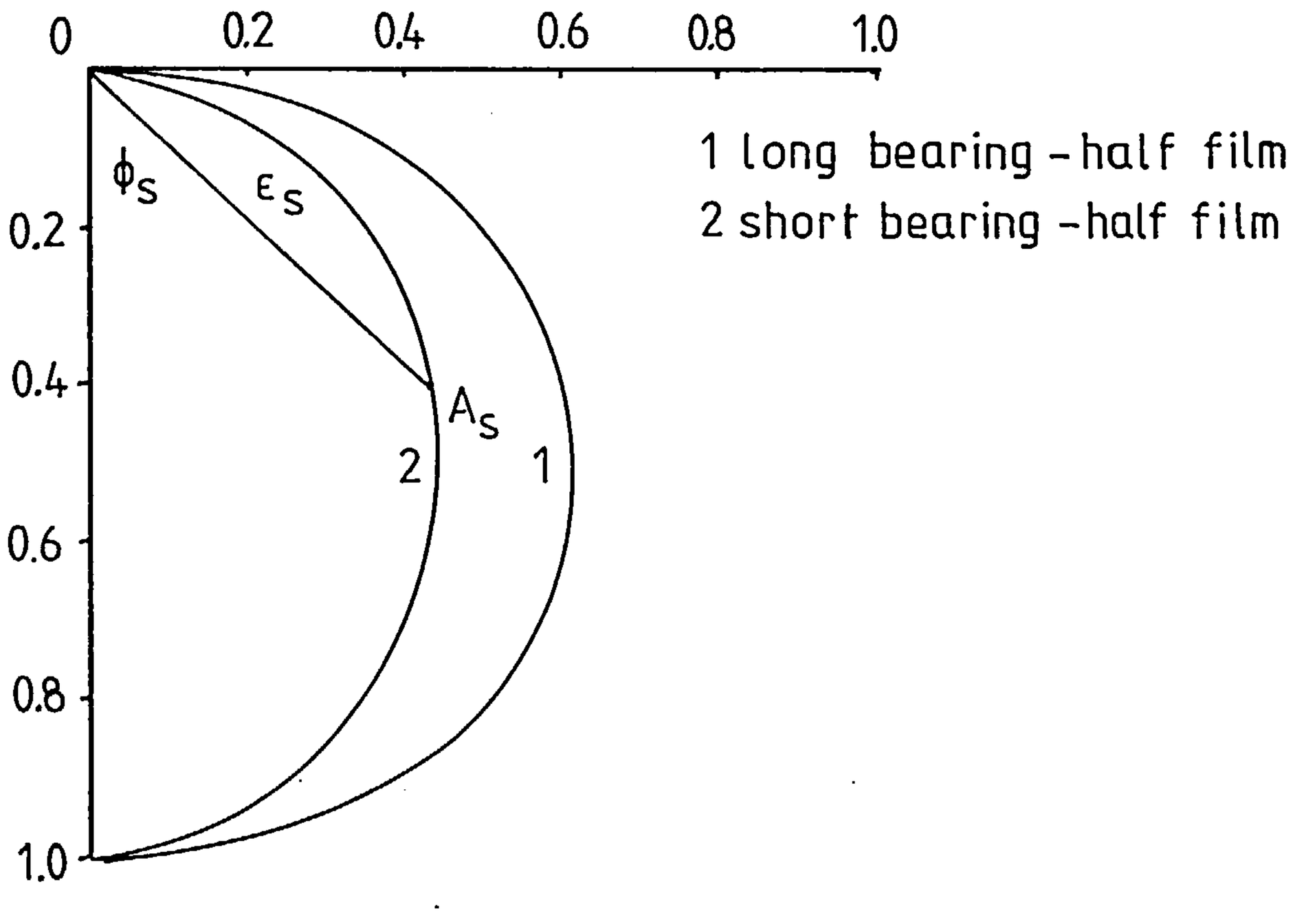

Figure 1.9 Steady state locus of the shaft centre for two models with different cavitation boundary conditions

1.6 Historical Review

The principle of hydrodynamic lubrication was first established by Beauchamp Tower (1883) when he noticed that if two loaded surfaces are kept apart by a film of oil, then a pressure distribution exists within the lubricant. This observation motivated Reynolds' (1886) to study the slow viscous flow of fluids in thin films, with the result that he provided the mathematical formulation for the pressure distribution between two bearing surfaces that is known today as Reynolds' equation.

Fluid film instability was initially identified experimentally by Newkirk (1924), although the first hydrodynamic study of the journal bearing had been carried out by Harrison (1919). He assumed an infinitely long bearing, operating with a complete film, and succeeded in deriving the radial and tangential force components. By neglecting the inertia of the shaft, he was able to show that stable whirl orbits could exist for $\epsilon<1$.

Stodola (1925) and Hummel (1926) independently reached the conclusion that the fluid film forces cause instability when $\epsilon<0.7$. Stodola developed a direct method to test the stability of an equilibrium position which is widely used today. His method is as follows: assume the journal to have mass m and the journal centre's position to be defined by cartesian co-ordinates (x,y). The fluid film force components F_x, F_y which depend on the position and velocity of the journal centre are linearised about the equilibrium position so that the equations of motion become:

$$m\frac{d^2x}{dt^2} = F_x\left(x,y,\frac{dx}{dt},\frac{dy}{dt}\right) = \frac{\partial F_x}{\partial x}x + \frac{\partial F_x}{\partial\left\{\frac{dx}{dt}\right\}}\frac{dx}{dt} + \frac{\partial F_x}{\partial y}y + \frac{\partial F_x}{\partial\left\{\frac{dy}{dt}\right\}}\frac{dy}{dt}$$

$$m\frac{d^2y}{dt^2} = F_y\left(x,y,\frac{dx}{dt},\frac{dy}{dt}\right) = \frac{\partial F_y}{\partial x}x + \frac{\partial F_y}{\partial\left\{\frac{dx}{dt}\right\}}\frac{dx}{dt} + \frac{\partial F_y}{\partial y}y + \frac{\partial F_y}{\partial\left\{\frac{dy}{dt}\right\}}\frac{dy}{dt}$$

Once the eight Taylor expansion coefficients are known, these two simultaneous linear differential equations can be readily tested for stability (see Chapter 5 for full details). Although Stodola recognised that it was appropriate to ignore subambient pressures when calculating the fluid film forces, he neglected the velocity (damping) terms in the linearised equations of motion, including only the displacement (stiffness) terms in his analysis. Robertson (1933) extended Stodola's work by including the damping terms, applying the technique to a journal bearing with a complete film, which he concluded was unstable.

In the last thirty years, the widespread introduction of high speed rotating machinery has led to a greater interest in the problem of journal bearing instability. It became clear that it was of two distinct types. Newkirk (1956), in an experimental study, contrasted the results obtained previously with a rigid shaft and a flexible shaft. The flexible shaft had a first critical speed in bending of 1210 r.p.m.; it was observed to whirl with a frequency of 1250 r.p.m. over the speed range 2300-5000 r.p.m. (resonant whip), the amplitude of this whirl increased with speed. The rigid shaft had no bending critical speeds below 30000 r.p.m.; oil whirl was observed at low speeds with a frequency slightly less than half running speed. Interestingly, this oil whirl died out at higher speeds between 7000 r.p.m. and 18000 r.p.m.

Sternlicht (1962) identified three different types of rotor instability: half frequency whirl, fractional frequency whirl and resonant whip. Smith (1970) also found three different types: light load instability, half frequency whirl and low frequency whirl. It is, however, generally agreed that half frequency whirl, fractional frequency whirl and light load instability are different manifestations of oil whirl; whereas low frequency whirl is really resonant whip. This plethora of terminology, with the additions of synchronous and nonsynchronous whirl, make a study of the literature most

confusing, especially for the nonspecialist. The author would like to suggest that in general, only the terms 'oil whirl' and 'resonant whip' should be used. The use of 'half frequency whirl' should be restricted to the description of the pure half frequency whirl observed in the case of the unloaded bearing.

Early analytical studies of the fluid film were restricted to Sommerfeld's (1904) solution to the long bearing. Another major development which occurred shortly after the second world war was Ocvirk's (1952) introduction of the short bearing approximation. The latter solution is now accepted as being the more realistic. This is reflected in the fact that although the first attempts to model a finite bearing were based on the long bearing e.g. Warner (1963), recent attempts have been based on the short bearing e.g. Pan (1980), Pan and Ibrahim (1980).

Two important contributions to the understanding of fluid film instability were made by Poritsky (1953) and Hori (1959). In a study confined to small eccentricities, Poritsky showed that although a flexible rotor operating in a long bearing with an uncavitated film is inherently unstable, if cavitation is introduced, it is possible to derive a stability criterion, i.e. for stability, the following must be satisfied:

$$m\omega^2 \left\{ \frac{1}{K_r} + \frac{1}{K_s} \right\} < 4 \quad \text{or} \quad \omega < 2\omega_1$$

where: K_r = rotor stiffness, K_s = oil stiffness

ω = rotational speed, ω_1 = rotor's first critical speed in bending

Although Poritsky's approach was rather crude in that fluid film damping was assumed to be linear, he succeeded in showing that for $\omega > 2\omega_1$, the rotor will whirl with frequency ω_1 as observed experimentally. He was also one of the first to appreciate the importance of cavitation as a stabilising agent.

Hori calculated the fluid film forces under the assumption that the bearing was infinitely long and that the lubricant occupied only the converging part of the gap between the shaft and the bush. By linearising the equations of motion about the steady state position in a similar fashion to that adopted by Stodola, he used Hurwitz criteria to derive a stability condition:

$$\frac{F}{mc\omega^2} > \kappa_1(\epsilon_s)\left\{ \kappa_2(\epsilon_s) + \frac{F}{mc\omega_1^2} \right\}$$

where: F = load supported by the bearing, m = rotor mass

ϵ_s = steady state value of the eccentricity ratio

ω_1 = first critical speed in bending of the rotor

c = radial clearance, κ_1, κ_2 = functions of ϵ_s

The second part of Hori's work consists of a part analytical, part experimental examination of the motion of a rotor mounted on a flexible shaft operating well above the threshold speed (the maximum speed for which the rotor is stable, as calculated by linear techniques). Although some of his assumptions are rather vague, he succeeded in showing that resonant whip cannot occur unless $\omega > 2\omega_1$, as well as explaining some of the observations of Newkirk and Lewis (1956) and Pinkus (1956).

Recent work in this area of the subject has harnessed the power of high speed digital computers to solve Reynolds' equation for finite L/D ratios and for noncircular bearing shapes. This has enabled several techniques to be developed to calculate the eight bearing coefficients, e.g. Woodcock and Holmes (1970), Lundholm (1971), Lund and Thomsen (1978). Akers, Michaelson and Cameron (1971) combined a numerical integration of Reynolds' equation with a Runge-Kutta solution of the equations of motion to calculate stability borderlines for a variety of L/D ratios. They achieved good agreement with results obtained by standard techniques. It has become common practice to use

a combined computational/experimental approach to confirm the accuracy of computer programs developed for stability analysis. Lund and Tonnesen (1978) obtained excellent agreement between experimental results obtained by an examination of two different rotor systems and numerically calculated stability borderlines, thus validating the use of theoretical models in bearing analysis. Allaire (1980) has presented a detailed survey of the stability characteristics of several bearing geometries by a similar combination of experimental and computational methods.

Interest in the nonlinear features of oil whirl has arisen from the observation that several machines have been successfully run at speeds in excess of the threshold speed e.g. Mitchell, Holmes and Byrne (1965-6), Newkirk and Lewis (1956) and Tondl (1965). However, with very few exceptions, mathematical investigations of the nonlinear motion have been based on numerical integration, the results of which have been inconclusive. Using both long and short bearing theory, Mitchell, Holmes and Byrne concluded that the journal was unstable for all rotor speeds if a complete oil film is assumed; whereas Reddi and Trumpler (1962) and Tolle and Muster (1969), also using a complete film, found that under certain conditions stable whirl orbits exist. Badgley and Booker (1969) considered the effects of cavitation by neglecting the subambient pressure region for the long bearing, the short bearing, and Warner's (1963) finite length approximation. However, their investigation was restricted to the consideration of the effects of initial transients on the linear stability borderline. McKay (1981) using a time-step technique, found that under certain conditions the long bearing with oscillating half film (originally developed by Hori) can sustain stable whirl orbits.

Lund (1966) made an analytical investigation of the short bearing by means of the method of averaging. Myers (1981) employed a similar technique for the

long bearing. Both these studies showed the existence of stable whirling at speeds just above and below critical, depending on the value of a certain speed independent parameter. In the case of Myers, a study of the same model by means of Hopf bifurcation and multiple scaling gave excellent agreement, but showed discrepancies with the method of averaging, suggesting an error in its application. The author is not aware of any further analytical studies other than the work of Lund and Myers.

Other numerical studies include work by Jennings (1960), Huggins (1963-4) and Someya (1963-4). Recently, attention appears to have concentrated on the use of numerical techniques to examine the effects of extraneous features such as load imbalance and rotating loads on whirling motion e.g. Kirk and Gunter (1975), Bannister (1980). Lund and Nielsen (1980) have adapted the method of averaging to examine the effect of mass imbalance.

CHAPTER 2

CAVITATION MODELS AND LINEAR ANALYSIS OF THE STABILITY OF THE EQUILIBRIUM POSITION

In Chapter 1, cavitation was discussed in general terms and the hydrodynamic pressure forces due to the fluid film were derived. These were found to be functions of the position and velocity of the journal within the bush. A steady state (equilibrium) position was found by equating the velocity components within the force expressions to zero, and balancing the steady state forces against the load (Figure 1.8). This led to a relationship between the load (F), the steady-state eccentricity ratio (ϵ_s) and the rotation speed (ω). In this chapter, the experimental and analytical basis of various attempts to model cavitation phenomena will be examined and the fluid film forces for particular cavitation models will be derived. In addition, linearised stability analysis will be used to determine the stability of the equilibrium position giving rise to a neutral curve in (ϵ_s, ν) parameter space (see Section 2.3) and also the frequency of small vibrations at the stability threshold (critical frequency). Finally the effect of shaft flexibility on the stability of the models will be considered.

2.1 The application of cavitation boundary conditions

The pressure distribution in a journal bearing is found by solving Reynolds' equation subject to appropriate boundary conditions. The simplest solution to the long bearing approximation, known as the Sommerfeld (1904) solution and representing a journal with a full fluid film (no cavitation), is obtained by applying the conditions:

$$p = 0 \quad \text{at} \quad \theta = 0,\ 2\pi \tag{2.1}$$

This solution ignores cavitation and leads to an antisymmetric pressure distribution in the static case (see Figure 2.1); as observed in Section 1.3 it has been shown to be inherently unstable. The simplest modification to this model is known as the Gumbel (1921) condition, for which the following

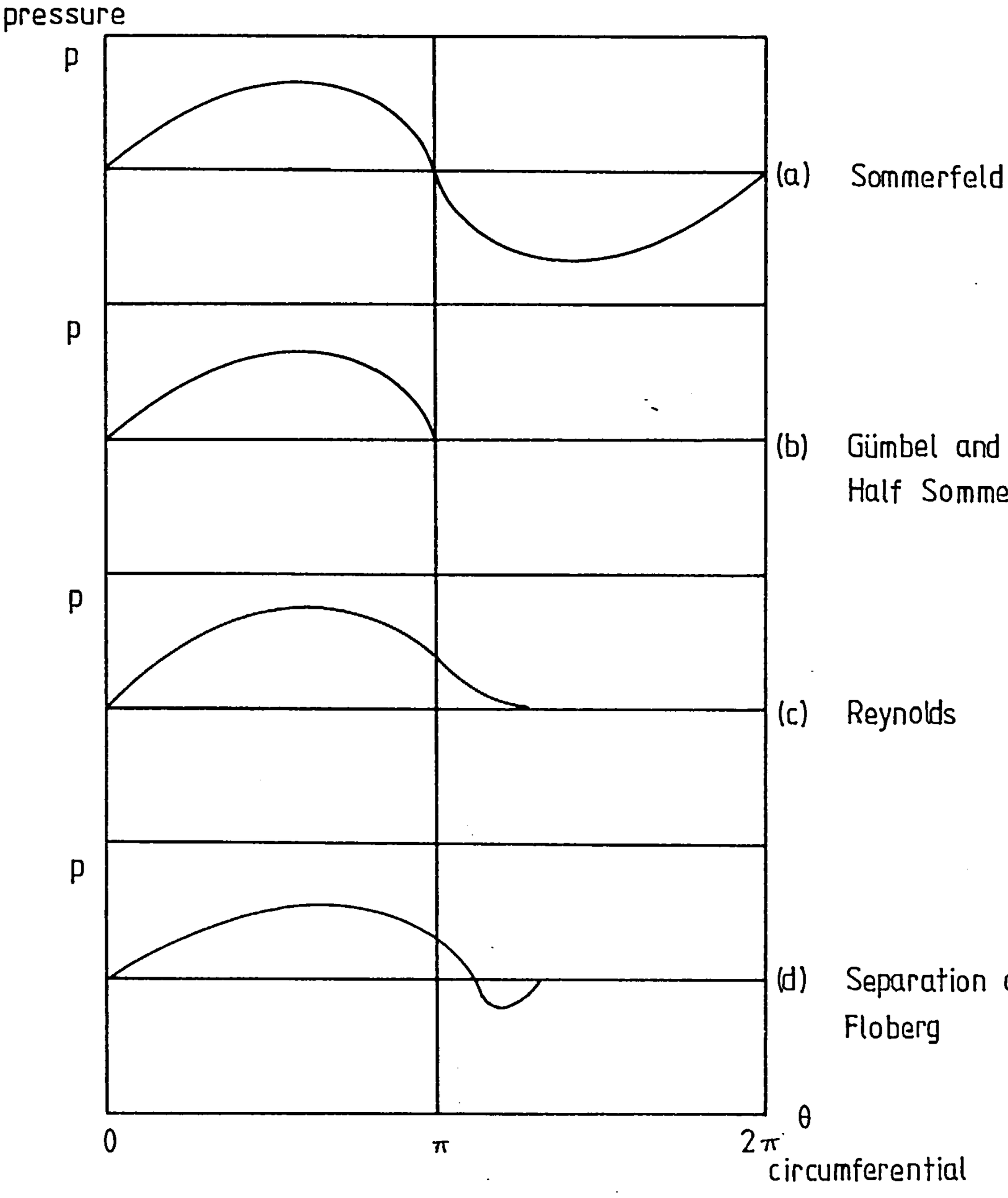

Figure 2.1 Pressure distributions in an infinite width journal bearing under static conditions

boundary conditions are specified:

$$p = 0 \quad \text{at} \quad \theta = 0,\ \pi$$

$$p = 0 \quad \text{at} \quad \pi < \theta < 2\pi$$

This model gives reasonably accurate results for the static properties of the bearing and consequently it hes been widely used as a 'first approximation' e.g. Hori (1959), McKay (1981). Another relatively straightforward modification to the non-cavitating model is the half Sommerfeld solution. Here, Reynolds' equation is integrated as for the Sommerfeld solution with boundary conditions (2.1); however subambient pressures are simply ignored when calculating the hydrodynamic forces. It is easy to confuse the Gumbel and half Sommerfeld solutions in the literature of the subject, since in the static case they are identical in predicting the existence of a cavity filling exactly the whole of the converging region (Figure 2.1). Consequently some authors have been imprecise as to which boundary conditions they are applying. The Gumbel solution has the fluid film filling exactly the whole of the converging region under both static and dynamic conditions; whereas under dynamic conditions, the half Sommerfeld solution (see Section 2.6) has:

$$p > 0 \quad \text{for} \quad 0 < \theta < \pi+\alpha \qquad (\alpha > 0)$$

$$\text{and } p = 0 \quad \text{for} \quad \pi+\alpha < \theta < 2\pi$$

As we shall see later on, this apparently small distinction gives rise to a very different neutral stability curve in (ϵ_s, ν) space.

To obtain a more accurate representation of the behaviour of the oil film, Reynolds' boundary conditions can be used. This condition constitutes a more realistic attempt to reconcile the mathematical model with experimental and visual evidence of the region around film rupture. This evidence (e.g. Dowson (1957)) suggests that the breakdown of the lubricant flow is characterised by a finger pattern of air cavities (see Figures 2.2 and 2.3). The flow rate per

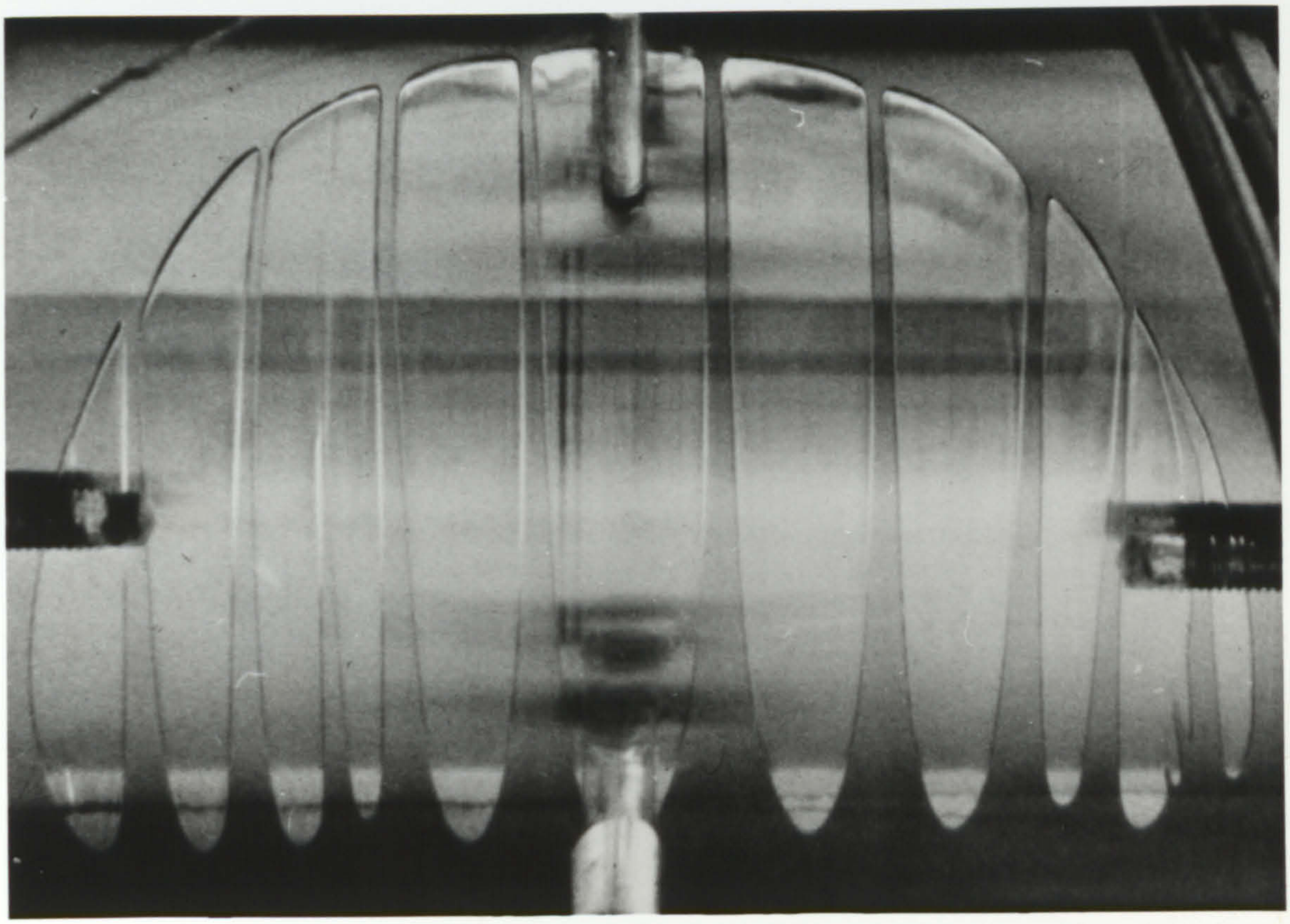

Figure 2.2
'Finger cavities' at the
lubricant/cavity interface

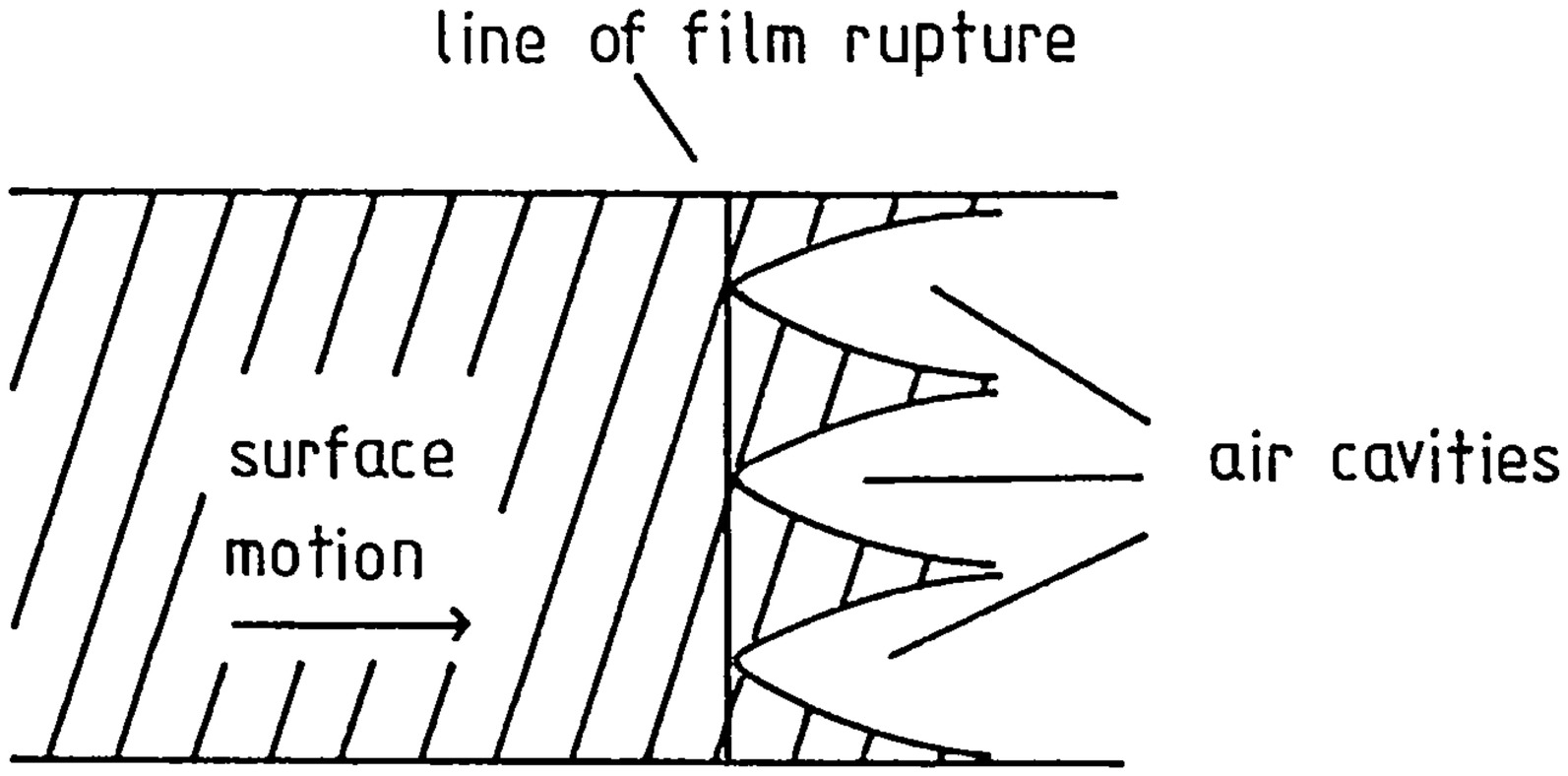

Figure 2.3 Plan view of film rupture

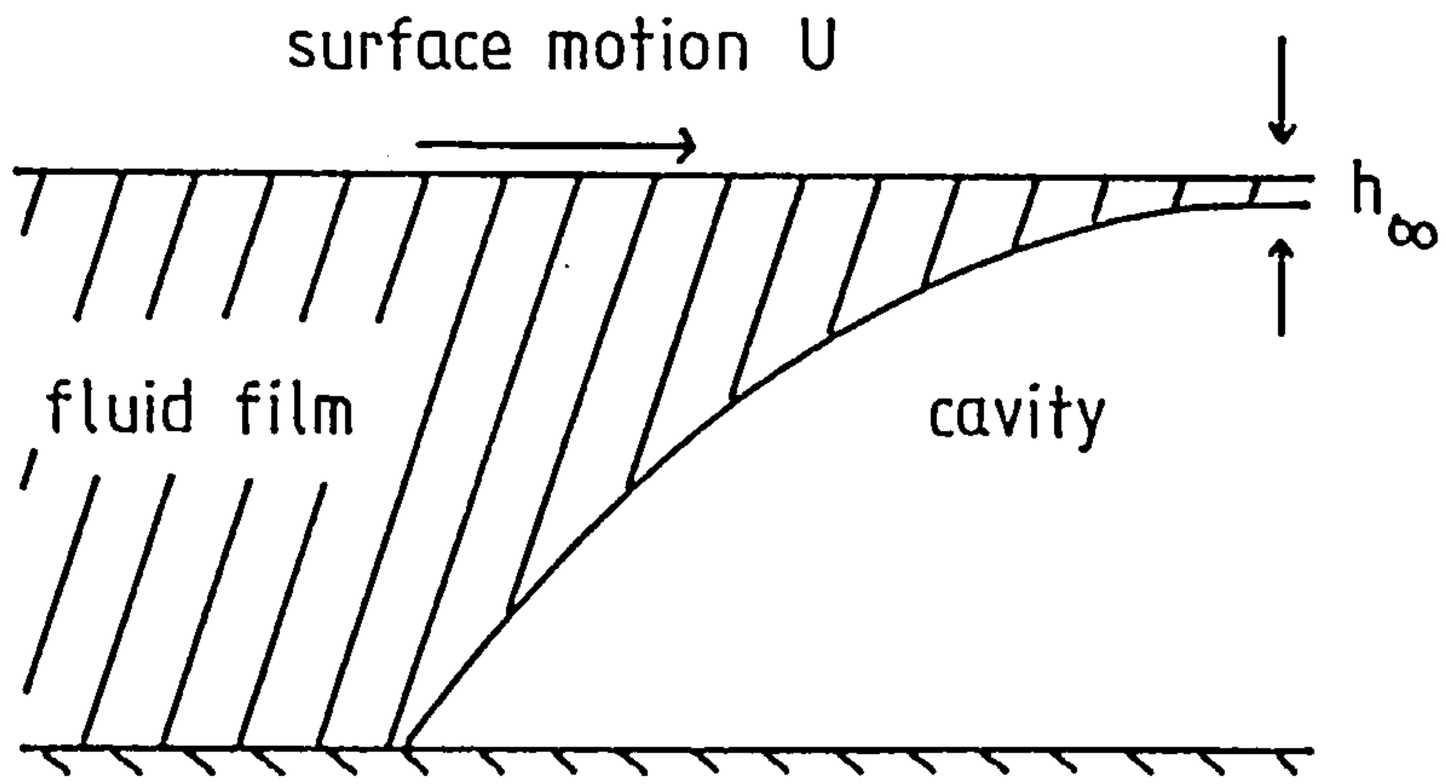

Figure 2.4 Flow separation

unit width is given by (equation (1.3)):

$$\frac{-h^3}{12\mu}\frac{dp}{dx} + \frac{Uh\rho}{2}$$

We have assumed that the pressure in the cavities is constant and ambient. Therefore if the cavities are sharply pointed, the flow rate per unit width immediately after rupture is given by:

$$\frac{Uh\rho}{2}$$

Consequently, continuity requirements imply that:

$$\frac{dp}{dx} = 0$$

The Gumbel and half Sommerfeld solutions fail to satisfy this continuity condition. The Reynolds' boundary conditions can be summarised as:

$$p = 0 \quad \text{at} \quad \theta = 0$$

$$p = \frac{dp}{d\theta} = 0 \quad \text{at} \quad \theta = \theta_1$$

$$p = 0 \quad \text{for} \quad \theta_1 < \theta < 2\pi$$

The Reynolds' boundary condition represents the most sophisticated model of cavitation commonly in use in bearing analysis. However, it is not ideal, since further evidence (Hopkins (1957), Birkhoff and Hays (1963)) suggests that just upstream of film rupture, the lubricant pressure drops below that of the cavity (Figure 2.1). As the use of Reynolds' condition cannot predict this subcavity pressure loop, new attempts have been made to explain the circumstances around film rupture. It has been suggested that a reverse flow eddy might provide a mechanism for cavity formation, with the result that a cavity would form where the fluid separates from the bush (where velocity and tangential stress are both zero) (Figure 2.4). In this case some of the fluid will be carried over or under the cavity attached to the rotating shaft. The

zero shear stress assumption leads to the condition:

$$\frac{dp}{dx} = \frac{2\mu U}{h^2} \qquad (2.2)$$

This pressure relationship combined with the chosen pressure value for the cavity can be used to determine the position of the lubricant/cavity interface. When (2.2) is satisfied and separation occurs (in general, when $\epsilon>0.3$), this condition implies that the cavity forms at the position of separation. Therefore, the application of this condition involves the assumption that the existence of a cavity does not affect separation. Nevertheless, this work does represent a step forward in explaining the presence of the subcavity loop and the absence of cavitation for lightly loaded bearings at low eccentricities ($\epsilon<0.3$). The method has since been reformulated by Coyne and Elrod (1970,1971) who carried out a planar analysis, taking account of surface tension, gravity and fluid inertia. Having determined the rupture interface they derived the following boundary conditions (gravity and fluid inertia are neglected here):

$$\frac{dp}{dx} = \frac{6\mu U}{h_c^2}\left(1-2\frac{h_\infty}{h_c}\right)$$

$$p = -\frac{T}{R_o}+\Delta p$$

h_∞ = uniform fluid film downstream of film rupture

R_o = radius of curvature of free film at separation point

T = surface tension between lubricant and air

Δp = measure of the pressure change across the transition region from the lubrication type flow just upstream of the cavity

Coyne and Elrod also succeeded in deriving the ratios (h_∞/h_c) and (R_o/h_∞) as functions of the capilliary number $\mu U/T$. The importance of these ratios in low Reynolds' number fluid dynamics has already been demonstrated by Bretherton (1960) and Taylor (1963).

The question arises as to when are the Coyne and Elrod conditions and the Reynolds' conditions valid. Coyne and Elrod assumed that the fluid/air interface is unperturbed, i.e. a straight line along the axis of the bearing. This situation arises at low pressures and low eccentricity ratios. The Reynolds' condition assumes that the interface is perturbed in a 'finger pattern' (see Figures 2.2 and 2.3), which is most likely to occur when moderate to high pressures are generated, i.e. at higher eccentricity ratios.

The problem of film reformation has not received the detailed treatment afforded film rupture, indeed in common usage the term 'cavitation conditions' has come to represent film rupture conditions; this thesis adopts this convention. Floberg (1975) has developed some rather complex governing equations, whilst Coyne and Elrod remarked that the general formulation of their equations was applicable to film reformation. Application of the Coyne and Elrod technique, however, leads to an infinite number of possible film shapes at reformation. Dowson and Taylor (1979) suggest that in an analysis of lightly loaded bearings across the eccentricity range, a mixture of physical models might produce the best results. Clearly there is scope for more research into the conditions governing film reformation.

The approach adopted in this thesis (except in the case of the short bearing. which will be considered later in this section) is that the film begins either at the line of maximum film thickness, or at the axial groove, if one is included in the model. This assumption is rather hard to justify, yet it is made in the light of the observations that film reformation occurs in the region (just upstream) of the position of maximum film thickness.

Dynamic Conditions

The cavitation models so far considered have been concerned with the

behaviour of the lubricant under static conditions (with the exception of the short bearing model, which implies its own dynamic conditions). If a linear or nonlinear dynamic analysis is to be carried out, the behaviour of the fluid film during a vibration of the journal must be known. In particular, does the lubricant remain in a fixed position relative to the shaft, or to the bush? Even during very small vibrations this can have a dramatic effect upon stability (see Section 2.10 for a discussion of this phenomenon).

Short Bearing Theory

The above discussion of cavitation boundary conditions is applicable to long and finite bearing theory. However, in recent years, short bearing theory has come into prominence as a more realistic description of the physics involved since typically L/D < 3/4 (Holmes (1960,1963), Lund (1966), Lund and Nielsen (1980)). Due to the nature of equation (1.13) it is not possible to implement arbitrary boundary conditions, because the pressure distribution imposes its own zero (i.e. cavitation) values. Recently Pan (1980) has examined a short bearing which can sustain negative pressures, but in general, only two short bearing models are available:

(1) Full film model. This has already been shown to be inherently unstable (Holmes (1963)), and will therefore be ignored.

(2) Half film model. In this model the fluid film extends from $\theta_1 < \theta < \pi + \theta_1$, where θ_1 is determined by the position and velocity of the journal.

Summary

The remainder of this chapter will be concerned with an investigation of journal bearing stability for various models incorporating the boundary conditions already discussed. Initially the simpler cavitation models are analysed, then the more sophisticated Reynolds' approximation is studied. The

latter condition has been chosen not only for the advantage of relative ease of application, but also because of its success in predicting those bearing properties that have been confirmed by experiment. The use of Reynolds' condition allows an additional sophistication to be built into the physical model, namely the introduction of fluid supply through an axial groove. Finally the a short bearing operating with a half film will be analysed.

2.2 The equations of motion

The derivation of the equations of motion and the analysis of their stability in this and the following section are a generalisation and extension of a technique developed by Hori (1959) to study the long bearing oscillating half film model. To derive the equations of motion, rectangular co-ordinate axes are introduced with the origin O at the equilibrium point of the journal centre (Figure 2.5). Denote the co-ordinates of the shaft centre and rotor centre by $A(\xi,\eta)$, $R(x',y')$ respectively (note that for a rigid shaft A and R are coincident).

It is important to point out that it is assumed that the shaft is sufficiently stiff for static deflections to be ignored. If static deflections were to be included, the problem would be greatly complicated by the presence of sinusoidal forcing terms in the equations of motion.

There are two forces acting on the rotor centre:

(1) The load due to gravity.

(2) The force due to the bending of the shaft.

Consequently the rotor centre has equations of motion:

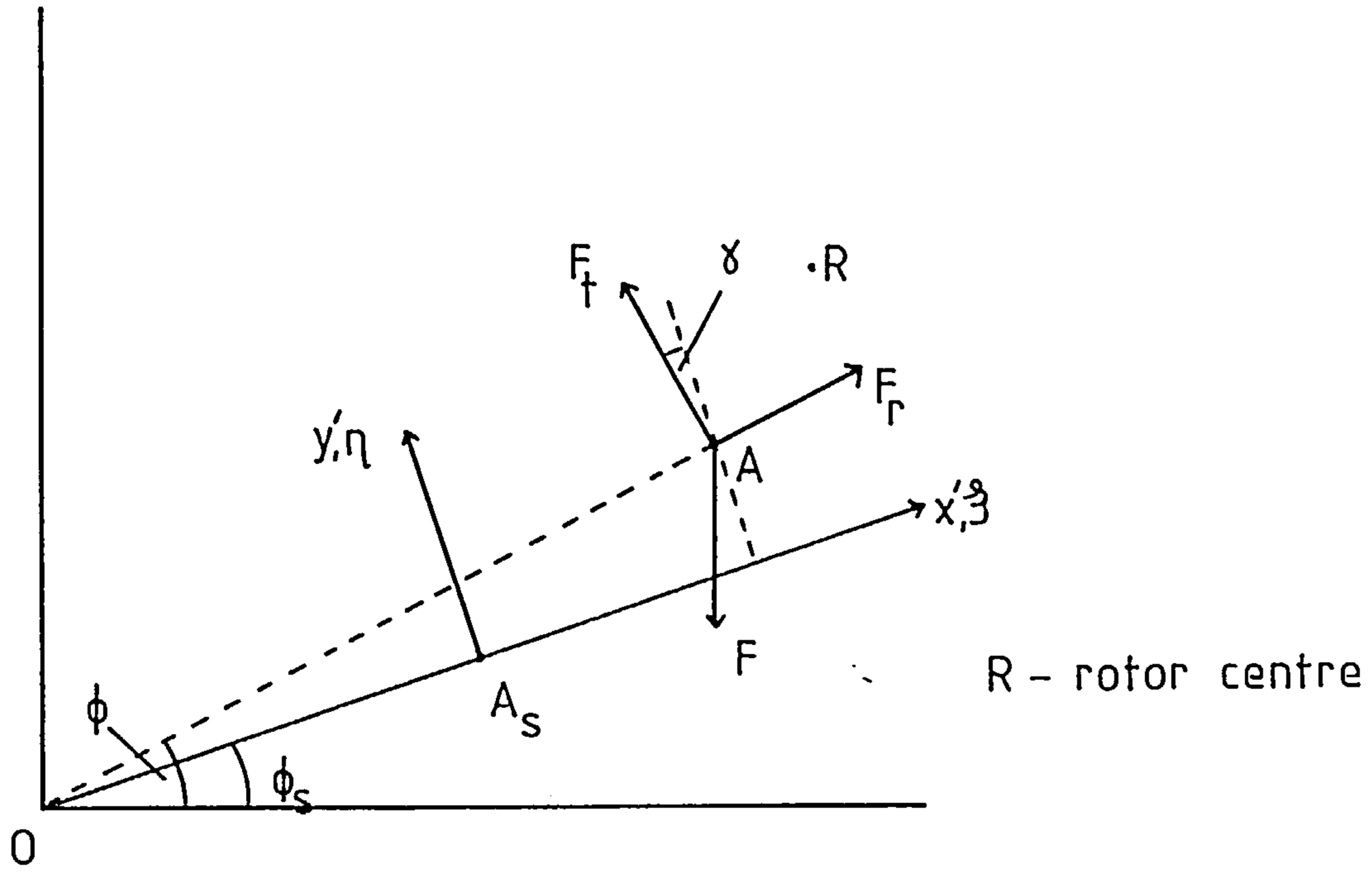

Figure 2.5 Co-ordinate system for the stability analysis

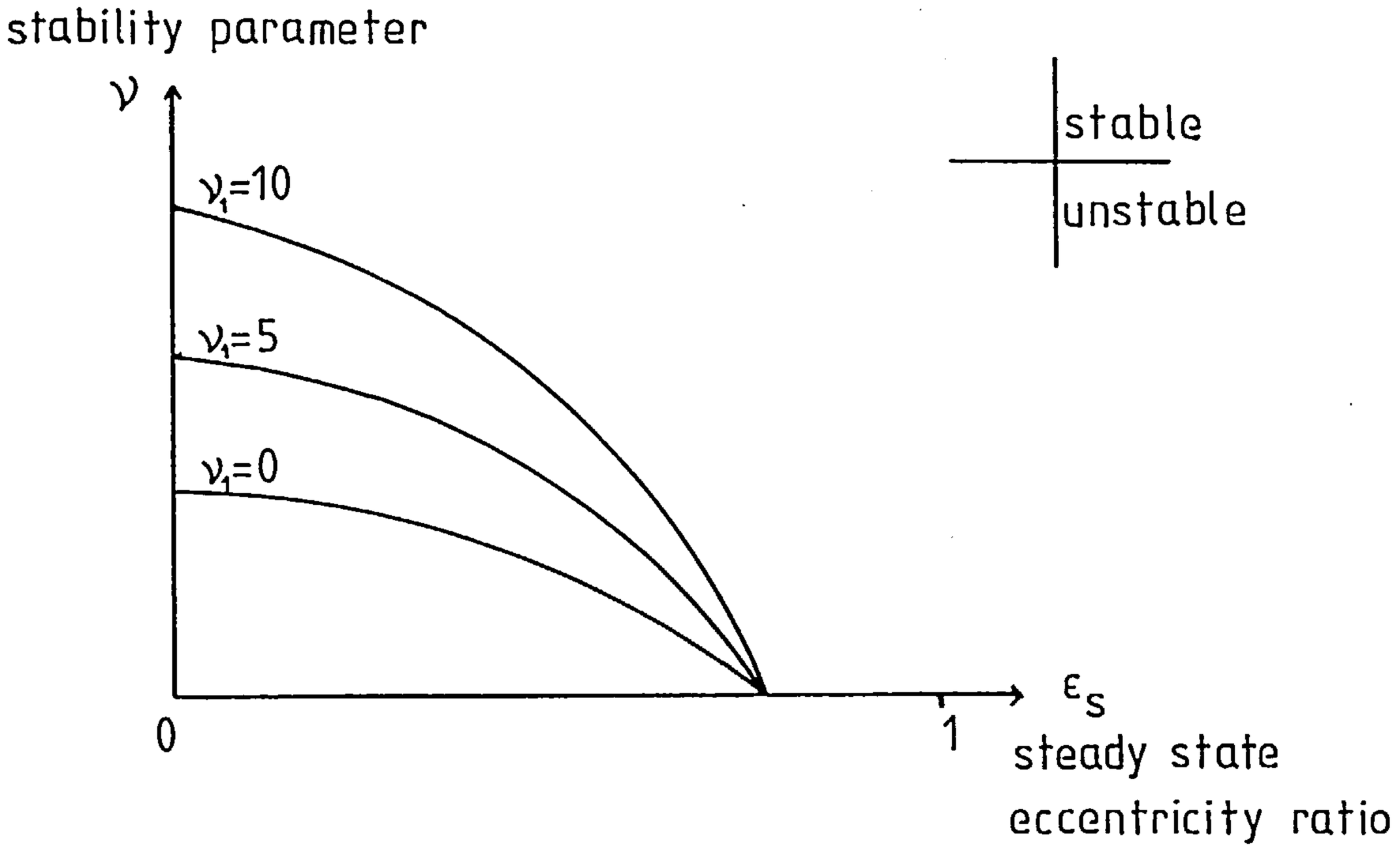

Figure 2.6 A typical stability chart

$$m\ddot{x}'+k(x'-\xi)+mg\sin\varphi_s = 0 \qquad (2.3)$$

$$m\ddot{y}'+k(y'-\eta)+mg\cos\varphi_s = 0 \qquad (2.4)$$

The force balance between the bending force in the shaft and the reaction at the bearings leads to the relationship:

$$k(x'-\xi) = -F_r\cos(\varphi-\varphi_s)+F_t\sin(\varphi-\varphi_s) \qquad (2.5)$$

$$k(y'-\eta) = -F_r\sin(\varphi-\varphi_s)-F_t\cos(\varphi-\varphi_s) \qquad (2.6)$$

Equations (2.3)-(2.6) represent four equations of motion describing the behaviour of the system. If the terms in ξ and η are eliminated they can be used to calculate the stability of the rotor.

2.3 Linearised stability analysis

Equations (2.3)-(2.6) can be linearised about the equilibrium point (ϵ_s,φ_s) for the purpose of examining the stability of the bearing. The first step is to perturb the eccentricity ratio and attitude angle about their equilibrium values:

$$\epsilon = \epsilon_s+\delta \quad ; \quad \delta \ll \epsilon_s \qquad (2.7)$$

$$\varphi = \varphi_s+\gamma \quad ; \quad \gamma \ll \varphi_s \qquad (2.8)$$

It can be seen from Figure 2.5, in which OA = e = ϵc, that:

$$\eta = c\epsilon\sin\gamma \quad ; \quad \xi = c\epsilon\cos\gamma-c\epsilon_s$$

$$\gamma \ll \varphi_s \rightarrow \cos\gamma \simeq 1 \ , \ \sin\gamma \simeq \gamma$$

$$\rightarrow \xi \simeq c\epsilon-c\epsilon_s = c\delta \quad ; \quad \eta \simeq c\epsilon_s\gamma$$

The equations of motion can be nondimensionalised by use of the following quantities (in addition to those introduced in (1.17) and (1.18)):

$$x = \frac{x'}{c} \quad ; \quad y = \frac{y'}{c} \quad ; \quad \nu = \frac{F}{mc\omega^2} \quad ; \quad \nu_1 = \frac{F}{mc\omega^2_1} \tag{2.9}$$

where ω_1 = the first critical speed in bending of the shaft ($=\sqrt{(k/m)}$).

Linearising the equations about the equilibrium position yields:

$$\ddot{x} + \frac{\nu}{\nu_1}(x-\delta) + \nu\sin\varphi_s = 0 \tag{2.10}$$

$$\ddot{y} + \frac{\nu}{\nu_1}(y-\epsilon_s\gamma) + \nu\cos\varphi_s = 0 \tag{2.11}$$

$$(x-\delta) + S\nu_1\bar{F}_r - \gamma S\nu_1\bar{F}_t = 0 \tag{2.12}$$

$$(y-\epsilon_s\gamma) + S\nu_1\bar{F}_r + \gamma S\nu_1\bar{F}_t = 0 \tag{2.13}$$

Equations (2.10)-(2.13) can be reduced to two third order linear equations in x and y by removing terms in δ and γ. The procedure is as follows (full details are given in Appendix 1):

(1) Note that the fluid film forces (equations (1.19)) can linearized to become:

$$\bar{F}_r = -A_r - B_r\delta + C_r\dot{\gamma} - D_r\dot{\delta} + E_r\gamma \tag{2.14}$$

$$\bar{F}_t = A_t + B_t\delta - C_t\dot{\gamma} + D_t\dot{\delta} + E_t\gamma \tag{2.15}$$

(2) Use (2.10),(2.11) to find $\delta,\dot{\delta},\gamma,\dot{\gamma}$ in terms of $x,y,\dot{x},\dot{y},\epsilon_s$ and φ_s.

(3) Substitute (2.14),(2.15) into (2.12),(2.13) and remove constant terms by considering an equilibrium position:

The system now reduces to:

$$a_1\nu_1\dddot{x}+(a_2\nu_1+1)\ddot{x}+a_1\nu\dot{x}+a_2\nu x-a_3\nu_1\dddot{y}+(a_4-a_5)\nu_1\ddot{y}$$
$$-a_3\nu\dot{y}+(a_4-a_5)\nu y = 0 \tag{2.16a}$$

$$b_1\nu_1\ddot{x}+b_2\nu_1\ddot{x}+b_1\nu\dot{x}+b_2\nu x-b_3\nu_1\ddot{y}-\{1+(b_4-b_5)\nu_1\}\ddot{y}$$

$$-b_3\nu\dot{y}+(b_4-b_5)\nu y = 0 \qquad (2.16b)$$

Each of the coefficients a_i, b_i are functions of ϵ_s alone. They are time-independent and constant for a given value of ϵ_s. The stability of (2.16a) and (2.16b) can be examined by a standard method, in which x and y are assumed to be of the form:

$$x = x_0 e^{sT} \quad ; \quad y = y_0 e^{sT}$$

This leads to a characteristic equation:

$$A_0 s^6+A_1 s^5+A_2 s^4+A_3 s^3+A_4 s^2+A_5 s^1+A_6 = 0 \qquad (2.17)$$

$$A_i = A_i(a_i, b_i, \nu, \nu_1)$$

For the equilibrium point to be stable, all the roots of the characteristic must have negative real parts, and we can find necessary and sufficient conditions for this by applying Hurwitz criteria (Gantmacher (1959)). These criteria state that for (2.17) to have roots with negative real parts, the following inequalities must be satisfied simultaneously:

$$A_6 > 0,\ A_5 > 0,\ A_4 > 0,\ A_3 > 0,$$

$$A_2 > 0,\ A_1 > 0,\ A_0 > 0. \qquad (2.18)$$

$$\begin{vmatrix} A_1 & A_3 & A_5 & 0 & 0 \\ A_0 & A_2 & A_4 & A_6 & 0 \\ 0 & A_1 & A_3 & A_5 & 0 \\ 0 & A_0 & A_2 & A_4 & A_6 \\ 0 & 0 & A_1 & A_3 & A_5 \end{vmatrix} > 0 \qquad (2.19)$$

$$\begin{vmatrix} A_1 & A_3 & A_5 \\ A_0 & A_2 & A_4 \\ 0 & A_1 & A_3 \end{vmatrix} > 0 \qquad (2.20)$$

In general, condition (2.18) is always satisfied, and after a considerable

amount of algebra, which is straightforward but tedious, (2.19) can be written in the form:

$$\nu > \kappa_1(\epsilon_s)\{\kappa_2(\epsilon_s)+\nu_1\} \qquad (2.21)$$

If (2.20) is written in a similar form to (2.21) it can be seen that it is a weaker condition than (2.19), i.e. if (2.19) is satisfied, so is (2.20). Since κ_1 and κ_2 are functions of ϵ_s alone, it is therefore possible to express the stability parameter ν in terms of the eccentricity ratio and the stiffness parameter ν_1. A typical stability graph is shown in Figure 2.6. It can be seen that in the case of the rigid shaft, for which:

$$\omega_1 \to \infty$$

$$\nu_1 \to 0$$

the stability criterion reduces to the traditional criterion used by other workers in this area of research (e.g. Myers (1981), Holmes (1960)):

$$\nu > L(\epsilon_s)$$

where the expression L is derived from a fourth order characteristic. In passing we note that it is possible to show that:

$$L(\epsilon_s) = \kappa_1(\epsilon_s)\kappa_2(\epsilon_s)$$

This does, however, involve a great deal of algebraic manipulation, which would be of little benefit since the result can easily be verified for any particular bearing model by simply comparing the numerical results yielded by the two methods.

The analysis so far has produced a pair of simultaneous linear third order O.D.E.'s in x and y, to which we have assumed existence of solutions of the form:

$$x = x_0 e^{sT} \quad ; \quad y = y_0 e^{sT}$$

At the threshold of stability, the small oscillations about the equilibrium position are neither growing nor shrinking, so s is wholly imaginary. In this case, suppose that the motion has critical frequency $\bar{\Omega}_s$, such that:

$$s = i\bar{\Omega}_s$$

on substitution into (2.17) we obtain:

$$-A_0\bar{\Omega}_s^6+iA_1\bar{\Omega}_s^5+A_2\bar{\Omega}_s^4-iA_3\bar{\Omega}_s^3-A_4\bar{\Omega}_s^2+iA_5\bar{\Omega}_s+A_6 = 0 \qquad (2.22)$$

Equating real and imaginary parts leads to:

$$-A_0\bar{\Omega}_s^6+A_2\bar{\Omega}_s^4-A_4\bar{\Omega}_s^2+A_6 = 0$$

$$A_1\bar{\Omega}_s^5-A_3\bar{\Omega}_s^3+A_5\bar{\Omega}_s = 0$$

solving the latter, we obtain:

$$\bar{\Omega}_s^2 = \frac{A_3 \pm (A_3^2 - 4A_1A_5)^{1/2}}{2A_1} \qquad (2.23)$$

which after some manipulation (see Appendix 1), yields solutions:

$$\bar{\Omega}_s^2 = \begin{matrix}\omega_1^2 \\ \omega_s^2\end{matrix} \qquad (2.24)$$

and $$\bar{\Omega}_s^2 = \nu_s f(\epsilon_s, \nu_1) \qquad (2.25)$$

Solution (2.24) is clearly a resonance solution, and corresponds to large vibrations occurring when twice the critical speed of the shaft is reached, and for which this type of linearized analysis is invalid. (2.25) is the appropriate solution for small vibrations. From (2.21), at the stability threshold:

$$\nu_s = \kappa_1(\epsilon_s)\{\kappa_2(\epsilon_s)+\nu_1\} \qquad (2.26)$$

Substituting (2.26) into (2.25), we obtain (see Appendix 1 for details):

$$\bar{\Omega}_s^2 = \kappa_1(\epsilon_s)$$

i.e. the critical frequency of small vibrations is independent of the shaft stiffness.

If we replace κ_1 by $\bar{\Omega}_s^2$ in (2.26), we find that for a flexible shaft ν_s is given by:

$$\nu_s = \nu_{s0}+\bar{\Omega}_s^2\nu_1 \qquad (2.27)$$

where ν_{s0} is the corresponding threshold value for a rigid shaft. In the case of the rigid shaft:

$$k \to \infty \quad ; \quad \omega_1 \to \infty \quad ; \quad \nu_1 \to 0$$

in this case (2.27) becomes:

$$\nu_s = \nu_{s0}$$

Hence the results for the rigid and flexible shafts are consistent.

n.b. Since deriving the expression (2.27) it has come to the author's attention that an equivalent result is stated by Allaire (1980). However, it is the author's opinion that the expression given here shows more clearly the relationship between the rigid and flexible cases.

We are now in a position to apply the linearised stability analysis to the various bearing models described in Section 2.1. It should be pointed out that since the algebra involved in deriving the hydrodynamic forces for these models can be found throughout the literature of the subject, it has not been

considered necessary to reproduce it in detail here, other than when it is of particular interest.

For the purposes of a comparison of these results with those produced by other techniques, it may be necessary to convert the values of the stability parameter ν to the nondimensional rotor speed $\bar{\omega}$. In fact, $\tilde{\omega}$ is used in the nonlinear part of this research, since it seemed more appropriate to a dynamic study of the behaviour at different speeds. The parameters are related by:

$$\nu = \frac{1}{\bar{\omega}^2}$$

2.4 A long bearing operating with an oscillating half film

In this model the fluid film extends from the line of maximum film thickness ($\theta=0$), to the line of minimum film thickness ($\theta=\pi$) in the converging half of the bearing. A cavity is assumed to exist in the diverging half (see Figure 2.7). The pressure in this cavity is assumed to be ambient, therefore it makes no contribution to the hydrodynamic force exerted on the shaft. It is important to point out, for comparison with other models, that the position of the cavity remains fixed relative to the shaft and not to the bush. As the shaft vibrates about its equilibrium position, the fluid film also vibrates in such a way that the extent of the lubricant is constantly between ($\theta=0$) and ($\theta=\pi$).

The appropriate boundary conditions are:

$$p(0) = p(\pi) = 0$$

Integrating (1.12) we obtain:

$$\frac{c^2}{6\mu R^2}\frac{dp}{d\theta} = \frac{\epsilon(\omega-2\dot{\varphi})(\cos\theta+C_1)}{(1+\epsilon\cos\varphi)^3} + \frac{2\dot{\epsilon}\sin\theta}{(1+\epsilon\cos\theta)^3}$$

$$\frac{c^2 p}{6\mu R^2} = \epsilon(\omega-2\dot{\varphi})\int\frac{(\cos\theta+C_1)d\theta}{(1+\epsilon\cos\theta)^3} + 2\dot{\epsilon}\int\frac{\sin\theta d\theta}{(1+\epsilon\cos\theta)^3} + C_2$$

The constants C_1, C_2 can be eliminated by using the above boundary conditions. The integrals can be performed by means of the Sommerfeld substitution (see Appendix 2), and we obtain the pressure distribution:

$$\frac{c^2 p}{6\mu R^2} = \frac{\epsilon(\omega-2\dot{\varphi})(2+\epsilon\sin\theta)\sin\theta}{(2+\epsilon^2)(1+\epsilon\cos\theta)^3}$$

$$+\dot{\epsilon}\left[4\frac{\sin\theta}{\pi}\left[\frac{(4-\epsilon^2)+3\epsilon\cos\theta}{(1-\epsilon^2)^{3/2}(2+\epsilon^2)v^2}\right] - \frac{4\cos^{-1}u}{\pi(1-\epsilon)^2} + \frac{1}{\epsilon}\left[\frac{1}{v^2} - \frac{1}{(1+\epsilon)^2}\right]\right]$$

$$u = \frac{\epsilon+\cos\theta}{1+\epsilon\cos\theta} \quad ; \quad v = 1+\epsilon\cos\theta$$

$\theta' = \theta$ measured from perturbed position

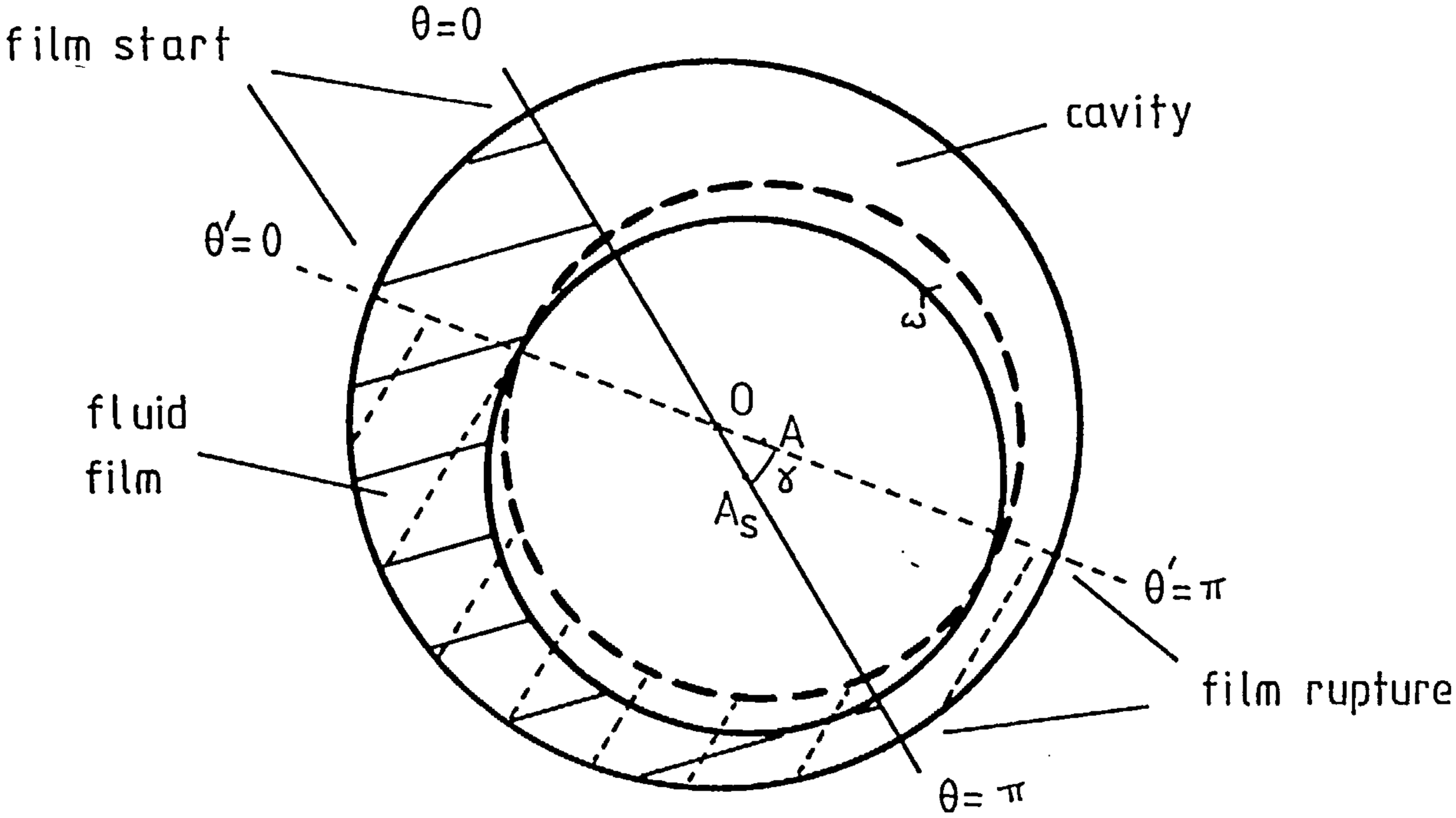

Figure 2.7 Long bearing - oscillating half film

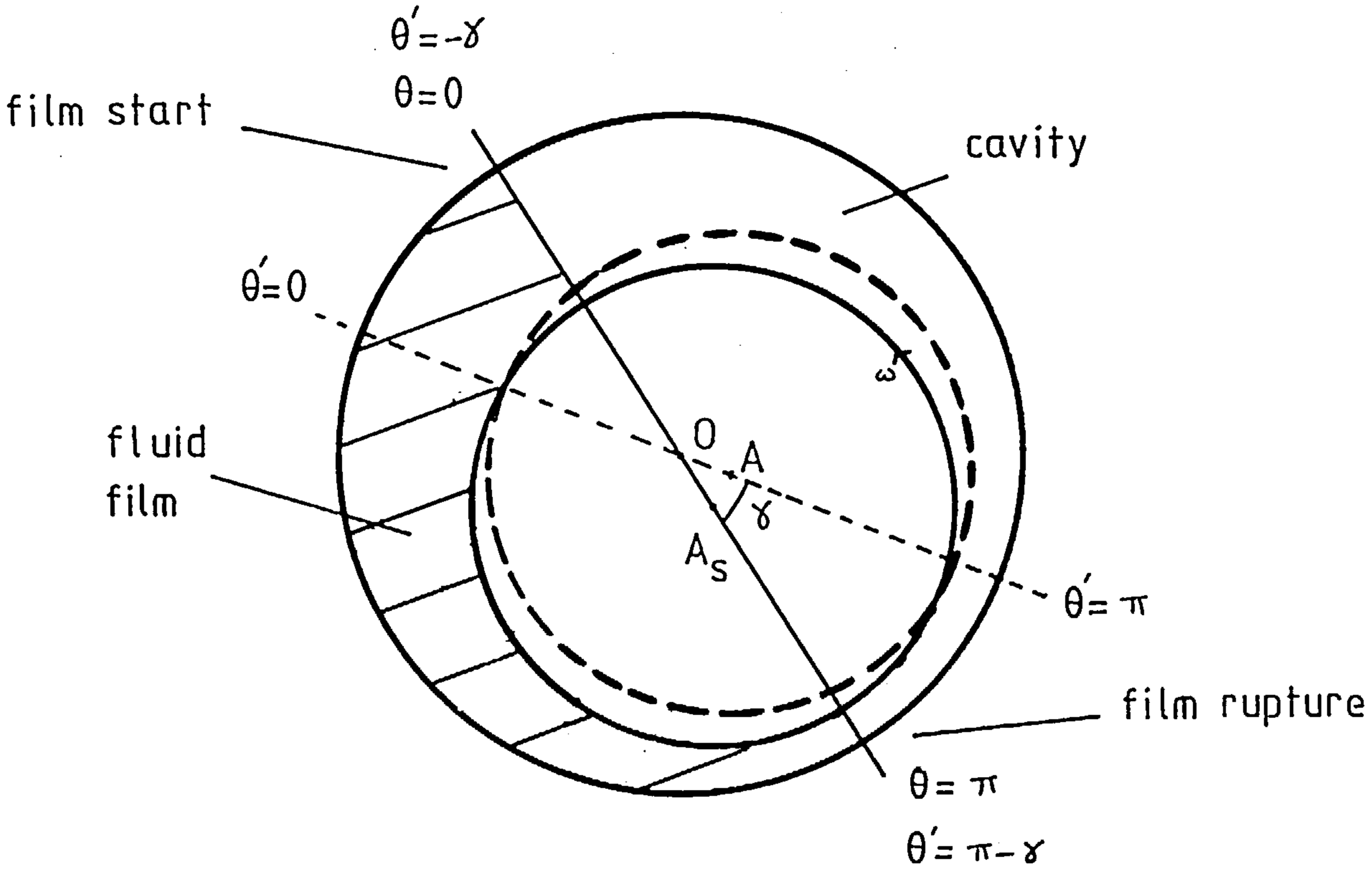

Figure 2.8 Long bearing - static half film

Evaluating the hydrodynamic force components by means of (1.15) we obtain:

$$-\frac{c^2 F_r}{LR^3\mu\omega} = \bar{F}_r = \frac{12\epsilon^2(1-2\varphi')}{(2+\epsilon^2)(1-\epsilon^2)} + \frac{6\{\pi^2(2+\epsilon^2)-16\}\epsilon'}{\pi(2+\epsilon^2)(1-\epsilon^2)^{3/2}} \qquad (2.28)$$

$$\frac{c^2 F_t}{LR^3\mu\omega} = \bar{F}_t = \frac{6\pi\epsilon(1-2\varphi')}{(1-\epsilon^2)^{1/2}(2+\epsilon^2)} + \frac{24\epsilon\epsilon'}{(1-\epsilon^2)(2+\epsilon^2)} \qquad (2.29)$$

Expressions (2.28) and (2.29) can be linearised by means of (2.7) and (2.8) to give:

$$\bar{F}_r = -\frac{12\epsilon_s^2}{pq} - \frac{24\epsilon_s(2+\epsilon_s^4)}{p^2q^2}\delta + \frac{24\epsilon_s^2}{pq}\gamma' - \frac{12\delta'}{q^{3/2}}\left\{\frac{\pi}{2} - \frac{8}{\pi p}\right\} \qquad (2.30)$$

$$\bar{F}_t = \frac{6\pi\epsilon_s}{pq^{1/2}} + \frac{6\pi(2-\epsilon_s^2+2\epsilon_s^4)\delta}{p^2q^{3/2}} - \frac{12\epsilon_s\pi\gamma'}{pq} + \frac{24\epsilon_s\delta'}{pq} \qquad (2.31)$$

$$[\ p = 2+\epsilon_s^2 \quad ; \quad q = 1-\epsilon_s^2\ ]$$

Given a bearing load F and a rotation speed ω, we can find the equilibrium value of the eccentricity ratio. It is possible to find the steady state value of the attitude angle and the load capacity by the use of (1.20) and (1.21). This can be achieved by putting $\epsilon'=0, \varphi'=0$ in (2.28) and (2.29), or $\delta'=0, \gamma'=0$ in (2.30) and (2.31).

This leads to:

$$\bar{F} = 6\epsilon_s\frac{\{\pi^2(1-\epsilon_s^2)+4\epsilon_s^2\}^{1/2}}{pq}$$

$$\tan\varphi_s = \frac{\pi(1-\epsilon_s^2)^{1/2}}{2\epsilon_s}$$

It is now possible to analyse the stability of this equilibrium position since (2.30) and (2.31) are in the required form of (2.14) and (2.15). By substituting the terms in A_r, A_t etc. into (2.21) a stability borderline can be established for various values of the shaft stiffness.

2.5 A long bearing operating with a static half film

This model is similar to the previous one in that under steady state conditions it has an oil film of 180° extent in the converging part of the bearing and a cavity in the diverging part. The crucial difference between the two is the behaviour of the oil film when the shaft vibrates about its equilibrium position. In this model the film remains at its equilibrium position (see Figure 2.8) during a vibration of the shaft, so that it extends from $\theta=-\gamma$ to $\theta=\pi-\gamma$ under dynamic conditions (note that $\gamma/\pi \ll 1$). At equilibrium, however, it fills the space $0\leqslant\theta\leqslant\pi$.

Since the extent of the fluid film in equilibrium is the same as in the oscillating half film model, the equilibrium properties of the two models (i.e. attitude angle, load capacity, etc.) are identical. However, it will be seen in Section 2.10 that the apparently insignificant difference in the behaviour of the fluid film under dynamic conditions has a great effect on the stability characteristics.

The pressure distribution can be found by integrating (1.12) with the new boundary conditions:

$$p(-\gamma) = p(\pi-\gamma) = 0 \quad ; \quad \gamma/\pi \ll 1$$

This enables the force components to be determined by means of (1.15). The hydrodynamic force components are:

$$\frac{-c^2F_r}{LR^3\mu\omega} = \frac{12\epsilon(1-2\dot{\varphi})}{(1-\epsilon^2)(2+\epsilon^2)} + \frac{6\{\pi^2(2+\epsilon^2)-16\}\dot{\epsilon}}{\pi(1-\epsilon^2)^{3/2}(2+\epsilon^2)} - \frac{96\epsilon\gamma}{\pi(2+\epsilon^2)(1-\epsilon^2)^{3/2}}$$

$$\frac{-c^2F_t}{LR^3\mu\omega} = \frac{6\pi\epsilon(1-2\dot{\varphi})}{(1-\epsilon^2)^{3/2}(2+\epsilon^2)} + \frac{24\epsilon\dot{\epsilon}}{(2+\epsilon^2)(1-\epsilon^2)} - \frac{12\epsilon^4\gamma}{(2+\epsilon^2)(1-\epsilon^2)}$$

These expressions are identical to those for the oscillating film model with

the addition of the γ terms which arise since the pressure distribution is no longer radially symmetric with respect to the shaft position. Similarly the linearised force expressions include terms involving γ.

$$\bar{F}_r = -\frac{12\epsilon_s^2}{pq} - \frac{24\epsilon_s(2+\epsilon_s^4)\delta}{p^2q^2} + \frac{24\epsilon_s^2\dot{\gamma}}{pq} - \frac{12\dot{\delta}}{q^{3/2}}\left[\frac{\pi-8}{2}\frac{}{\pi p}\right] + \frac{96\epsilon_s\gamma}{\pi p^2 q^{3/2}} \quad \ldots\ldots(2.32)$$

$$\bar{F}_t = \frac{6\pi\epsilon_s}{q^{1/2}p} + \frac{6\pi(2-\epsilon_s^2+2\epsilon_s^4)\delta}{p^2q^{3/2}} - \frac{12\epsilon_s\pi\dot{\gamma}}{q^{1/2}p} + \frac{24\epsilon_s\dot{\delta}}{pq} - \frac{12\epsilon_s^4\gamma}{p^2q} \quad (2.33)$$

The equilbrium values of load capacity and attitude angle can be found as before. Since (2.32) and (2.33) are in the form of (2.14) and (2.15) a stability borderline can be found by their substitution into (2.21).

2.6 A long bearing operating with a half Sommerfeld film

In this model, no constraints are placed on the pressure distribution, other than the assumption that the pressure build-up begins at the line of maximum film thickness (θ=0). Equation (1.12) is integrated by means of the Sommerfeld substitution using the boundary conditions:

$$p = 0 \quad ; \quad \theta = 0, 2\pi$$

This is the identical procedure carried out when finding the pressure distribution for a full (uncavitated) film. In this case, however, a cavity is assumed to exist wherever subambient pressures are predicted (see Figure 2.9). On integrating (1.12), we obtain:

$$\frac{c^2p}{6\mu R^2} = \frac{\epsilon(\omega-2\dot{\varphi})(2+\epsilon\cos\theta)\sin\theta}{(2+\epsilon^2)(1+\epsilon\cos\theta)^2} + \frac{\dot{\epsilon}}{\epsilon}\left\{\frac{1}{(1+\epsilon\cos\theta)^2} - \frac{1}{(1+\epsilon)^2}\right\} \quad (2.34)$$

$$\rightarrow p = 0 \quad ; \quad \theta = 0, 2\pi, \pi+\alpha$$

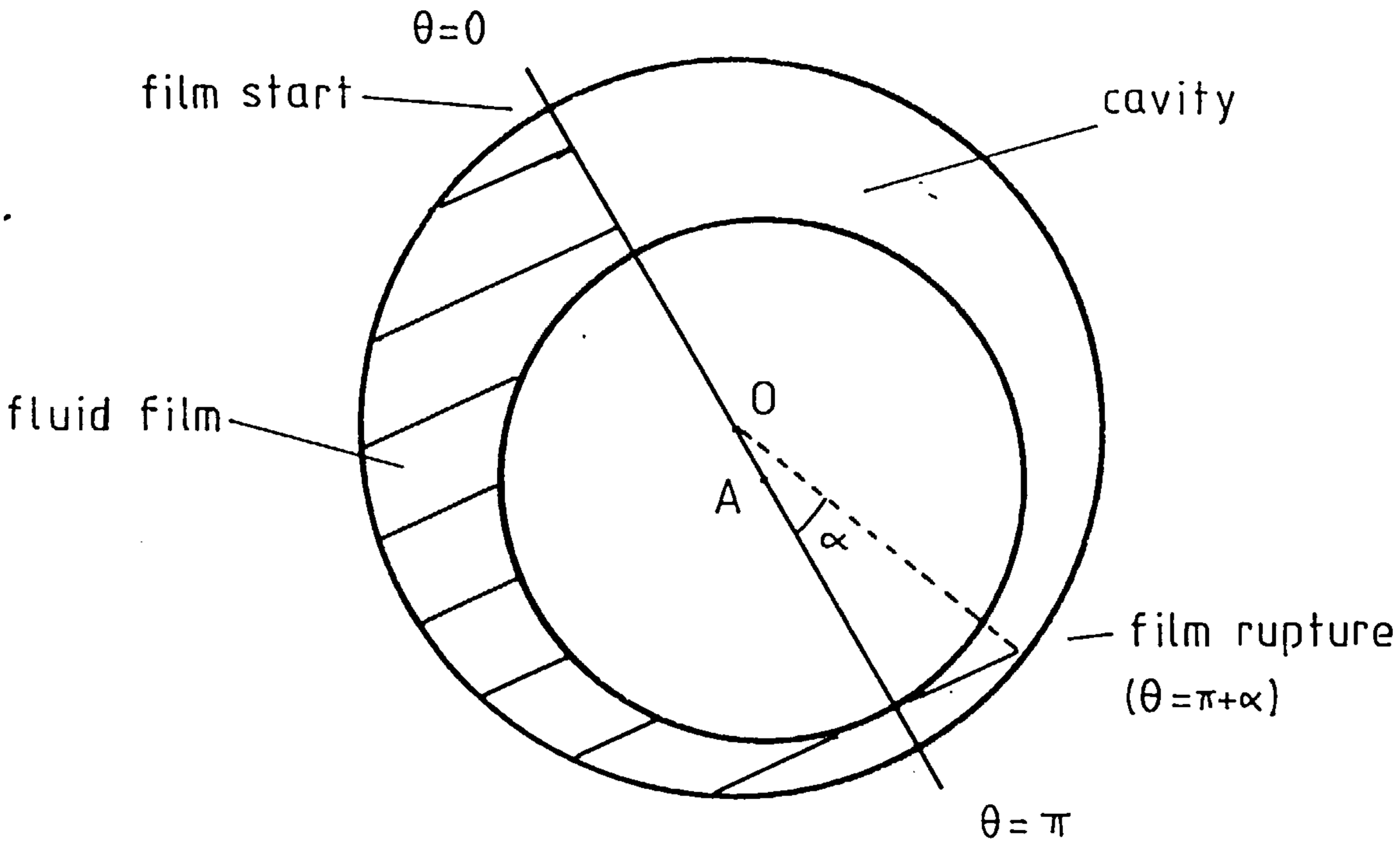

Figure 2.9 Long bearing - Half Sommerfeld film

where α satisfies

$$\frac{-\epsilon(\omega-2\dot{\varphi})(2-\epsilon\cos\alpha)\sin\alpha}{(2+\epsilon^2)(1-\epsilon\cos\alpha)^2} + \frac{\dot{\epsilon}}{\epsilon}\left\{\frac{1}{(1+\epsilon\cos\alpha)^2} - \frac{1}{(1+\epsilon)^2}\right\} = 0 \quad (2.35)$$

We assume a cavity exists (p = 0) in the region $\pi+\alpha<\theta<2\pi$. In the steady state α is zero and hence the equilibrium properties of this model are the same as in the previous two. When considering the full nonlinear motion of the journal, α must be determined numerically from (2.35); however, during a small amplitude vibration of the journal, α is small and can be found from (2.35) by neglecting second order terms:

$$\alpha = \frac{4(2+\epsilon_s)\dot{\delta}}{\epsilon_s(1+\epsilon_s)^2(2-\epsilon_s)} \quad (2.36)$$

The linearised force terms can now be found by substituting (2.34) into (1.15) and using (2.36) wherever α occurs. The linearised force components are:

$$\bar{F}_r = -\frac{12\epsilon_s^2}{pq} - \frac{24\epsilon_s(2+\epsilon_s^4)\delta}{p^2q^2} + \frac{24\epsilon_s\dot{\gamma}}{pq} - \frac{6\pi\dot{\delta}}{q^{3/2}}$$

$$\bar{F}_t = \frac{6\epsilon_s\pi}{pq^{1/2}} + \frac{6\pi(2-\epsilon_s^2+2\epsilon_s^4)\delta}{p^2q^{3/2}} - \frac{12\pi\epsilon_s\dot{\gamma}}{pq^{1/2}} + \frac{24(1-\epsilon_s)\dot{\delta}}{q^2}$$

These expressions are very similar to those for the oscillating half film model, only the $\dot{\delta}$ terms differ. However, the stability characteristics for the two models are very different, as we shall see later.

2.7 A long bearing operating with a film satisfying Reynolds' Boundary conditions

In this model the oil film is assumed to begin at the line of maximum film thickness and to end beyond the point of minimum film thickness at the point where both the pressure and pressure gradient are zero. In the first instance, the oil film is assumed to be oscillating, as in the case of Section 2.3, i.e. its position remains fixed relative to the shaft during a vibration (see Figure 2.10). This assumption will be modified later, and in the next section the model will be further refined by the inclusion of oil supply through an axial groove. Therefore, to avoid reproduction of the algebra, the θ_1-term (corresponding to the film start) will be retained in the calculations, although it is zero for this particular model. The algebra for all these models is especially tedious, and has been kept to an absolute minimum here so as not to obscure the main features of the work. Full details of the derivation of the pressure distribution and hydrodynamic forces for this and the following section can be found in the Ph.D. thesis of C.J. Myers (1981).

The Reynolds' boundary conditions for the oscillating film model are:

$$p = 0 \quad ; \quad \theta = 0$$

$$p = \frac{dp}{d\theta} = 0 \quad ; \quad \theta = \theta_2$$

Integrating (1.12) we obtain:

$$\frac{dp}{d\theta} = \frac{6\mu R^2}{c^2}\left\{\frac{\epsilon(\omega-2\dot{\varphi})\cos\theta+2\dot{\epsilon}\sin\theta+C_1}{(1+\epsilon\cos\theta)^3}\right\}$$

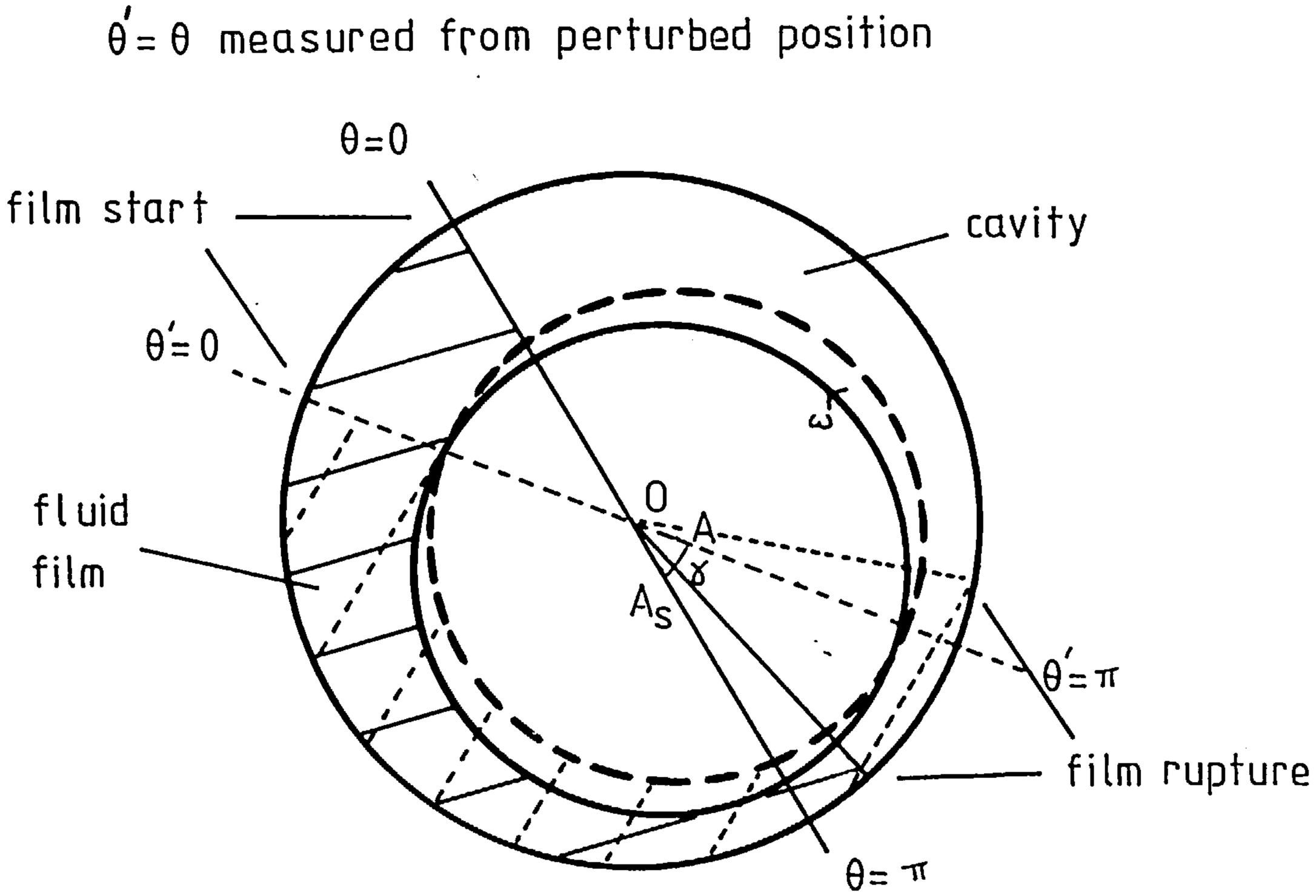

Figure 2.10a Reynolds' boundary conditions – oscillating film

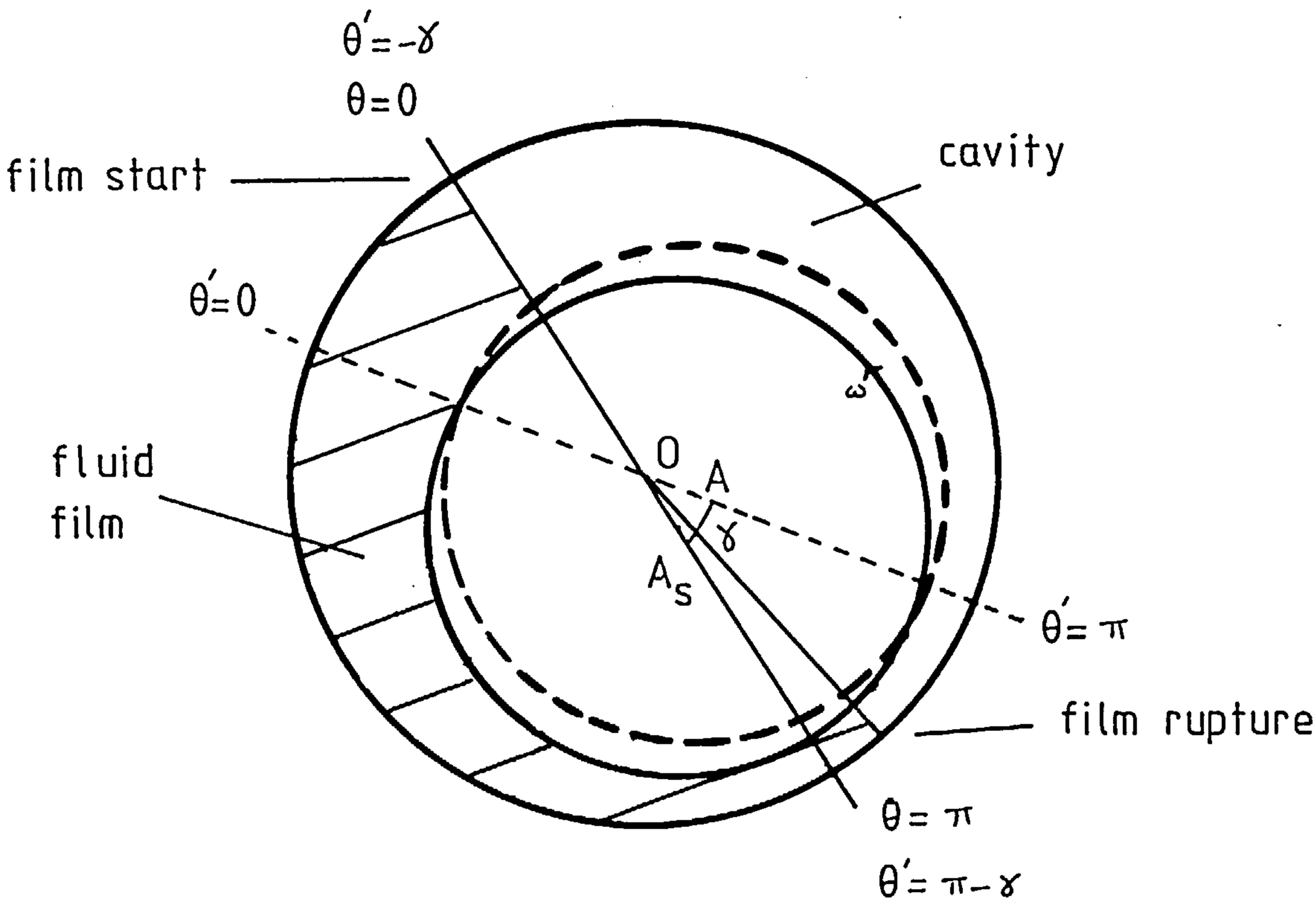

Figure 2.10b Reynolds' boundary conditions – static film

Since:

$$\frac{dp}{d\theta} = 0 \text{ at } \theta = \theta_2$$

this implies that:

$$\frac{dp}{d\theta} = \frac{6\mu R^2}{c^2}\left[\frac{\epsilon(\omega-2\dot{\varphi})(\cos\theta-\cos\theta_2)+2\dot{\epsilon}(\sin\theta-\sin\theta_2)}{(1+\epsilon\cos\theta)^3} \right]$$

This equation can be solved by the Sommerfeld substitution, and θ_2 can be found numerically by solving $p(\theta_2)=0$. We have:

$$\frac{c^2 p}{6\mu R^2} = \frac{\epsilon(\omega-2\dot{\varphi})F(\epsilon,\psi,\psi_1,\psi_2)}{4(1-\epsilon^2)^{3/2}(1-\epsilon\cos\psi_2)} + \frac{2\dot{\epsilon}Q(\epsilon,\psi,\psi_1,\psi_2)}{4(1-\epsilon^2)^2(1-\epsilon\cos\psi_2)} \qquad (2.37)$$

The variables ψ, ψ_1 and ψ_2 are the Sommerfeld angles corresponding to θ, θ_1 and θ_2 respectively. As previously mentioned, θ_1 and hence ψ_1 are zero for the oscillating case, but they are retained here so as to make the application of the method to the static and axial grove cases easier. The steady state value of ψ_2 can be found numerically by solving:

$$F(\epsilon_s,\psi_{2s},\psi_{1s},\psi_{2s}) = 0 \qquad (2.38)$$

We can now find the steady state pressure distribution:

$$\frac{c^2 p}{6\mu R^2\omega} = \frac{\epsilon_s F(\epsilon_s,\psi,\psi_{1s},\psi_{2s})}{4(1-\epsilon_s^2)^{3/2}(1-\epsilon\cos\psi_{2s})}$$

The hydrodynamic force components can be found by substituting (2.37) into (1.15) and after linearisation they are of the form:

$$\bar{F}_r = -A_r - B_r\delta + C_r\dot{\gamma}' - D_r\dot{\delta}' \qquad (2.39)$$

$$\bar{F}_t = A_t + B_t\delta - C_t\dot{\gamma}' + D_t\dot{\delta}' \qquad (2.40)$$

$$A_r = A_r(\epsilon_s,\psi_{1s},\psi_{2s}) \text{ etc.}$$

These expressions are of the required form for the stability analysis, since they are functions of ϵ_s. The variable ψ_{1s} is specified by the type of Reynolds' model chosen; in this case it is zero, but for the axial groove model ψ_{1s} is a function of ϵ_s. In both cases ψ_{2s} is dependent on ϵ_s from (2.38).

The model with Reynolds' boundary conditions and static fluid film is partly analogous to the static half film model discussed in Section 2.5. It is assumed that lubricant is supplied to the bearing through an axial groove positioned at the line of maximum film thickness, i.e. at an angle $\pi-\varphi_s$ before the load-line (see Figure 2.11). During a vibration of the shaft, the beginning of the fluid film remains fixed relative to the bush. In equilibrium, the oscillating and static versions of the Reynolds' boundary conditions are identical, but they have very different stability characteristics.

2.8 A long bearing operating with the lubricant supplied through an axial groove

Of all the long bearing models considered, this is the most refined, incorporating an axial groove (a groove aligned with the axis of the bearing), thus removing the need to assume that the pressure becomes superambient at the line of maximum film thickness. We assume that the pressure build-up begins at the groove and continues until $p=dp/d\theta=0$. The groove is fixed in space, and its position is measured with respect to an imaginary line through the centre of the bearing, parallel to the load on the journal. The angle between the line of centres and the groove is denoted by β (see Figure 2.11). In all the previous models examined, the pressure build-up has begun at the line of maximum film thickness ($\theta=0$), but here it

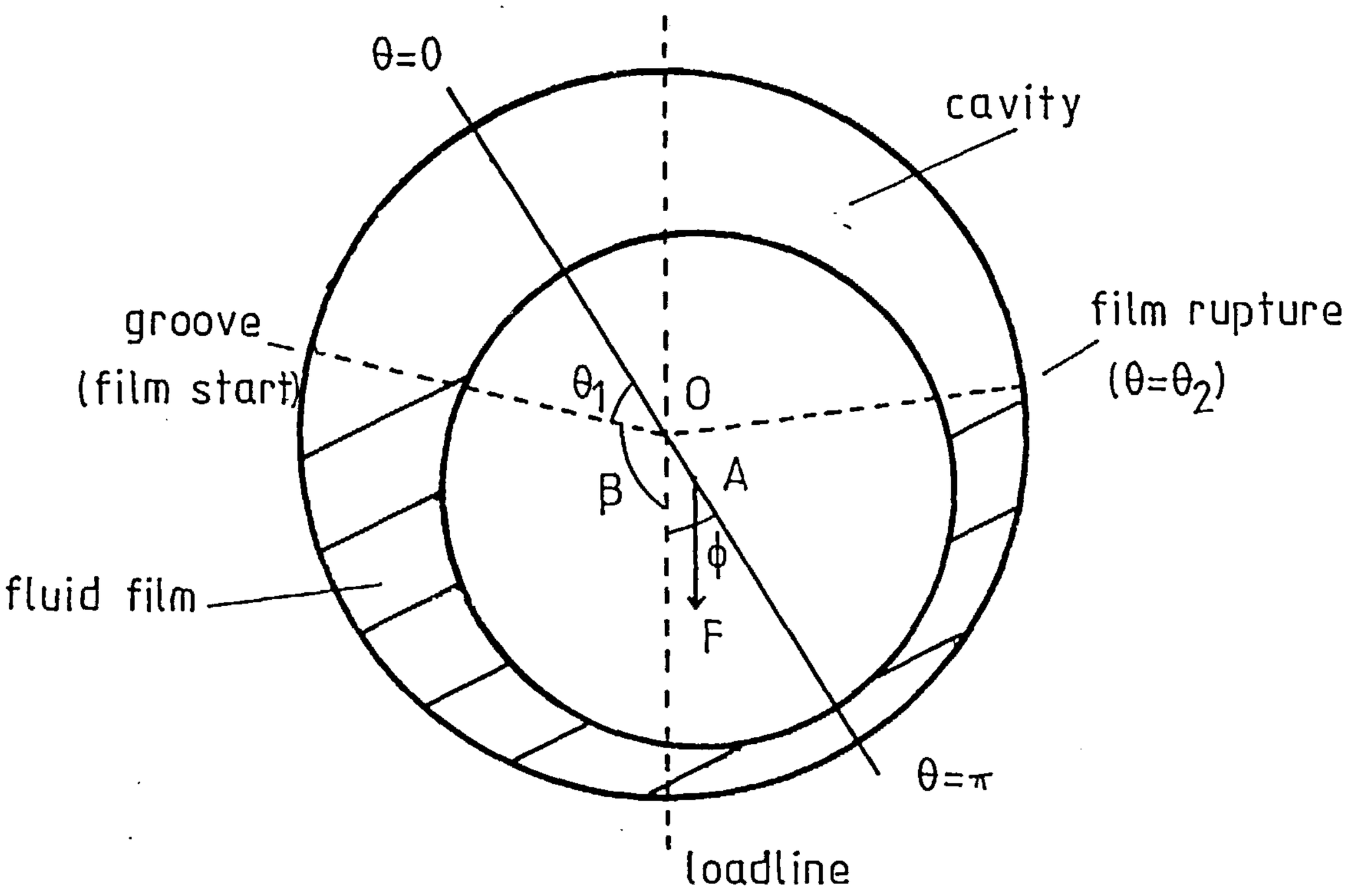

Figure 2.11 The axial groove bearing

is necessary to locate the groove i.e. to find θ_{1s}, for every equilibrium position. This is done numerically using the relationship:

$$\theta_{1s} + \beta + \varphi_s = \pi$$

During a vibration, θ_1 does not remain constant, but changes from θ_1 to $\theta_1-\gamma$. If the model is to be an accurate description of the lubricant behaviour, this 'γ-variation' must be taken into account. Interestingly, Lundholm (1971) omitted to include this variation in his work on axial groove bearings; once he became aware of the error, he produced an addendum to his results (Lundholm (1973)).

The hydrodynamic force components are found as in the previous section, noting that $\Psi_1 \neq 0$. Linearisation yields:

$$\bar{F}_r = -A_r(\epsilon_s,\beta)-B_r(\epsilon_s,\beta)\delta+C_r(\epsilon_s,\beta)\dot{\gamma}-D_r(\epsilon_s,\beta)\dot{\delta}+E_r(\epsilon_s,\beta)\gamma \quad (2.41)$$

$$\bar{F}_t = A_t(\epsilon_s,\beta)+B_t(\epsilon_s,\beta)\delta-C_t(\epsilon_s,\beta)\gamma+D_t(\epsilon_s,\beta)\dot{\delta}+E_t(\epsilon_s,\beta)\gamma \quad (2.42)$$

The expressions $A_r...D_t$ in (2.41) and (2.42) are identical to those in (2.39) and (2.40). A full stability analysis can be carried out for any particular groove position, provided that the groove is not more than 180° before the load-line. It will be seen in Section 2.10 that the groove position has a significant effect upon the stability characteristics of the bearing. If $\beta>180°$ the groove would be positioned well into the diverging region, where we would normally expect a cavity to be found; in this case, the numerical scheme to find θ_{1s} fails to converge. It is possible to construct a mathematical model with $\beta>180°$, in which the fluid film terminates at the axial groove, but since this configuration is fundamentally different from the other lubrication models examined in this thesis, it has not been considered here; indeed, as such it is of no practical interest.

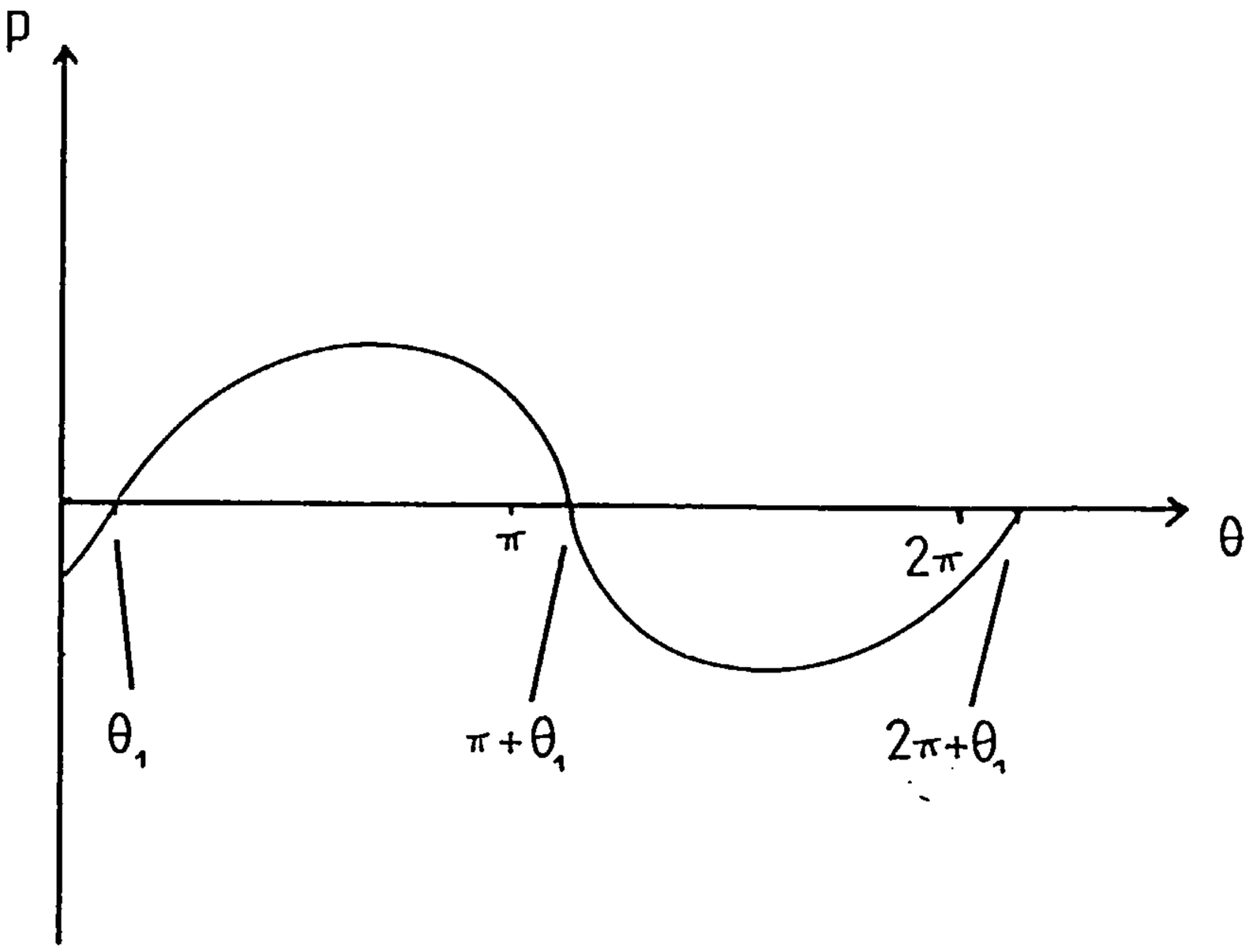

Figure 2.12 Pressure distribution for the short bearing

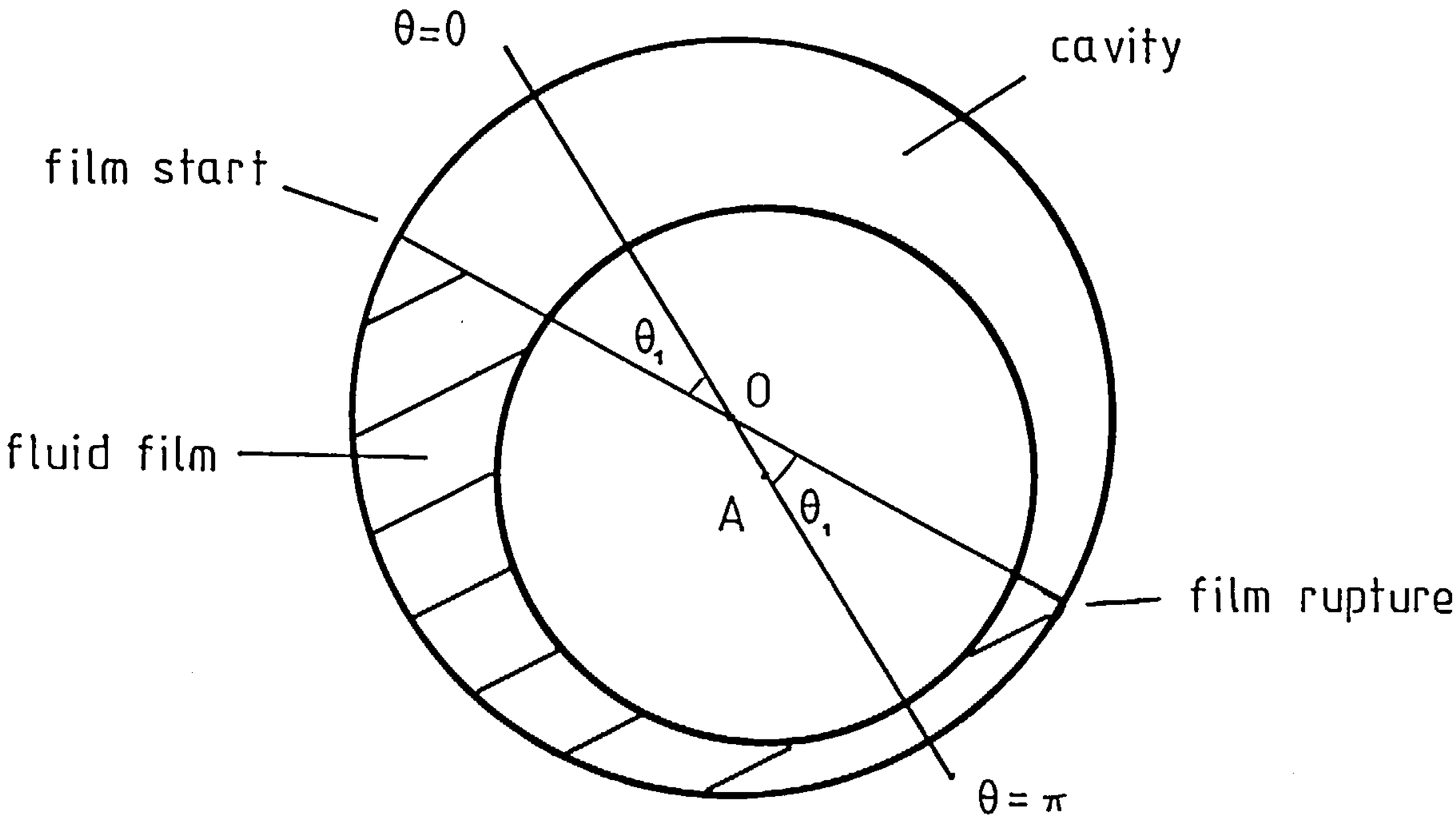

Figure 2.13 Short bearing - half film

2.9 A short bearing operating with a half film

The final model to be examined is a short bearing operating with a half (or π) film. For the short bearing, the assumptions made in simplifying Reynolds' equation do not allow the arbitrary imposition of boundary conditions as in the long bearing models previously considered. In this case, we must impose the conditions:

$$p = 0 \quad ; \quad z = 0, L$$

i.e. the pressure must be ambient at the bearing ends, since they are open to the atmosphere. This leads to the pressure distribution (integrating (1.13)):

$$\frac{c^2 p}{\mu L^2} = \frac{3z(z-L)}{L^2}\left\{ \frac{-\epsilon(\omega-2\dot{\varphi})\sin\theta+2\dot{\epsilon}\cos\theta}{(1+\epsilon\cos\theta)^3} \right\} \tag{2.43}$$

which implies:

$$p = 0 \text{ at } \theta = \theta_1, \pi+\theta_1, 2\pi+\theta_1$$
$$\tan\theta_1 = \frac{2\dot{\epsilon}}{\epsilon(\omega-2\dot{\varphi})} \tag{2.44}$$

Thus the imposition of boundary conditions at the bearing ends completely determines the nature of the circumferential pressure distribution. In equilibrium, the pressure is identically zero at the lines of maximum and minimum film thickness, but under dynamic conditions the zero points depend on the position and velocity of the shaft through (2.44). A typical pressure distribution is shown in Figure 2.12.

Since the values of θ giving zero pressure are determined via (2.44), we are faced with two possible physical models. The full film model has been shown to be inherently unstable (Holmes (1963)), and will, therefore be ignored here. The half film model, in which a cavity is assumed to exist in the

region $\theta_1 < \theta < 2\pi+\theta_1$ will be considered in detail (see Figure 2.13).

The hydrodynamic forces are found by integrating the pressure distribution (2.43) in (1.16) from θ_1 to $\pi+\theta_1$. A direct integration is possible (see Chapter 4), but for the linear analysis adopted here, use of the Sommerfeld substitution is more convenient.

In a small vibration of the shaft about its equilibrium position, ϵ and φ are small quantities, and so θ_1 will also be small, since (2.44) reduces to:

$$\theta_1 = \tan^{-1}\left[\frac{2\dot{\delta}}{\epsilon_s\omega}\right] = \tan^{-1}\left[\frac{2\delta'}{\epsilon_s}\right]$$

In practice, all occurrences of θ_1 in the force integrals cancel out, or are of second order, since in equilibrium, or to first order for small vibrations, the pressure distribution is antisymmetric about $\theta=\pi+\theta_1$. Consequently, when evaluating the linearised fluid film forces, the same result can be obtained by integrating from 0 to π. Clearly this approach cannot be adopted in a full nonlinear analysis of the motion, since the second order terms would not be trivial in this case. The linearised forces are:

$$\bar{F}_r = -\frac{\epsilon_s^2}{q} - \frac{2\epsilon_s(1+\epsilon_s^2)\delta}{q^3} + \frac{2\epsilon_s^2\gamma'}{q^2} - \frac{\pi(1+2\epsilon_s^2)\dot{\delta}}{2q^{5/2}}$$

$$\bar{F}_t = \frac{\pi\epsilon_s}{4q^{3/2}} + \frac{\pi(1+2\epsilon_s^2)\delta}{4q^{5/2}} - \frac{\pi\gamma'}{2q^{3/2}} + \frac{2\epsilon_s\dot{\delta}}{q^2}$$

Note that for the short bearing, $\bar{F}_r$ and $\bar{F}_t$ are defined as:

$$\bar{F}_r = \frac{F_r}{\overline{FS}_m} \quad ; \quad \bar{F}_t = \frac{F_t}{\overline{FS}_m}$$

2.10 Results and discussion

A full stability analysis has been carried out by the author for all the models discussed in Sections 2.4-2.9, but since this work has generated a very large amount of data, only the most important results have been included in this thesis. Figures 2.14-2.19 display the essential features.

Figure 2.14 shows the stability borderline for the case of the rigid shaft, for all those models operating without an axial groove. If a bearing is operating in a region of parameter space below the relevant borderline, then the equilibrium position will be unstable (i.e. at least one of the roots of the characteristic equation will have a positive real part). If it is operating above the stability borderline, then it will be stable. One feature common to all models is the existence of a particular value for the steady state eccentricity ratio ϵ_s^*, above which the bearing is always stable. With the exception of the long bearing static half film model, ϵ_s^* always lies in the range $0.75<\epsilon_s^*<0.85$ (the tendency of journals to become stable when $\epsilon>0.7$ was first observed by Stodola (1925)). The oscillating half film model is by far the least stable, and the half Sommerfeld model displays even greater stability at low eccentricities, with the additional feature of predicted stable behaviour at $\epsilon_s=0$, corresponding to an unloaded, or vertical shaft. The only difference in the hydrodynamic force components in each of these models is the presence of a γ-term in the static half film case, and a slight modification to the δ'-term for the half Sommerfeld boundary conditions.

The most sophisticated model, incorporating Reynolds' boundary conditions, has very similar stability characteristics to the half Sommerfeld film (as seen in Figure 2.14); although the static Reynolds' film is surprisingly less stable than the oscillating version, which is contrary to the results obtained for the half film. The two static film versions do have remarkably

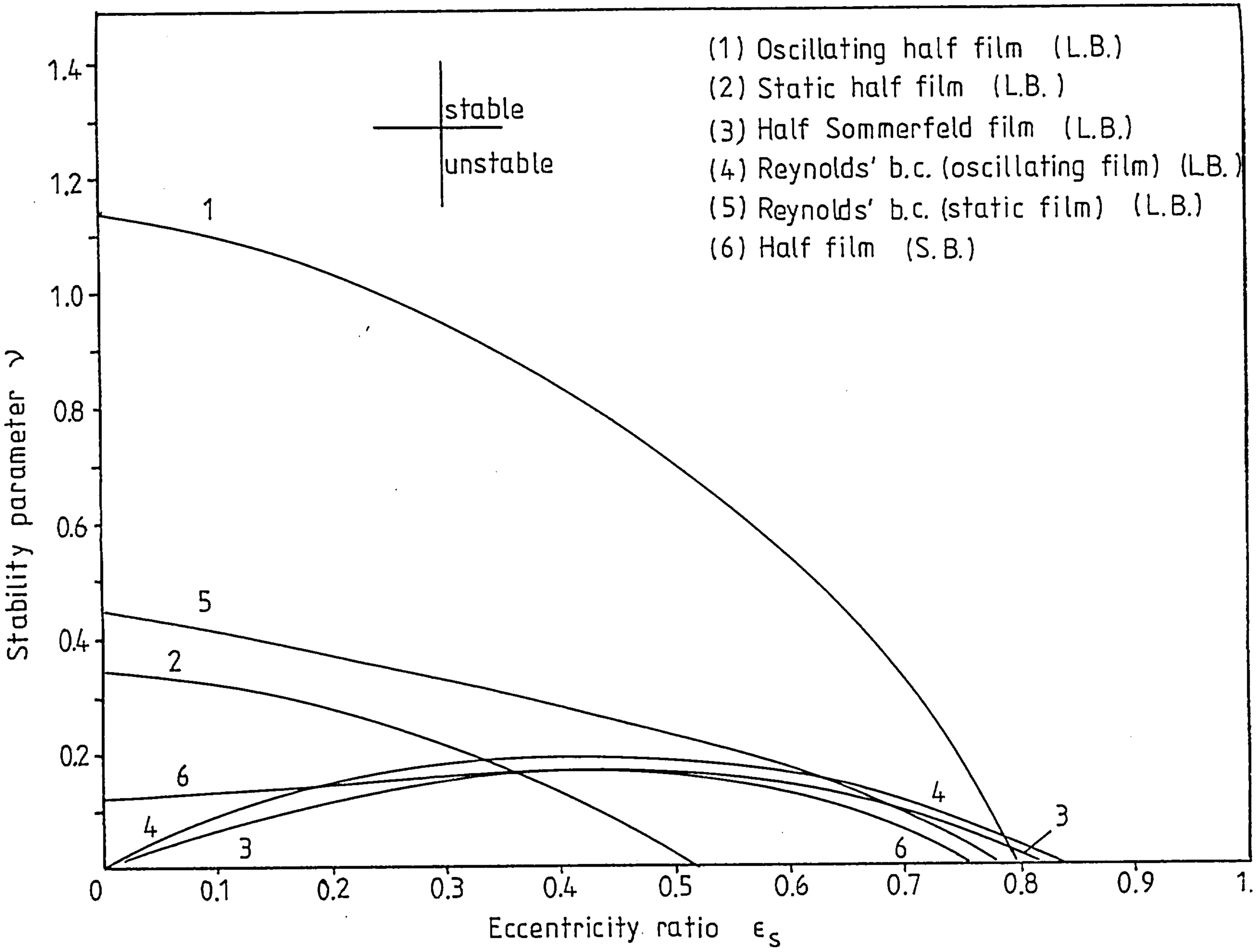

Figure 2.14 Stability borderlines for different cavitation models (rigid shaft)

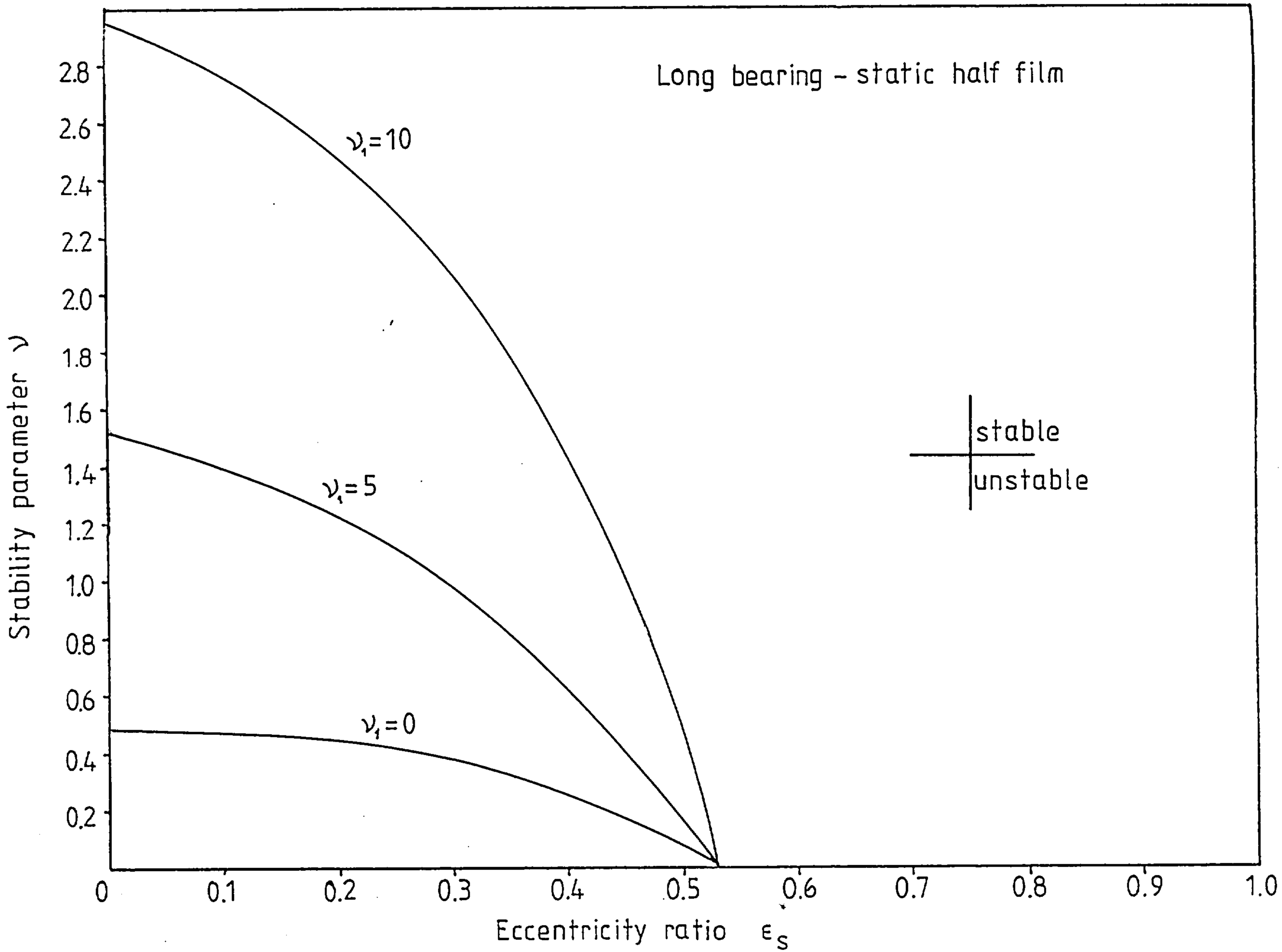

Figure 2.15 The effect of shaft stiffness on the stability borderline

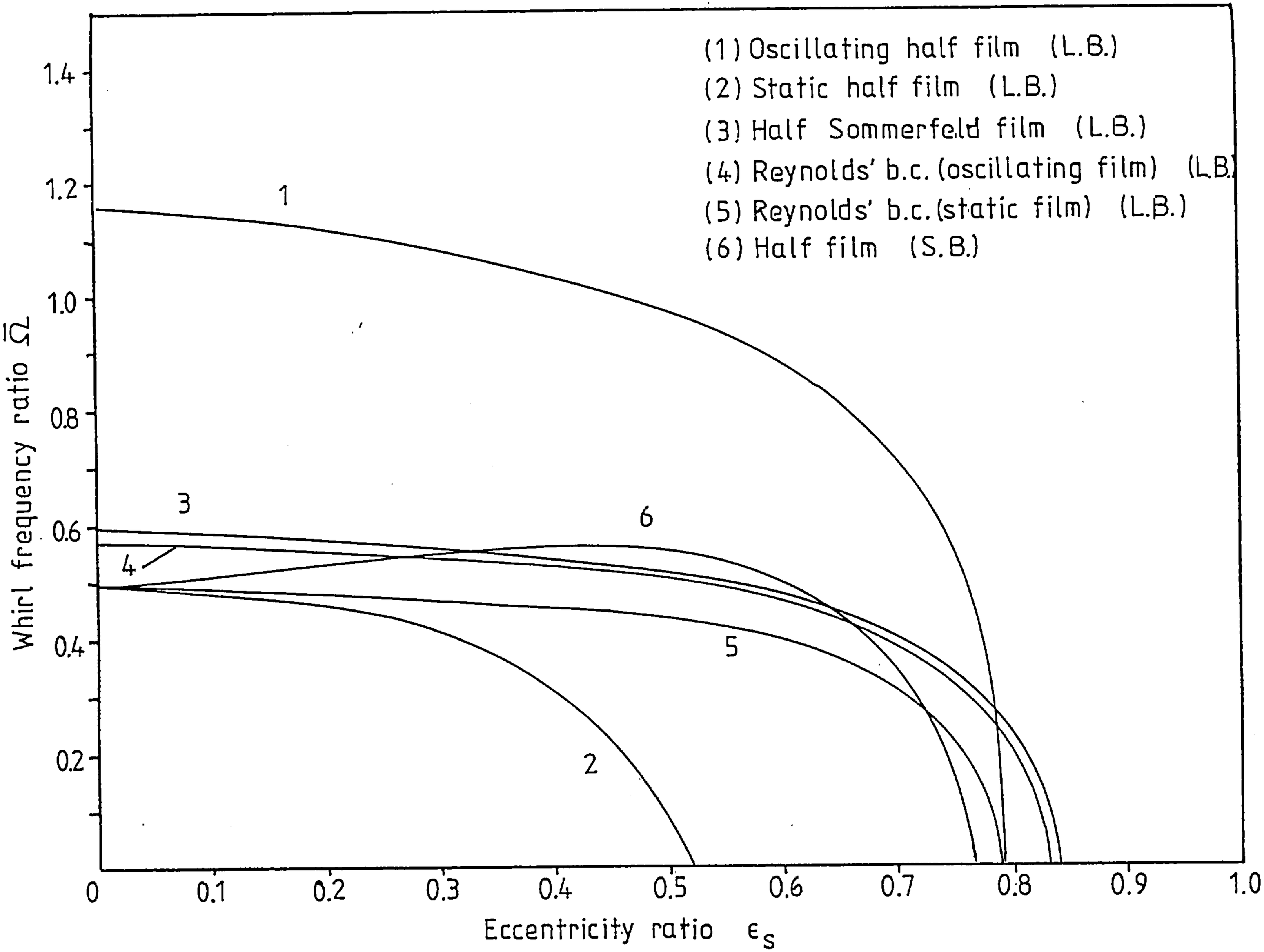

Figure 2.16 Critical frequencies for different cavitation models

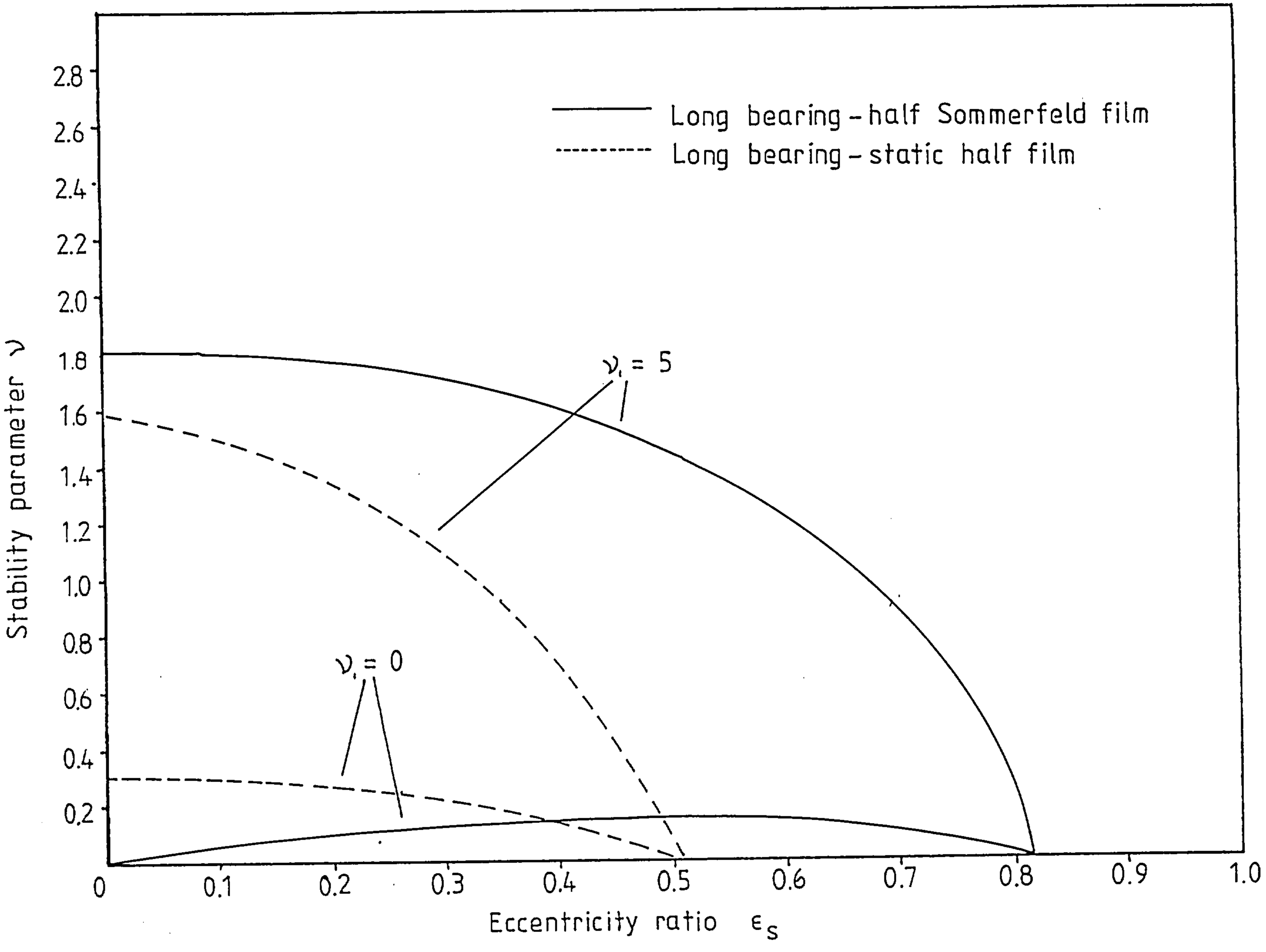

Figure 2.17 The effect of shaft stiffness on different cavitation models

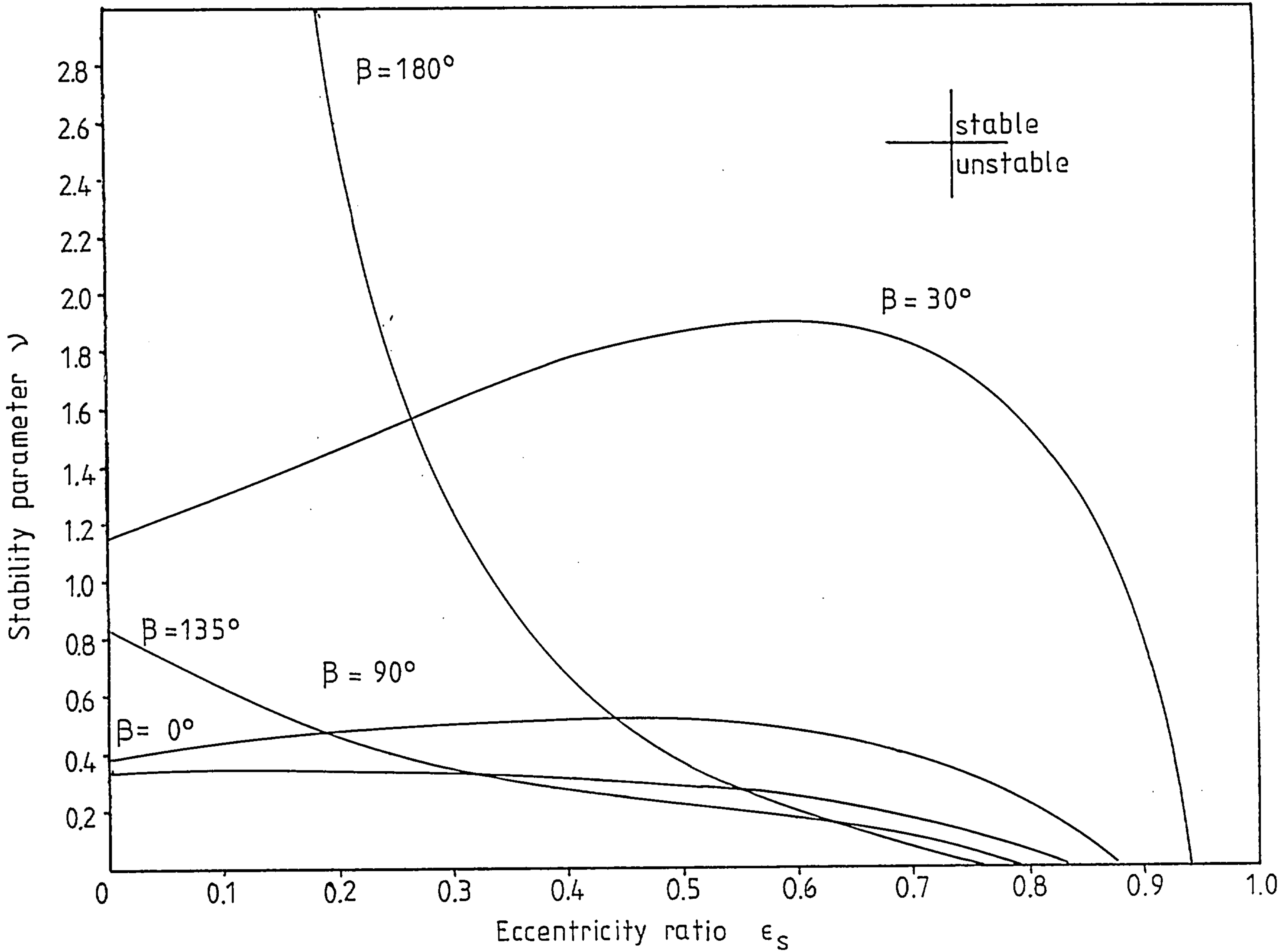

Figure 2.18 Stability borderlines for the axial groove bearing

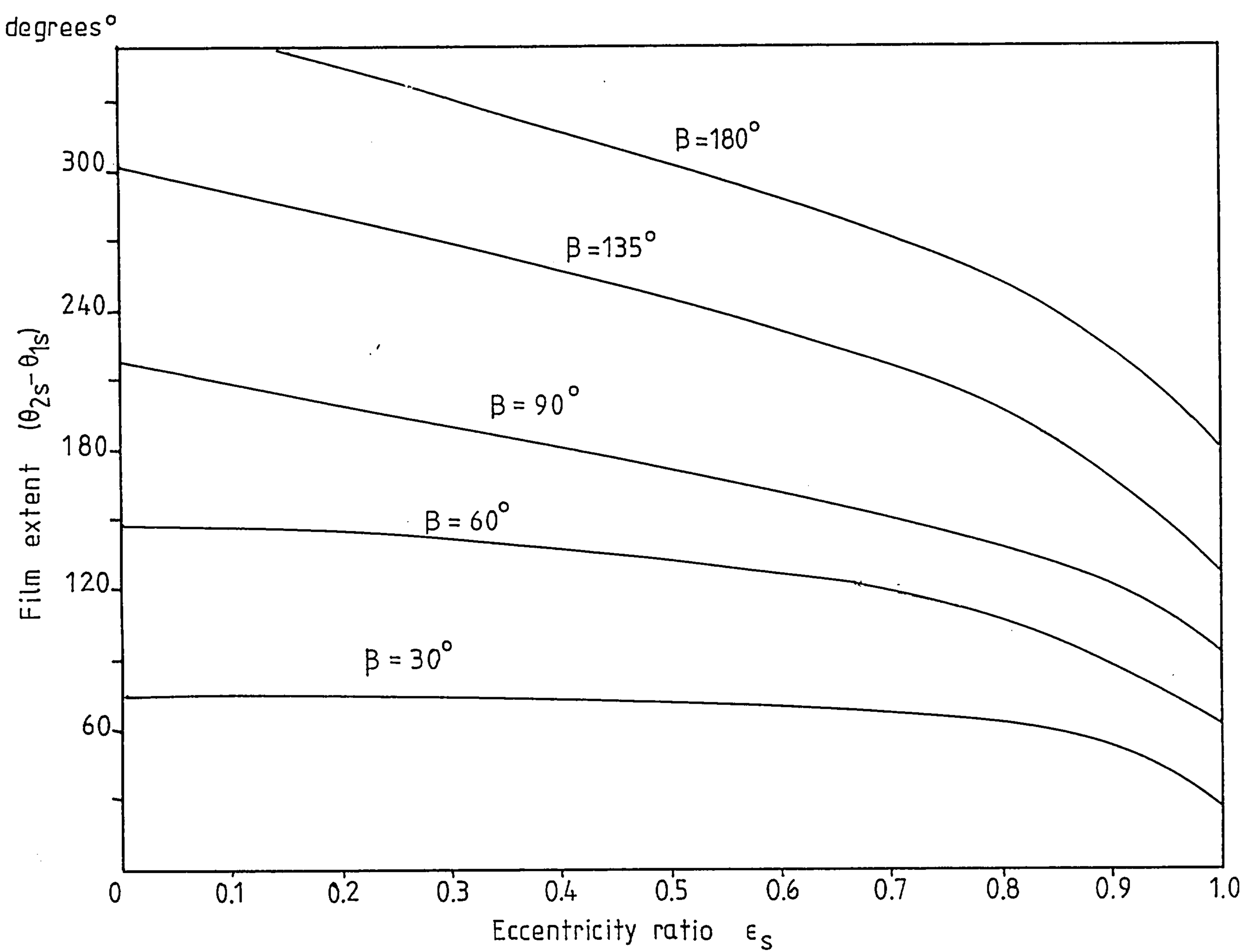

Figure 2.19 Film extent for the axial groove bearing

similar stability borderlines, being generally less stable than the other models (with the exception of the oscillating half film, which as will be discussed later, has features inconsistent with oil whirl). A rather speculative explanation is that the natural movement of the oil film with the shaft has a stabilising effect by approaching a new equilibrium position as the shaft vibrates. If the oil film is constrained to remain in the same place, any perturbation of the shaft position is more likely to lead to instability, since the oil film cannot maintain the fine balance of the equilibrium position. However, it is not clear why the static half film model should become automatically stable at a much lower value of ϵ_s than all the other models.

Although the simplifying assumptions for the short bearing half film model are very different, its stability characteristics are, rather surprisingly, similar to those for the long bearing models.

Intuitively, one would expect that shaft flexibility would make the system less stable. This is indeed the case, although it should be stressed that flexibility adds no new qualitative features to the stability charts. Equation (2.27) shows that the threshold value of the stability parameter for a flexible shaft at a given eccentricity ratio, is simply the value of the parameter for a rigid shaft at that eccentricity, plus a quantity due to the flexibility. This quantity is given by the square of the appropriate value of the critical frequency multiplied by the stiffness parameter ν_1. The stability chart for the long bearing static half film model for various values of ν_1 is shown in Figure 2.15. One feature that remains unaffected by shaft flexibility is the value of ϵ_s^* for each model. The effect of shaft flexibility is simply to lower the stability threshold, rather than to change the nature of the onset of instability. This was first demonstrated by Hagg and Warner (1953) and shows that oil whirl is caused exclusively by forces

generated within the oil film.

The critical frequency for each model is shown in Figure 2.16. It can be seen that the majority of the cavitation models fulfill the necessary criterion for oil whirl, i.e. a whirl frequency close to half that of the shaft frequency. In each case $\bar{\Omega}_s$ decreases monotonically to zero as the eccentricity ratio approaches the value ϵ_s^*. The critical frequency for the long bearing oscillating half film model is much higher than that predicted for the other models; in fact over most of the range of ϵ_s, $\bar{\Omega}_s$ is well in excess of 0.5. This suggests that this model is unsuitable as a tool in the investigation of oil whirl, since the motivation for studying the subject was provided by the original observations by Newkirk et al. (1924), (1925), (1930) etc. of small vibrations at frequencies close to half the value of the shaft speed.

The importance of critical frequency becomes clear when we examine its implications for the flexible shaft. Figure 2.17 shows a comparison of the threshold values of ν for two values of ν_1 for the half Sommerfeld and static half film models. It shows that at low eccentricities the half Sommerfeld model is more stable if the shaft is rigid, whereas for ν_1=5 the static half film model is more stable. This is due to the higher value of $\bar{\Omega}_s$ for the half Sommerfeld film.

Figure 2.18 shows the effects on stability of different axial groove positions for the case of the rigid shaft. For groove positions less than 30° before the load line, the journal is very unstable (hence the results are not shown here), but stability improves as β is increased to 90°. Beyond this point, the stability deteriorates for all except the highest eccentricity ratios. As discussed in Section 2.8 it is not possible to consider values of β greater than 180°, for which this physical model is inappropriate. It

appears that for journals operating over a range of speeds and loads, a groove position around 90° before the load line is the most stable.

The axial groove model demonstrates the importance of cavity size; Figure 2.19 shows the film extent for different groove positions. The stability results suggest that both too much and too little cavitation are conducive to instability (as remarked earlier, it is well known that a bearing operating with a complete film is unstable). One explanation of this might be that a film operating with a short lubricant arc e.g. β=30° would be more susceptible to disturbances of the shaft from the equilibrium position, since the shorter contact area with the shaft is less able to provide a large enough restoring force to provide stability.

To illustrate the results, consider a rotor mounted on a shaft supported by two plain journal bearings. The dimensions of the system are as follows:

L = 0.05m	μ = 0.01Pa s
D = 0.05m	F = 300N (total load = 600N)
R = 0.025m	c = 0.00025m

If we assume a rotation frequency of 5000rpm, it is possible to calculate the equilibrium position and its stability for each cavitation model. The results are summarised in Table 2.1; three sets of results are shown, which correspond to: a rigid shaft, a shaft with first critical speed in bending of 3000rpm and a shaft with first critical speed in bending of 10000rpm. The table shows the discrepancies in the results obtained by using different models, and hence the importance of modelling the fluid film correctly if these results are to be meaningful.

Another interesting feature is the relatively small effect of shaft flexibility on oil whirl in a real rotor system. For the higher critical speed the threshold speeds are reduced, but not by enough to change the

Table 2.1

A typical rotor sytem - variation in the threshold speed for different cavitation models and shaft stiffnesses

			rigid shaft		flexible shaft			
			$\omega_1 = \infty$		ω_1=3000rpm		ω_1=100000rpm	
model	ϵ_s	ν_{s0}	ω_s	stability	ω_s	stability	ω_s	stability
1	.44	.77	2150	unstable	1750	unstable	2100	unstable
2	.44	.08	6700	stable	5700	stable	6700	stable
3	.44	.15	5600	stable	3700	unstable	5500	stable
4	.37	.17	4600	unstable	3650	unstable	4450	unstable
5	.37	.27	3650	unstable	3200	unstable	3650	unstable
6	.64	.43	2900	unstable	2550	unstable	2850	unstable
7	.49	.27	3650	unstable	3150	unstable	3550	unstable
8	.35	.28	3600	unstable	3150	unstable	3500	unstable
9	.58	.14	5150	stable	4050	unstable	5050	stable

Key to models:

1 Long bearing - oscillatng half film
2 Long bearing - static half film
3 Long bearing - half Sommerfeld film
4 Long bearing - Reynolds' conditions (oscillating)
5 Long bearing - Reynolds' conditions (static)
6 Long bearing - axial groove 60° before loadline
7 Long bearing - axial groove 90° before loadline
8 Long bearing - axial groove 120° before loadline
9 Short bearing - half film

stability of any of the models (although it would be possible to achieve this effect by a careful choice of parameters). The reason for this effect is the small value of ν_1 for all but the slowest critical speeds. A critical speed of 10000rpm gives ν_1=0.036. This is far too small to give the spectacular effects shown in Figure 2.17. There is a substantial effect on stability if the shaft has a critical speed of 3000rpm, giving ν_1=0.398. However, if the shaft were rotating at 5000rpm it would be operating close to twice its critical speed, where oil whip effects come into play (see Section 1.4). Since oil whip is a large amplitude motion, it is likely to swamp any oil whirl.

The intention of this chapter has been to extend the application of linear techniques to flexible rotors across a variety of cavitation models, in order to confirm the small but significant role played by shaft flexibility in the onset of instability. Although the effects shown in Figure 2.17 are unikely to be observed, this work has succeeded in highlighting the widely differing implications of shaft flexibilty for different cavitation models and the necessity for accurate modelling of the fluid film behaviour for the successful design of systems with flexible shafts.

This chapter has been concerned with the calculation of threshold values for the stability parameter to define regions in (ϵ_s, ν) space in which small vibrations are naturally damped. However, just inside these stable regions the damping may be very weak. Hahn (1976) concluded that just inside the stable region, although the bearing may be theoretically stable, the degree of damping may be insufficient for stable running in practice. There is wide theoretical evidence, e.g. Lund (1966), Myers (1981), of the existence of whirl orbits existing as limit cycles just above and below the threshold value. Since a small amplitude whirl orbit might well be an acceptable mode of operation, the next stage is to examine nonlinear effects around the

region of neutral stability in order to confirm or deny the existence of whirl orbits, and to ascertain whether or not they are stable.

Before progressing to the remainder of this thesis, it is important to justify the omission of a detailed analysis of the effect on bearing dynamic characteristics of the latest developments in cavitation theory e.g. Coyne and Elrod, Floberg and the recent work of Pan (1980) on the improved short bearing model. It has been the author's intention not to provide a supplementary contribution to the theory of cavitation, but to give a flavour of the mathematics that can be used to study the implicatons of film rupture and reformation on journal bearing dynamic behaviour. Since the majority of these advanced studies are concerned with the static situation, it is more appropriate in a work of this kind to confine our attention to the more familiar models, whilst at the same time investigating their different implications for oil whirl. Such is the complexity of the latest cavitaton models, that it will be necessary to resort to numerical techniques to carry out an anlytical study of their behaviour. An introduction as to how this can be achieved is included in Chapter 8. However, as the short bearing half film model represents the best compromise between relative mathematical simplicity and accurate physical representation, it is the author's intention to make a detailed study of this model using the nonlinear theory developed in Chapter 3.

2.11 Conclusions

1. The choice of cavitation models is the crucial factor affecting the predicted stability of a journal bearing system. It is important to model cavity behaviour correctly under both static and dynamic conditions.
2. Shaft flexibility has a destabilising effect which is related to the value of the critical frequency. The introduction of flexibility does not,

however, affect the value of ϵ_s^*, the eccentricity ratio above which a model is always stable.

3. Shaft flexibility adds no new qualitative features to the stability charts. Its effect on oil whirl is relatively small, except in the case of very flexible shafts, where it is likely to be swamped by oil whip.

4. The long bearing with an oscillating half film displays features inconsistent with oil whirl.

CHAPTER 3

NONLINEAR ANALYTICAL TECHNIQUES

The examination of journal bearing behaviour has, thus far, been restricted to analysis considering the linear terms in the two equations of motion of the rotor. The next stage is to reintroduce the nonlinear terms in order to obtain a more accurate description of the behaviour close to the stability borderline. Three analytical techniques are used: Hopf bifurcation, the method of multiple scales and the method of averaging. Due to the complexity of the journal bearing equations (a fourth order system with highly nonlinear forcing terms), the application of these techniques is by no means straightforward; a clear exposition of the techniques is called for before their application to the journal bearing problem. The objective of this chapter is, therefore, to consider each method in turn, outline the underlying theory and describe the method of application to a simple nonlinear, second order system.

3.1 Hopf bifurcation

Bifurcation theory deals with the bifurcation of periodic orbits from certain critical points (steady states) of a general n-dimensional ($n\geq 2$), real, first order system of autonomous ordinary differential equations of the form:

$$\frac{d}{dt}\underline{x} = \underline{F}(\underline{x},\nu) \tag{3.1}$$

where ν is a real parameter and $\underline{a}^{\nu}$ is a critical point. It is assumed that $\underline{F}$ is analytic in a neighbourhood of $(\underline{x},\nu)=(\underline{a}^0,0)$, and that the Jacobian $\underline{F}_{\underline{x}}(\underline{a}^0,0)$ has exactly two non-zero purely imaginary eigenvalues $\pm i\Omega_0$ with the remaining n-2 eigenvalues having non-zero real parts. Hopf (1942) proved that a periodic orbit bifurcates from the critical point $(\underline{x},\nu)=(\underline{a}^0,0)$ as long as $\alpha'(0)\neq 0$ where $\alpha(\nu)+i\Omega(\nu)$ denotes the eigenvalue of $\underline{F}_{\underline{x}}$ that is a continuous extension of $+i\Omega_0$. Hopf also provides information about the uniqueness of

these bifurcated orbits, although by itself Hopf's theorem is imprecise about predicting the stability of bifurcated orbits and the direction of bifurcation.

The direction of bifurcation is defined by the values of ν for which it occurs. In general it can only occur for one of the following cases:

$$\nu < 0 \quad ; \quad \nu = 0 \quad ; \quad \nu > 0$$

If bifurcation occurs for $\nu<0$, i.e. for values of ν less than its critical value, the bifurcation is said to be subcritical. If it occurs for $\nu>0$, i.e. for values of ν above critical, the bifurcation is said to be supercritical. The existence of a bifurcation at $\nu=0$ is a special case and will not be dealt with in this thesis. Hassard, Kazarinoff and Wan (1981) suggest that it is an open question whether a bifurcation can occur at $\nu=0$.

The questions of bifurcation direction and stability are clearly important ones if the technique is to be used in the analysis of periodic phenomena. Several authors have attempted to simplify its application e.g. Marsden and McCracken (1976) and Friedrichs (1965). Using a slightly different approach to that of Hopf, Friedrichs established an existence theorem for the two dimensional problem by making the additional assumption that $\underline{F}$ is only three times continuously differentiable. An advantage of Friedrichs' formulation is a more explicit dependence of orbit properties on free parameters.

The work of Hopf was further extended by Poore (1976), who, as well as extending it to n dimensions, greatly simplified the problem by establishing algebraic criteria which are sufficient to guarantee that the bifurcated periodic orbit exists only for $\nu<0$ or $\nu>0$ in a sufficiently small neighbourhood of $(\underline{x},\nu)=(\underline{a}^0,0)$. If these criteria are met, the direction of bifurcation, the change in period of oscillation and the stability of the

bifurcated orbit are reduced to an algebraic problem.

It is the author's intention to utilise Poore's results in the analysis of the nonlinear behaviour of the journal bearing. It will therefore be advantageous to examine briefly the theorems on which they are based. Before applying the technique however, it is necessary to specify those conditions which must be satisfied if a bifurcated orbit is to exist.

Conditions for Hopf bifurcation

(1) A critical point $(\underline{x},\nu)=(\underline{a}^0,0)$ exists such that the Jacobian matrix $\underline{F}_{\underline{x}}(\underline{a}^0,0)$ has exactly two non-zero, purely imaginary eigenvalues $\pm i\Omega_0$, where $\Omega_0>0$. If $n>2$ the remaining $n-2$ eigenvalues have nonzero real parts.

(2) $\underline{F}(\underline{x},\nu) \in C^k[Dx(-\nu_0,\nu_0)]$ where D is a domain in R^n containing $\underline{a}^0$. Also $\nu_0>0$, although it can be small, and $k\geqslant 3$.

(3) $\alpha'(0)>0$, where $\alpha(\nu)+i\Omega(\nu)$ denotes the eigenvalue of $\underline{F}_x$ that is a continuous extension of $+i\Omega_0$.

(4) If $n>2$, the $n-2$ eigenvalues with nonzero real parts have negative real parts.

In practice conditions (1) and (4) are often satisfied when there is an exchange in the stability of a critical point as two (complex conjugate) eigenvalues cross the imaginary axis as a parameter is varied. Condition (3) is not strictly necessary, but it has been introduced to avoid a confusion which has developed in the literature over the meaning of 'subcritical' and 'supercritical'. Any system can be modified to satisfy this condition by substituting $\gamma=-\nu$. The implicit function theorem now guarantees the existence of a solution $\underline{a}^\nu$ which satisfies $\underline{F}(\underline{a}^\nu,\nu)=0$, and is k-times continuously differentiable.

It is necessary to introduce a change of variables:

$$\underline{x} = \underline{a}^{\nu} + \mu\underline{y} \; ; \qquad (1+\mu\eta)s = t$$

$$A^{\nu} = \underline{F}_{\underline{x}}(a^{\nu},\nu) \; ; \qquad \nu B^{\nu} = A^{\nu} - A^{0} ; \qquad B^{0} = \left.\frac{dA^{\nu}}{d\nu}\right|_{\nu=0} \tag{3.2}$$

$$\mu^{2}Q(\underline{y},\mu,\nu) = F(\underline{a}^{\nu}+\mu\underline{y},\nu) - \mu A^{\nu}\underline{y} \; ; \qquad \nu = \mu\delta$$

μ,δ,η are parameters to be defined. This transformation reduces (3.1) to:

$$\frac{d}{ds}\underline{y} = A^{0}\underline{y} + \mu\underline{G}(\underline{y},\mu,\delta,\eta) \tag{3.3}$$

$$\underline{G}(\underline{y},\mu,\delta,\eta) = \delta B^{\mu\delta}\underline{y} + \eta A^{\mu\delta}\underline{y} + (1+\mu\eta)\underline{Q}(\underline{y},\mu,\delta,\mu\delta)$$

It is now possible to make several observations:

(1) At μ=0 (3.3) has two linearly independent $2\pi/\Omega_0$-periodic solutions corresponding to the eigenvalues $\pm i\Omega_0$ of A^0.

(2) The problem of periodic solutions of (3.3) is a perturbation problem in μ.

(3) Since $\underline{x} = \underline{a}^{\nu} + \mu\underline{y}$, μ is a measure of the amplitude of the periodic orbit.

(4) In general, the bifurcated periodic orbit will not be differentiable in ν at ν = 0, but will be differentiable in μ at μ=0.

(5) The parameter δ determines the relationship between ν and μ.

(6) The parameter η shows the change in the period of oscillation as μ varies.

(7) μ is the independent small parameter; η and δ are to be determined.

Theorem 1

If (3.1) satisfies conditions (1), (2) and (3) and the transformation (3.2) is performed, then for some sufficiently small $\mu>0$ there exist real functions $\delta=\delta(\mu)$ and $\eta=\eta(\mu) \in C^{k-2}[(-\mu_1,\mu_1)]$ satisfying $\delta(0)=\eta(0)=0$, such that for $T=2\pi p/\Omega_0$ (p = positive integer):

$$\underline{x}(t,\mu) = \underline{a}^{\nu} + \mu \underline{Y}\left(\frac{1}{1+\mu\eta(\mu)}, \mu\right) \qquad (3.4)$$

is a $(1+\mu\eta(\mu))$T-periodic solution of:

$$\frac{d}{dt}\underline{x} = \underline{F}(\underline{x}, \nu(\mu))$$

for $\nu=\mu\delta(\mu)$. If $\delta=\delta(\mu)$ and $\eta=\eta(\mu)$ in (3.3), then $y=y(s,\mu)$ is a T-periodic solution of (3.3) with $y(s,\mu) \in C^{k-2}[-\mu_1,\mu_1]$, uniformly in s.

The main implications of this theorem are as follows:

(1) Since $\nu = \nu(\mu) = \mu\delta(\mu) = \mu^2\delta'(0)+O(\mu^3)$ as $\mu\to 0$, the bifurcated periodic orbit for (3.4) exists for $(\underline{x},\nu)$ in a sufficiently small neighbourhood of $(\underline{a}^{\nu},0)$ only for $\nu>0$ if $\delta'(0)>0$ and only for $\nu<0$ if $\delta'(0)<0$. Hence the sign of $\delta'(0)$ determines the direction of bifurcation.

(2) Those critical points $\underline{a}^{\nu}$ where $\delta'(0)=0$ are special cases in which it is necessary to compute $\delta''(0)$ or possibly higher derivatives in order to determine the direction of bifurcation. These degenerate cases are not considered in this thesis (the work involved in calculating $\delta''(0)$ is formidable), but brief reference will be made to them in later sections.

(3) The period of oscillation of $\underline{x}(t,\mu)$ in (3.4) is $T(1+\mu\eta(\mu)) = (1+\mu^2\eta'(0)+O(\mu^3))2\pi p/\Omega_0$ as $\mu\to 0$. This period of orbit increases or decreases from $T=2\pi p/\Omega_0$ according to the sign of $\eta'(0)$.

Theorem 2

If $\alpha'(0)\delta'(0)>0$ and Condition (4) holds, then the bifurcated periodic orbit will be asymptotically stable. If either of these conditions fail, then the bifurcated orbit will be unstable near the bifurcation point.

Theorem 3

Let $\underline{F}(\underline{x},\nu)$ satisfy the conditions for Theorem 1, and let $\underline{u}$ and $\underline{v}$ denote the left and right eigenvectors respectively of the eigenvalue $+i\Omega_0$ of the matrix A^0. If $\underline{u}$ and $\underline{v}$ are normalised by the requirement $\underline{u}.\underline{v} = 1$, then:

$$\dot{\alpha}'(0)\dot{\delta}'(0) + i(\dot{\omega}'(0)\dot{\delta}'(0)+\Omega_0\dot{\eta}'(0))$$

$$= k^2\Bigg\{ -u_l\frac{\partial^3 F_l}{\partial x_j\partial x_k\partial x_p} v_j v_k \bar{v}_p + 2u_l\frac{\partial^2 F_l}{\partial x_j\partial x_k} v_j (A^{0-1})_{kr}\frac{\partial^2 F_r}{\partial x_p\partial x_q} v_p \bar{v}_q$$

$$+ u_l\frac{\partial^2 F_l}{\partial x_j\partial x_k} \bar{v}_j((A^0-2i\Omega_0 I)^{-1})_{kr}\frac{\partial^2 F_r}{\partial x_p\partial x_q} v_p v_q \Bigg\} \qquad (3.5)$$

where k is an arbitrary constant, $(A^{0-1})_{kr}$ denotes the element in the k^{th} row and the r^{th} column of A^{0-1} and repeated indices within each term imply a sum from 1 to n. Equation (3.5) represents a pair of real equations for $\delta'(0)$ and $\eta'(0)$. Although their values can only be found to within an arbitrary positive constant k^2, this is sufficient to indicate whether the period of these orbits is increasing or decreasing.

It is important to emphasise the first implication of Theorem 1, which states that bifurcation can only occur for $\nu>0$ (supercritical) or $\nu<0$ (subcritical) depending on whether the sign of $\delta'(0)$ is positive or negative respectively. Bifurcations are, therefore, unique (a formal statement of uniqueness exists, but it is omitted here, since it is the application rather than the theory of this technique that is of interest). The stability of the bifurcated orbits follows from Theorem 2. Since $\alpha'(0)$ is positive under Condition 3, the stability is also decided by the sign of $\delta'(0)$. Supercritical orbits are, therefore, stable and subcritical orbits are unstable. The two possible types of behaviour are shown in Figure 3.1. Figure 3.1a shows an unstable limit cycle; any perturbtion from this cycle will cause the system to 'wind away'

3.1a unstable limit cycle

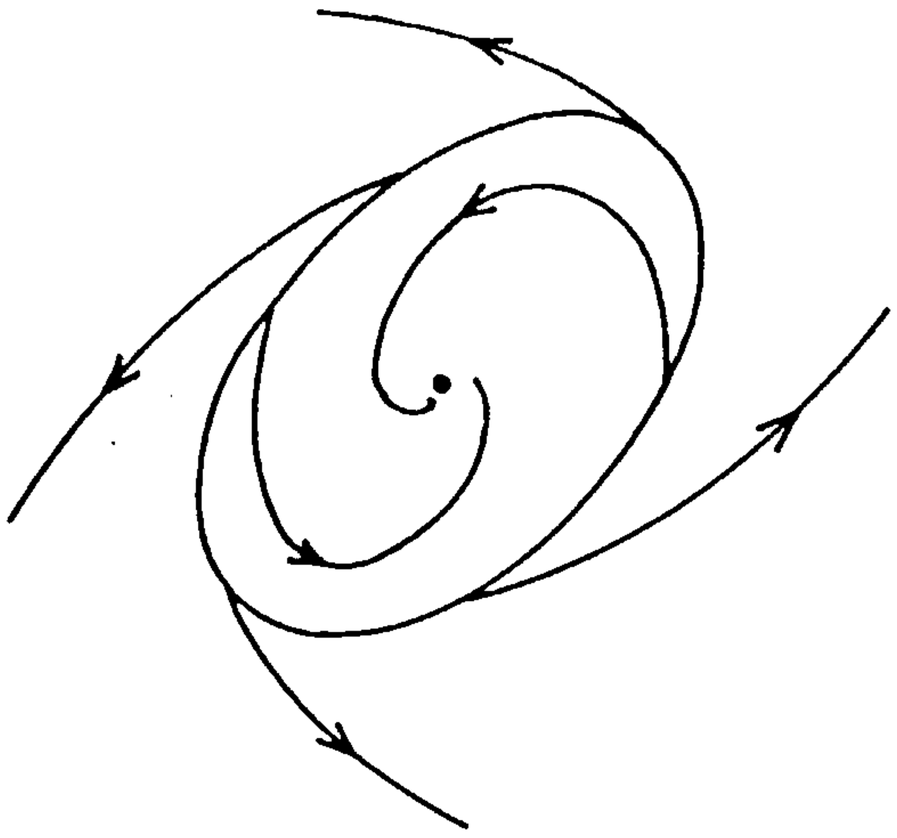

3.1b stable limit cycle

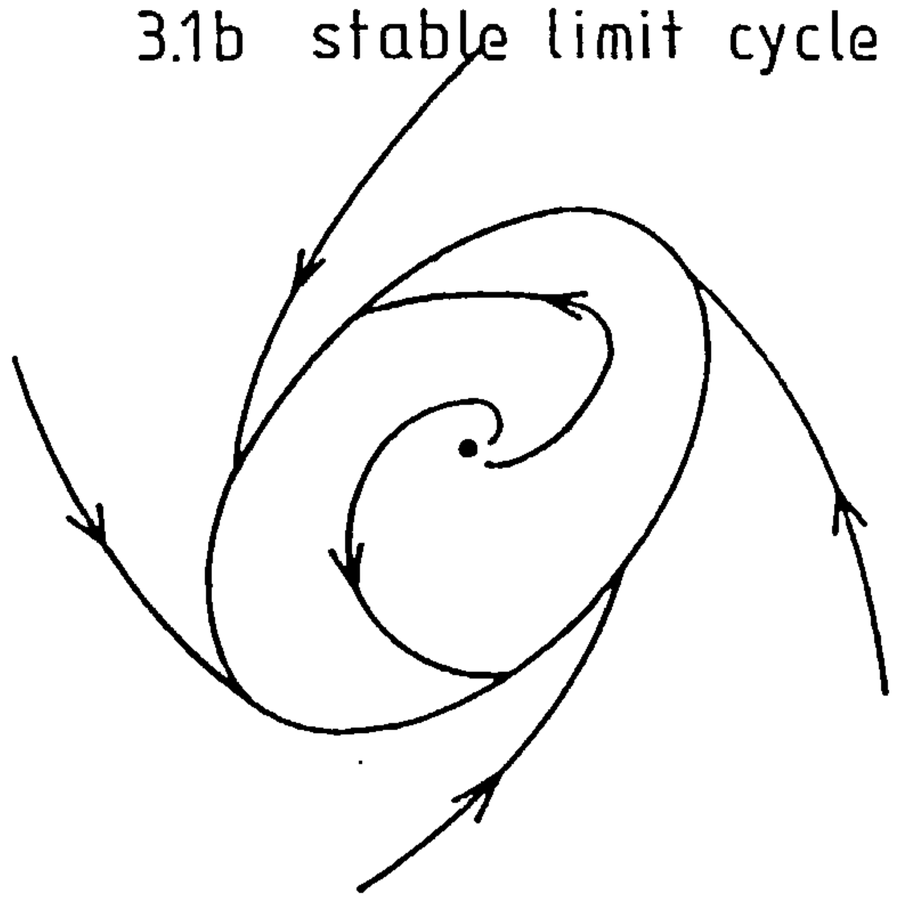

Figure 3.1 Limit cycles

amplitude

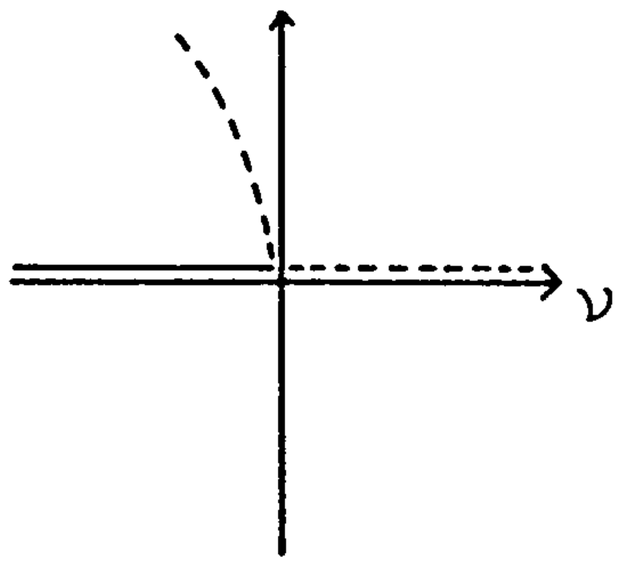

unstable

stable

$\nu < 0$ stable critical point
or unstable limit cycle

$\nu > 0$ unstable critical point

3.2a subcritical bifurcation

amplitude

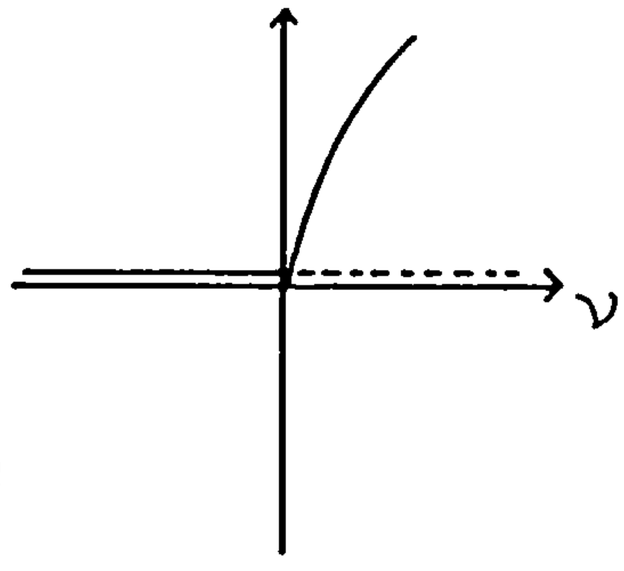

$\nu < 0$ stable critical point

$\nu > 0$ stable limit cycle
or unstable critical point

3.2b supercritical bifurcation

Figure 3.2 Hopf bifurcation

either to an equilibrium point, or to completely unstable behaviour. Figure 3.1b shows a stable limit cycle; if the system is perturbed from this limit cycle, it will 'wind back' to its original orbit.

Figure 3.2 shows the two types of possible behaviour as the bifurcation parameter approaches its critical value (ν=0). For both supercritical and subcritical bifurcation, the system has a stable equilibrium point for ν<0 and an unstable equilibrium point for ν>0 (as predicted by linear theory). Figure 3.2a shows subcritical bifurcation, for which an unstable limit cycle exists for ν<0. Figure 3.2b shows supercritical bifurcation; in this case the system can manifest a stable limit cycle for ν>0.

Remark Note the shape of the amplitude/bifurcation patameter curve in Figure 3.2. We have:

$$\text{amplitude} \simeq k\mu \qquad \text{(for some constant k)}$$

$$\nu = \mu^2\delta'(0) + O(\mu^3)$$

$$\rightarrow \text{amplitude} \simeq l\sqrt{\nu} \qquad \text{(for some constant l)}$$

Application of Hopf Bifurcation

It is possible to illustrate the above ideas by applying Hopf bifurcation to a simple second order system. Consider a damped harmonic oscillator whose motion is described by:

$$\ddot{x} + d^2\dot{x} + \omega_0^2 x = 0 \qquad (3.6)$$

where d^2 is assumed to be constant. By subjecting the oscillator to a mechanism which provides nonlinear negative damping, the equation of motion becomes:

$$\ddot{x} + \dot{x}(d^2-L(x)) + \omega_0^2 x = 0 \qquad (3.7)$$

in which we shall assume L(x) to be of the form:

$$L(x) = l^2 - \gamma x^2 \qquad (3.8)$$

and l^2 and γ to be constants. If we examine the linear system:

$$\ddot{x} + \dot{x}(d^2-l^2) + \omega_0^2 x = 0 \qquad (3.9)$$

we obtain a characteristic:

$$\lambda = \frac{-(d^2-l^2) \pm ((d^2-l^2)^2-4\omega_0^2)^{1/2}}{2} \qquad (3.10)$$

Thus the stability of the equilibrium point x=0 is governed by the following criteria (this situation is illustrated in Figure 3.3a):

$l^2 < d^2$ stable

$l^2 > d^2$ unstable

$l^2 = d^2$ neutrally stable

The application of Hopf bifurcation techniques should enable us to investigate the nonlinear behaviour close to the point where the stability changes, i.e. at $l^2 = d^2$, where the positive and negative damping are in balance. Introduce a bifurcation parameter:

$$\nu = l^2-d^2$$

The system becomes:

$$\ddot{x} + \dot{x}(\gamma x^2-\nu) + \omega_0^2 x = 0 \qquad (3.11)$$

Replacing this second order system by two first order ordinary differential equations, we obtain:

3.3a linear

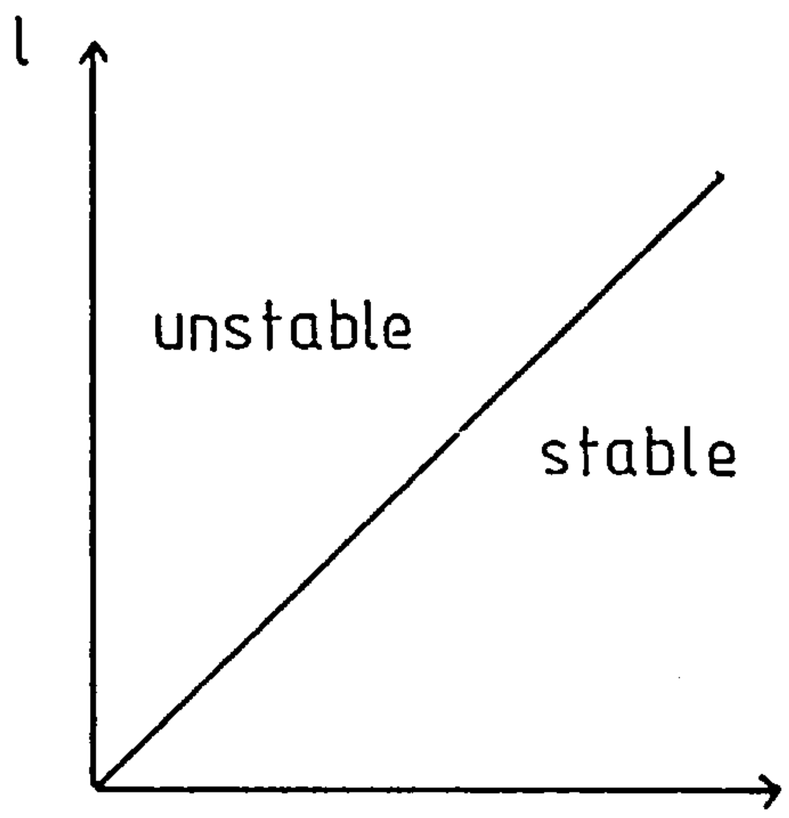

3.3b nonlinear

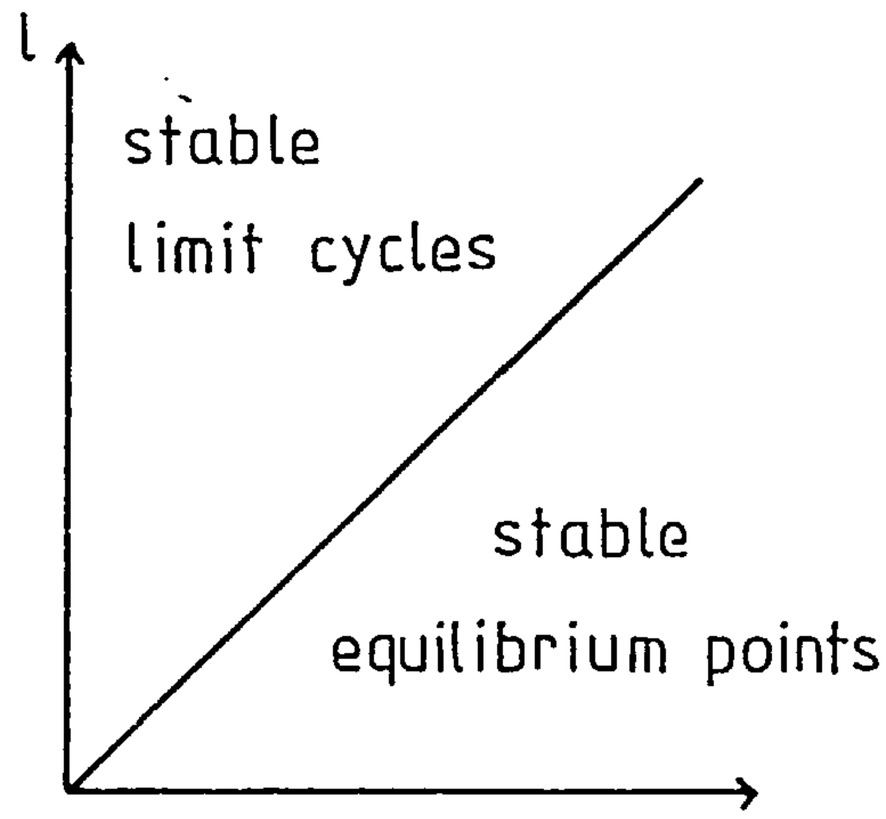

Figure 3.3 System behaviour near the stability borderline

$$\dot{x}_1 = x_2 = F_1 \qquad (3.12a)$$

$$\dot{x}_2 = -x_2(\gamma x_1^2 - \nu) - \omega_0^2 x_1 = F_2 \qquad (3.12b)$$

Hence we have the Jacobian:

$$A^{\nu} = \begin{bmatrix} 0 & 1 \\ -2\gamma x_1 x_2 - \omega_0^2 & -(\gamma x_1^2 - \nu) \end{bmatrix} \qquad (3.13)$$

$$A^0 = \begin{bmatrix} 1 & 0 \\ -\omega_0^2 & 0 \end{bmatrix}$$

A^0 has eigenvalues: $\lambda = \pm i\omega_0$. From (3.13) or (3.10) we can obtain:

$$\left.\frac{d\lambda}{d\nu}\right|_{\nu=0} = \frac{1}{2}$$

$$\dot{\alpha}(0) = \frac{1}{2} \quad ; \quad \dot{\Omega}(0) = 0$$

We also require the following eigenvectors and matrix inverses, all of which are straightforward to calculate:

$$\underline{u} = (i\omega_0 \quad 1) \quad ; \quad \underline{v} = \begin{bmatrix} -i/2\omega_0 \\ i/2\omega_0 \end{bmatrix}$$

$$A^{0-1} = \begin{bmatrix} 0 & -1/\omega_0^2 \\ 1 & 0 \end{bmatrix} \quad ; \quad (A^0 - 2i\Omega_0 I)^{-1} = \begin{bmatrix} \frac{2i}{3\omega_0} & \frac{1}{3\omega_0} \\ -\frac{1}{3} & \frac{2i}{3\omega_0} \end{bmatrix}$$

If the second and third order derivatives of $\underline{F}$ are evaluated at $x_1=x_2=0$ and $\nu=0$, only $\partial^3 F_2/\partial^2 x_1 \partial x_2$ is found to be non-zero, i.e.:

$$\frac{\partial^3 F_2}{\partial x_1^2 \partial x_2} = -2\gamma$$

The summation (3.5) can be reduced to:

$$\dot{\alpha}(0)\dot{\delta}(0) + i(\dot{\Omega}(0)\dot{\delta}(0)+\Omega_0\dot{\eta}(0))$$

$$= k^2 \left\{ -u_2 \frac{\partial^3 F_2}{\partial x_1 \partial x_1 \partial x_2} v_1 v_1 \bar{v}_2 \; -u_2 \frac{\partial^3 F_2}{\partial x_1 \partial x_2 \partial x_1} v_1 v_2 \bar{v}_1 \; -u_2 \frac{\partial^3 F_2}{\partial x_2 \partial x_1 \partial x_1} v_2 v_1 \bar{v}_1 \right\}$$

$$= 2k^2\gamma . \frac{1}{8\omega_0^2}$$

$$\rightarrow \dot{\alpha}(0)\dot{\delta}(0) + i\Omega_0\dot{\eta}(0) = \frac{k^2\gamma}{4\omega_0^2}$$

$$\rightarrow \dot{\delta}(0) = \frac{k^2\gamma}{2\omega_0^2} \qquad (3.14)$$

$$\dot{\eta}(0) = 0 \qquad (3.15)$$

Therefore a supercritical bifurcation exists for this system, i.e. stable limit cycles exist for $\nu>0$ (for $l^2>d^2$, see Figure 3.3b). The period of these orbits, however, does not vary from the critical value $2\pi/\omega_0$.

3.2 The method of multiple scales

This method can be used to extend the range of application (the time span for which solutions are valid) of the standard perturbation technique. For certain systems, the standard procedure provides a solution that is only valid for small time. For example consider the simple second order system:

$$\ddot{x} + x = \epsilon x \quad ; \quad \epsilon \ll 1 \tag{3.16}$$

This has a solution:

$$x = a\cos\left[(1-\epsilon)^{1/2}\tau + \alpha\right] \tag{3.17}$$

The standard approach is to look for solutions of the form:

$$x = x_0(\tau) + \epsilon x_1(\tau) + \epsilon^2 x_2(\tau) + \ldots. \tag{3.18}$$

Substituting (3.18) into (3.16) and equating coefficients of equal powers of ϵ leads to:

$$\ddot{x}_0 + x_0 = 0 \tag{3.19}$$

$$\ddot{x}_1 + x_1 = x_0 \tag{3.20}$$

$$\ddot{x}_2 + x_2 = x_1 \tag{3.21}$$

The general solution of (3.19) is:

$$x_0 = a\cos(\tau+\alpha) \tag{3.22}$$

on substituting into (3.20) and solving, we obtain:

$$x_1 = \frac{a\tau}{2}\sin(\tau+a) \tag{3.23}$$

substituting for x_1 in (3.21) and solving for x_2, we obtain:

$$x_2 = \frac{a}{8}\left\{-\tau^2\cos(\tau+\alpha) + a\tau\sin(\tau+\alpha)\right\} \qquad (3.24)$$

Therefore:

$$x(\epsilon,\tau) = a\cos(\tau+\alpha) + \frac{1}{2}\epsilon a\tau\sin(\tau+\alpha)$$

$$+ \epsilon^2\frac{a}{8}\left\{\tau\sin(\tau+\alpha)-\tau^2\cos(\tau+\alpha)\right\} + O(\epsilon^3)$$

This expansion will eventually fail, since the second and third terms cease to be small compared to the first term, which was implicitly assumed when expansion (3.18) was carried out. As long as τ is of O(1), the first three terms are O(1), $O(\epsilon)$, $O(\epsilon^2)$ respectively. However, if τ is $O(\epsilon^{-1})$, the first three terms are all O(1). This type of failure occurs for any finite number of terms in this particular series.

It is possible to find another series representation for (3.17) by considering the first two terms in the Taylor series for $(1-\epsilon)^{1/2}$. This leads to:

$$x(\epsilon,\tau) = a\cos\{(\tau-\epsilon\frac{\tau}{2})+\alpha\} + \frac{\epsilon^2 a\tau}{8}\sin\{(\tau-\epsilon\frac{\tau}{2})+\alpha\} + \ldots$$

This expansion is valid for τ of $O(\epsilon^{-1})$; it is possible to extend this approach to obtain any desired accuracy of solution to (3.16).

The above example shows that alternative series expansions, valid for longer time, exist for these singular perturbation problems. However, the above procedure can only be carried out if the analytical solution is already known. Since this is not normally the case, a new approach is needed to generate approximate solutions; this is the method of multiple scales. Several detailed expositions of the theory exist e.g. Nayfeh (1972) and Cole (1968). Essentially the method looks for a solution that is characterised by

behaviour along two different time scales. These are 'fast time', which relates to the short term dynamic behaviour of the system and 'slow time', which governs slower variations over a longer time span. The technique is ideally suited to the search for limit cycles in journal bearings; here fast time relates to the motion of the individual orbits, slow time is the time scale on which the orbit evolves to the limit cycle amplitude.

Application of the method of multiple scales

The application of this method and its consistency with Hopf bifurcation, can be seen by examining the simple second order system examined in Section 3.1

$$\ddot{x} + \dot{x}(\gamma x^2 - \nu) + \omega_0^2 x = 0 \qquad (3.11)$$

Bifurcation theory shows that stable periodic orbits bifurcate from $(x,\nu)=(0,0)$. To investigate these orbits by multiple scaling, put:

$$\nu = \mu^2 \qquad (3.25)$$

Introduce time scales:

$$\tau^* = \mu^2 \tau \qquad \text{"slow time"} \qquad (3.26)$$

$$s = (1+\mu\omega_1+\mu^2\omega_2+\mu^3\omega_3+....)\tau \qquad \text{"fast time"} \qquad (3.27)$$

and look for a solution of the form:

$$\Delta x = \mu x_1(s,\tau^*)+\mu^2 x_2(s,\tau^*)+\mu^3 x_3(s,\tau^*)+... \qquad (3.28)$$

Much of the literature on this subject is rather vague on the choice of forms (3.25)-(3.28). However, if a system has already been analysed by bifurcation theory, the correct forms are easy to identify.

(1) Since $\nu=\mu^2\delta'(0)+O(\mu^3)$, choose $\nu=\mu^2$.

(2) Since (via Hopf) the amplitude is proportional to μ, look for a series with leading term $O(\mu)$.

(3) The correct scaling for slow time is given by the growth rate of the linearised exponential as $\nu \to 0$:

$$e^{\alpha(\nu)\tau} \to e^{\alpha'(0)\nu\tau} \quad \text{as} \quad \nu \to 0$$

Consequently the slow time scale must be $O(\nu\tau)$, i.e. $O(\mu^2\tau)$.

The ω_i and x_i are calculated according to the principal that secular terms in x_i (terms with an explicit dependence on s) must be suppressed. Consequently the functions x_i should display modulation only in the slow time τ^*. Finally it should be pointed out that (3.28) is expressed as a series for Δx since small perturbation solutions about an equlibrium position (x=0) are sought. It is possible to derive the following identities from (3.25)-(3.28):

$$\frac{d\Delta x}{d\tau} = \mu\left(\frac{\partial x_1}{\partial s}\right)+\mu^2\left(\frac{\partial x_2}{\partial s}+\omega_1\frac{\partial x_1}{\partial s}\right)+\mu^3\left(\frac{\partial x_3}{\partial s}+\omega_1\frac{\partial x_2}{\partial s}+\omega_2\frac{\partial x_1}{\partial s}+\frac{\partial x_1}{\partial \tau^*}\right) \quad (3.29)$$

$$\frac{d^2\Delta x}{d\tau^2} = \mu\left(\frac{\partial^2 x_1}{\partial s^2}\right)+\mu^2\left(\frac{\partial^2 x_2}{\partial s^2}+2\omega_1\frac{\partial^2 x_1}{\partial s^2}\right)+\mu^3\left(\frac{\partial^2 x_3}{\partial s^2}+2\omega_1\frac{\partial^2 x_2}{\partial s^2}+2\omega_2\frac{\partial^2 x_1}{\partial s^2}+\omega_1^2\frac{\partial^2 x_1}{\partial s^2}+2\frac{\partial^2 x_1}{\partial s\partial \tau^*}\right) \quad (3.30)$$

Substituting (3.28)-(3.30) into (3.11) yields as far as third order:

Order (μ): $$\frac{\partial^2 x_1}{\partial s^2} + \omega_0^2 x_1 = 0 \quad (3.31)$$

Order (μ^2): $$\frac{\partial^2 x_2}{\partial s^2} + \omega_0^2 x_2 = -2\omega_1\frac{\partial^2 x_1}{\partial s^2} \quad (3.32)$$

Order (μ^3): $$\frac{\partial^2 x_3}{\partial s^2} + \omega_0^2 x_3 = \frac{\partial x_1}{\partial s}(1-\gamma x_1^2) - 2\omega_1\frac{\partial^2 x_2}{\partial s^2} - 2\omega_2\frac{\partial^2 x_1}{\partial s^2} - \omega_1^2\frac{\partial^2 x_1}{\partial s^2} - 2\frac{\partial^2 x_1}{\partial s\partial \tau^*} \quad (3.33)$$

The solution to (3.31) is:

$$x_1 = A_1(\tau^*)e^{i\omega_0 s} + \overline{A_1(\tau^*)}e^{-i\omega_0 s} \qquad (3.34)$$

The function $A_1(\tau^*)$ and its complex conjugate $\overline{A_1(\tau^*)}$ are to be determined later. The substitution of (3.34) into (3.32) leads to:

$$\frac{\partial^2 x_2}{\partial s^2} + \omega_0^2 x_2 = 2\omega_1\omega_0^2(A_1 e^{i\omega_0 s} + \overline{A}_1 e^{-i\omega_0 s})$$

Clearly the suppression of secular terms requires that $\omega_1=0$, giving solutions:

$$x_2 = A_2(\tau^*)e^{i\omega_0 s} + \overline{A_2(\tau^*)}e^{-i\omega_0 s}$$

$A_2(\tau^*)$ is to be found later. Equation (3.33) now becomes:

$$\frac{\partial^2 x_3}{\partial s^3} + \omega_0^2 x_3 = \left\{(iA_1 + 2\omega_2\omega_0 A_1 - i\gamma A_1|A_1|^2 - 2i\frac{dA_1}{d\tau^*})\ \omega_0 e^{i\omega_0 s} - i\gamma\omega_0 A_1 e^{3i\omega_0 s}\right\} + \text{complex conjugate}$$

in order to suppress secular terms we require:

$$2i\frac{dA}{d\tau^*} = A_1(i + 2\omega_2\omega_0 - i\gamma|A_1|^2) \qquad (3.35)$$

This is a complex amplitude equation for A_1. It can be solved by separating the real and imaginary parts. To do this, write:

$$A_1(\tau^*) = R(\tau^*)e^{i\theta(\tau^*)}$$

which then yields:

$$\frac{dR}{d\tau^*} = \frac{R}{2}(1-\gamma R^2) \qquad \text{amplitude equation} \qquad (3.36)$$

$$\frac{d\theta}{d\tau}^{*} = -\omega_2\omega_0 \qquad \text{phase shift equation} \qquad (3.37)$$

We are primarily concerned with the amplitude equation, since the condition for the existence of stationary orbits is that:

$$\frac{dR}{d\tau}^{*} = 0$$

Equation (3.36) gives the amplitude of these orbits:

$$R = \frac{1}{\gamma^{1/2}} = R_e$$

the stability of these orbits follows immediately, since:

$$R > R_e \rightarrow \frac{dR}{d\tau}^{*} < 0$$

$$R < R_e \rightarrow \frac{dR}{d\tau}^{*} > 0$$

i.e. if R is less than R_e, the system will spiral outwards, if R is greater than R_e it will spiral inwards. This corresponds to the stable limit cycle shown in Figure 3.1b. Integrating (3.37) and incorporating (3.34) and (3.28), it can be shown that the system approaches a limit cycle of the form:

$$\Delta x = \sqrt{\nu}\,\frac{2}{\sqrt{\gamma}}\cos\{\omega_0\tau(1+O(\nu^{3/2}))\} + O(\nu) \qquad (3.38)$$

The period of solution (3.38) is given by:

$$T = \frac{2\pi}{\omega_0(1+O(\nu^{3/2}))} = \frac{2\pi}{\omega_0}(1+O(\mu^3)) \qquad (3.39)$$

In order to examine the existence of stationary orbits for $\nu<0$, put:

$$\nu = -\mu^2$$

A repetition of the above analysis, incorporating this modification, leads to the amplitude equation:

$$\frac{dR}{d\tau^*} = \frac{R}{2}(-1-\gamma R^2)$$

This gives negative $dR/d\tau^*$ for all values of R except R=0, consequently all orbits spiral towards the equlibrium point.

The results of this analysis exactly match those obtained by Hopf bifurcation, and in addition provide extra information relating to the evolution toward the limit cycle solution. In the region $\nu>0$ there is a stable limit cycle, and in the region $\nu<0$ all states regress to the (linear) equilibrium point. This corresponds to a supercritical bifurcation.

Remarks

(1) The inexact nature of (3.38) is due to presence of ω_2 in (3.35), which is indeterminate at this order of approximation. It does not appear, however, in the amplitude equation which is the most important result of this analysis.

(2) The coefficient of R in the amplitude equation represents the linear growth rate $\alpha'(0)=1/2$.

3.3 The method of averaging

The method of averaging, as a technique for solving dynamical problems with a restraining force, was first developed by Krylov and Bogoliubov (1947) and later extended by Bogoliubov and Mitropolski (1961). It is very similar in concept to the method of multiple scales; Morrison (1966) has shown that in certain cases the two methods are equivalent. However, for the journal bearing problem, the relationship between the two techniques has been unclear (see the discussion at the end of Chapter 7); this thesis will attempt to remove the existing discrepancies.

The method of averaging, in common with the previous two methods described, relies on the existence of a small parameter in the restraining force (the system must be weakly nonlinear), as in equation (3.16) which is repeated here:

$$\ddot{x} + x = \epsilon x \quad ; \quad \epsilon \ll 1 \tag{3.16}$$

An equation of this type is said to be in standard form. The application of the method of averaging assumes the existence of an asymptotic expansion of the form:

$$x = a\cos\psi + \epsilon u_1(a,\psi) + \epsilon^2 u_2(a,\psi) + \ldots. \tag{3.40}$$

The expansion (3.40) is simply a perturbation of the solution to the corresponding linear problem. Each u_i is periodic in ψ, and a,ψ are assumed to vary in time according to:

$$\frac{da}{d\tau} = \epsilon A_1(a) + \epsilon^2 A_2(a) + \ldots. \tag{3.41}$$

$$\frac{d\psi}{d\tau} = \Omega_0 + \epsilon\psi_1(a) + \epsilon^2\psi_2(a) + \ldots. \tag{3.42}$$

Therefore, in common with the method of multiple scales, this method provides

information about the evolution to limit cycle solutions. A necessary requirement to uniquely determine the A_i and ψ_i is that the u_i contain no terms in $\cos\psi$, hence the first term in (3.40) represents the full first harmonic of the solution. A brief outline of the procedure to find the u_i, A_i and ψ_i is as follows. First the derivatives of x with respect to T are transformed using (3.40)-(3.42). These results are then substituted into (3.16) in order to equate like powers of ϵ. The A_i and ψ_i can then be found using the principle that secular terms in the u_i must vanish.

Application of the method of averaging

The consistency of this technique with the two previously examined can be seen by its application to the example:

$$\ddot{x} + \dot{x}(\gamma x^2 - \nu) + \omega_0^2 x = 0 \qquad (3.11)$$

The existence of stationary orbits in the region $\nu>0$ can be examined by putting:

$$\nu = \mu^2 \qquad (3.43)$$

As in the case of multiple scaling, it is possible to use the results from bifurcation theory to obtain an indication of the correct choice of forms (3.43)-(3.46).

(1) Since $\nu = \mu^2\delta'(0) + O(\mu^3)$, put $\nu=\mu^2$.

(2) Since the amplitude is proportional to μ, look for a series:

$$\Delta x = \mu a\cos\psi + \mu^2 u_1(a,\psi) + \mu^3 u_2(a,\psi) + \ldots. \qquad (3.44)$$

(3) In the application of multiple scaling, the correct form for slow time is given by the growth rate of the linearised exponential as $\nu\to 0$, i.e. $\tau^*=\mu^2\tau$. Consequently an expansion of the form:

$$\frac{da}{d\tau} = \mu A_1(a) + \mu^2 A_2(a) + ... \qquad (3.45)$$

will be consistent with multiple scaling and bifurcation theory if $A_1=0$, since slow time relates to the growth in amplitude of the whirl orbits. It will be seen that this is the case.

(4) Hopf bifurcation sugests that the leading term in the phase shift equation should be valid to $O(\mu^3)$, since the change in the period of oscillations is given by a factor $1+\mu^2\eta'(0)+O(\mu^3)$ and in this case $\eta'(0)=0$. Hence an expansion of the form:

$$\frac{d\psi}{d\tau} = \Omega_0 + \mu\psi_1(a) + \mu^2\psi_2(a) + \mu^3\psi_2(a) + ... \qquad (3.46)$$

will be consistent with the previous two methods if $\psi_1=\psi_2=0$. This is indeed so.

The following results can be obtained from (3.44)-(3.46):

$$\frac{d\Delta x}{d\tau} = \mu(-\Omega_0 a\sin\psi) + \mu^2(A_1\cos\psi + \Omega_0\frac{\partial u_1}{\partial\psi} - \psi_1 a\sin\psi)$$

$$+ \mu^3(A_1\frac{\partial u_1}{\partial a} + A_2\cos\psi + \Omega_0\frac{\partial u_2}{\partial\psi} + \psi_1\frac{\partial u_1}{\partial\psi} - \psi_2 a\sin\psi) \qquad (3.47)$$

$$\frac{d^2\Delta x}{d\tau^2} = \mu(-\Omega_0^2 a\cos\psi) + \mu^2(\Omega_0^2\frac{\partial^2 u_1}{\partial\psi^2} - 2\Omega_0 A_1\sin\psi - 2\Omega_0\psi_1 a\cos\psi)$$

$$+ \mu^3\{A_1\frac{dA_1}{da}\cos\psi - A_1\frac{d\psi_1}{da}a\sin\psi + 2\Omega_0 A_1\frac{\partial^2 u_1}{\partial a\partial\psi} - 2\Omega_0\psi_2 a\cos\psi$$

$$- 2\psi_1 A_1\sin\psi - 2\Omega_0 A_2\sin\psi + \Omega_0^2\frac{\partial u_2}{\partial\psi^2} + 2\Omega_0\psi_1^2\frac{\partial u_1}{\partial\psi^2} - a^2\psi_1\cos\psi\} \qquad ....(3.48)$$

Now substitute (3.44), (3.47) and (3.48) into (3.11) and equate powers of μ.

Order (μ): $\qquad -\Omega_0^2 a\cos\psi + \omega_0^2 a\cos\psi = 0 \qquad (3.49)$

Order (μ^2):
$$\Omega_0^2 \frac{\partial^2 u_1}{\partial \psi^2} + \omega^2 u_1 = 2\Omega_0 a\dot{\psi}_1 \cos\psi + 2\Omega_0 A_1 \sin\psi \qquad (3.50)$$

Order (μ^3):
$$\Omega_0^2 \frac{\partial^2 u_2}{\partial \psi^2} + \omega_0^2 u_2 = \gamma\Omega_0 a^3 \cos^2\psi \sin\psi - \Omega_0 a \sin\psi - 2\Omega_0 \dot{\psi}_1 \frac{\partial^2 u_1}{\partial \psi^2}$$
$$+ a\dot{\psi}_1^2 \cos\psi + 2\Omega_0 \Psi_2 a \cos\psi - A_1 \frac{dA_1}{da} \cos\psi + A_1 \frac{d\dot{\psi}_1}{da} a \sin\psi$$
$$- 2\Omega_0 A_1 \frac{\partial^2 u_1}{\partial a \partial \psi} + 2\dot{\psi}_1 A_1 \sin\psi + 2\Omega_0 A_2 \sin\psi) \qquad (3.51)$$

(3.49) implies that:

$$\Omega_0 = \pm \omega_0$$

This represents the solution to the linear problem. From (3.50) it can be seen that if u_1 is to contain no secular terms, we must have:

$$A_1 = \dot{\psi}_1 = 0$$

(3.51) is now reduced to:

$$\frac{\partial^2 u_2}{\partial \psi^2} + u_2 = \frac{1}{\omega_0^2} \left\{ \gamma a^3 \cos^2\psi \sin\psi - a\sin\psi + 2\dot{\psi}_2 a\cos\psi + 2A_2 \sin\psi \right\}$$

$$= \frac{1}{\omega_0^2} \left\{ (\gamma \frac{a^3}{4} + 2A_2 - a)\sin\psi + 2\dot{\psi}_2 a\cos\psi + \gamma \frac{a^3}{4} \sin 3\psi \right\}$$

If u_2 is to contain no secular terms, both the coefficients of $\sin\psi$ and $\cos\psi$ must be zero. This implies:

$$\dot{\psi}_2 = 0 \qquad (3.52)$$

$$A_2 = \frac{a}{2} (1 - \gamma \frac{a^2}{4}) \qquad (3.53)$$

For stationary orbits we require A_2=0 (see (3.45)). This requirement gives the amplitude of these orbits:

$$a = \frac{2}{\sqrt{\gamma}}$$

The amplitude equation (3.53) is equivalent to the analogous equation obtained in the two-timing technique (3.36); the divisor 4 appears in (3.53) because of the different form of expansions (3.28) and (3.40). The resulting limit cycles are thus of the form:

$$\Delta x = \frac{\mu 2}{\sqrt{\gamma}} \cos \left\{ \tau(\Omega_0 + O(\mu^3)) \right\} + O(\mu^2)$$

$$\Delta x = \frac{\sqrt{\nu} 2}{\sqrt{\gamma}} \cos \left\{ \omega_0 \tau(1 + O(\nu^{\frac{3}{2}})) \right\} + O(\nu) \qquad (3.54)$$

This is in complete agreement with (3.38), the result obtained by multiple scaling. A further check on the consistency is provided by the fact that the conditions:

$$A_1 = \psi_1 = \psi_2 = 0$$

are satisfied.

Accuracy of the method of averaging

Equation (3.54) represents the first approximation to the system (3.11). In this case it would be possible to find the second approximation by calculating u_1, and even the third approximation by calculating u_2. In general, however, this is not possible, since the amount of computation require to find the u_i rapidly becomes unacceptably large. It is, however, necessary to consider u_1 and u_2 in order to ensure the existence of stationary orbits. Consider the following solution:

$$x = \mu a \cos\psi + \mu^2 u_1(a,\psi) + \mu^3 u_2(a,\psi)$$

$$\frac{da}{d\tau} = \mu A_1(a) + \mu^2 A_2(a)$$

$$\frac{d\psi}{d\tau} = \Omega_0 + \mu\psi_1(a) + \mu^2\psi_2(a)$$

The change in the value of a as τ changes from zero to τ is given by:

$$\Delta a = a(\tau) - a(0) \simeq \tau\bar{A}_1\mu$$

where A_1 denotes the average value of A_1 in the period $(0,\tau)$. The error in $da/d\tau$ is $O(\mu^3)$, and after a time τ has elapsed the error in 'a' will be be $O(\mu^3\tau)$. If $\tau=O(\mu^{-1})$, the error will be $O(\mu^2)$, consequently it would be meaningless to retain the u_1 term in the solution for any but the shortest time span. In order to include the u_1 term it would be necessary to work to order to $O(\mu^3)$ in A and ψ. In general finding A_n and ψ_n entails working to order n+1 or n+2; for n=3 this would require considerable effort, which would yield no extra information of significance. Bogoliubov and Mitropolski suggest that in all but the most unusual cases the qualitative features of the nonlinear behaviour are present in the first approximation. Consequently, this thesis will restrict itself to the first approximation.

CHAPTER 4

THE APPLICATION OF HOPF BIFURCATION TO THE EQUATIONS OF MOTION GOVERNING OIL WHIRL IN THE 'SHORT' BEARING

4.1 Introduction to the use of nonlinear techniques

This chapter is concerned with the application of those analytical techniques developed in Chapter 3 to the short bearing operating with a half film (see Section 2.9). Hopf bifurcation theory is used to prove the existence of small amplitude closed orbits close to the stability borderline; further information about the nature of these limit cycles can then be found by employing the method of multiple scales and the method of averaging. The authenticity of these results is confirmed by a numerical integration of the equations of motion. It is then possible to derive criteria for the existence of oil whirl for this particular physical model, and to compare the effectiveness of the different techniques for predicting rotor behaviour.

For the remainder of this thesis, the bearing system described in the Introduction will be modified. In Chapter 2, it was found that shaft flexibility has a very small effect on the system's linear stability. This may or not be the case for the nonlinear behaviour, but the inclusion of flexibility necessitates the study of a cumbersome sixth order system; it is therefore ignored, and the shaft is assumed to be rigid ($\omega_1=\infty$, $\nu_1=0$). This has the effect of simplifying the analysis by reducing the equations of motion (2.3)-(2.6) to two second order nonlinear ordinary differential equations.

The analytical techniques under consideration examine the effect of varying a small parameter. In this investigation the variable parameter is the nondimensional rotor speed $\bar{\omega}$ relative to its equilibrium value $\bar{\omega}_s$. The reason for this choice is that $\bar{\omega}$ is the parameter most easily changed in an experimental investigation, and engineers are most interested in bearing performance at different running speeds. It is possible to find $\bar{\omega}_s$, the critical running speed corresponding to ϵ_s, by the methods of Chapter 2, but

for these purposes it is more convenient to use standard linear techniques. Full details if these calculations can be found in several references e.g. Holmes (1960), Lundholm (1969). For convenience, a brief outline of the technique is given here.

4.2 Standard theory of linear stability analysis

For a horizontal, massless, rigid shaft, supporting a rotor of mass 2m, the equations of motion in polar coordinates are (see Figure 1.4):

$$m\left\{\frac{d^2e}{dt^2} - e\left[\frac{d\varphi}{dt}\right]^2\right\} = F\cos\varphi + F_r\left(e,\varphi,\frac{de}{dt},\frac{d\varphi}{dt}\right) \qquad (4.1a)$$

$$m\left\{e\frac{d^2\varphi}{dt^2} + 2\frac{de}{dt}\frac{d\varphi}{dt}\right\} = -F\sin\varphi + F_t\left(e,\varphi,\frac{de}{dt},\frac{d\varphi}{dt}\right) \qquad (4.1b)$$

These equations may be nondimensionalised by means of the quantities defined in (1.17) and (1.18) to give:

$$\epsilon'' - \epsilon\varphi'^2 = \frac{1}{\bar{\omega}^2}\left\{\cos\varphi + S_m\bar{F}_r(\epsilon,\varphi,\epsilon',\varphi')\right\} \qquad (4.2a)$$

$$\epsilon\varphi'' + 2\epsilon'\varphi' = -\frac{1}{\bar{\omega}^2}\left\{\sin\varphi - S_m\bar{F}_t(\epsilon,\varphi,\epsilon',\varphi')\right\} \qquad (4.2b)$$

Clearly, equations (4.2) apply for any cavitation model (for the long bearing model the Sommerfeld number S replaces S_m). For the short bearing half film model, the hydrodynamic forces can be found by integrating the pressure distribution (2.43) from θ_1 to $\pi+\theta_1$ in (1.16). They can be expressed as follows:

$$\bar{F}_r = \epsilon(1-2\varphi')I_1 + 2\epsilon' I_2 \qquad (4.3a)$$

$$\bar{F}_t = \epsilon(1-2\varphi')I_3 + 2\epsilon' I_1 \qquad (4.3b)$$

where integrals I_1, I_2 and I_3 are given in Appendix 3.

The equations of motion (4.2) have a steady state solution as discussed in Section 1.5 and defined by (1.20). Since the equations are nonlinear it is not possible to solve them analytically; consequently it is necessary to linearise them in order to examine the stability of the steady state position.

It is convenient to introduce a cartesian coordinate system (fixed with respect to the bush), with the origin at the bearing centre as shown in Figure 4.1.

(X,Y) are nondimensional quantities analogous to (x,y) defined in (2.9). The polar coordinates (ϵ,φ) are related to the Cartesian coordinates by the relationship (see Appendix 4):

$$X = \epsilon\cos\varphi \quad ; \quad Y = \epsilon\sin\varphi \tag{4.4}$$

The total forces acting on the shaft become:

$$\bar{F}_X = \frac{1}{S_m} + \bar{F}_r\cos\varphi - \bar{F}_t\sin\varphi \tag{4.5a}$$

$$\bar{F}_Y = \bar{F}_r\sin\varphi + \bar{F}_t\cos\varphi \tag{4.5b}$$

This leads to the nondimensional equations of motion:

$$\ddot{X} = \frac{S_m}{\bar{\omega}^2}\,\bar{F}_X(X,Y,\dot{X},\dot{Y},S_m) \tag{4.6a}$$

$$\ddot{Y} = \frac{S_m}{\bar{\omega}^2}\,\bar{F}_Y(X,Y,\dot{X},\dot{Y},S_m) \tag{4.6b}$$

In order to perform the linear and nonlinear analysis on these equations of motion, a perturbation ($\Delta X,\Delta Y$) from the equilibrium position (X_s,Y_s) is considered (Figure 4.1b). This is defined by:

$$\Delta X = X - X_s \quad ; \quad \Delta Y = Y - Y_s$$

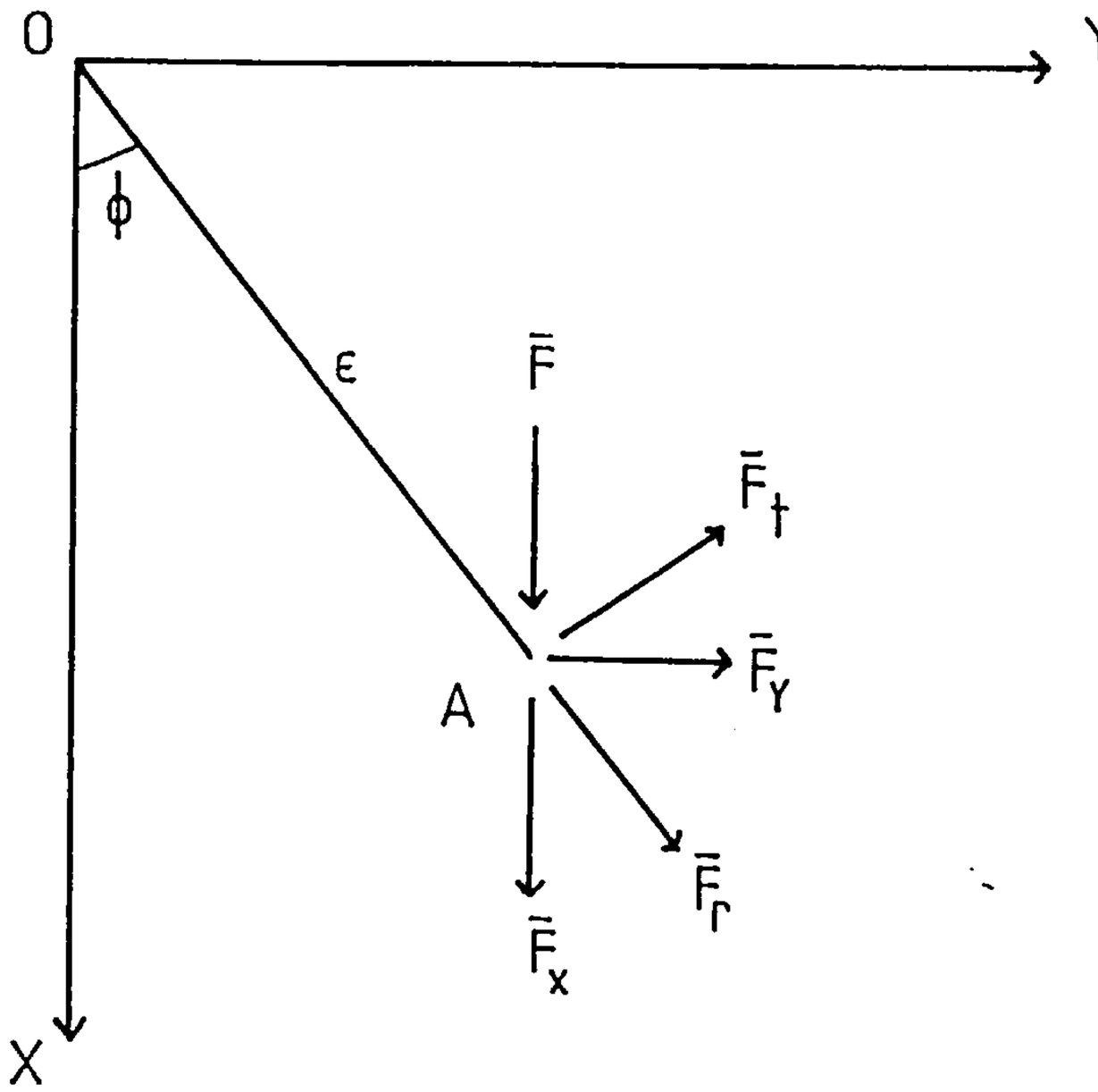

4.1a

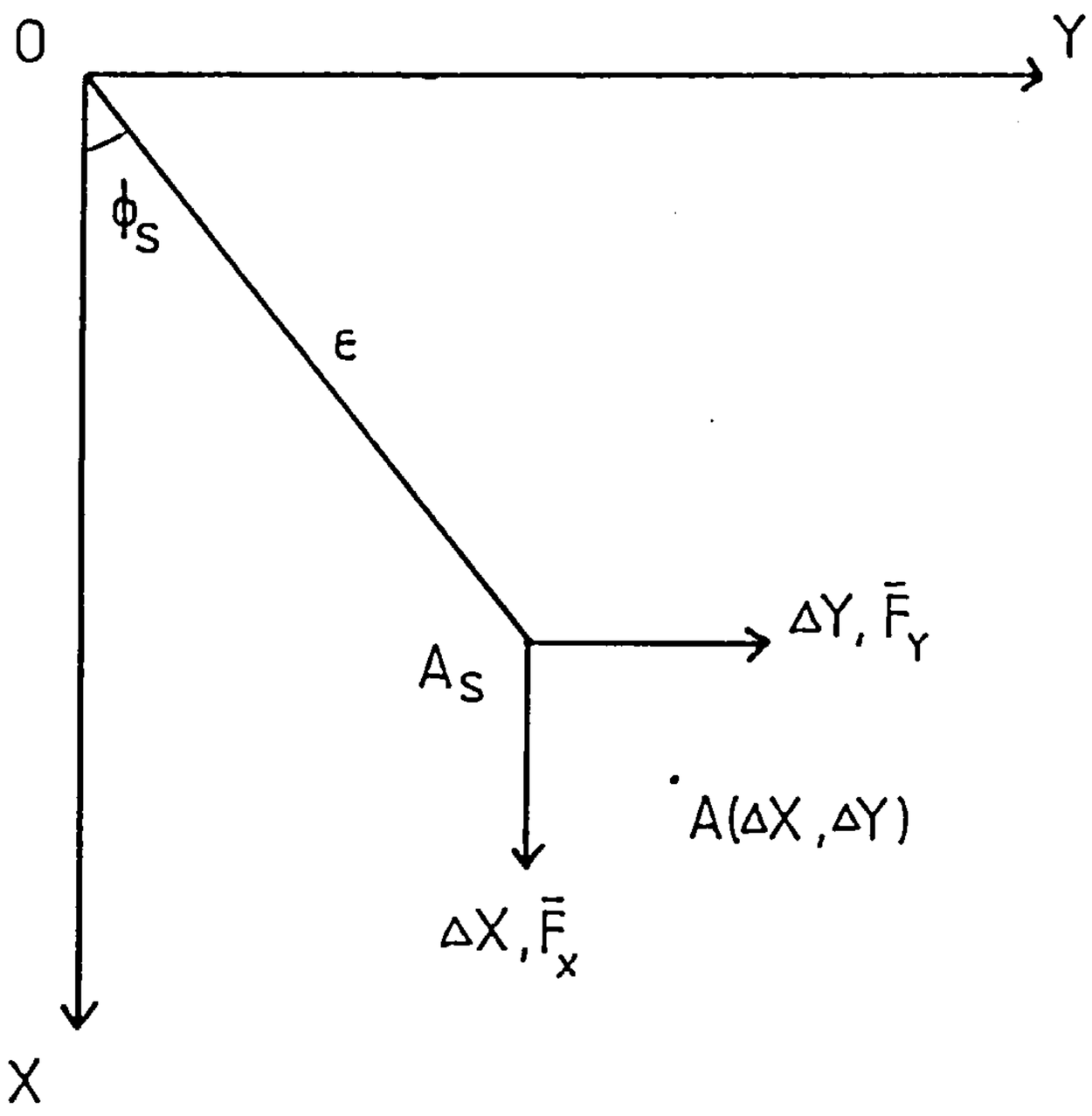

4.1b

Figure 4.1 Co-ordinate system for the nonlinear analysis

Define stiffness and damping coefficients as follows:

$$K_{XX} = -S_m\left\{\frac{\partial \bar{F}_X}{\partial X}\right\}_s \quad ; \quad B_{XX} = -S_m\left\{\frac{\partial \bar{F}_X}{\partial \dot{X}}\right\}_s$$

$$K_{XY} = -S_m\left\{\frac{\partial \bar{F}_X}{\partial Y}\right\}_s \quad ; \quad B_{XY} = -S_m\left\{\frac{\partial \bar{F}_X}{\partial \dot{Y}}\right\}_s \qquad (4.7)$$

$$K_{YX} = -S_m\left\{\frac{\partial \bar{F}_Y}{\partial X}\right\}_s \quad ; \quad B_{YX} = -S_m\left\{\frac{\partial \bar{F}_Y}{\partial \dot{X}}\right\}_s$$

$$K_{YY} = -S_m\left\{\frac{\partial \bar{F}_Y}{\partial Y}\right\}_s \quad ; \quad B_{YY} = -S_m\left\{\frac{\partial \bar{F}_Y}{\partial \dot{Y}}\right\}_s$$

The subscript s indicates steady state conditions $X_s=Y_s=0$.

Equations (4.6) can be linearised about the equilbrium point (X_s,Y_s) (note that $\bar{F}_{Xs}=\bar{F}_{Ys}=0$) to give:

$$\Delta\ddot{X} + \frac{1}{\bar{\omega}^2}\left\{ B_{XX}\Delta\dot{X} + B_{XY}\Delta\dot{Y} + K_{XX}\Delta X + K_{XY}\Delta Y \right\} = 0 \qquad (4.8a)$$

$$\Delta\ddot{Y} + \frac{1}{\bar{\omega}^2}\left\{ B_{YX}\Delta\dot{X} + B_{YY}\Delta\dot{Y} + K_{YX}\Delta X + K_{YY}\Delta Y \right\} = 0 \qquad (4.8b)$$

As in Section 2.3, the stability of these equations can be investigated by assuming the existence of a solution of the form:

$$\Delta X = \Delta X_0 e^{\bar{\lambda}\tau} \quad ; \quad \Delta Y = \Delta Y_0 e^{\bar{\lambda}\tau}$$

This leads to a characteristic equation:

$$\bar{\lambda}^4 + \frac{1}{\bar{\omega}^2}(B_{XX}+B_{YY})\,\bar{\lambda}^3 + \frac{1}{\bar{\omega}^2}\left\{(K_{XX}+K_{YY}) + \frac{1}{\bar{\omega}^2}(B_{XX}B_{YY}-B_{XY}B_{YX})\right\}\bar{\lambda}^2$$

$$+ \frac{1}{\bar{\omega}^4}(B_{XX}K_{YY}+B_{YY}K_{XX}-B_{XY}K_{YX}-B_{YX}K_{XY})\,\bar{\lambda} + \frac{1}{\bar{\omega}^4}(K_{XX}K_{YY}-K_{XY}K_{YX}) = 0 \qquad \ldots(4.9)$$

which can be written in the form:

$$\bar{\lambda}^4 + A_1\bar{\lambda}^3 + A_2\bar{\lambda}^2 + A_3\bar{\lambda} + A_4 = 0 \qquad (4.10)$$

solutions of this quartic can be examined by means of a reduced version of the Hurwitz criteria (2.18)-(2.20). These state that necessary and sufficient conditions fo the roots to have negative real parts are:

$$\text{(i) } A_1 > 0,\ \text{(ii) } A_2 > 0,\ \text{(iii) } A_3 > 0,\ \text{(iv) } A_4 > 0,$$

$$\text{(v) } R_5 = A_3(A_1A_2 - A_3) - A_1^2A_4 > 0$$

For equation (4.9) these become:

$$\text{(i)} \qquad \frac{1}{\bar{\omega}^2}(B_{XX}+B_{YY}) > 0$$

$$\text{(ii)} \qquad \frac{1}{\bar{\omega}^2}\left\{(K_{XX}+K_{YY}) + \frac{1}{\bar{\omega}^2}(B_{XX}B_{YY}-B_{XY}B_{YX})\right\} > 0$$

$$\text{(iii)} \qquad \frac{1}{\bar{\omega}^4}(B_{XX}K_{YY}+B_{YY}K_{XX}-B_{XY}K_{YX}-B_{YX}K_{XY}) > 0$$

$$\text{(iv)} \qquad \frac{1}{\bar{\omega}^2}(K_{XX}K_{YY}-K_{XY}K_{YX}) > 0$$

In general conditions (i) to (iv) are always satisfied, and so condition (v) becomes the effective test for stability. This can be expressed as a condition on $\tilde{\omega}$, i.e. for stability, the following must be satisfied:

$$\bar{\omega} < \bar{\omega}_s = \left[\frac{R}{S - T}\right]^{1/2} \qquad (4.11)$$

where:

$$R = B_{XX}B_{YY}-B_{XY}B_{YX}$$

$$S = \frac{(B_{XX}+B_{YY})(K_{XX}K_{YY}-K_{XY}K_{YX})}{B_{XX}K_{YY}+B_{YY}K_{XX}-B_{XY}K_{YX}-B_{YX}K_{XY}}$$

$$T = \frac{B_{XX}K_{XX}+B_{YY}K_{YY}+B_{XY}K_{YX}+B_{YX}K_{XY}}{B_{XX}+B_{YY}}$$

A similar execrcise to that carried out in Section 2.3 can be performed to find the critical frequency $\bar{\Omega}_s$. At the stability threshold, two of the roots of (4.9) are purely imaginary ($\bar{\lambda}=\pm i\bar{\Omega}_s$); hence write:

$$\bar{\lambda} = + i\bar{\Omega}_s$$

After substitution into (4.9), the following expression can be obtained by equating real and imaginary parts:

$$\bar{\Omega}_s = \left\{ \frac{B_{XX}K_{YY}+ B_{YY}K_{XX}- B_{XY}K_{YX}- B_{YX}K_{XY}}{(B_{XX}+ B_{YY})\ \bar{\omega}^2} \right\}^{1/2} \qquad (4.12)$$

As expected the results for $\bar{\omega}_s$ and $\bar{\Omega}_s$ defined by (4.11) and (4.12) are in complete agreement with those obtained by the methods described in Section 2.3. Their values are plotted against ϵ_s in Figure 4.2.

The next stage in the analysis is to determine the effect on the system as a whole of a change in the value of the chosen perturbation parameter $\bar{\omega}$.

4.3 The system parameter

For a journal bearing with fixed geometry and lubricant properties, there are only two parameters which can be varied in practice. These are the load F and the rotation speed ω; in nondimensional terms these are represented by the modified Sommerfeld number S_m and the nondimensional rotor speed $\bar{\omega}$.

$$S_m = \frac{L^3 R\omega\mu}{Fc^2} \qquad \bar{\omega} = \omega(mc/F)^{1/2} \qquad (4.13)$$

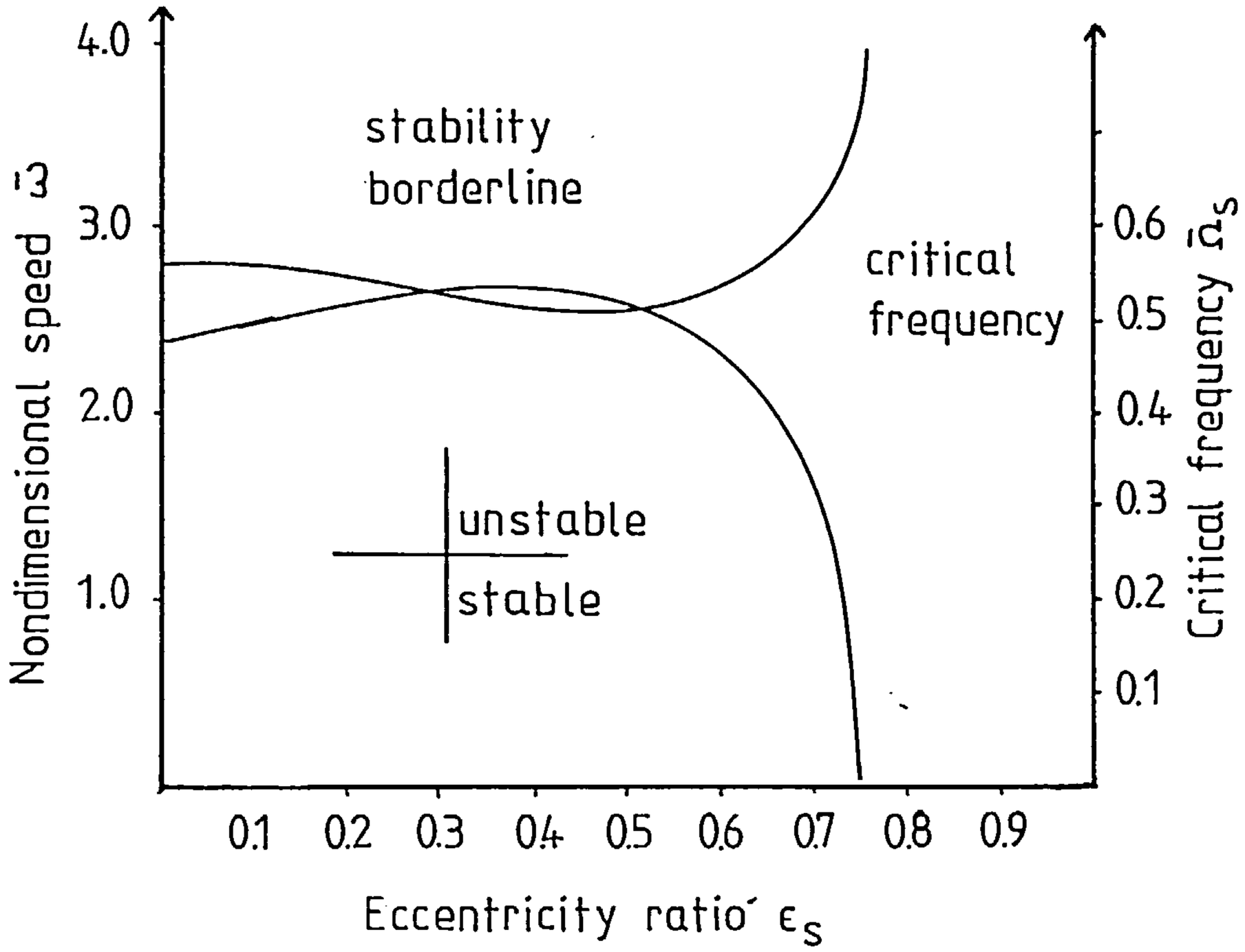

Figure 4.2 The short bearing – half film at neutral stability

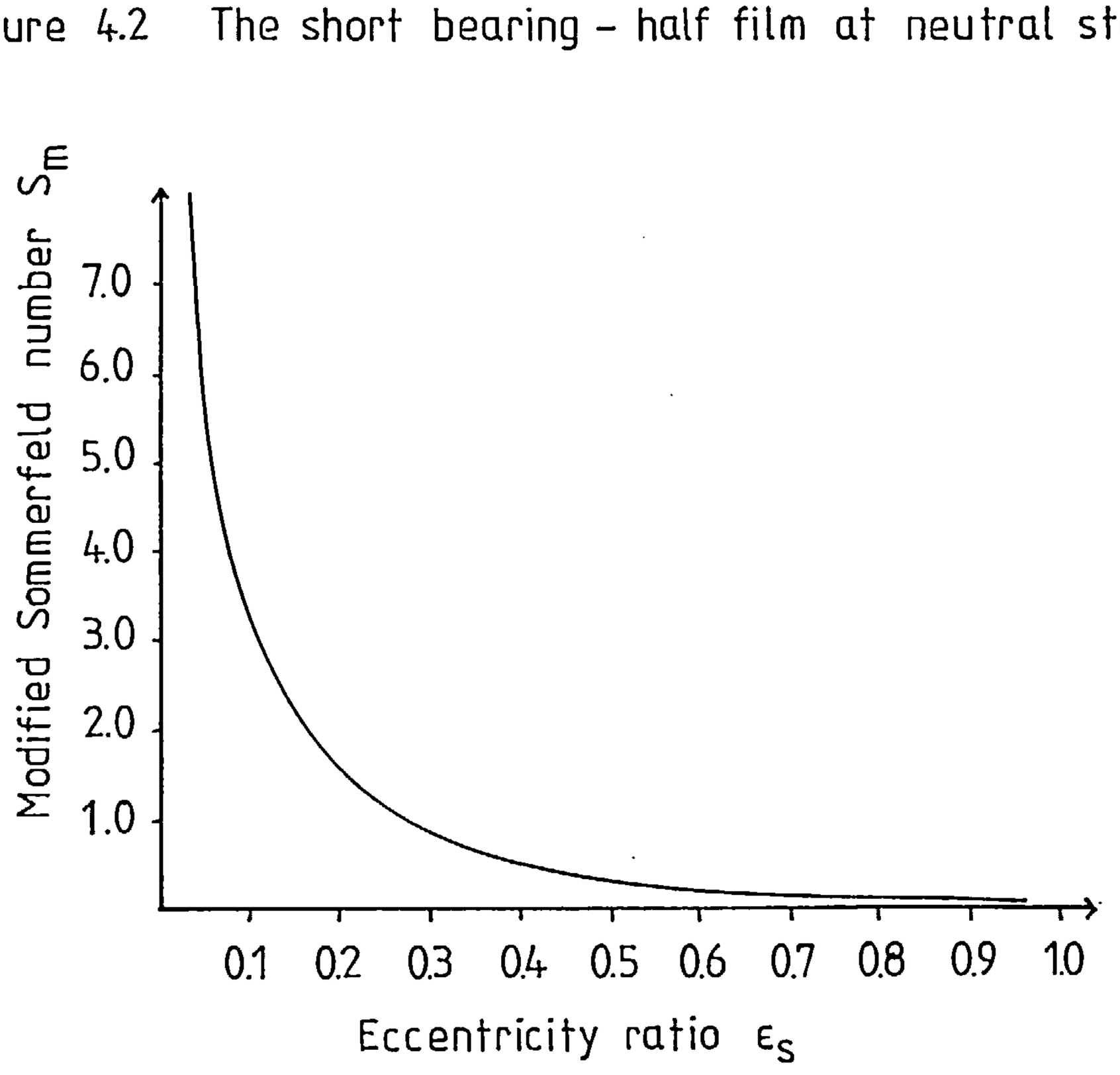

Figure 4.3 The modified Sommerfeld number

There is a direct relationship between the load and the equilibrium position (see Section 1.5). By (4.13) the load is related to the Modified Sommerfeld Number and for every value of S_m there is a corresponding equilibrium position ϵ_s. The relationship between S_m and ϵ_s is shown in Figure 4.3.

Clearly, the effect of a change in the rotor speed is to alter S_m via (4.13), which in turn affects ϵ_s via (1.21). For example, consider a system operating with $\bar{\omega}=\bar{\omega}_1$ just below $\bar{\omega}_s$; an increase in $\bar{\omega}$ might cause a change in the system behavior from a stable equilbrium position at $\epsilon=\epsilon_{s1}$ to small orbits in the linearly unstable region with centre at $\epsilon=\epsilon_{s2}$. This is shown in Figure 4.4.

If the techniques described in Chapter 4 are to be used to investigate the behaviour of a real system, it is necessary to define a system parameter which remains unaffected by variations in rotor speed. Lund and Saibel (1967) introduced such a parameter for their work on this model. Define a system parameter σ as:

$$\sigma = \frac{S_m}{\bar{\omega}} = \frac{L^3 R\mu}{(Fmc^5)^{1/2}}$$

It is important to point out that the system parameter remains fixed for a particular rotor system (i.e. bearing geometry, load and lubricant viscosity). For a given value of σ it is possible to draw an operation line showing the change in ϵ_s as $\bar{\omega}$ is varied. Figure 4.5 shows this relationship for σ=0.4. Clearly the area of greatest interest is the region around the point where the operation line crosses the stability borderline. This research will consider the behaviour of the journal bearing for various fixed values of the system parameter. Consequently it is necessary to consider the relationship between $\bar{\omega}$ and ϵ_s, which can be found as follows:

$$\frac{d\bar{\omega}}{d\epsilon_s} = \frac{d}{d\epsilon_s}\left\{ \frac{S_m(\epsilon_s)}{\sigma} \right\} = \frac{1}{\sigma}\frac{dS_m(\epsilon_s)}{d\epsilon_s} \qquad (4.14)$$

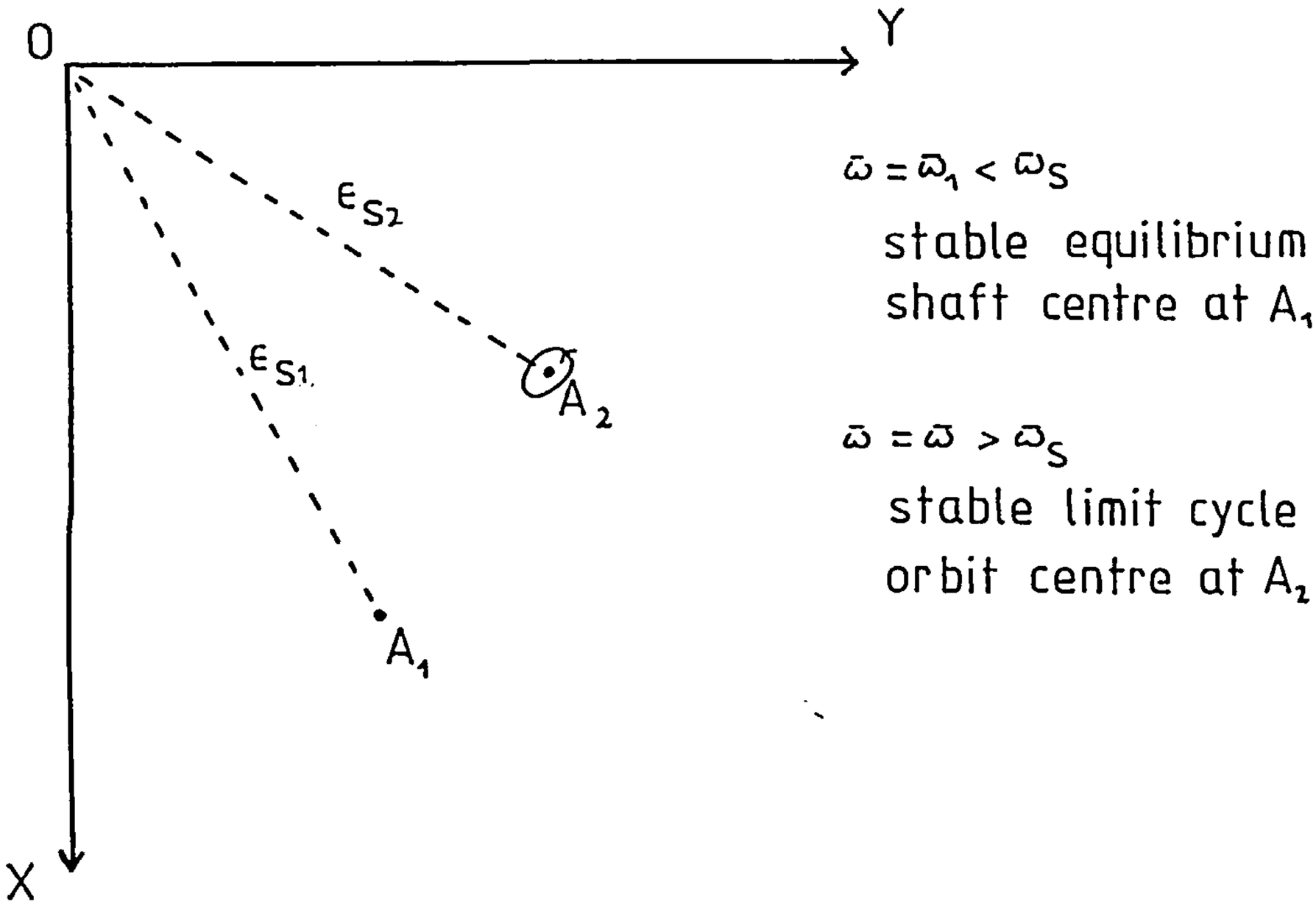

Figure 4.4 Behaviour of the shaft centre at different values of $\bar{\omega}$

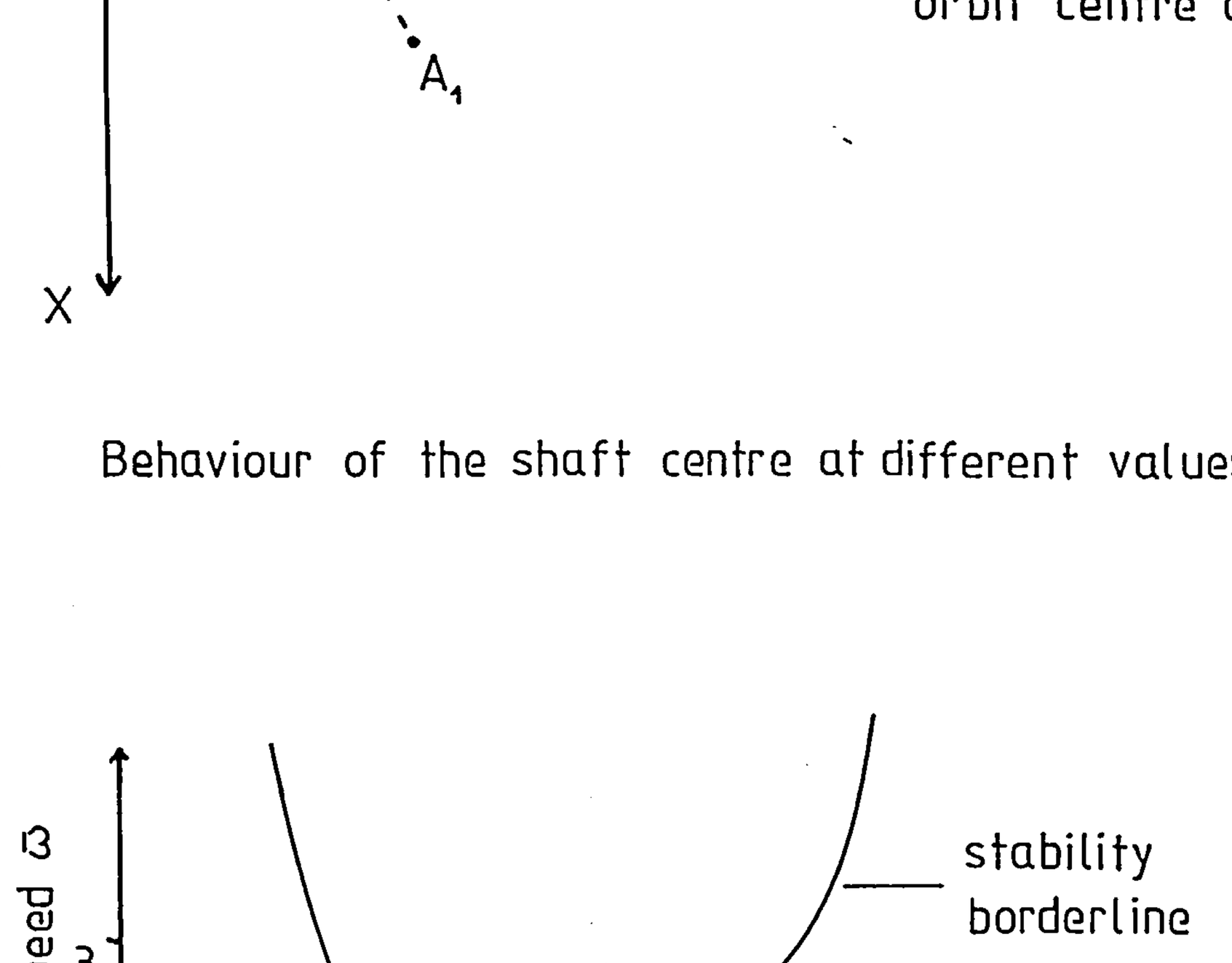

Figure 4.5 The system parameter

4.4 Hopf bifurcation applied to the equations of motion

Before applying Hopf bifurcation theory to the equations of motion (4.6), it is necessary to convert them to a first order system, which is done by writing:

$$X_1 = X \; ; \; X_2 = \dot{X} \; ; \; X_3 = Y \; ; \; X_4 = \dot{Y}$$

Equations (4.6) now become:

$$\dot{X}_1 = X_2 \tag{4.15a}$$

$$\dot{X}_2 = \frac{S_m}{\bar{\omega}^2} \bar{F}_X(X_1, X_2, X_3, X_4, S_m) \tag{4.15b}$$

$$\dot{X}_3 = X_4 \tag{4.15c}$$

$$\dot{X}_4 = \frac{S_m}{\bar{\omega}^2} \bar{F}_Y(X_1, X_2, X_3, X_4, S_m) \tag{4.15d}$$

$$\text{i.e.} \quad \frac{d\underline{X}}{d\tau} = \underline{F}(\underline{X}, \bar{\omega}, S_m)$$

These equations have a steady state solution:

$$\underline{F}(\underline{X}, \bar{\omega}, S_m) = 0$$

which implies:

$$X_{1s} = \epsilon_s \cos\varphi_s \; ; \; X_{2s} = 0 \; ; \; X_{3s} = \epsilon_s \sin\varphi_s \; ; \; X_{4s} = 0$$

This solution is governed by S_m; for every value of S_m, there corresponds a unique value of ϵ_s. The stability of this equilibrium postion can be examined by the method described in Section 4.1; for the first order system (4.15) the characteristic equation equivalent to (4.9) can be obtained by writing down the Jacobian:

$$A(\bar{\omega}) = (\nabla_{\underline{X}} \underline{F}(\underline{X}, \bar{\omega}, S_m))_{\underline{X}=\underline{X}_s}$$

$$= \begin{bmatrix} 0 & 1 & 0 & 0 \\ \frac{-K_{\underline{X}X}}{\bar{\omega}^2} & \frac{-B_{\underline{X}X}}{\bar{\omega}^2} & \frac{-K_{\underline{X}Y}}{\bar{\omega}^2} & \frac{-B_{\underline{X}Y}}{\bar{\omega}^2} \\ 0 & 0 & 0 & 1 \\ \frac{-K_{\underline{Y}X}}{\bar{\omega}^2} & \frac{-B_{\underline{Y}X}}{\bar{\omega}^2} & \frac{-K_{\underline{Y}Y}}{\bar{\omega}^2} & \frac{-B_{\underline{Y}Y}}{\bar{\omega}^2} \end{bmatrix}$$

The eigenvalues of $A(\bar{\omega})$ satisfy (4.9). For an equilibrium point to be stable, the rotor speed must satisfy the condition $\bar{\omega}<\bar{\omega}_s$. If this criterion is satisfied, then all four roots of (4.9) will have negative real parts. At $\bar{\omega}=\bar{\omega}_s$ (neutral stability) two of the roots are purely imaginary and the remaining two have negative real parts. For $\bar{\omega}>\bar{\omega}_s$ the two wholly imaginary eigenvalues now have positive real parts. Equilibrium points are always stable above $\epsilon_s \simeq 0.75$ (see Figure 4.2); consequently a bifurcation point exists at the stability borderline for every value of ϵ_s less than approximately 0.75. Figure 4.2 shows that the critical frequency is never zero in this range, therefore the eigenvalues never pass through the origin, since the critical frequency corresponds to the wholly imaginary eigenvalue at neutral stabilty $+i\bar{\Omega}_s$. Finally, it can be seen that $d\bar{\alpha}/d\bar{\omega}$ is always positive at neutral stability, if the system is becoming unstable, where $\bar{\alpha}$ is defined in Condition 4, Section 3.1 as the the real part of $\bar{\lambda}$.

Conditions (1) to (4) of Section 3.1 are satisfied; hence a Hopf bifurcation has been proved to exist for all values of ϵ_s up to approximately 0.75. Since $d\bar{\alpha}/d\bar{\omega}>0$ and the remaining eigenvalues have negative real parts, Theorem 2 implies that stable whirl orbits exist only at speeds above the threshold (supercritical bifurcation), conversely for $\bar{\omega}<\bar{\omega}_s$ whirl orbits are unstable (subcritical bifurcation). In order to calculate the direction of bifurcation

for each value of ϵ_s and the change in period of whirl orbits as $\bar{\omega}$ moves away from its threshold value, the algebraic formula defined in Theorem 3 are utilised. To do this, it is necessary to calculate the following:

(1) $\left\{\frac{d\bar{\alpha}}{d\bar{\omega}}\right\}_{\bar{\omega}=\bar{\omega}_s}$; $\left\{\frac{d\bar{\Omega}}{d\bar{\omega}}\right\}_{\bar{\omega}=\bar{\omega}_s}$

($\bar{\alpha},\bar{\Omega}$ are analogous to α,Ω in Section 3.1)

Method The characteristic (4.9) is expanded in a Taylor series about $\bar{\omega}=\bar{\omega}_s$ and first order terms are retained. Note that:

$$\text{at } \bar{\omega} = \bar{\omega}_s \; ; \quad \bar{\lambda}_s = i\bar{\Omega}_s$$

$$\text{at } \bar{\omega} = \bar{\omega}_s + \delta\bar{\omega} \quad , \quad \bar{\lambda} = i\bar{\Omega}_s + \left\{\frac{d\alpha}{d\bar{\omega}}\right\}_{\bar{\omega}=\bar{\omega}_s} \delta\bar{\omega} + i\left\{\frac{d\Omega}{d\bar{\omega}}\right\}_{\bar{\omega}=\bar{\omega}_s} \delta\bar{\omega}$$

$$\bar{\lambda} = \bar{\lambda}_s + \delta\bar{\lambda} \qquad (4.16)$$

Expression (4.16) can be substituted into the characteristic expansion and real and imaginary terms equated. This yields real equations for $d\bar{\alpha}/d\bar{\omega}$ and $d\bar{\Omega}/d\bar{\omega}$ (see Appendix 5).

(2) $\underline{u}, \underline{v}$

(the left and right eigenvectors corresponding to eigenvalue $+i\bar{\Omega}_s$ of the matrix $A(\bar{\omega}_s)$, normalised so that $\underline{u}.\underline{v}=1$)

Method A straightforward process of algebraic manipulation.

(3) $\dfrac{\partial^2 F_l}{\partial x_j \partial x_k}$; $\dfrac{\partial^3 F_l}{\partial x_i \partial x_j \partial x_k}$ $\qquad i,j,k,l = 1,2,3,4$

Method These derivatives can be found analytically using the transformation (4.4), some details of which are included in Appendix 4.

(4) $(A(\bar{\omega}_s))^{-1}$; $(A(\bar{\omega}_s)-2i\tilde{\Omega}_s I)^{-1}$

Method These matrix inverses can be found by standard techniques, which involve the solution of a system of simultaneous linear algebraic equations.

Performing the above algebra was an extremely tedious operation, the process taking several weeks to complete and check. The most arduous task was the calculation of the second and third derivatives of the force vectors, although the author was fortunate in that J.W. Lund (1966) had performed the calculations in his own Ph.D. thesis. It was the extreme tedium of this aspect of the research that prompted the numerical approach adopted in Chapter 6.

4.5 Results

The analysis has been carried out for equilbrium positions in the range $0.01 \leqslant \epsilon_s \leqslant 0.75$ (for $\epsilon_s > 0.75$ the short bearing half film model is always stable). The results are shown in Table 4.1. The $(\epsilon_s, \bar{\omega})$ parameter space can be split into two regions.

Region 1 $\epsilon_s \leqslant 0.14$ In this region $\delta'(0)<0$, therefore subcritical bifurcation takes place. Since $\alpha'(0)\delta'(0)<0$ the orbits are unstable. By the uniqueness theorem of Hopf, no small amplitude orbits may exist for $\bar{\omega} > \bar{\omega}_s$. Also $\eta'(0)>0$ so the period of the unstable orbit increases from its threshold value $2\pi p/\bar{\Omega}_s$.

Region 2 $0.15 \leqslant \epsilon_s \leqslant 0.75$ In this region $\delta'(0)>0$, therefore supercritical bifurcation occurs. The bifurcated orbits are stable. Since $\eta'(0)>0$ the period of these orbits increases as $\bar{\omega}$ moves away from its threshold value.

The implications of these results for two different rotor systems with system

Table 4.1

Results obtained by Hopf bifurcation for the short bearing operating with a half film

ϵ_s	S_m	$\bar{\omega}_s$	$\bar{\Omega}_s$	σ	$\delta'(0)$	$\alpha'(0)\delta'(0)$	$\eta'(0)$
0.01	31.82	2.76	0.50	11.51	< 0	< 0	> 0
0.05	6.33	2.76	0.50	2.29	< 0	< 0	> 0
0.10	3.11	2.74	0.51	1.13	< 0	< 0	> 0
0.14	2.17	2.72	0.51	0.80	< 0	< 0	> 0
0.15	2.01	2.72	0.51	0.74	> 0	> 0	> 0
0.20	1.45	2.68	0.51	0.54	> 0	> 0	> 0
0.30	0.86	2.61	0.52	0.33	> 0	> 0	> 0
0.40	0.54	2.55	0.52	0.21	> 0	> 0	> 0
0.50	0.33	2.54	0.52	0.13	> 0	> 0	> 0
0.60	0.20	2.70	0.47	0.07	> 0	> 0	> 0
0.70	0.10	3.63	0.35	0.03	> 0	> 0	> 0
0.75	0.07	9.74	0.13	0.01	> 0	> 0	> 0

parameter σ=0.06 and σ=2.0 are shown in Figure 4.6.

<u>σ=0.06</u> The operation line crosses the stability borderline at $\bar{\omega}$=2.81, ϵ_s=0.625 in the supercritical region. As the speed is increased, the equilibrium position moves towards the centre of the bearing (ϵ_s is decreasing). This equilibrium position remains stable until $\bar{\omega}$ reaches a value of 2.81. At this point the operation line crosses into the linearly unstable region; however, bifurcation theory shows that small stable limit cycles exist around the equilibrium point. At higher speeds, the corresponding equilibrium points will continue to be the centres of stable whirl orbits. The question of how far it is possible to increase $\bar{\omega}$ before the theory breaks down will be discussed in Section 7.2.

<u>σ=2.0</u> The operation line crosses the stability borderline at $\bar{\omega}$=2.76, ϵ_s=0.061 in the subcritical region. As in the previous case, ϵ_s decreases with increasing $\bar{\omega}$; this equilibrium point remains stable until $\bar{\omega}$ approaches 2.76, here bifurcation theory predicts that small unstable whirl orbits surround the equilibrium point. The behaviour, therefore, will depend an the initial conditions, i.e. the values of ϵ and φ at τ=0. If they are close to ϵ_s and φ_s, then the system will move towards a stable critical point, otherwise it will move into an unstable limit cycle of growing amplitude. For $\bar{\omega}>\bar{\omega}_s$ there are no limit cycles, consequently the system is completely unstable.

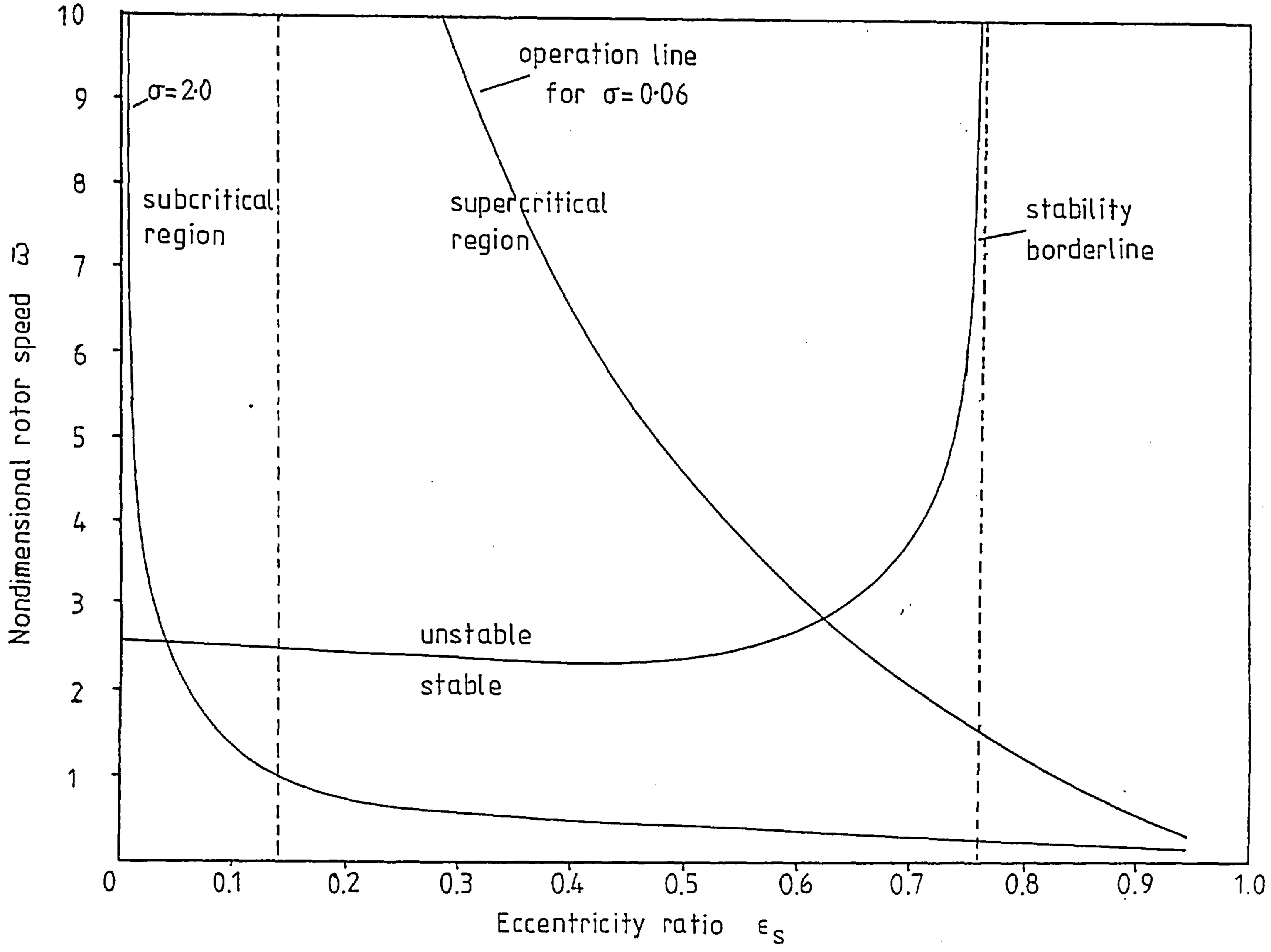

Figure 4.6 Hopf bifurcation results for the short bearing – half film model

CHAPTER 5

THE APPLICATION OF THE METHOD OF MULTIPLE SCALES TO THE EQUATIONS OF MOTION GOVERNING OIL WHIRL IN THE 'SHORT' BEARING

5.1 The application of the method of multiple scales

In Section 3.2 the method of multiple scales was discussed in detail and its application to a second order system in 'standard form' was demonstrated. Equations (4.6), which represent the equations of motion for the journal bearing, are however not in 'standard form' due to the absence of a small parameter. It is, therefore, necessary to introduce a modification to the technique. This can easily be demonstrated by reference to a simple example.

Consider a second order system:

$$\frac{d^2x}{d\tau^2} = g(x, \frac{dx}{d\tau}, \omega)$$

Suppose that an equilibrium solution exists:

$$x = x_s \; ; \quad \frac{dx}{d\tau} = 0 \quad ; \quad \omega = \omega_s$$

In order to introduce a small parameter perturb the rotational speed about its equilibrium value to:

$$\omega = \omega_s + \delta\omega$$

It is possible to apply 'small parameter' techniques to the above system by considering a Taylor expansion of the force expression about the equilibrium position; thus a strongly nonlinear system can be considered to be weakly nonlinear close to a critical point. The appropriate form of $\delta\omega$ depends on the nature of the problem, a consideration of the results obtained by Hopf bifurcation can give an indication as to the most efficient choice.

The above approach can be adopted in the analysis of the equations (4.6) by using a similar expansion about:

$$X = X_s \; ; \quad Y = Y_s \; ; \quad \dot{X} = 0 \quad ; \quad \dot{Y} = 0 \quad ; \quad \bar{\omega} = \bar{\omega}_s$$

When applying the two-timing technique to larger dimensional systems, it is necessary to assume monofrequency oscillations. This is the case for system (4.6); it is postulated that the system vibrates with the same frequency in both the X and Y directions.

In order to investigate the existence of small amplitude, periodic solutions to (4.6), we define the following forms:

$$\mu^2 = \bar{\omega} - \bar{\omega}_s \qquad (\text{for } \bar{\omega} > \bar{\omega}_s) \tag{5.1}$$

$$\tau^* = \mu^2 \tau \tag{5.2}$$

$$s = (1+\mu\omega_1+\mu^2\omega_2+\mu^3\omega_3+\ldots)\tau^* \tag{5.3}$$

and look for solutions of the form:

$$\Delta X(s,\tau^*) = \mu X_1(s,\tau^*) + \mu^2 X_2(s,\tau^*) + \mu^3 X_3(s,\tau^*) + \ldots \tag{5.4a}$$

$$\Delta Y(s,\tau^*) = \mu Y_1(s,\tau^*) + \mu^2 Y_2(s,\tau^*) + \mu^3 Y_3(s,\tau^*) + \ldots \tag{5.4b}$$

As observed in Section 3.2 the correct scaling for these forms can be deduced from a consideration of the Hopf bifurcation results.

(1) Theorem 1 (Section 3.1) implies that $\delta\bar{\omega}=\mu^2\delta'(0)+O(\mu^3)$. Therefore in perturbing $\bar{\omega}$ to $\bar{\omega}_s+\delta\bar{\omega}$, the correct form is (5.1).

(2) The transformation of variables (3.2) implies that the amplitude of the small periodic orbits is proportional to μ, therefore look for expansions in ΔX and ΔY in powers of μ as in (5.4)

(3) The correct scaling for 'slow time' is governed by the linearised growth rate of the exponential function as $\delta\bar{\omega}\to 0$:

$$e^{\alpha(\delta\bar{\omega})\tau} \to e^{\alpha'(0)\delta\bar{\omega}\tau} \qquad \text{as } \delta\bar{\omega} \to 0$$

$$= e^{\alpha'(0)\mu^2\tau}$$

Thus the slow time scale must be $O(\mu^2\tau)$.

The forms (5.1)-(5.4) are identical to those employed for the damped harmonic oscillator used as an example in Chapter 3. The derivatives remain as in (3.29) and (3.30)

$$\frac{d\Delta X}{d\tau} = \mu\left(\frac{\partial X_1}{\partial s}\right)+\mu^2\left(\frac{\partial X_2}{\partial s}+\omega_1\frac{\partial X_1}{\partial s}\right)+\mu^3\left(\frac{\partial X_3}{\partial s}+\omega_1\frac{\partial X_2}{\partial s}+\omega_2\frac{\partial X_1}{\partial s}+\frac{\partial X_1}{\partial \tau^*}\right) \quad (5.5a)$$

$$\frac{d^2\Delta X}{d\tau^2} = \mu\left(\frac{\partial^2 X_1}{\partial s^2}\right)+\mu^2\left(\frac{\partial^2 X_2}{\partial s^2}+2\omega_1\frac{\partial^2 X_1}{\partial s^2}\right)+\mu^3\left(\frac{\partial^2 X_3}{\partial s^2}+2\omega_1\frac{\partial^2 X_2}{\partial s^2}+2\omega_2\frac{\partial^2 X_1}{\partial s^2}\right.$$

$$\left.+\omega_1^2\frac{\partial^2 X_1}{\partial s^2}+2\frac{\partial^2 X_1}{\partial s\partial \tau^*}\right) \quad (5.6a)$$

Similar expressions exist for $d\Delta Y/d\tau$ and $d^2\Delta Y/d\tau^2$, which are denoted by (5.5b) and (5.6b). Before carrying out the two-timing analysis, it is necessary to appreciate some results from the elementary theory of ordinary differential equations. Consider the following system of two simultaneous o.d.e's:

$$\frac{d^2x}{d\tau^2} - a_3\frac{dx}{d\tau} - a_4\frac{dy}{d\tau} - a_1x - a_2y = q_1e^{i\bar{\Omega}\tau}+ m_1e^{2i\bar{\Omega}\tau}+ n_1 + \text{complex conjugate} \quad (5.7a)$$

$$\frac{d^2y}{d\tau^2} - b_3\frac{dx}{d\tau} - b_4\frac{dy}{d\tau} - b_1x - b_2y = q_2e^{i\bar{\Omega}\tau}+ m_2e^{2i\bar{\Omega}\tau}+ n_2 + \text{complex conjugate} \quad (5.7b)$$

(q_1, q_2, m_1, m_2 complex, n_1, n_2 real)

Neglecting transients, the solutions to equations (5.7) may be written:

$$x(\tau) = Ae^{i\bar{\Omega}\tau}+ r_1\tau e^{i\bar{\Omega}\tau}+ s_1e^{i\bar{\Omega}\tau}+ u_1e^{2i\bar{\Omega}\tau}+ \frac{v_1}{2} + c.c. \quad (5.8a)$$

$$y(\tau) = \lambda Ae^{i\bar{\Omega}\tau}+\lambda r_1\tau e^{i\bar{\Omega}\tau}+ s_2e^{i\bar{\Omega}\tau}+ u_2e^{2i\bar{\Omega}\tau}+ \frac{v_2}{2} + c.c. \quad (5.8b)$$

where A is constant and:

$$A\begin{bmatrix} 1 \\ \lambda \end{bmatrix}$$

represents the eigenvector corresponding to the eigenvalue $+i\bar{\Omega}$ of the homogeneous form of (5.7). The quantities r_1, s_1, s_2, u_1, u_2, v_1, v_2 can be found by calculating the appropriate particular integral. This is an elementary but rather tedious exercise. It follows from the linearity of the equations that:

$$r_1 = (B_1 \quad B_2) \begin{bmatrix} q_1 \\ q_2 \end{bmatrix} \qquad B_1, B_2 \text{ constant}$$

Therefore the elimination of secular terms from (5.8) requires:

$$r_1 = B_1 q_1 + B_2 q_2 = 0 \tag{5.9}$$

We are now ready to expand the right hand side side of equations (4.6) about the equilibrium position. For reasons of brevity only the results for (4.6a) are given here, the expressions for (4.6b) are very similar, with the a_i's replaced by b_i's, and a's by b's in the numbering scheme.

$$\begin{aligned}
\Delta\ddot{X} = \frac{1}{\bar{\omega}_s^2}\left[1 - \frac{2\mu^2}{\bar{\omega}_s}\right] \Bigg\{ & \left(a_1 + \mu^2 \frac{da_1}{d\bar{\omega}}\right)\Delta X + \left(a_2 + \mu^2 \frac{da_2}{d\bar{\omega}}\right)\Delta Y \\
& + \left(a_3 + \mu^2 \frac{da_3}{d\bar{\omega}}\right)\Delta\dot{X} + \left(a_4 + \mu^2 \frac{da_4}{d\bar{\omega}}\right)\Delta\dot{Y} + \frac{a_5}{2}\Delta X^2 + a_6 \Delta X \Delta Y + a_7 \Delta X \Delta\dot{X} \\
& + a_8 \Delta X \Delta\dot{Y} + \frac{a_9}{2}\Delta Y^2 + a_{10}\Delta Y\Delta\dot{X} + a_{11}\Delta Y\Delta\dot{Y} + \frac{a_{12}}{2}\Delta\dot{X}^2 + a_{13}\Delta\dot{X}\Delta\dot{Y} \\
& + \frac{a_{14}}{2}\Delta\dot{Y}^2 + \frac{a_{15}}{6}\Delta X^3 + \frac{a_{16}}{2}\Delta X^2\Delta Y + \frac{a_{17}}{2}\Delta X^2\Delta\dot{X} + \frac{a_{18}}{2}\Delta X^2\Delta\dot{Y} \\
& + \frac{a_{19}}{2}\Delta X\Delta Y^2 + a_{20}\Delta X\Delta Y\Delta\dot{X} + a_{21}\Delta X\Delta Y\Delta\dot{Y} + \frac{a_{22}}{2}\Delta X\Delta\dot{X}^2 + a_{23}\Delta X\Delta\dot{X}\Delta\dot{Y} \\
& + \frac{a_{24}}{2}\Delta X\Delta\dot{Y}^2 + \frac{a_{25}}{6}\Delta Y^3 + \frac{a_{26}}{2}\Delta Y^2\Delta\dot{X} + \frac{a_{27}}{2}\Delta Y^2\Delta\dot{Y} + \frac{a_{28}}{2}\Delta Y\Delta\dot{X}^2 \\
& + a_{29}\Delta Y\Delta\dot{X}\Delta\dot{Y} + \frac{a_{30}}{2}\Delta Y\Delta\dot{Y}^2 + \frac{a_{31}}{6}\Delta\dot{X}^3 + \frac{a_{32}}{2}\Delta\dot{X}^2\Delta\dot{Y} + \frac{a_{33}}{2}\Delta\dot{X}\Delta\dot{Y}^2 \\
& + \frac{a_{34}}{6}\Delta\dot{Y}^3 \Bigg\}
\end{aligned} \tag{5.10a}$$

where:

$$a_1 = S_m \left[\frac{\partial \bar{F}}{\partial X} X \right]_s , \quad a_2 = S_m \left[\frac{\partial \bar{F}}{\partial Y} X \right]_s , \quad \ldots , \quad a_{34} = S_m \left[\frac{\partial \bar{F}}{\partial \dot{Y}} X \right]_s$$

the derivatives are evaluated at $\bar{\omega}=\bar{\omega}_s$.

Now substitute (5.4)-(5.6) into (5.10a) and (5.10b) and equate powers of μ. This leads to:

Order (μ):

$$\frac{\partial^2 X_1}{\partial s^2} - \bar{a}_3 \frac{\partial X_1}{\partial s} - \bar{a}_4 \frac{\partial Y_1}{\partial s} - \bar{a}_1 X_1 - \bar{a}_2 Y_1 = 0 \qquad (5.11a)$$

Order (μ^2):

$$\frac{\partial^2 X_2}{\partial s^2} - \bar{a}_3 \frac{\partial X_2}{\partial s} - \bar{a}_4 \frac{\partial Y_2}{\partial s} - \bar{a}_1 X_2 - \bar{a}_2 Y_2 = -2\omega_1 \frac{\partial^2 \dot{X}_1}{\partial s^2} + \bar{a}_3 \omega_1 \frac{\partial X}{\partial s}_1$$

$$+ \bar{a}_4 \omega_1 \frac{\partial Y}{\partial s}_1 + \frac{\bar{a}}{2}_5 X_1^2 + \bar{a}_6 X_1 Y_1 + \bar{a}_7 X_1 \frac{\partial X}{\partial s}_1 + \bar{a}_8 X_1 \frac{\partial Y}{\partial s}_1 + \frac{\bar{a}}{2}_9 Y_1^2$$

$$+ \bar{a}_{10} Y_1 \frac{\partial X}{\partial s}_1 + \bar{a}_{11} Y_1 \frac{\partial Y}{\partial s}_1 + \frac{\bar{a}}{2}_{12} \left[\frac{\partial X}{\partial s}_1 \right]^2 + \bar{a}_{13} \frac{\partial X}{\partial s}_1 \frac{\partial Y}{\partial s}_1$$

$$+ \frac{\bar{a}}{2}_{14} \left[\frac{\partial Y}{\partial s}_1 \right]^2 \qquad (5.12a)$$

Order (μ^3):

$$\frac{\partial^2 X_3}{\partial s^2} - \bar{a}_3 \frac{\partial X_3}{\partial s} - \bar{a}_4 \frac{\partial Y_3}{\partial s} - \bar{a}_1 X_3 - \bar{a}_2 Y_3 = -2\omega_1 \frac{\partial^2 \dot{X}_2}{\partial s^2} - 2\omega_2 \frac{\partial^2 \dot{X}_1}{\partial s^2}$$

$$- 2\frac{\partial^2 X}{\partial s \delta \tau^*}_1 - \omega_1^2 \frac{\partial^2 X}{\partial s^2}_1 + \bar{a}_3 \left(\frac{\partial X}{\partial \tau^*}_1 + \omega_2 \frac{\partial X}{\partial s}_1 + \omega_1 \frac{\partial X}{\partial s}_2 \right) + \bar{a}_4 \left(\frac{\partial Y}{\partial \tau^*}_1 + \omega_2 \frac{\partial Y}{\partial s}_1 + \omega_1 \frac{\partial Y}{\partial s}_2 \right)$$

$$+ \left(-\frac{2a}{\bar{\omega}_s^3}_3 + \frac{1}{\bar{\omega}_s^2} \frac{da}{d\bar{\omega}}_3 \right) \frac{\partial X}{\partial s}_1 + \left(-\frac{2a}{\bar{\omega}_s^3}_4 + \frac{1}{\bar{\omega}_s^2} \frac{da}{d\bar{\omega}}_4 \right) \frac{\partial Y}{\partial s}_1 + \left(-\frac{2a}{\bar{\omega}_s^3}_1 + \frac{1}{\bar{\omega}_s^2} \frac{da}{d\bar{\omega}}_1 \right) X_1$$

$$+ \left(-\frac{2a}{\bar{\omega}_s^3}_2 + \frac{1}{\bar{\omega}_s^2} \frac{da}{d\bar{\omega}}_2 \right) Y_1 + \bar{a}_5 X_1 X_2 + \bar{a}_6 (X_1 Y_2 + Y_1 X_2) + \bar{a}_9 Y_1 Y_2$$

$$+ \bar{a}_7\left\{X_1(\omega_1\frac{\partial X}{\partial s}_1 + \frac{\partial X}{\partial s}_2) + X_2\frac{\partial X}{\partial s}_1\right\} + \bar{a}_8\left\{X_1(\omega_1\frac{\partial Y}{\partial s}_1 + \frac{\partial Y}{\partial s}_2) + X_2\frac{\partial Y}{\partial s}_1\right\}$$

$$+ \bar{a}_{10}\left\{Y_1(\omega_1\frac{\partial X}{\partial s}_1 + \frac{\partial X}{\partial s}_2) + Y_2\frac{\partial X}{\partial s}_1\right\} + \bar{a}_{11}\left\{Y_1(\omega_1\frac{\partial Y}{\partial s}_1 + \frac{\partial Y}{\partial s}_2) + Y_2\frac{\partial Y}{\partial s}_1\right\}$$

$$+ \bar{a}_{12}\frac{\partial X}{\partial s}_1\frac{\partial X}{\partial s}_2 + \bar{a}_{13}(\frac{\partial X}{\partial s}_1\frac{\partial Y}{\partial s}_2 + \frac{\partial Y}{\partial s}_1\frac{\partial X}{\partial s}_2) + \bar{a}_{14}\frac{\partial Y}{\partial s}_1\frac{\partial Y}{\partial s}_2 + \frac{\bar{a}}{6}_{15}X_1^3$$

$$+ \frac{\bar{a}}{2}_{16}X_1^2Y_1 + \frac{\bar{a}}{2}_{17}X_1^2\frac{\partial X}{\partial s}_1 + \frac{\bar{a}}{2}_{18}X_1^2\frac{\partial Y}{\partial s}_1 + \frac{\bar{a}}{2}_{19}X_1Y_1^2 + \bar{a}_{20}X_1Y_1\frac{\partial X}{\partial s}_1$$

$$+ \bar{a}_{21}X_1Y_1\frac{\partial Y}{\partial s}_1 + \frac{\bar{a}}{2}_{22}X_1\left[\frac{\partial X}{\partial s}_1\right]^2 + \bar{a}_{23}X_1\frac{\partial X}{\partial s}_1\frac{\partial Y}{\partial s}_1 + \frac{\bar{a}}{2}_{24}X_1\left[\frac{\partial Y}{\partial s}_1\right]^2$$

$$+ \frac{\bar{a}}{6}_{25}Y_1^3 + \frac{\bar{a}}{2}_{26}Y_1^2\frac{\partial X}{\partial s}_1 + \frac{\bar{a}}{2}_{27}Y_1^2\frac{\partial Y}{\partial s}_1 + \frac{\bar{a}}{2}_{28}Y_1\left[\frac{\partial X}{\partial s}_1\right]^2 + \bar{a}_{29}Y_1\frac{\partial X}{\partial s}_1\frac{\partial Y}{\partial s}_1$$

$$+ \frac{\bar{a}}{2}_{30}Y_1(\frac{\partial Y}{\partial s}_1)^2 + \frac{\bar{a}}{6}_{31}\left[\frac{\partial X}{\partial s}_1\right]^3 + \frac{\bar{a}}{2}_{32}\left[\frac{\partial X}{\partial s}_1\right]^2\frac{\partial Y}{\partial s}_1 + \frac{\bar{a}}{2}_{33}\frac{\partial X}{\partial s}_1\left[\frac{\partial Y}{\partial s}_1\right]^2$$

$$+ \frac{\bar{a}}{6}_{34}\left[\frac{\partial Y}{\partial s}_1\right]^3 \qquad (5.13a)$$

Define $\bar{a}_1$ etc. by:

$$\bar{a}_1 = a_1/\ \bar{\omega}_s^2$$

The solution of equations (5.11) is:

$$X_1(s,\tau^*) = A_1(\tau^*)e^{i\bar{\Omega}_s s} + \text{complex conjugate} \qquad (5.14a)$$

$$Y_1(s,\tau^*) = \lambda A_1(\tau^*)e^{i\bar{\Omega}_s s} + \text{complex conjugate} \qquad (5.14b)$$

If these expressions are substituted into equation (5.12), it can be seen that the elimination of secular terms requires that ω_1=0. It is then possible to write the right hand side of (5.12) in the form:

$$A_1^2(\tau^*)m_1e^{2i\bar{\Omega}_s s} + |A_1|^2\frac{n}{2}_1 + \text{complex conjugate}$$

$$A_1^2(\tau^*)m_2e^{2i\bar{\Omega}_s s} + |A_1|^2\frac{n}{2}_2 + \text{complex conjugate}$$

and the solution is therefore:

$$X_2(s,\tau^*) = A_2(\tau^*)e^{i\bar{\Omega}_s s} + A_1^2(\tau^*)u_1 e^{2i\bar{\Omega}_s s}$$

$$+ |A_1(\tau^*)|^2 v_{\frac{1}{2}1} + \text{complex conjugate} \qquad (5.15a)$$

$$Y_2(s,\tau^*) = \lambda A_2(\tau^*)e^{i\bar{\Omega}_s s} + A_1^2(\tau^*)u_2 e^{2i\bar{\Omega}_s s}$$

$$+ |A_1(\tau^*)|^2 v_{\frac{1}{2}2} + \text{complex conjugate} \qquad (5.15b)$$

The process for finding u_1,u_2,v_1,v_2 is identical to that for finding u_1,u_2,v_1,v_2 in equations (5.8). The next stage in the analysis is the substitution of expressions (5.14) and (5.15) into (5.13). It is not possible to write down the solution to (5.13), but it is possible to specify a requirement for the elimination of secular terms. These terms arise from the presence of $\exp(i\bar{\Omega}_s s)$ on the right hand side of (5.13), for which the coefficients are:

$$q_1 = \gamma_1 \frac{dA_1}{d\tau^*} + A_1(\gamma_2 + \gamma_3|A_1|^2)$$

$$q_2 = \gamma_4 \frac{dA_1}{d\tau^*} + A_1(\gamma_5 + \gamma_6|A_1|^2)$$

The elimination of secular terms requires (see equation (5.9)):

$$B_1\left\{\gamma_1 \frac{dA_1}{d\tau^*} + A_1(\gamma_2+\gamma_3|A_1|^2)\right\} + B_2\left\{\gamma_4 \frac{dA_1}{d\tau^*} + A_1(\gamma_5+\gamma_6|A_1|^2)\right\} = 0$$

This relationship can be manipulated to yield the complex amplitude equation:

$$\frac{dA_1}{d\tau^*} = A_1(\eta_2 - \eta_3|A_1|^2)$$

It is possible to separate real and imaginary parts by writing:

$$A_1(\tau^*) = R(\tau^*)e^{i\theta(\tau^*)}$$

$$\eta_2 = \eta_{2r} + i\eta_{2i} \quad ; \quad \eta_3 = \eta_{3r} + i\eta_{3i}$$

which yields amplitude and phase shift equations which are analogous to equations (3.36) and (3.37):

$$\frac{dR}{d\tau}_{*} = R(\eta_{2r} - \eta_{3r}R^2) \qquad \text{Amplitude Equation} \qquad (5.16)$$

$$\frac{d\theta}{d\tau}_{*} = \eta_{2i} - \eta_{3i}R^2 \qquad \text{Phase Shift Equation} \qquad (5.17)$$

The coefficient of R in the amplitude equation corresponds to the linear growth rate $d\bar{\alpha}/d\bar{\omega}$ and for $\bar{\omega}>\bar{\omega}_s$ this is positive, since the system is becoming unstable. Therefore periodic solutions (stationary orbits) can exist for $\eta_{3r}>0$. The stability of these orbits follows from an identical argument to that adopted in Section 3.2. For stationary orbits we require:

$$\eta_{2r} - \eta_{3r}R^2 = 0$$

$$\rightarrow R = \left| \frac{\eta_{2r}}{\eta_{3r}} \right|^{1/2}$$

For $\bar{\omega}>\bar{\omega}_s$, there are two possible cases:

(1) $\eta_{3r} > 0$ $\qquad R \rightarrow \sqrt{|\eta_{2r}/\eta_{3r}|}$ as $\tau \rightarrow \infty$

The solution of (4.6) approaches a stable limit cycle of the following form as $\bar{\omega}\rightarrow\bar{\omega}_s$:

$$\Delta X(\tau) = 2\left|\frac{\eta_{2r}}{\eta_{3r}}\right|^{1/2}|\bar{\omega}-\bar{\omega}_s|^{1/2}\cos\left\{(1+O(\bar{\omega}-\bar{\omega}_s))\bar{\Omega}_s\tau\right\} + O(\bar{\omega}-\bar{\omega}_s)$$

... (5.18a)

$$\Delta Y(\tau) = 2|\lambda|\left|\frac{\eta_{2r}}{\eta_{3r}}\right|^{1/2}|\bar{\omega}-\bar{\omega}_s|^{1/2}\sin\left\{(1+O(\bar{\omega}-\bar{\omega}_s))\bar{\Omega}_s\tau+\psi_1\right\} + O(\bar{\omega}-\bar{\omega}_s)$$

...(5.18b)

$$\psi_1 = \tan^{-1}(\lambda_r/\lambda_i) \quad ; \quad \lambda = \lambda_r + \lambda_i$$

The period of this orbit is:

$$\frac{2\pi}{\bar{\Omega}_s} \left(1 + O(\omega-\bar{\omega}_s)\right)$$

(2) $\eta_{3r} < 0$ The amplitude equation (5.16) shows that $dR/d\tau^* > 0$ for all τ^*. Therefore the motion is unstable.

In order to investigate the existence of orbits at speeds below the threshold, the alternative substitution:

$$\bar{\omega} = \bar{\omega}_s - \mu^2$$

can be used. If the analysis is repeated, an identical amplitude equation to (5.16) is obtained. However, in this case the sign of the coefficient of R is reversed, since $\eta_{2r} = -(d\bar{\alpha}/d\omega) < 0$. There are two cases to consider:

(3) $\eta_{3r} > 0$ Equation (5.16) implies that $R(\tau^*) \to 0$ as $\tau \to 0$, since $dR/d\tau^* < 0$ for all R. Therefore the system moves towards its equilibrium position.

(4) $\eta_{3r} < 0$ A periodic solution is possible with:

$$R = R_c = \left| \frac{\eta_{2r}}{\eta_{3r}} \right|^{1/2}$$

However, this orbit is unstable, since for $R > R_c$, $dR/d\tau^* > 0$ and for $R < R_c$, $dR/d\tau^* < 0$. Theoretically an orbit can exist, provided $R(\tau^*=0) = R_c$, but it is unstable.

The cases (1) to (4) are shown in Figure 5.1

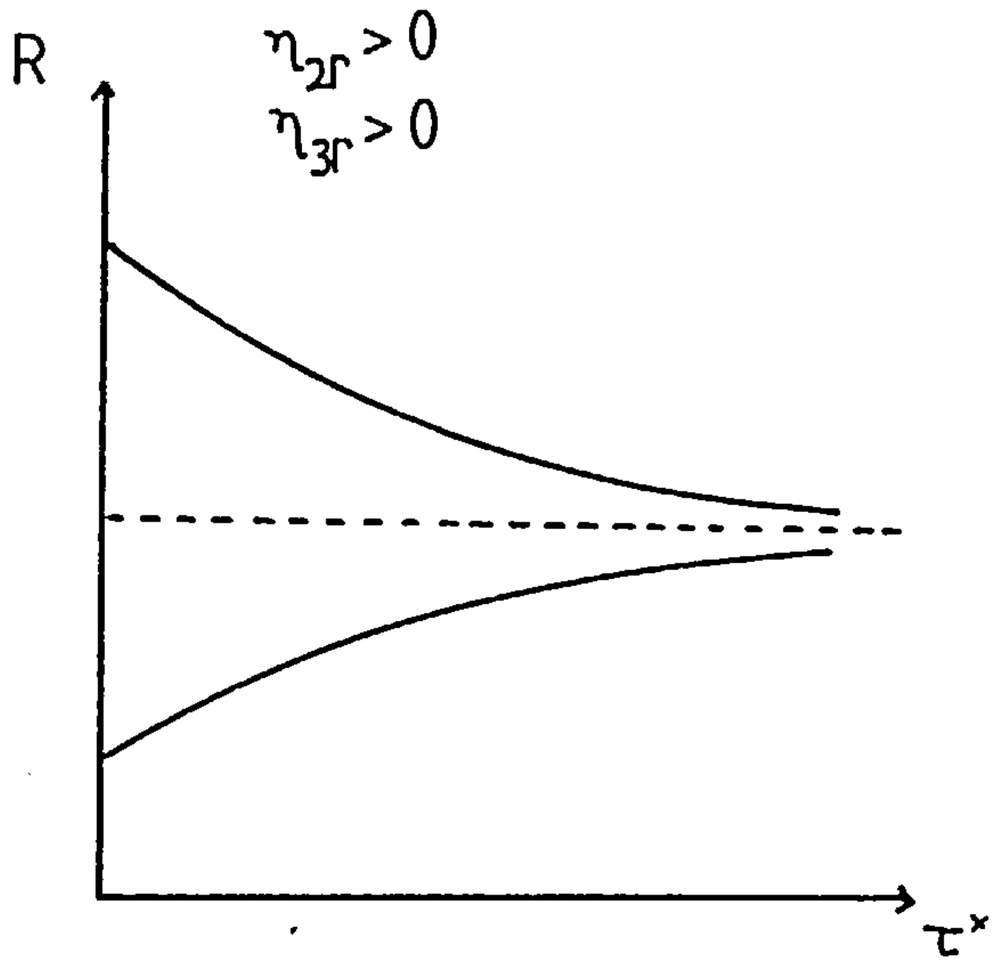

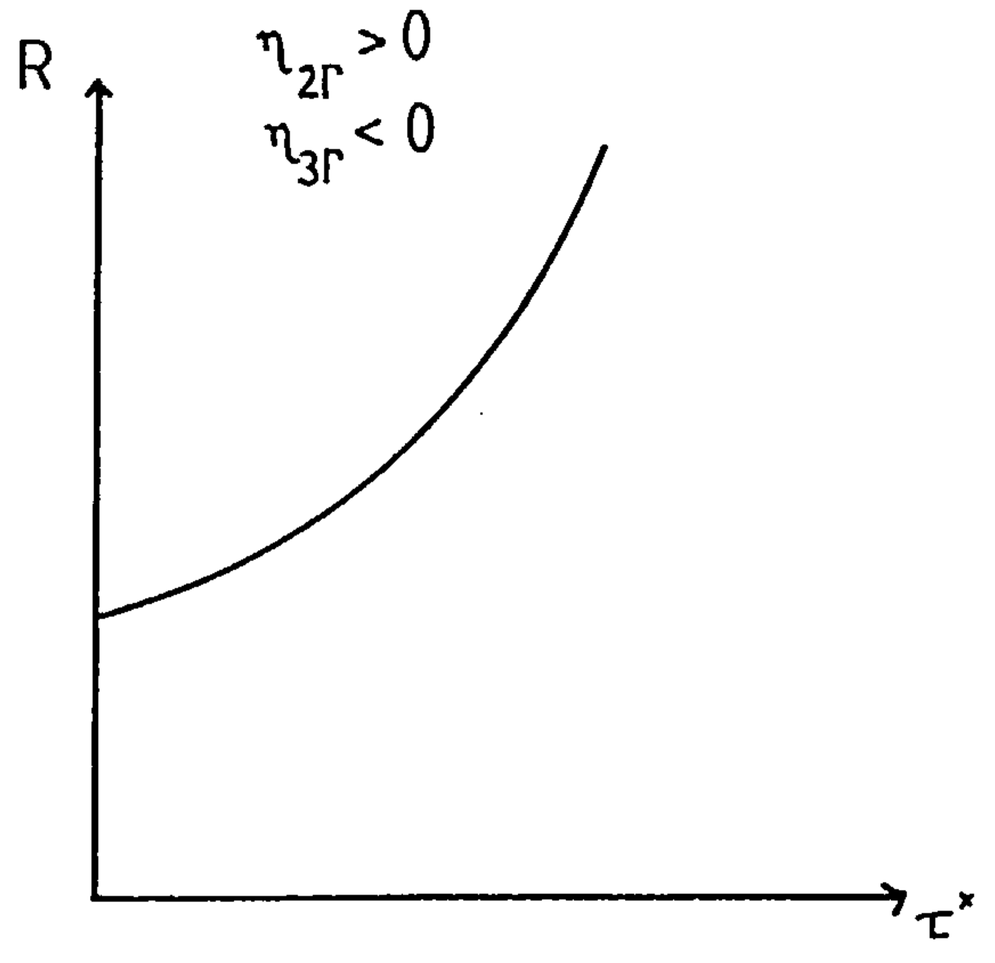

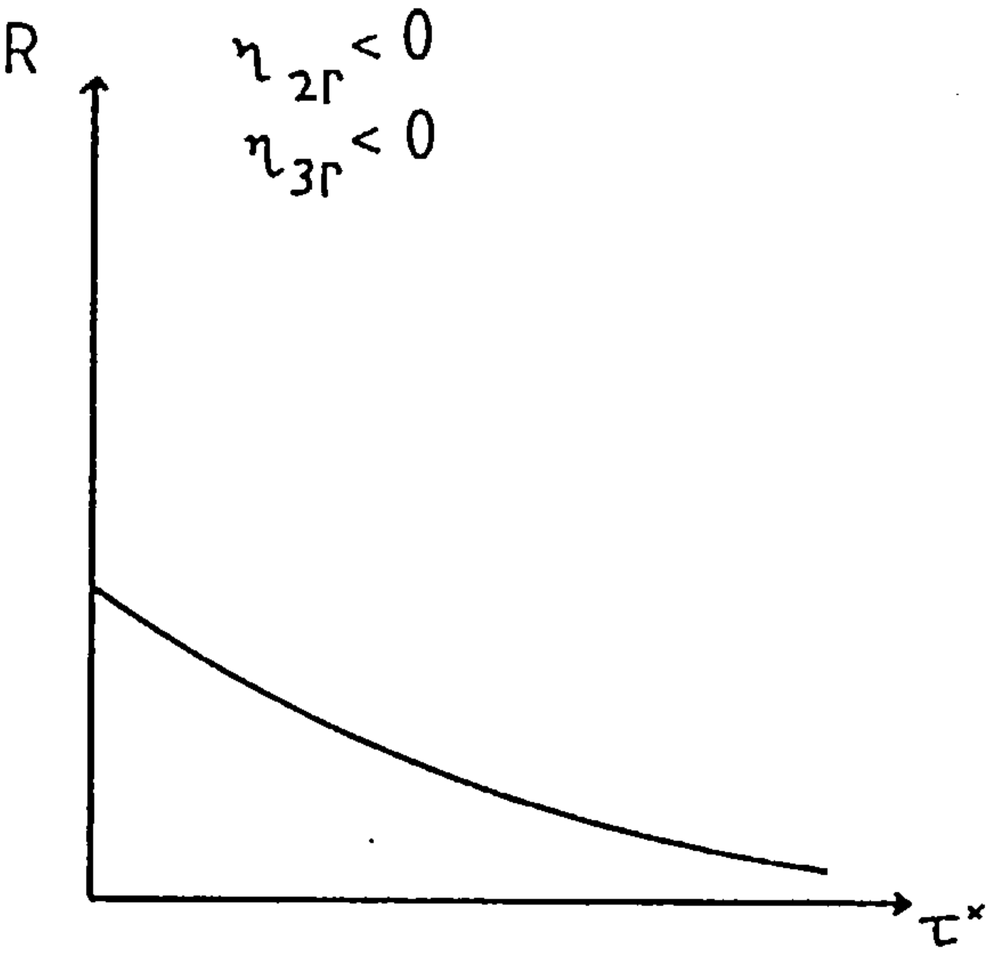

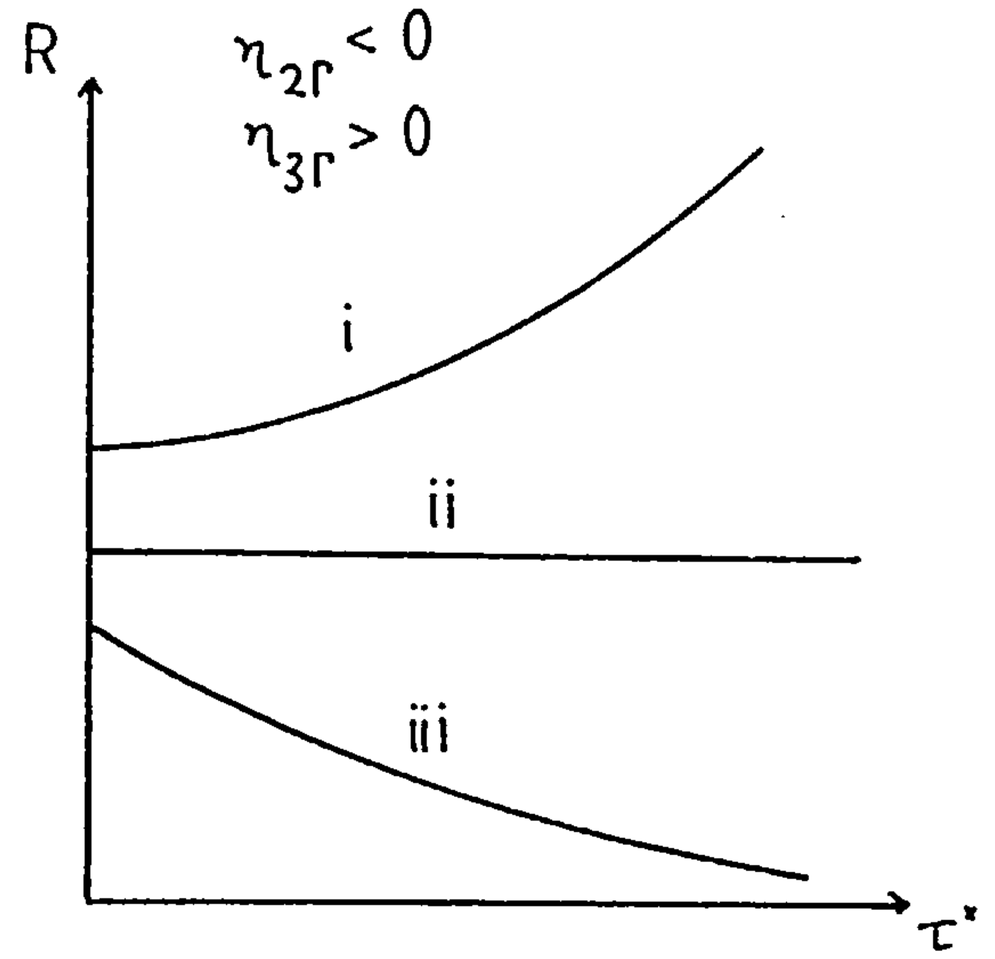

i $R(0) > R$

ii $R(0) = R$

iii $R(0) < R$

Figure 5.1 The relationship between the orbit amplitude and 'slow' time

5.2 Results

In order to carry out a detailed investigation, the values of η_{2r} and η_{3r} must be found for all possible values fo ϵ_s. As in the previous section, this is done for equilibrium positions in the range $0.01 \leqslant \epsilon_s \leqslant 0.75$. The type of nonlinear behaviour observed is governed by the value of η_{3r}. If $\eta_{3r} > 0$ then stable limit cycles exist for $\bar{\omega} > \bar{\omega}_s$, if $\eta_{3r} < 0$ then unstable limit cycles exist for $\bar{\omega} < \bar{\omega}_s$. These two types of behaviour correspond to supercritical and subcritical bifurcation respectively. The results are shown in Table 5.1. The parameter space splits into two regions which exactly match those found using Hopf bifurcation.

Region 1 $\epsilon_s \leqslant 0.14$ In this region $\eta_{3r} < 0$, therefore the behaviour is subcritical.

Region 2 $0.15 \leqslant \epsilon_s \leqslant 0.75$ In this region $\eta_{3r} > 0$, therefore the behaviour is supercritical.

Table 5.1

Results obtained by the method of multiple scales for the short bearing operating with a half film

ϵ_s	S_m	$\bar{\omega}_s$	$\bar{\Omega}_s$	σ	η_{2r}	η_{3r}	amp
0.01	31.82	2.76	0.50	11.51	0.01	-0.02	0.61
0.05	6.33	2.76	0.50	2.29	0.03	-0.07	0.67
0.10	3.11	2.74	0.50	1.13	0.06	-0.07	0.95
0.14	2.17	2.72	0.51	0.80	0.07	-0.002	5.88
0.15	2.01	2.72	0.51	0.74	0.08	0.02	2.07
0.20	1.45	2.68	0.51	0.54	0.09	0.12	0.84
0.30	0.86	2.61	0.52	0.33	0.09	0.24	0.60
0.40	0.54	2.55	0.52	0.21	0.08	0.25	0.56
0.50	0.33	2.54	0.52	0.13	0.06	0.26	0.48
0.60	0.20	2.70	0.47	0.07	0.04	0.46	0.28
0.70	0.10	3.63	0.35	0.03	0.01	1.03	0.09
0.75	0.07	9.74	0.13	0.01	.0003	1.01	0.02

$$\text{amp} = \sqrt{(\eta_{2r}/\eta_{3r})}$$

CHAPTER 6

THE APPLICATION OF THE METHOD OF AVERAGING TO THE THE EQUATIONS OF MOTION GOVERNING OIL WHIRL IN THE 'SHORT' BEARING

6.1 The application of the method of averaging

There are a number of parallels between the applications of the method of averaging and the method of multiple scales to equations (4.6). As in Chapter 5, it is necessary to modify these equations by introducing a perturbation about the threshold speed $\bar{\omega}_s$. The method of averaging utilises a similar expansion about the equlibrium point:

$$X = X_s \; ; \; Y = Y_s \; ; \; \dot{X} = 0 \quad ; \; \dot{Y} = 0 \quad ; \; \bar{\omega} = \bar{\omega}_s$$

and in addition assumes the existence of monofrequency oscillations. The existence of small, stationary, periodic orbits in the region $\bar{\omega}>\bar{\omega}_s$ will be investigated by expressing the rotor speed in the form:

$$\bar{\omega} = \bar{\omega}_s + \mu^2 \tag{6.1}$$

Suppose that there exists a solution of the form:

$$\Delta X = \mu a\cos\psi+\mu^2 u_1(a,\psi)+\mu^3 u_2(a,\psi) \; +.... \tag{6.2a}$$

$$\Delta Y = \mu r a\cos(\psi+\xi)+\mu^2 v_1(a,\psi)+\mu^3 v_2(a,\psi)+.... \tag{6.2b}$$

such that r and ξ are constants denoting the shape and phase of the elliptical orbits of the first approximation. a and ψ are given by:

$$\frac{da}{d\tau} = \mu A_1(a)+\mu^2 A_2(a)+.... \tag{6.3}$$

$$\frac{d\psi}{d\tau} = \bar{\Omega}_s+\mu\psi_1(a)+\mu^2\psi_2(a)+.... \tag{6.4}$$

Once again, it is a consideration of bifurcation theory which suggests the above forms for (6.1)-(6.4). The arguments are similar to those adopted in Sections 3.3 and 5.1. Since the above forms are identical to (3.43)-(3.46), the derivatives are:

$$\frac{d\Delta X}{d\tau} = \mu(-\bar{\Omega}_s a\sin\psi) + \mu^2(A_1\cos\psi+\bar{\Omega}_s\frac{\partial u}{\partial\psi}_1-\psi_1 a\sin\psi)$$

$$+ \mu^3(A_1\frac{\partial u}{\partial a}_1+A_2\cos\psi+\bar{\Omega}_s\frac{\partial u}{\partial\psi}_2+\psi_1\frac{\partial u}{\partial\psi}_1-\psi_2 a\sin\psi) \qquad (6.5a)$$

$$\frac{d^2\Delta X}{d\tau^2} = \mu(-\bar{\Omega}_s^2 a\cos\psi) + \mu^2(\bar{\Omega}_s^2\frac{\partial^2 u}{\partial\psi^2}_1-2\bar{\Omega}_s a\psi_1\cos\psi -2\bar{\Omega}_s A_1\sin\psi)$$

$$+ \mu^3(\bar{\Omega}_s^2\frac{\partial^2 u}{\partial\psi^2}_2+2\bar{\Omega}_s\psi_1\frac{\partial^2 u}{\partial\psi^2}_1-a\psi_1^2\cos\psi-2\bar{\Omega}_s\psi_2 a\cos\psi+A_1\frac{dA}{da}_1\cos\psi$$

$$-A_1\frac{d\psi}{da}_1 a\sin\psi+2\Omega_s A_1\frac{\partial^2 u}{\partial a\partial\psi}_1-2\psi_1 A_1\sin\psi-2\Omega_s A_2\sin\psi) \qquad (6.6a)$$

Similar expressions exist for $d\Delta Y/d\tau$ and $d^2\Delta Y/d\tau^2$:- (6.5b) and (6.6b)

Expressions (6.2), (6.5) and (6.6) are now substituted into (5.10) in order to equate powers of μ. As in the previous section, only the results for (5.10a) are given here, where the results from (5.10b) are referred to later in the text, they will be denoted by the suffix 'b'. The following abbreviations are used.

$$c_1 = \cos\psi \quad ; \quad s_1 = \sin\psi$$

$$c_2 = \cos(\psi+\xi) \quad ; \quad s_2 = \sin(\psi+\xi)$$

Order (μ):

$$-\bar{\Omega}_s^2 a c_1 = -\bar{a}_3\bar{\Omega}_s a s_1 - \bar{a}_4\bar{\Omega}_s r a s_2 + \bar{a}_1 a c_1 + \bar{a}_2 r a c_2 \qquad (6.7a)$$

Order (μ^2)

$$\bar{\Omega}_s^2\frac{\partial^2 u}{\partial\psi^2}_1 - 2\bar{\Omega}_s a\psi_1 c_1 - 2\bar{\Omega}_s A_1 s_1 = \bar{a}_3(A_1 c_1 - \psi_1 a s_1 + \bar{\Omega}_s\frac{\partial u}{\partial\psi}_1)$$

$$+ \bar{a}_4(A_1 r c_2 - \psi_1 r a s_2 + \bar{\Omega}_s\frac{\partial v}{\partial\psi}_1) + \bar{a}_1 u_1 + \bar{a}_2 v_1 + \frac{\bar{a}}{2}_5 a^2 c_1^2$$

$$+ \bar{a}_6 r a^2 c_1 c_2 - \bar{a}_7\Omega_s a^2 c_1 s_1 - \bar{a}_8\bar{\Omega}_s r a^2 c_1 s_2 + \frac{\bar{a}}{2}_9 r^2 a^2 c_2^2 - \bar{a}_{10} r a^2 c_2 s_1$$

$$- \bar{a}_{11} r^2 a^2 \bar{\Omega}_s c_2 s_2 + \frac{\bar{a}}{2}_{12} \bar{\Omega}_s^2 a^2 s_1^2 + \bar{a}_{13} \bar{\Omega}_s^2 r a^2 s_1 s_2 + \frac{\bar{a}}{2}_{14} \bar{\Omega}_s^2 r^2 a^2 s_2^2$$

...(6.8a)

Order (μ^3)

$$\bar{\Omega}_s^2 \frac{\partial u}{\partial \psi^2}_2 + 2\bar{\Omega}_s \psi_1 \frac{\partial u}{\partial \psi^2}_1 - a\psi_1^2 c_1 - 2\bar{\Omega}_s \psi_2 a c_1 + A_1 \frac{dA}{da}_1 c_1 - A_1 \frac{d\psi}{da}_1 a s_1$$

$$+ 2\bar{\Omega}_s A_1 \frac{\partial^2 u}{\partial a \partial \psi}_1 - 2\psi_1 A_1 s_1 - 2\bar{\Omega}_s A_2 s_1 = \frac{1}{\bar{\omega}^2} \Big\{ a_3 (A_2 c_1 + \bar{\Omega}_s \frac{\partial u}{\partial \psi}_2 + A_1 \frac{\partial u}{\partial a}_1$$

$$+ \psi_1 \frac{\partial u}{\partial \psi}_1 - \psi_2 a s_1) - \frac{da}{d\bar{\omega}}_3 \bar{\Omega}_s a s_1 + a_4 (A_2 r c_2 + \bar{\Omega}_s \frac{\partial v}{\partial \psi}_2 + A_1 \frac{\partial v}{\partial a}_1 + \psi_1 \frac{\partial v}{\partial \psi}_1$$

$$- \psi_2 r a s_2) - \frac{da}{d\bar{\omega}}_4 \bar{\Omega}_s r a s_2 + a_1 u_2 + \frac{da}{d\bar{\omega}}_1 a c_1 + a_2 v_2 + \frac{da}{d\bar{\omega}}_2 r a c_2 \Big\}$$

$$+ \frac{\bar{a}}{2}_5 (2 a u_1 c_1) + \bar{a}_6 (a v_1 c_1 + r a u_1 c_2) + \frac{\bar{a}}{2}_9 (2 r a v_1 c_2)$$

$$+ a_7 (a c_1 (A_1 c_1 + \Omega_s \frac{\partial u}{\partial \psi}_1 - \psi_1 a s_1) - a \Omega_s u_1 s_1)$$

$$+ \bar{a}_8 (a c_1 (A_1 r c_2 + \bar{\Omega}_s \frac{\partial v}{\partial \psi}_1 - \psi_1 r a s_2) - r a \bar{\Omega}_s u_1 s_2)$$

$$+ \bar{a}_{10} (r a c_2 (A_1 c_1 + \bar{\Omega}_s \frac{\partial u}{\partial \psi}_1 - \psi_1 a s_1) - a \bar{\Omega}_s v_1 s_1)$$

$$+ \bar{a}_{11} (r a c_2 (A_1 r c_2 + \bar{\Omega}_s \frac{\partial v}{\partial \psi}_1 - \psi_1 r a s_2) - r a \bar{\Omega}_s v_1 s_2)$$

$$+ \frac{\bar{a}}{2}_{12} (-2\bar{\Omega}_s a s_1 (A_1 c_1 + \bar{\Omega}_s \frac{\partial u}{\partial \psi}_1 - \psi_1 a s_1)$$

$$+ a_{13} (-\Omega_s a s_1 (A_1 r c_2 + \Omega_s \frac{\partial v}{\partial \psi}_1 - \psi_1 r a s_2) - \Omega_s r a s_2 (A_1 c_1 + \Omega_s \frac{\partial u}{\partial \psi}_1 - \psi_1 a s_1))$$

$$+ \frac{\bar{a}}{2}_{14} (-2\bar{\Omega}_s r a s_2 (A_1 r c_2 + \bar{\Omega}_s \frac{\partial v}{\partial \psi}_1 - \psi_1 r a s_2)$$

$$+ \frac{\bar{a}}{6}_{15} a^3 c_1^3 + \frac{\bar{a}}{2}_{16} r a^3 c_1^2 c_2 + \frac{\bar{a}}{2}_{17} (-a^3 \bar{\Omega}_s c_1^2 s_1) + \frac{\bar{a}}{2}_{18} (-a^3 \bar{\Omega}_s r c_1^2 s_2)$$

$$+ \frac{\bar{a}}{2}_{19} (a^3 r^2 c_1 c_2^2) + \bar{a}_{20} (-\bar{\Omega}_s r a^3 c_1 c_2 s_1) + \bar{a}_{21} (-\bar{\Omega}_s^2 r\ a^3 c_1 c_2 s_2)$$

$$+ \frac{\bar{a}}{2}_{22}(\bar{\Omega}_s^2 a^3 c_1 s_1^2) + \bar{a}_{23}(\bar{\Omega}_s^2 r a^3 c_1 s_1 s_2) + \frac{\bar{a}}{2}_{24}(\bar{\Omega}_s^2 r^2 a^3 c_1 s_2^2)$$

$$+ \frac{\bar{a}}{6}_{25}(r^3 a^3 c_2^3) + \frac{\bar{a}}{2}_{26}(-\bar{\Omega}_s r^2 a^3 c_2^2 s_1) + \frac{\bar{a}}{2}_{27}(-\bar{\Omega}_s r^3 a^3 c_2^2 s_2)$$

$$+ \frac{\bar{a}}{2}_{28}(\bar{\Omega}_s^2 r a^3 c_2 s_1^2) + \bar{a}_{29}(\bar{\Omega}_s^2 r^2 a^3 c_2 s_1 s_2) + \frac{\bar{a}}{2}_{30}(\bar{\Omega}_s^2 r^3 a^3 c_2 s_2^2)$$

$$+ \frac{\bar{a}}{6}_{31}(-\bar{\Omega}_s^3 a^3 s_1^3) + \frac{\bar{a}}{6}_{32}(-\bar{\Omega}_s^3 r a^3 s_1^2 s_2) + \frac{\bar{a}}{2}_{33}(-\bar{\Omega}_s^3 r^2 a^3 s_1 s_2^2)$$

$$+ \frac{\bar{a}}{6}_{34}(-\bar{\Omega}_s^3 r^3 a^3 s_2^3)$$

$$- \frac{2}{\bar{\omega}^3}\left\{-a_3 \bar{\Omega}_s a s_1 - \bar{a}_4 \Omega_s r a s_2 + a_1 a c_1 + a_2 r a c_2\right\} \qquad (6.9a)$$

Consider the $O(\mu)$ expressions, and equate terms in $\cos\psi, \sin\psi$ to obtain:

$$-\frac{\bar{\Omega}_s^2}{r} = -\bar{a}_4 \bar{\Omega}_s \sin\xi + \frac{\bar{a}_1}{r} + \bar{a}_2 \cos\xi$$

$$0 = -\frac{\bar{a}_1}{r}\bar{\Omega}_s - \bar{a}_4 \bar{\Omega}_s \cos\xi - \bar{a}_2 \sin\xi$$

$$-\bar{\Omega}_s^2 \cos\xi = -\bar{b}_4 \bar{\Omega}_s \sin\xi + \frac{\bar{b}_1}{r} + \bar{b}_2 \cos\xi$$

$$-\bar{\Omega}_s^2 \sin\xi = -\frac{\bar{b}_3}{r}\bar{\Omega}_s - \bar{b}_4 \bar{\Omega}_s \cos\xi - \bar{b}_2 \sin\xi$$

Two of these equations are redundant, the remaining pair can be solved to find r and ξ:

$$r = \frac{-\bar{a}_1 - \bar{\Omega}_s^2}{-a_4 \Omega_s \sin\xi + a_2 \cos\xi}$$

$$\tan\xi = \frac{(-\bar{b}_2 - \bar{\Omega}_s)(-\bar{a}_1 - \bar{\Omega}_s) - \bar{a}_2 \bar{b}_1}{(-\bar{a}_1 - \bar{\Omega}_s^2)(-\bar{b}_4 \bar{\Omega}_s) - \bar{b}_1 \bar{a}_4 \bar{\Omega}_s}$$

The presence of terms involving $\cos\psi$ and $\sin\psi$ in (6.8) can lead to the appearance of secular terms in u_1 and v_1; in order to suppress them it is

necessary to equate the coefficients of $\cos\psi$ and $\sin\psi$ to zero. This can be achieved by putting:

$$A_1 = \psi_1 = 0 \tag{6.10}$$

The solutions of (6.8) can be written:

$$u_1 = p_1+q_1\cos 2\psi+r_1\sin 2\psi \quad ; \quad v_1 = p_2+q_2\cos 2\psi+r_2\sin 2\psi$$

The p_i, q_i and r_i are all functions of a^2. Result (6.10) leads to a considerable simplification of (6.9). These equations can now be written:

$$\bar{\Omega}_s^2\frac{\partial^2 u_2}{\partial\psi^2}-\bar{\Omega}_s\bar{a}_1\frac{\partial u_2}{\partial\psi}-\bar{\Omega}_s\bar{a}_2\frac{\partial v_2}{\partial\psi}-\bar{a}_3u_2-\bar{a}_4v_2 =$$

$$\cos\psi(2\bar{\Omega}_s\psi_2 a+\bar{a}_1A_2+\bar{a}_2A_2r\cos\xi-\bar{a}_2\psi_2 ra\sin\xi+f_1(a))$$

$$+\ \sin\psi(2\bar{\Omega}_sA_2-\bar{a}_1\psi_2 a-\bar{a}_2A_2r\sin\xi-\bar{a}_2\psi_2 ra\cos\xi+f_2(a))$$

$$+\ \text{higher harmonics} \tag{6.11a}$$

$$\bar{\Omega}_s^2\frac{\partial^2 v_2}{\partial\psi^2}-\bar{\Omega}_s\bar{b}_1\frac{\partial u_2}{\partial\psi}-\bar{\Omega}_s\bar{b}_2\frac{\partial v_2}{\partial\psi}-\bar{b}_3u_2-\bar{b}_4v_2 =$$

$$\cos\psi(2\bar{\Omega}_s\psi_2 ra\cos\xi+2\bar{\Omega}_srA_2\sin\xi+\bar{b}_1A_2+\bar{b}_2A_2r\cos\xi-\bar{b}_2\psi_2 ra\sin\xi+f_3(a))$$

$$+\ \sin\psi(2\bar{\Omega}_sA_2r\cos\xi-2\bar{\Omega}_s\psi_2 ra\sin\xi-\bar{b}_1\psi_2 a-\bar{b}_2A_2r\sin\xi-\bar{b}_2\psi_2 ra\cos\xi+f_4(a))$$

$$+\ \text{higher harmonics} \tag{6.11b}$$

The terms f_1 to f_4 are formed by the product of u_1 and v_1 with powers of $\cos\psi$, $\sin\psi$, $\cos(\psi+\xi)$ and $\sin(\psi+\xi)$. It is possible to write:

$$f_i(a) = g_i(a)+h_i(a^3)$$

where the g_i and h_i are functions of a and a^3 respectively. Before proceeding to the next stage of the analysis, it is necessary to introduce an elementary result from the theory of ordinary differential equations (Cohen (1972)).

Lemma

Given a pair of ordinary differential equations:

$$\frac{d^2x}{d\tau^2}-a_1\frac{dx}{d\tau}-a_2\frac{dy}{d\tau}-a_3x-a_4y = a\cos\tau+b\sin\tau$$

$$\frac{d^2y}{d\tau^2}-b_1\frac{dx}{d\tau}-b_2\frac{dy}{d\tau}-b_3x-b_4y = c\cos\tau+d\sin\tau$$

the condition for the elimination of secular terms in x and y is:

$$B_{1r}a+B_{1c}b+B_{2r}c+B_{2c}d = 0$$

$$-B_{1r}b+B_{1c}a-B_{2r}d+B_{2c}c = 0$$

where $B_{1r},B_{2r},B_{1c},B_{2c}$ are linear functions of $a_1 \ldots b_4$. It is a straightforward but tedious process to find them (this result is analogous to (5.9)).This lemma can be applied to (6.11) and the conditions for the elimination of secular terms in u_2 and v_2 become:

$$\Psi_2 a\eta_1+A_2\eta_2 =$$

$$-B_{1r}g_1-B_{1c}g_3-B_{2r}g_5-B_{2c}g_7-B_{1r}g_2-B_{1c}g_4-B_{2r}g_6-B_{2c}g_8 \qquad (6.12a)$$

$$\Psi_2 a\eta_3+A_2\eta_4 =$$

$$B_{1r}g_3-B_{1c}g_1+B_{2r}g_7-B_{2c}g_5+B_{1r}g_4-B_{1c}g_2+B_{2r}g_8-B_{2c}g_6 \qquad (6.12b)$$

where, η_1 to η_4 are all functions of $a_1 \ldots b_4, r, \xi, \bar{\Omega}_S$. Equations (6.12) can be written in the form:

$$\eta_1\Psi_2 a+\eta_2 A_2 = \mu_1 a+\mu_2 a^3$$

$$\eta_3\Psi_2 a+\eta_4 A_2 = \mu_3 a+\mu_4 a^3$$

Solving gives:

$$\psi_2 a = \frac{(\mu_1 a+\mu_2 a^3)\eta_4-(\mu_3 a+\mu_4 a^3)\eta_2}{\eta_1\eta_4-\eta_2\eta_3} \qquad (6.13)$$

$$A_2 = \frac{(\mu_1 a+\mu_2 a^3)\eta_3-(\mu_3 a+\mu_4 a^3)\eta_1}{\eta_3\eta_2-\eta_1\eta_4} \qquad (6.14)$$

It is possible to write (6.14) in the form:

$$A_2 = a(\kappa_1-a^2\kappa_2) \qquad (6.15)$$

For the existence of periodic orbits up to $O(\mu^3)$ (see the discussion at the end of Section 6.3), we require $A_2=0$. Also, since in general $\kappa_1>0$, we require $\kappa_2>0$. In this case stationary orbits exist for:

$$a^2 = a_e^2 = \frac{\kappa_1}{\kappa_2}$$

The orbits are given by:

$$\Delta X = \mu a_e \cos\psi \quad ; \quad \Delta Y = \mu r a_e \cos(\psi+\xi) \qquad (6.16)$$

The stability of these orbits is guaranteed, since:

$$a > a_e \rightarrow A_2 < 0 \rightarrow \frac{da}{d\tau} < 0$$

$$a < a_e \rightarrow A_2 > 0 \rightarrow \frac{da}{d\tau} > 0$$

In order to examine the existence of whirl orbits at speeds just below the threshold speed, put

$$\bar{\omega} = \bar{\omega}_s - \mu^2$$

Reworking the analysis leads to an identical equation to (6.15). In this case, however, $\kappa_1<0$ in general. Consequently, the condition for the

existence of stationary orbits becomes $\kappa_2<0$. Clearly these orbits cannot be stable.

The method of averaging displays four types of behaviour, which are identical to those observed in the case of multiple scaling:

$\bar{\omega} > \bar{\omega}_s$

(1) $\kappa_1 > 0$, $\kappa_2 > 0$. Stable whirl orbits of type (6.16).

(2) $\kappa_1 > 0$, $\kappa_2 < 0$. The system is completely unstable.

$\bar{\omega} < \bar{\omega}_s$

(3) $\kappa_1 < 0$, $\kappa_2 > 0$. The system moves towards an equilibrium point.

(4) $\kappa_1 < 0$, $\kappa_2 < 0$. Unstable whirl orbits exist.

6.2 Results

The results are shown in Table 6.1. They are in exact agreement with those obtained by Hopf bifurcation and multiple scaling. As before, the parameter space can be split into two regions.

Region 1 $\epsilon_s \leq 0.14$ Unstable limit cycles exist for $\bar{\omega}<\bar{\omega}_s$.

Region 2 $0.15 \leq \epsilon_s \leq 0.75$ Stable limit cycles exist for $\bar{\omega}>\bar{\omega}_s$.

6.3 Comparison with the results obtained by Lund

The initial motivation for the work described in this chapter was the failure to obtain agreement for the short bearing half film model between the results obtained by Hopf bifurcation and multiple scaling, and those obtained by Lund (1966) using a method of averaging. In order to introduce a small parameter into the system of equations (4.6), Lund relies on the concept of a small error from a computed solution. In several instances this method gives

Table 6.1

Results obtained by the method of averaging for the short bearing operating with a half film

ϵ_s	$\bar{\omega}_s$	$\bar{\Omega}_s$	σ	r	ξ°	κ_1	κ_2	a
0.01	2.76	0.500	11.51	-1.00	89.6	0.0069	-0.0047	1.2196
0.05	2.76	0.501	2.29	-1.00	88.2	0.0333	-0.0187	1.3362
0.1	2.74	0.503	1.13	-0.99	86.2	0.0601	-0.0165	1.9088
0.14	2.72	0.506	0.80	-0.97	84.4	0.0746	-0.0006	11.7668
0.15	2.72	0.506	0.74	-0.97	84.0	0.0773	0.0045	4.1438
0.2	2.68	0.511	0.54	-0.95	81.4	0.0858	0.0303	1.6834
0.30	2.61	0.519	0.33	-0.91	74.8	0.0863	0.0608	1.1918
0.40	2.55	0.524	0.21	-0.88	65.8	0.0762	0.0613	1.1156
0.50	2.54	0.515	0.13	-0.87	54.2	0.0596	0.0637	0.9670
0.60	2.70	0.474	0.07	-0.92	40.0	0.0360	0.1141	0.5614
0.70	3.63	0.345	0.03	-1.04	22.1	0.0088	0.2575	0.1850
0.75	9.74	0.127	0.01	-1.15	6.9	0.0003	0.2543	0.0332

fundamentally different results from those found by the methods adopted here. Since the method used in this thesis is restricted in its validity to rotor speeds close to the threshold, it is not possible to confirm evidence of hysteresis found by Lund; however it is of interest to make a comparison with his results, wherever it is possible to do so. In order to do this, the author first carried out Lund's analysis to confirm the accuracy of his results.

Figure 6.1 compares the predicted response of the journal to a small change in the rotor speed from the threshold, as found by this work and by Lund. For each value of σ there is a corresponding threshold speed and equilibrium eccentricity ratio, where the operation line crosses the stability borderline. Results are shown for four such values of σ; since the linear theory used to calculate $\bar{\omega}_s$ and ϵ_s is common to both methods, it is possible to make a comparison. The behaviour close to the threshold speed is shown by the direction of the slope of the amplitude/rotor speed curve. A line sloping to the right indicates the existence of whirl orbits above the threshold speed; a line sloping to the left indicates their existence for $\bar{\omega}<\bar{\omega}_s$. Figure 6.1 shows that for very small eccentricities (ϵ_s=0.051) there is agreement on the existence of whirl orbits at speeds below the threshold, but disagreement on stability. For medium eccentricities (ϵ_s=0.251 and ϵ_s=0.450) there is complete agreement with Lund's results, whereas for higher eccentricities (ϵ_s=0.600) the two methods disagree as to whether limit cycles exist at speeds above or below the threshold speed.

The stability of Lund's whirl orbits was originally found by forming the variational equations from the averaged equations of motion. This method is clearly anomalous in that it predicts stable orbits in the subcritical region, e.g for σ=2.24. An alternative approach is possible, based on forming the variational equations from the original equations of motion (Lund and

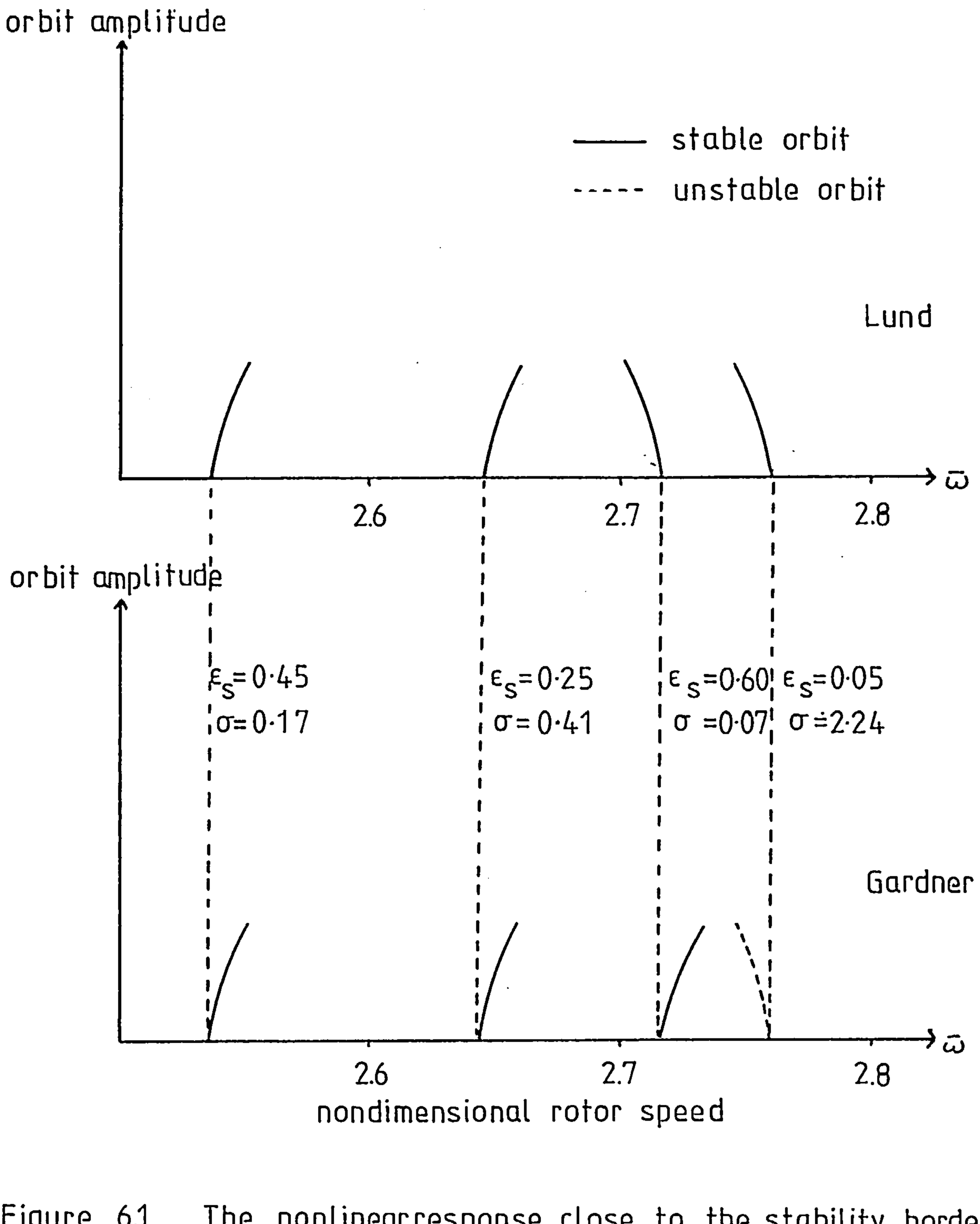

Figure 6.1 The nonlinearresponse close to the stability borderline:- comparison of the results obtained by two different applications of the method of averaging

Nielsen (1981)). It was the author's original intention to examine this alternative course as a possible clue to the reasons for the discrepancies in the results obtained by the two 'different' methods of averaging. However, this was abandoned when it became clear that the methods were in disagreement not only over stability, but also over the direction of bifurcation in the case of σ=0.07. Here Lund's method predicts small stable whirl orbits below the threshold speed well into the supercritical region, contrary to the Hopf bifurcation results. The author's method was subsequently vindicated by numerical integration (see Chapter 7).

No satisfactory explanation has, as yet, been found for the existing discrepancies. It is felt, however, that if the anomalies within the Lund method could be eliminated, it might well prove a powerful tool in the analysis of nonlinear rotor behaviour, since it has two important advantages over the method adopted in this thesis.

(1) It is not restricted in its validity to values of $\bar{\omega}$ close to $\bar{\omega}_s$.

(2) It is relatively simple to apply and does not require the calculation of second and third order derivatives.

CHAPTER 7

THE APPLICATION OF NUMERICAL INTEGRATION TO THE EQUATIONS OF MOTION GOVERNING OIL WHIRL IN THE 'SHORT' BEARING AND A DISCUSSION OF THE RESULTS OBTAINED BY NONLINEAR TECHNIQUES

7.1 Numerical integration of the equations of motion

In order to confirm the results of the previous three sections and to identify any other periodic behaviour which might occur as $\bar{\omega}$ changes, the equations of motion (4.6) were integrated numerically using standard library routines developed by the Numerical Algorithm Group (NAG libraries). These routines integrate a series of first order, nonlinear, ordinary differential equations (equations (4.15)) using a variable order, variable step Adams' method (Hall and Watt (1976)). The programs were run on the University of Leeds Amdahl V7 computer and the results displayed visually by means of a Calcomp graph plotter.

The approach adopted was to follow the development of solutions as $\bar{\omega}$ increased for two values of the system parameter, whose corresponding operation lines crossed the stability borderline in the two different regions identified by analytical methods. The values chosen were σ=0.06 and σ=2.0 (see Section 4.3 and Figure 4.6). Particular attention was paid to the effect on the subsequent motion of the starting position of the journal centre (ϵ_0, φ_0). Several values of σ were, in fact, investigated in order to eliminate any special phenomena peculiar to the two chosen values. None were observed. The results of the analysis are shown in Figures 7.1-7.3 and summarised in Table 7.1.

Figure 7.1 shows the behaviour for a system operating with σ=2.0, crossing the stability borderline in the subcritical region. At values of $\bar{\omega}$ well below the threshold value of 2.76, the system is stable, although the time taken for convergence to the equilibrium position grows with increasing $\bar{\omega}$ (Figures 7.1a and 7.1b). The behaviour as $\bar{\omega}$ approaches $\bar{\omega}_s$ depends on the initial position. Close to the equilibrium point the system is stable, although convergence is slow (Figure 7.1c). For values of ϵ_0 and φ_0 further away from

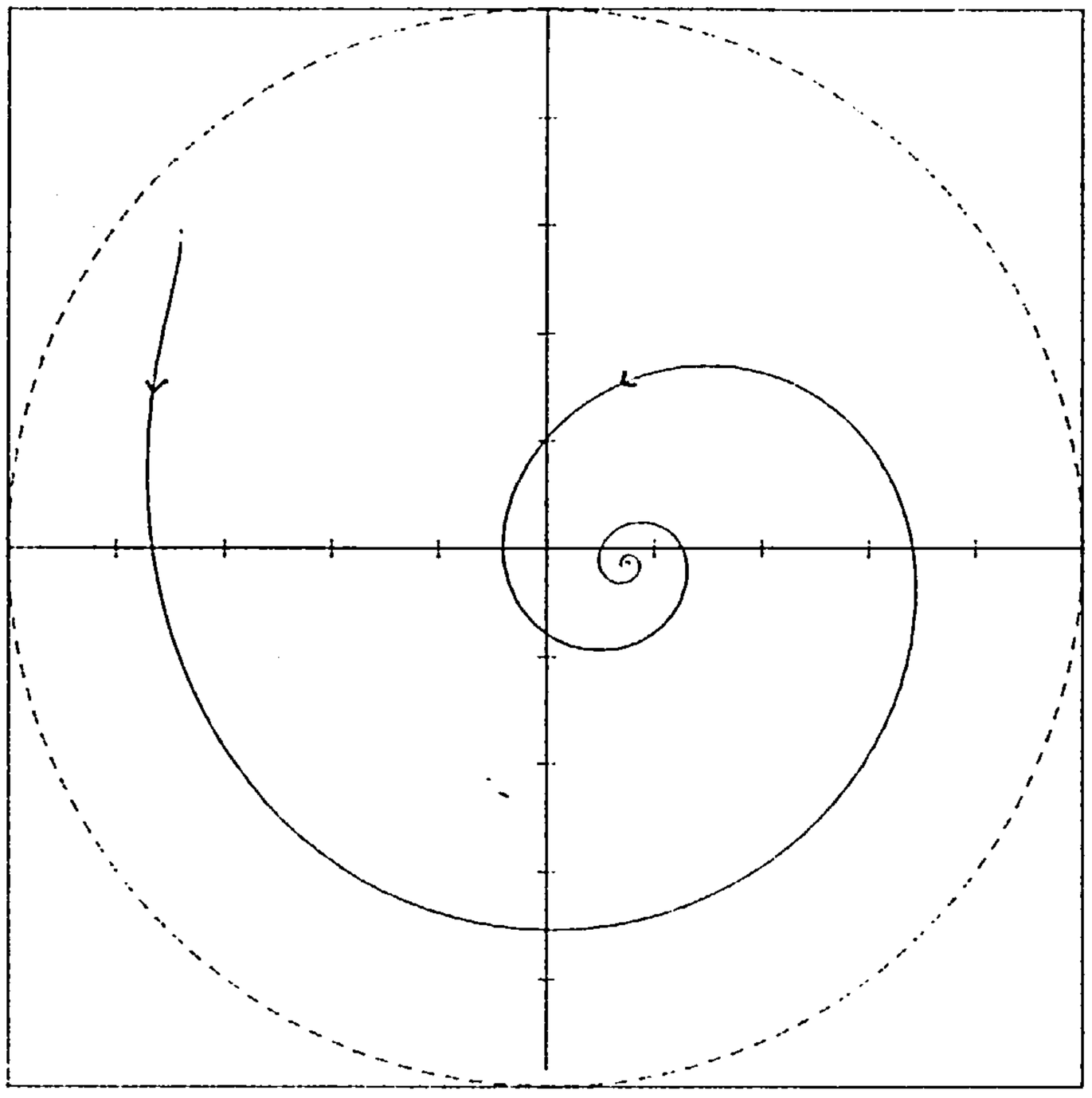

Figure 7.1a

$\sigma = 2.0 \quad \varpi = 1.0$

$\epsilon_o = 0.9 \quad \phi_o = 4.0$

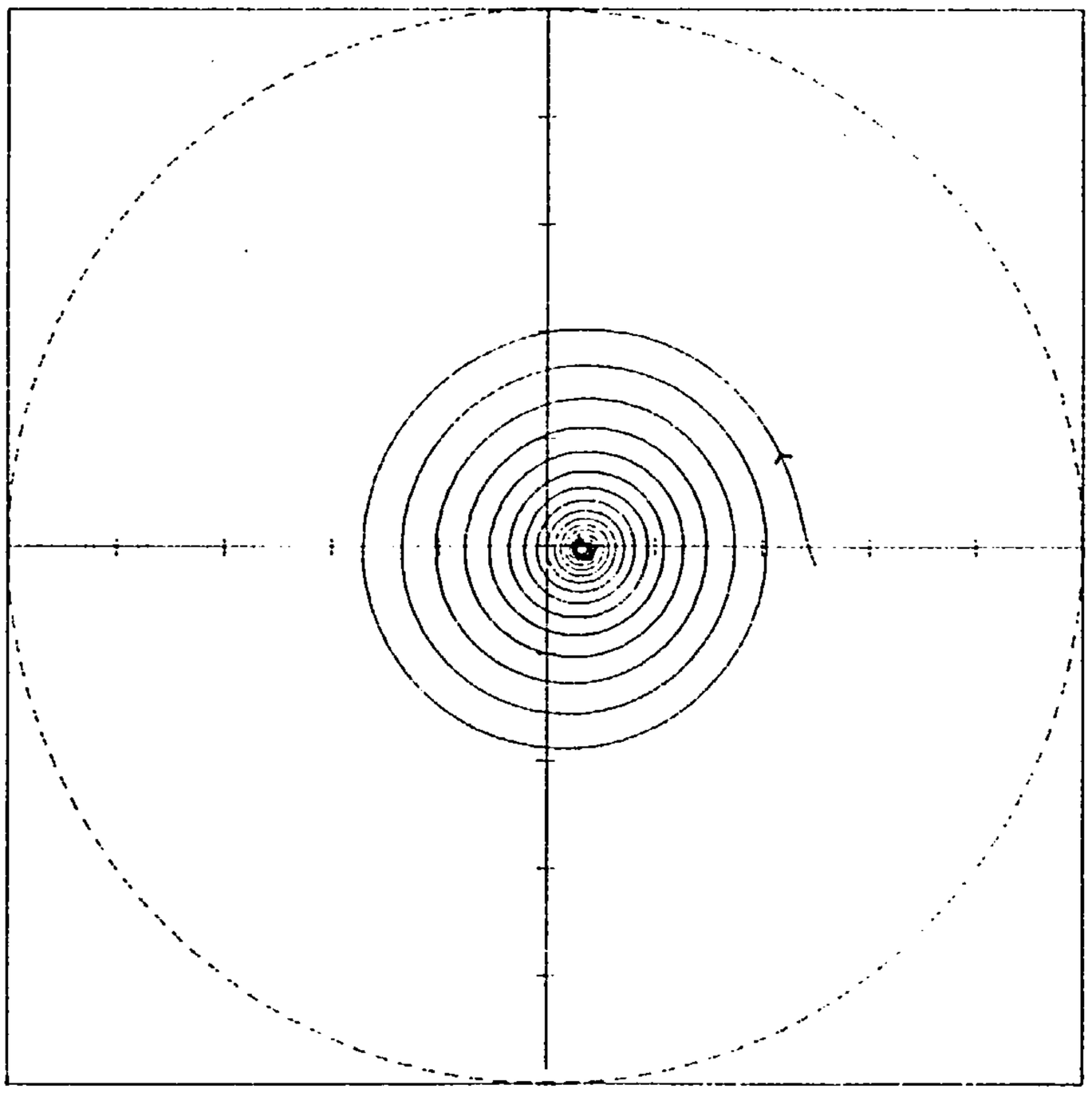

Figure 7.1b

$\sigma = 2.0 \quad \varpi = 2.3$

$\epsilon_o = 0.5 \quad \phi_o = 1.5$

Figure 7.1c

$\sigma = 2.0$ $\varpi = 2.65$

$\epsilon_0 = 0.1$ $\phi_0 = 1.0$

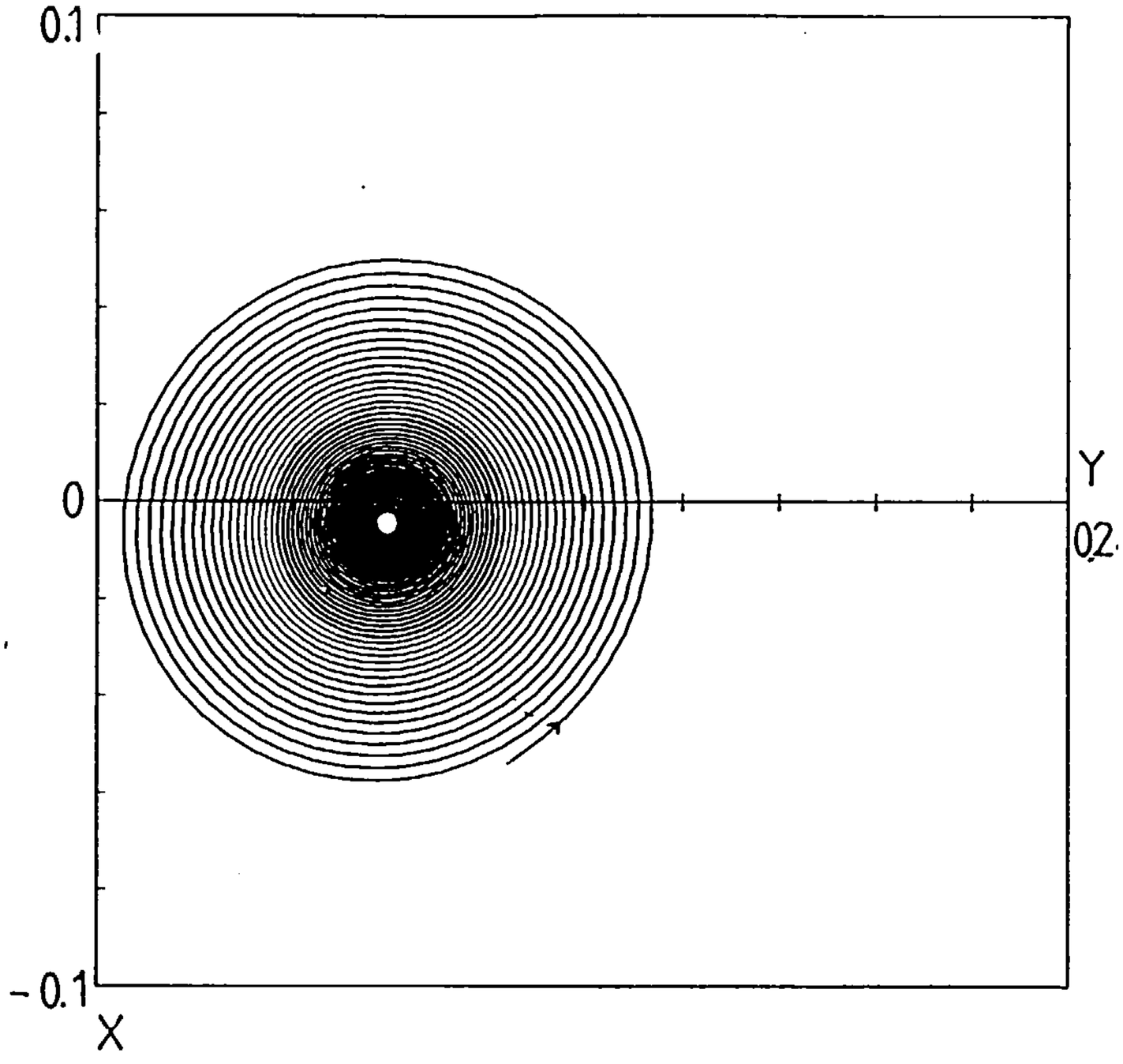

Figure 7.1d

$\sigma = 2.0$ $\varpi = 2.65$

$\epsilon_0 = 0.9$ $\phi_0 = 4.0$

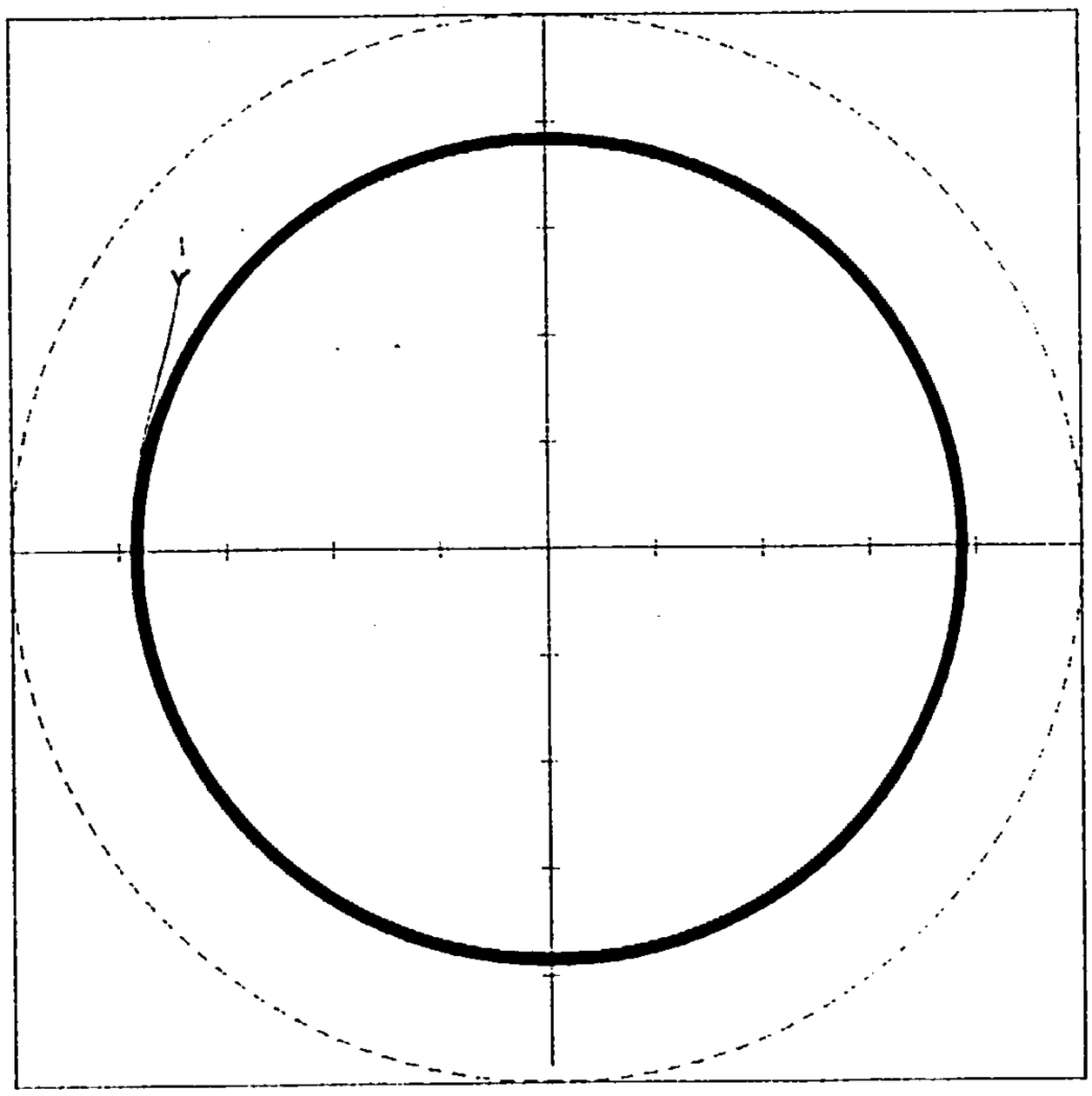

Figure 7.1e

$\sigma = 2.0$ $\varpi = 2.72$

$\epsilon_o = 0.5$ $\phi_o = 4.0$

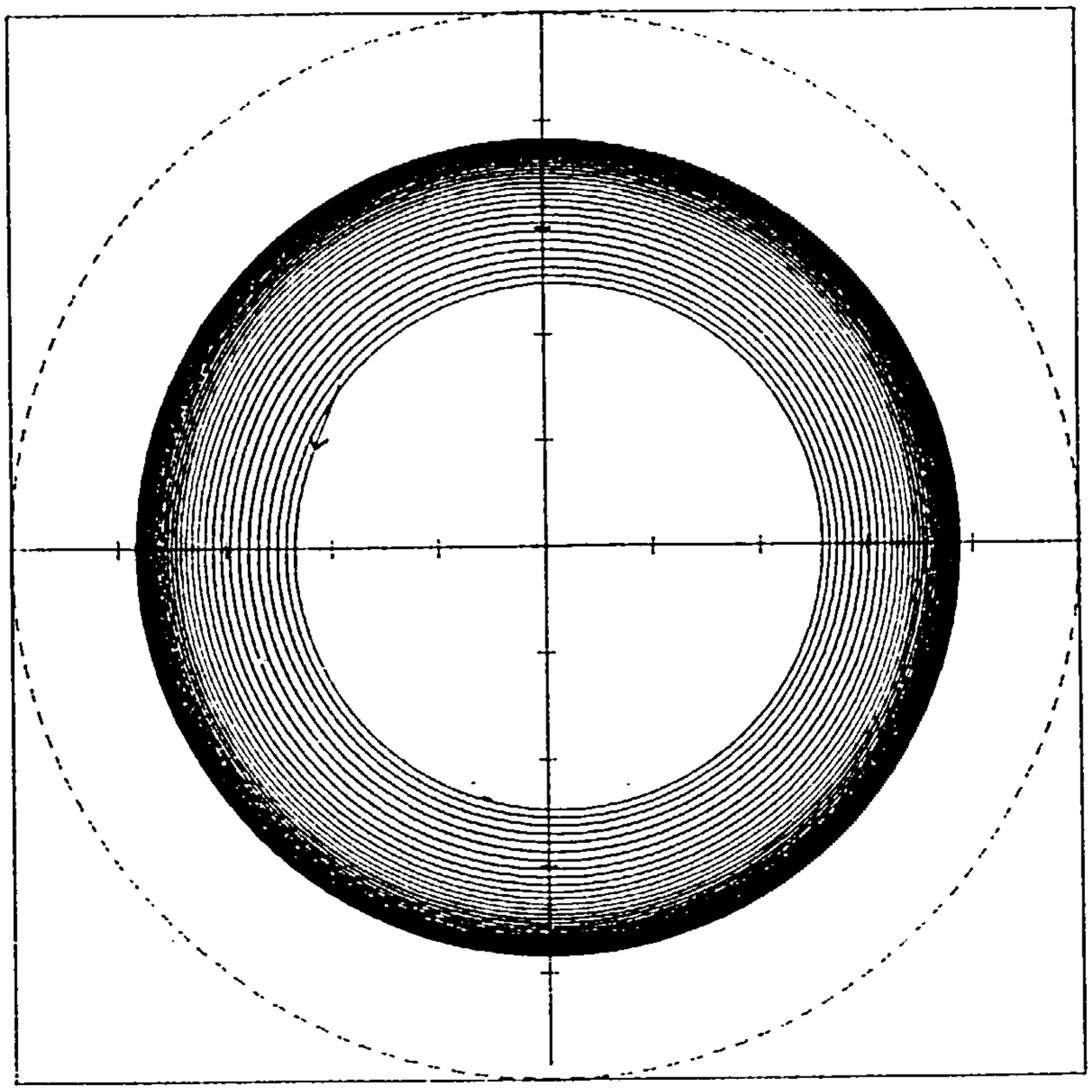

Figure 7.1f

$\sigma = 2.0$ $\varpi = 2.8$

$\epsilon_o = 0.1$ $\phi_o = 1.0$

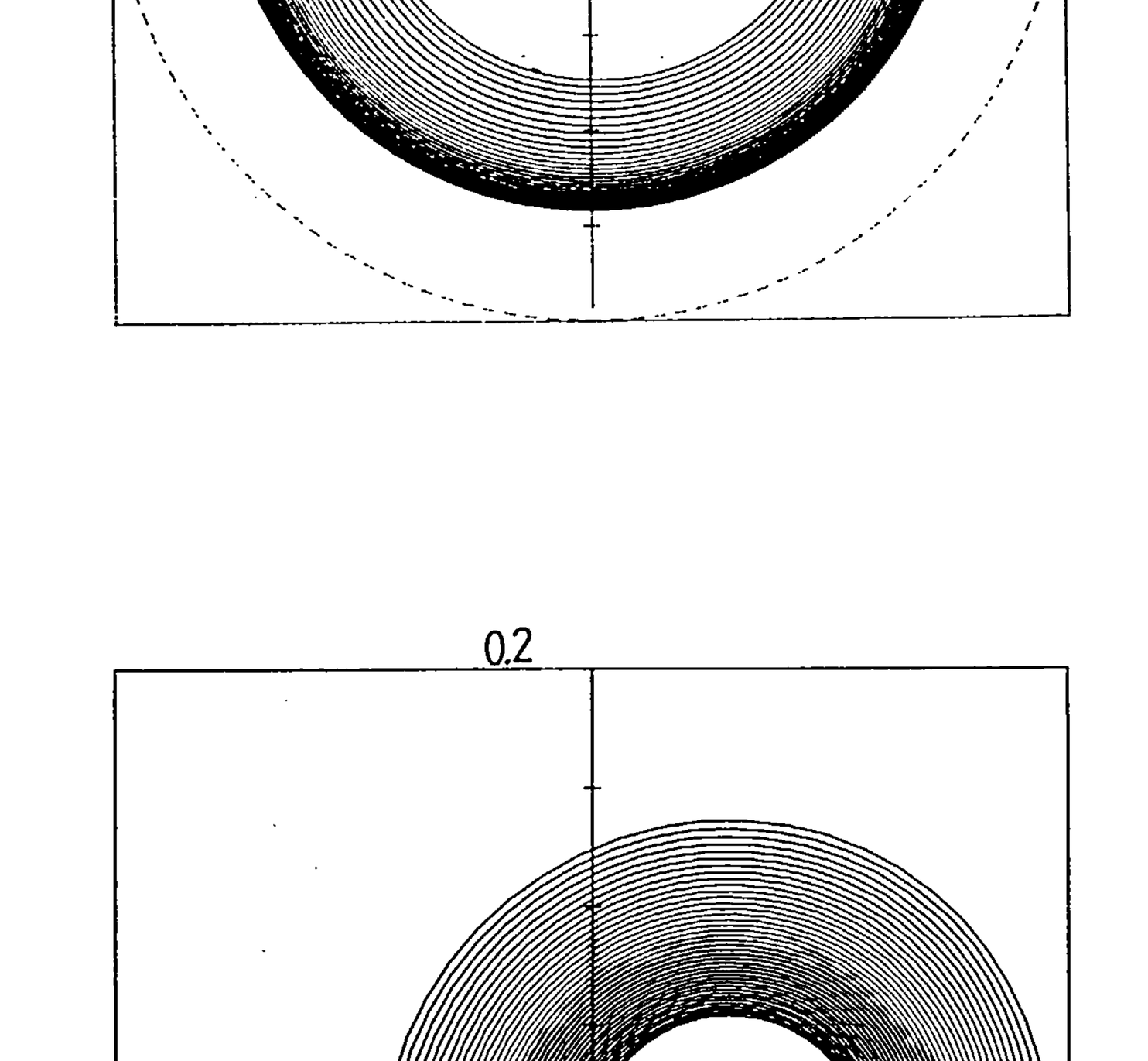

Figure 7.1g

$\sigma = 2.0$ $\bar{\omega} = 2.8$

$\epsilon_o = 0.4$ $\phi_o = 1.0$

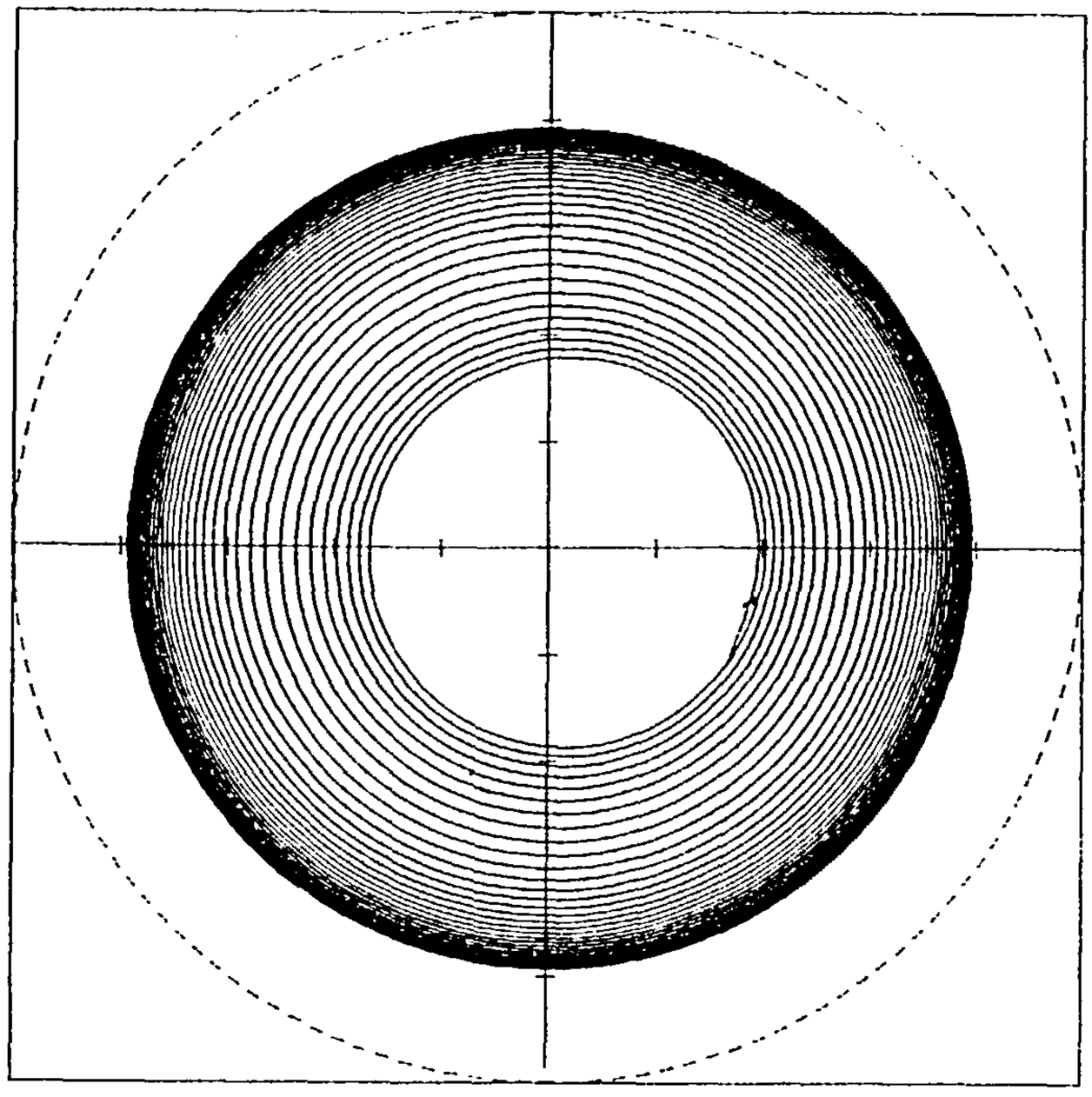

Figure 7.1h

$\sigma = 2.0$ $\bar{\omega} = 3.5$

$\epsilon_o = 0.4$ $\phi_o = 0.0$

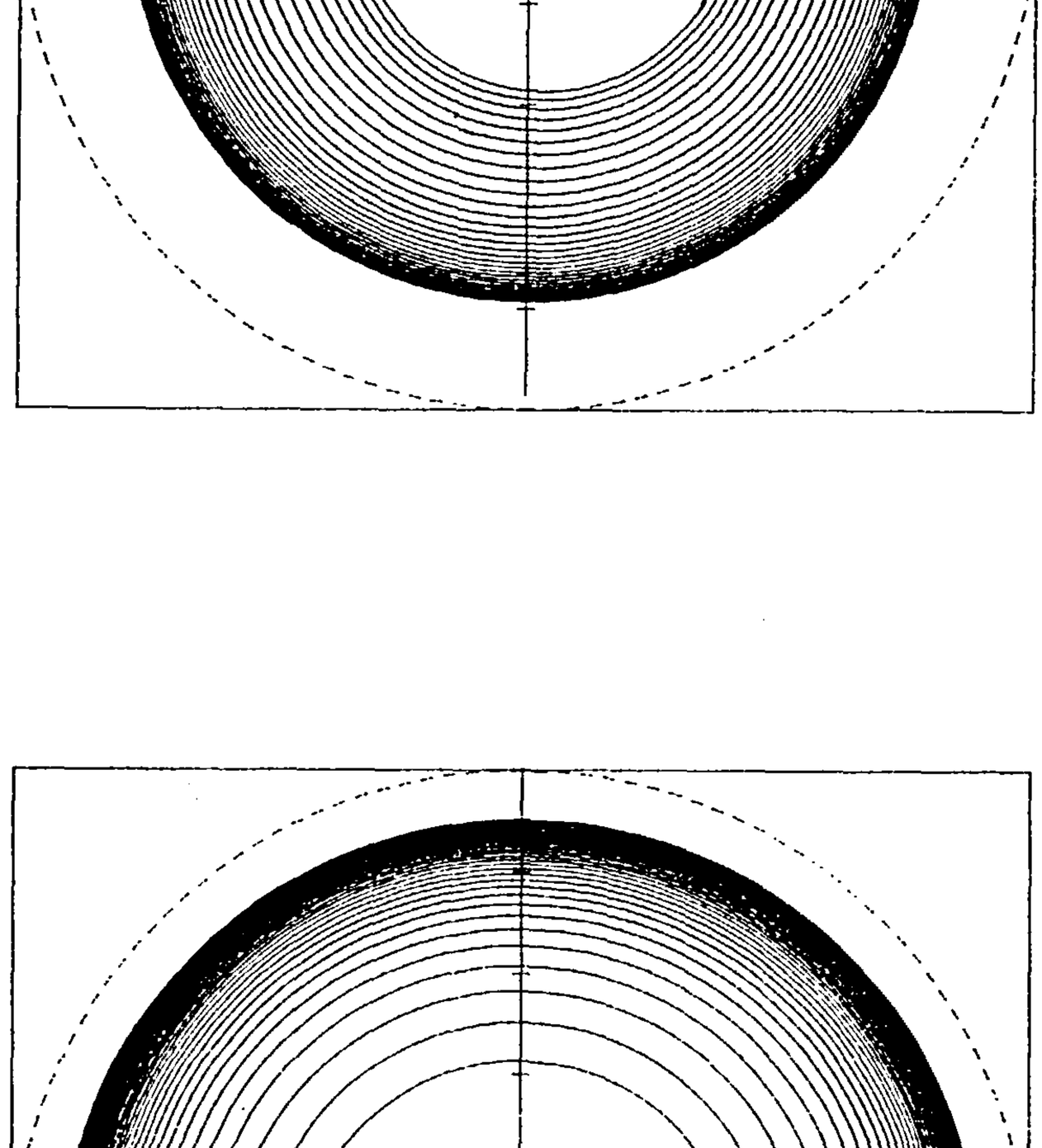

Figure 7.1i

$\sigma = 2.0 \quad \omega = 8.0$

$\epsilon_o = 0.4 \quad \phi_o = 0.0$

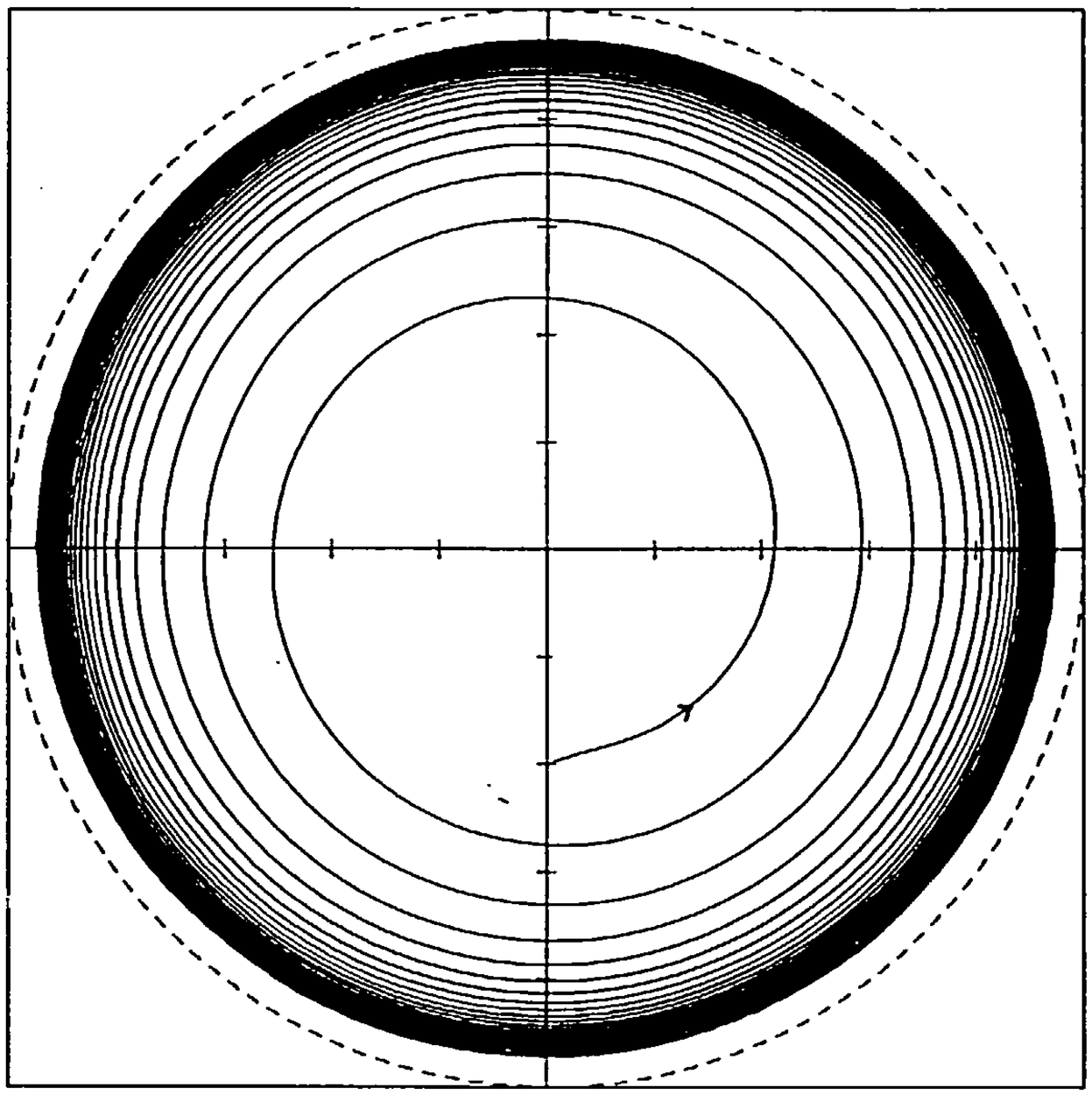

Figure 7.2a

$\sigma = 0.06 \quad \varpi = 1.5$

$\epsilon_o = 0.9 \quad \phi_o = 4.0$

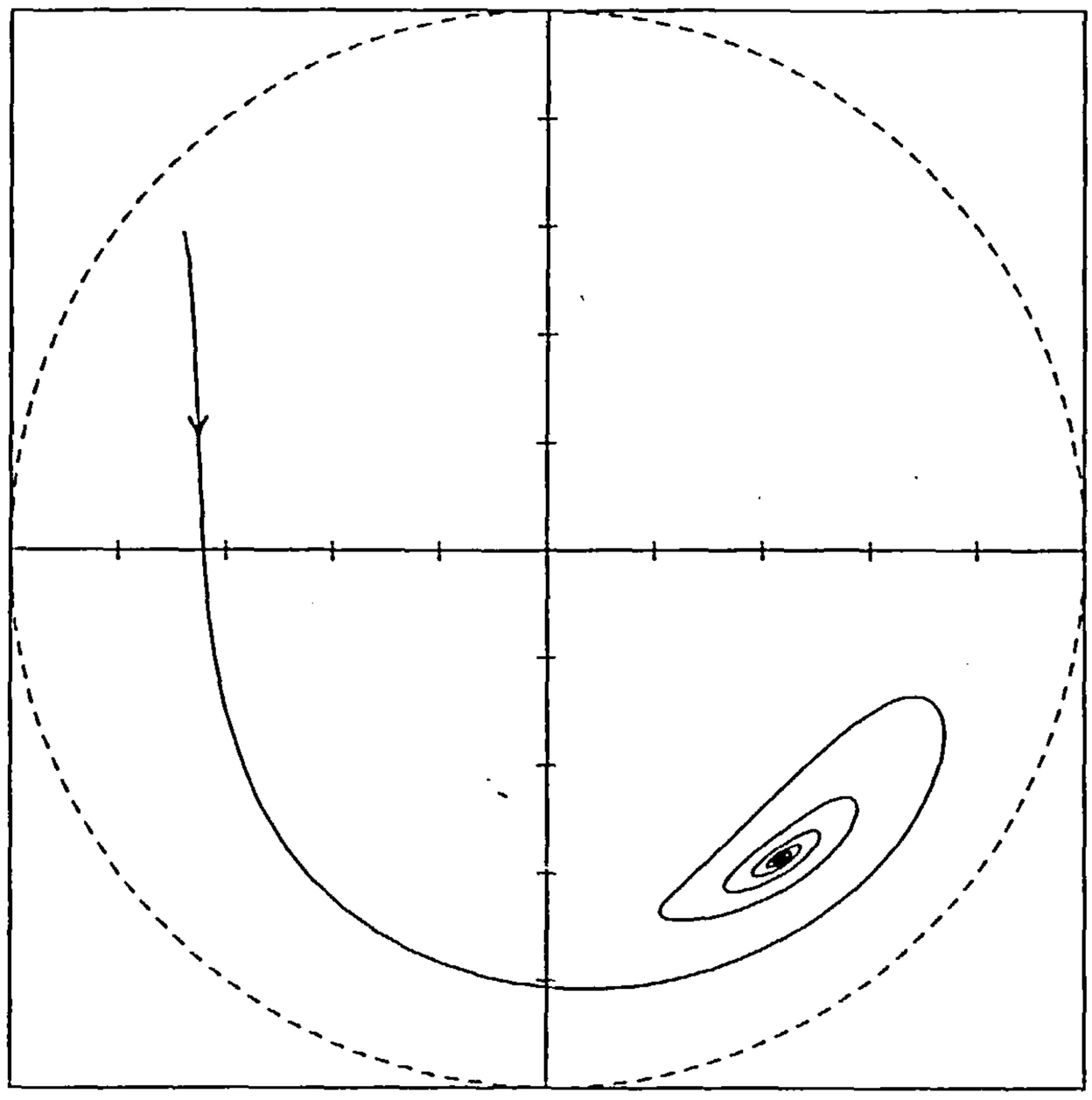

Figure 7.2b

$\sigma = 0.06 \quad \varpi = 2.2$

$\epsilon_o = 0.9 \quad \phi_o = 4.0$

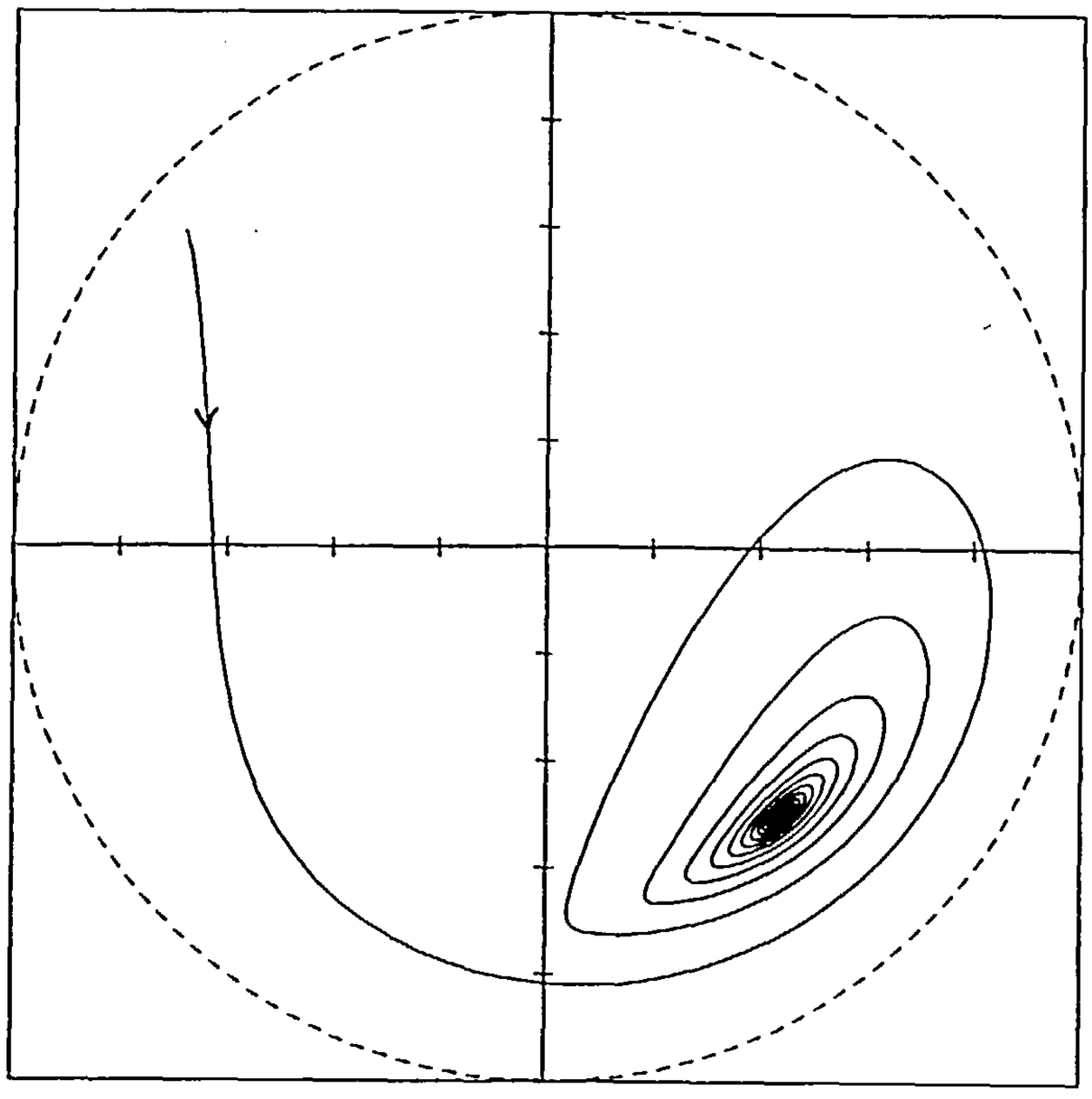

Figure 7.2c

σ=0.06 $\bar{\omega}$=2.79

ϵ_o=0.9 ϕ_o=4.5

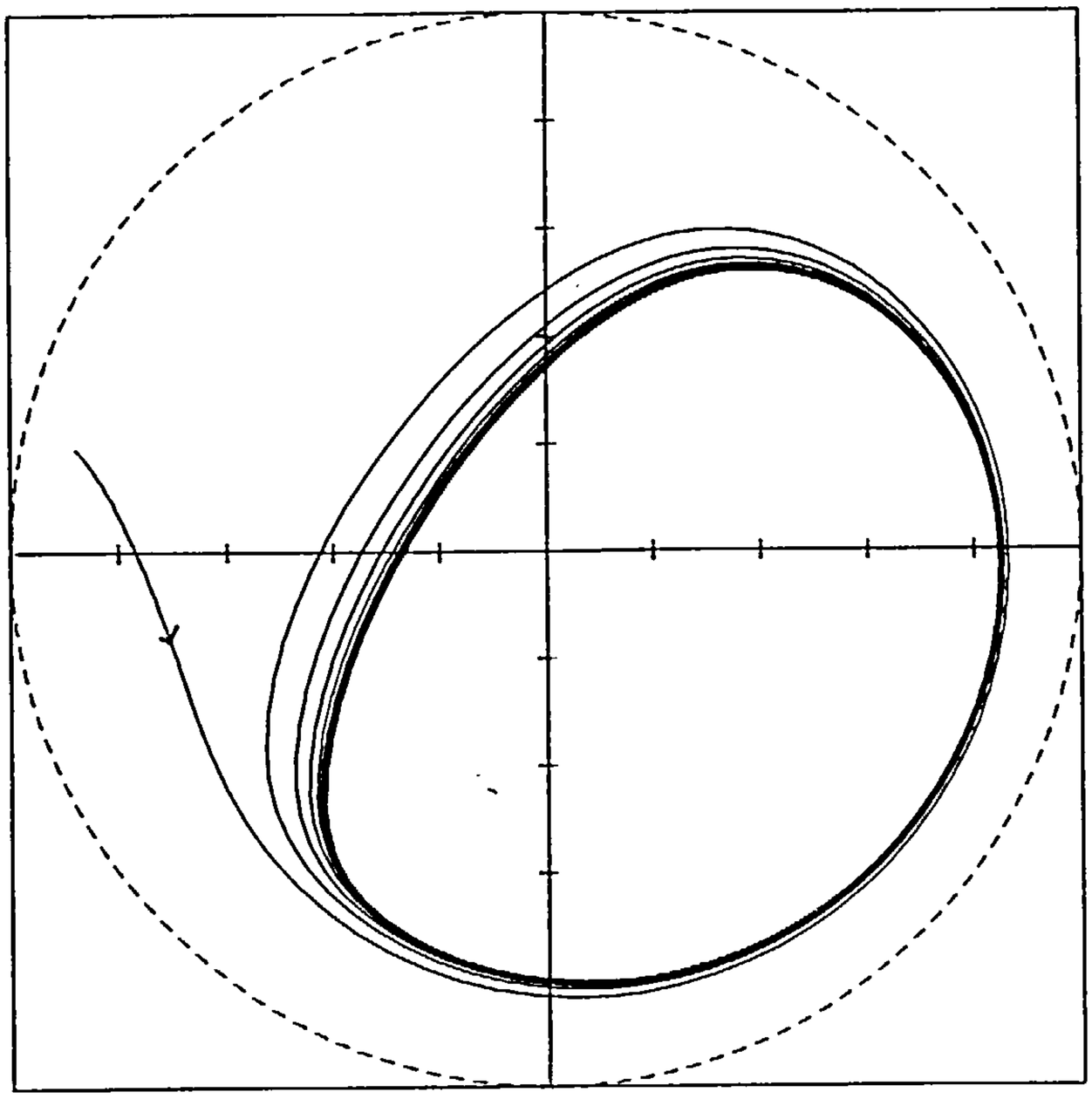

Figure 7.2d

σ=0.06 $\bar{\omega}$=2.85

ϵ_o=0.8 ϕ_o=0.7

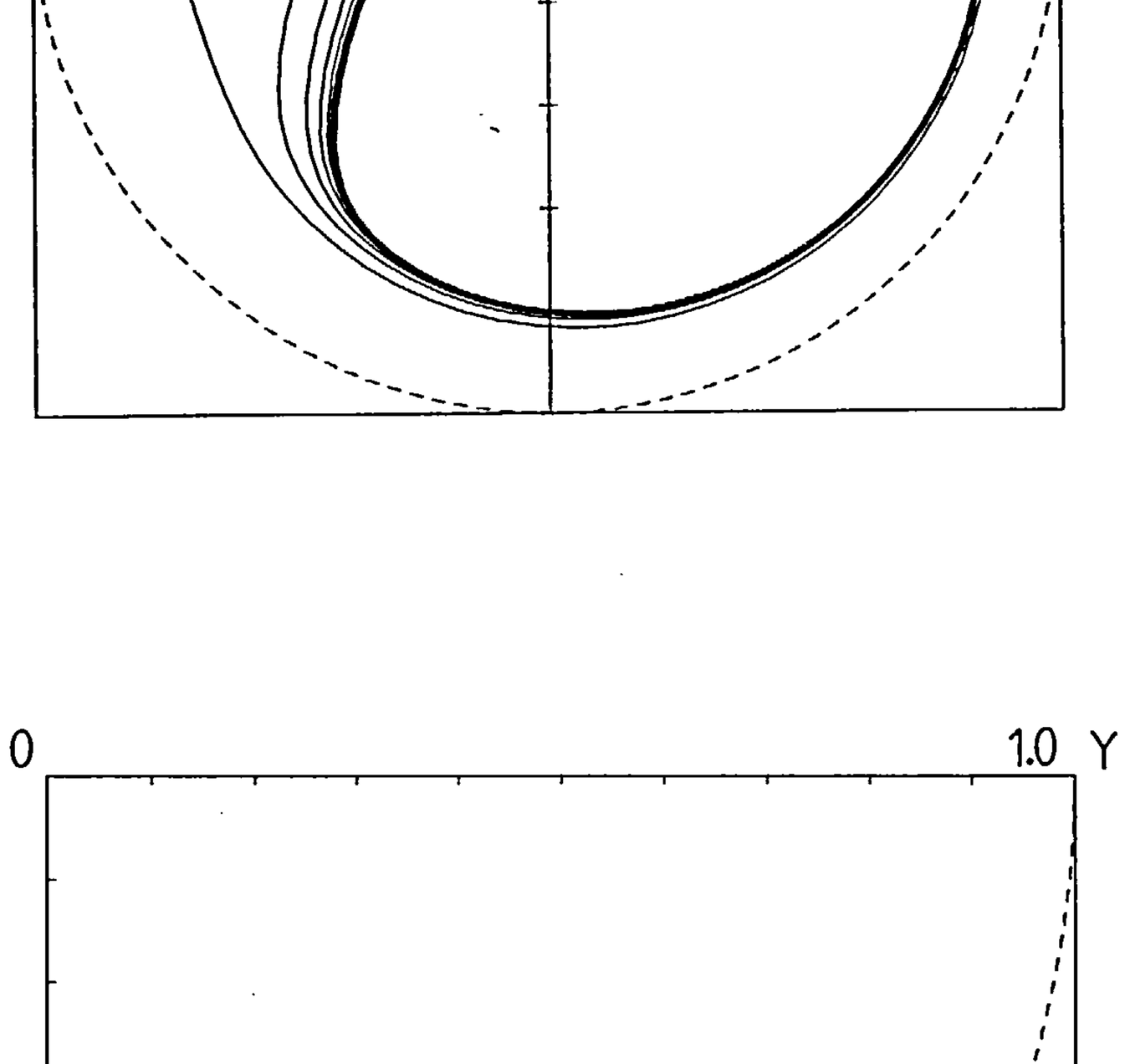

Figure 7.2e

$\sigma = 0.06 \quad \bar{\omega} = 2.85$

$\epsilon_o = 0.9 \quad \phi_o = 4.0$

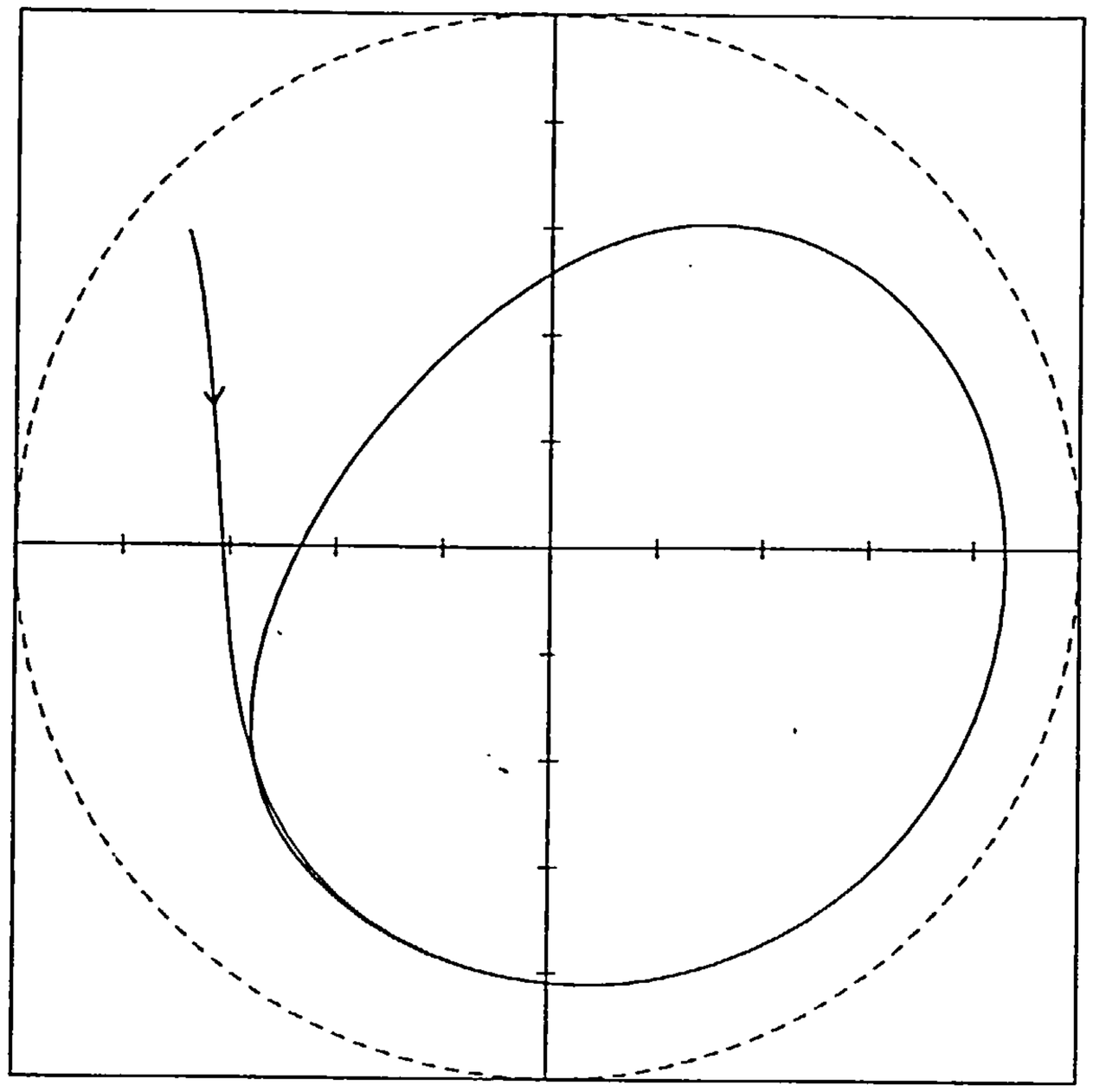

Figure 7.2f

$\sigma = 0.06 \quad \bar{\omega} = 2.92$

$\epsilon_o = 0.8 \quad \phi_o = 0.7$

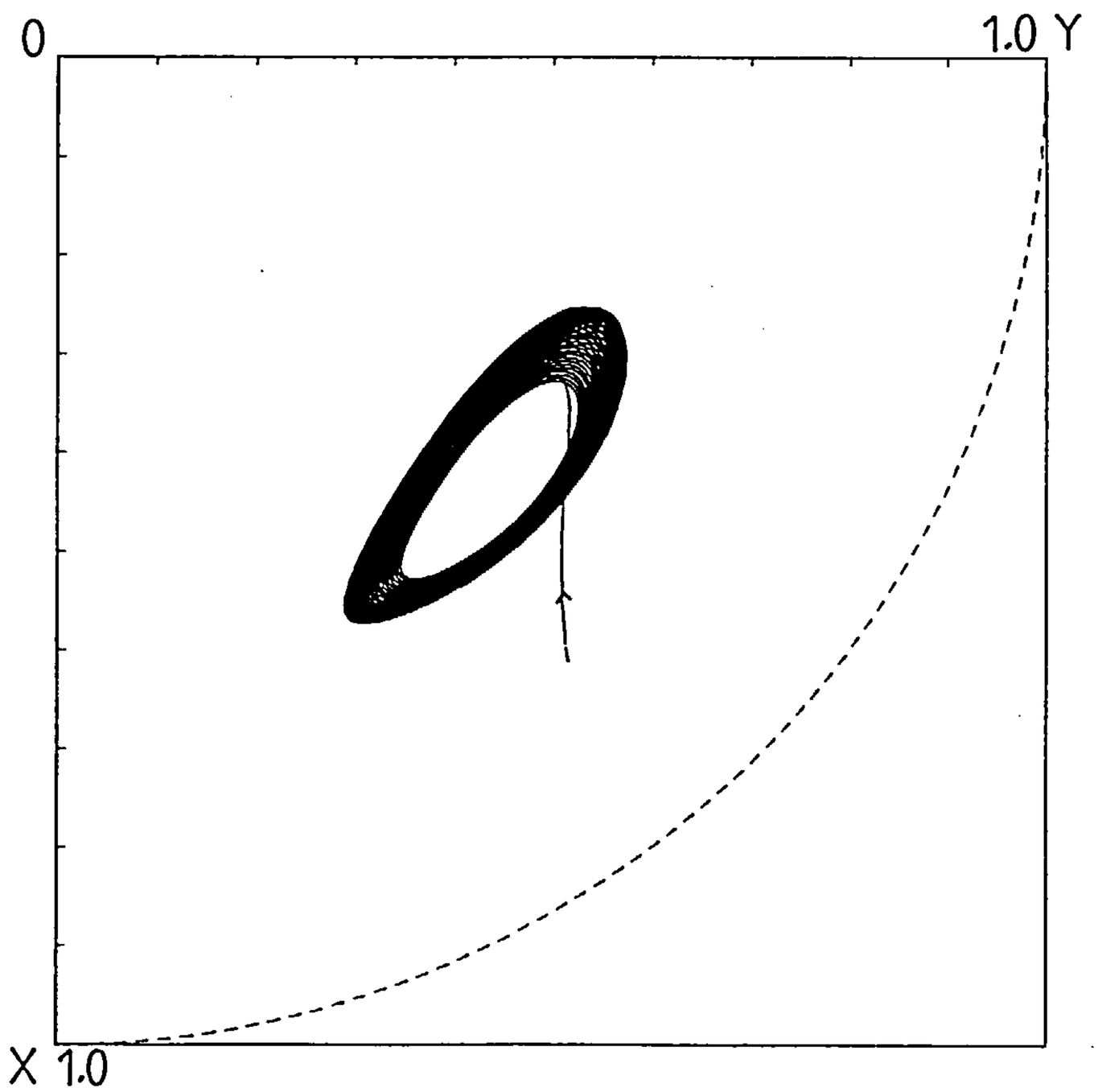

Figure 7.2g

$\sigma = 0.06 \quad \bar{\omega} = 2.92$

$\epsilon_o = 0.8 \quad \phi_o = 0.0$

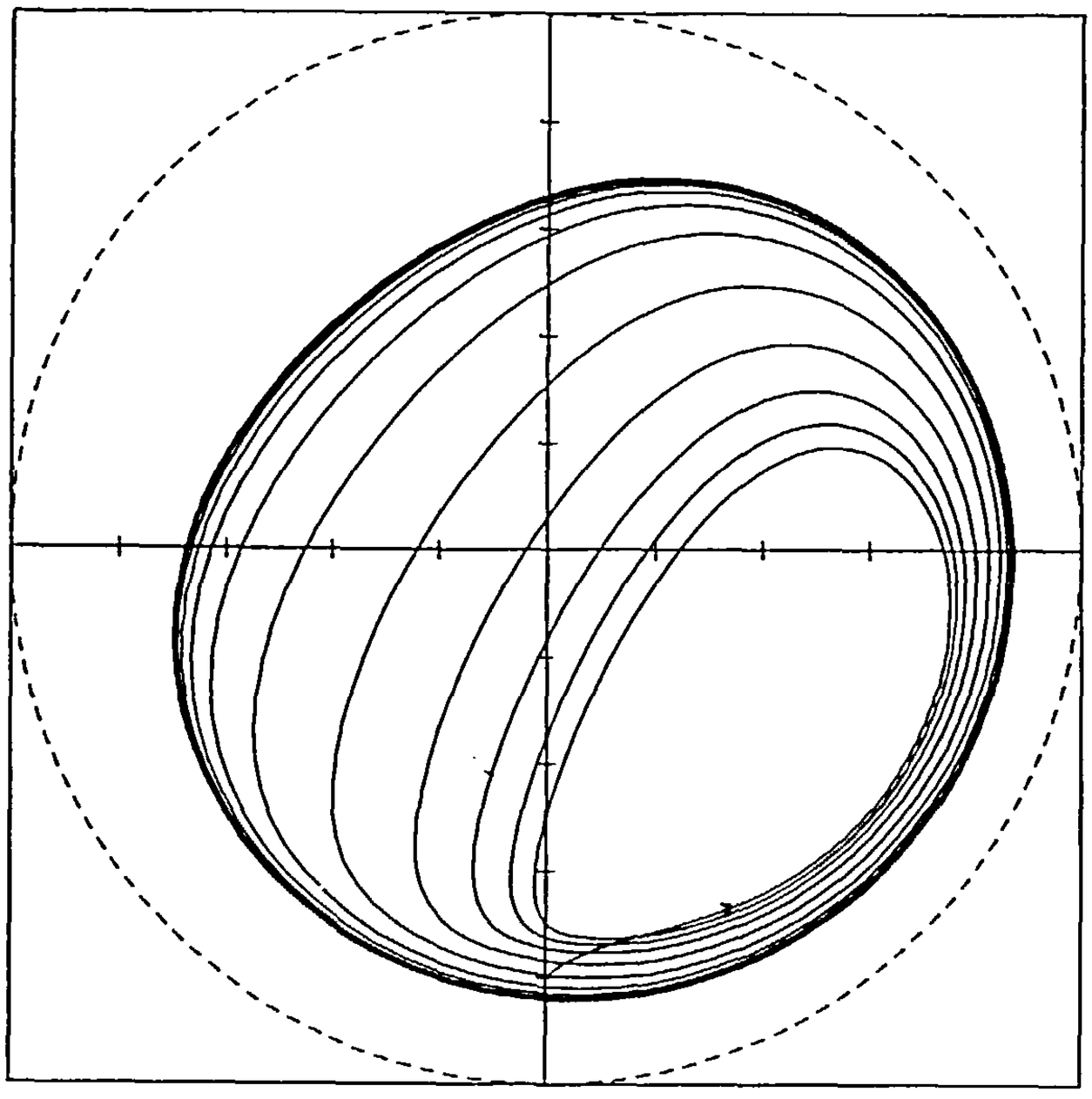

Figure 7.2h

$\sigma = 0.06 \quad \bar{\omega} = 2.95$

$\epsilon_o = 0.8 \quad \phi_o = 0.7$

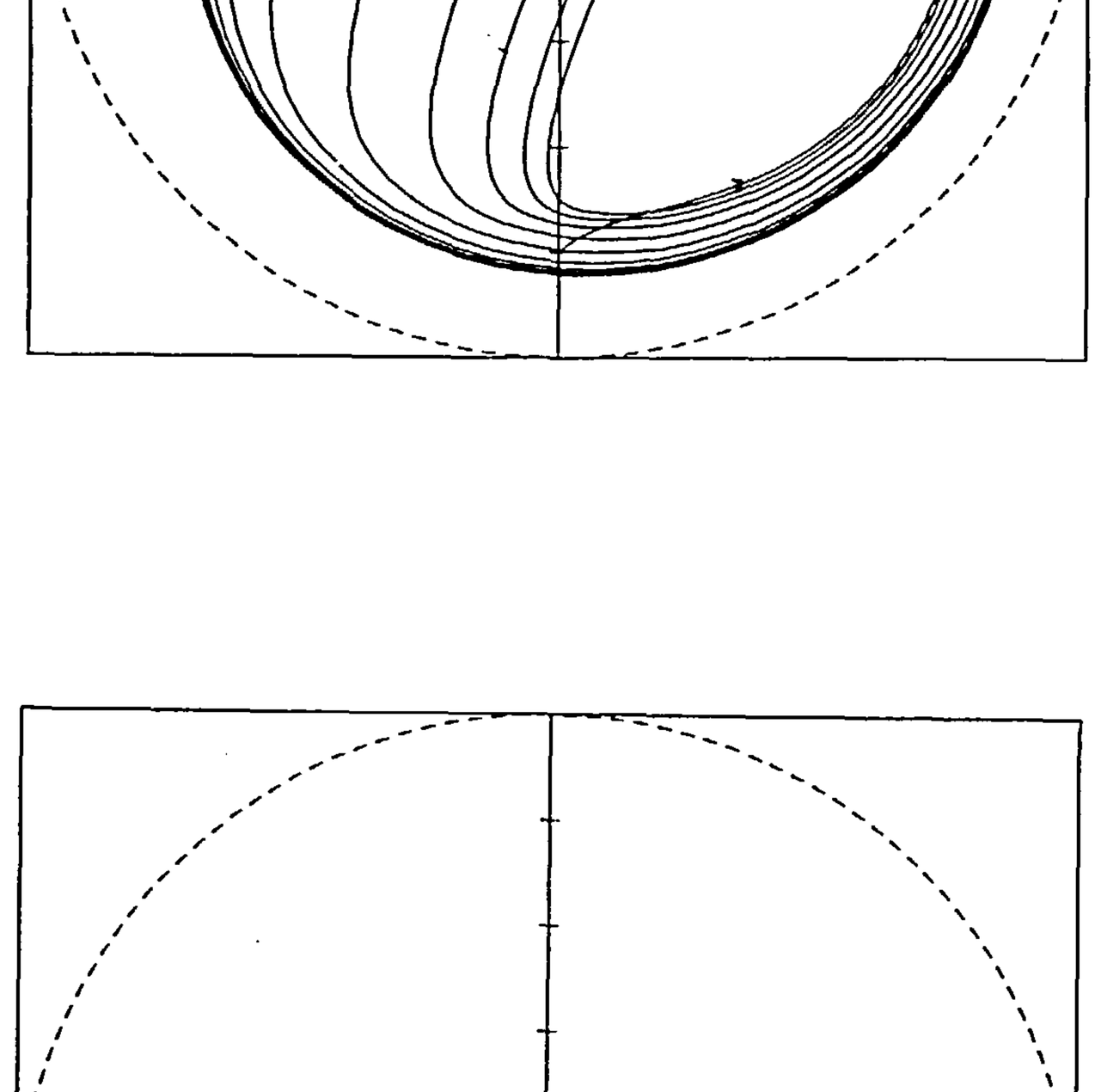

Figure 7.2i

σ=0.06 $\bar{\omega}$=2.96

ϵ_o=0.8 ϕ_o=0.7

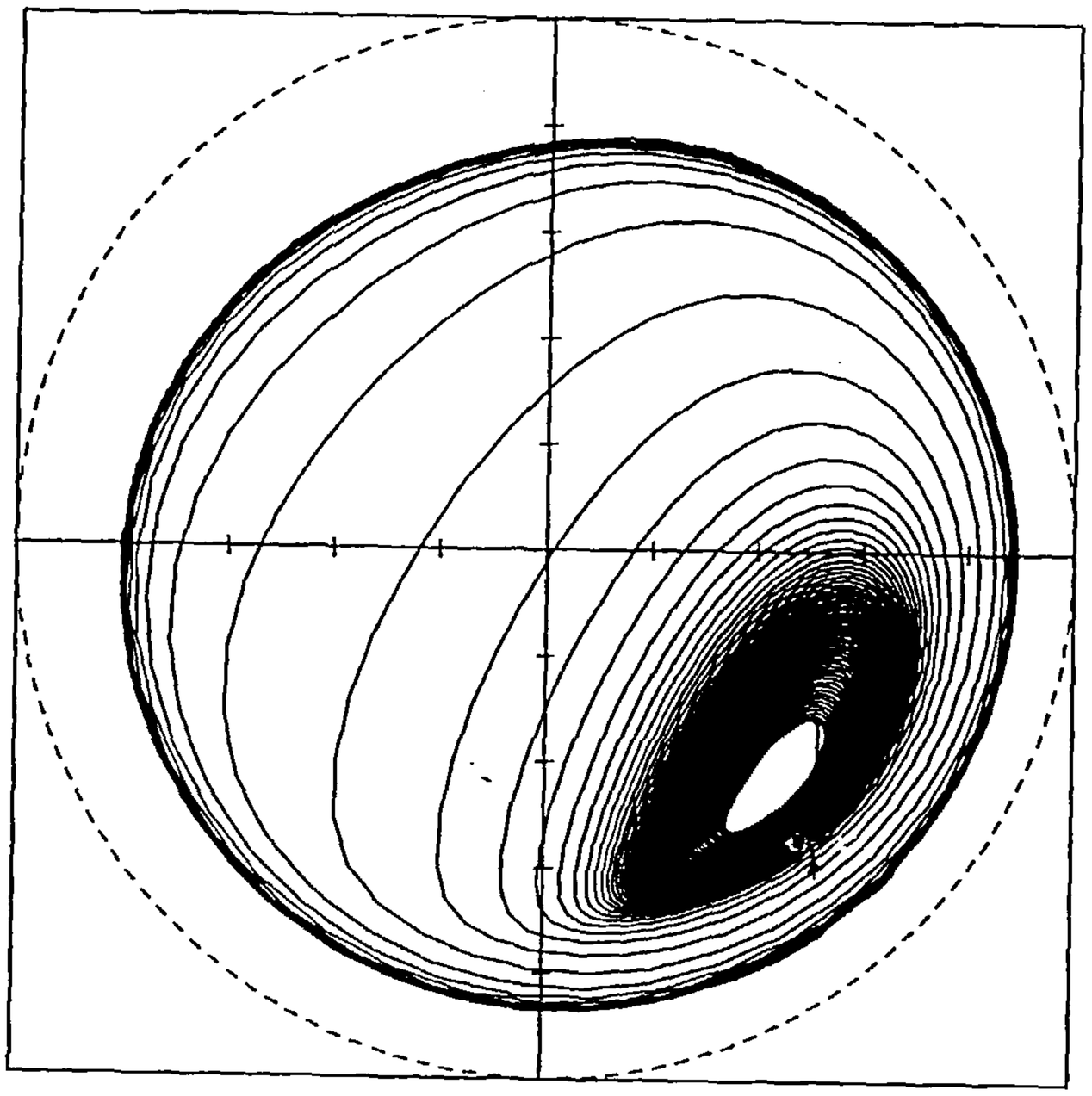

Figure 7.2j

σ=0.06 $\bar{\omega}$=3.0

ϵ_o=0.7 ϕ_o=0.9

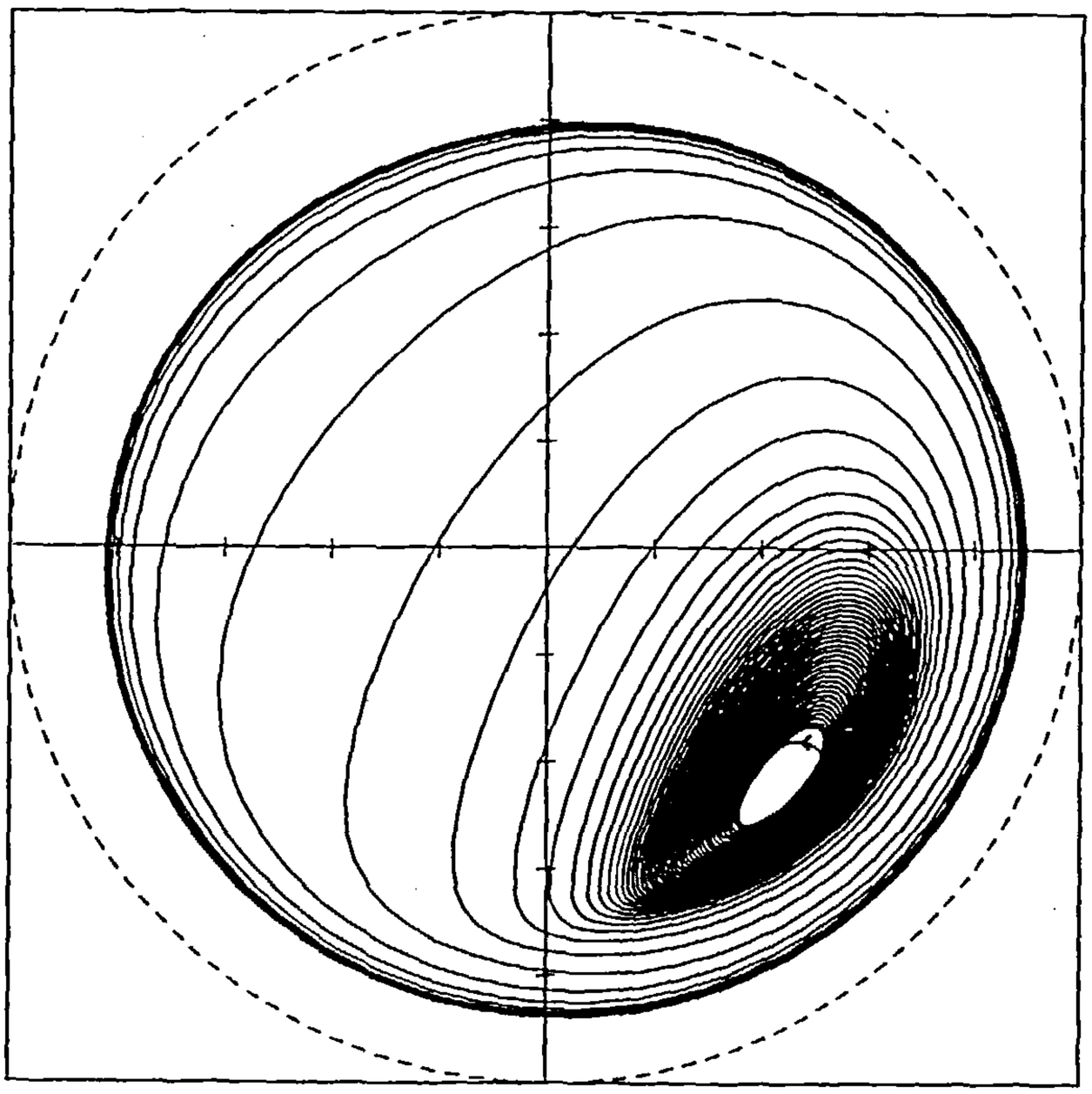

Figure 7.2k

$\sigma=0.06 \quad \varpi=4.5$

$\epsilon_o=0.6 \quad \phi_o=0.7$

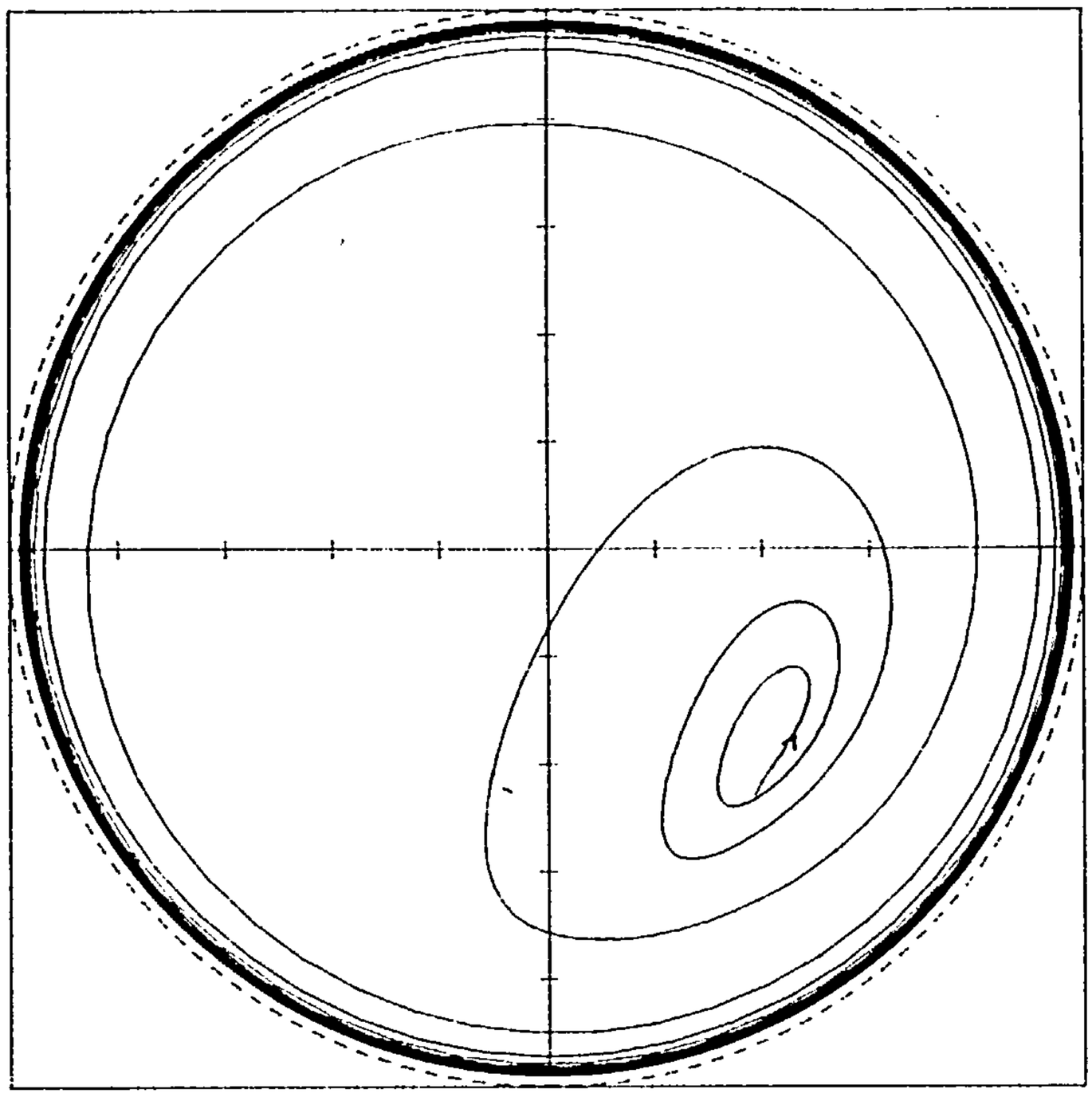

Figure 7.3a

$\sigma = 2.0$ $\omega = 1.0$

$\epsilon_o = 0.9$ $\phi_o = 4.0$

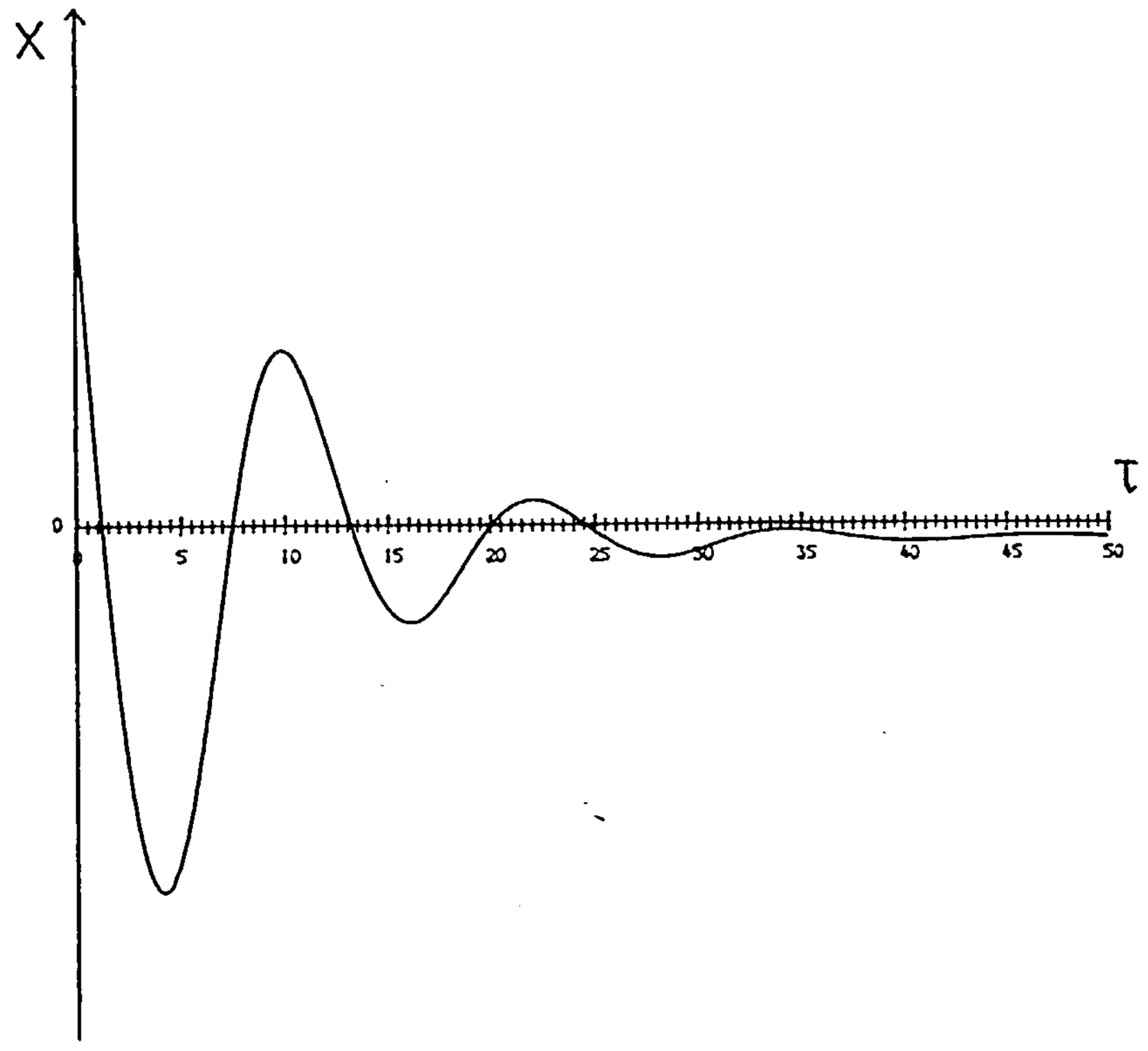

Figure 7.3b

$\sigma = 0.06$ $\bar{\omega} = 1.5$

$\epsilon_o = 0.9$ $\phi_o = 4.0$

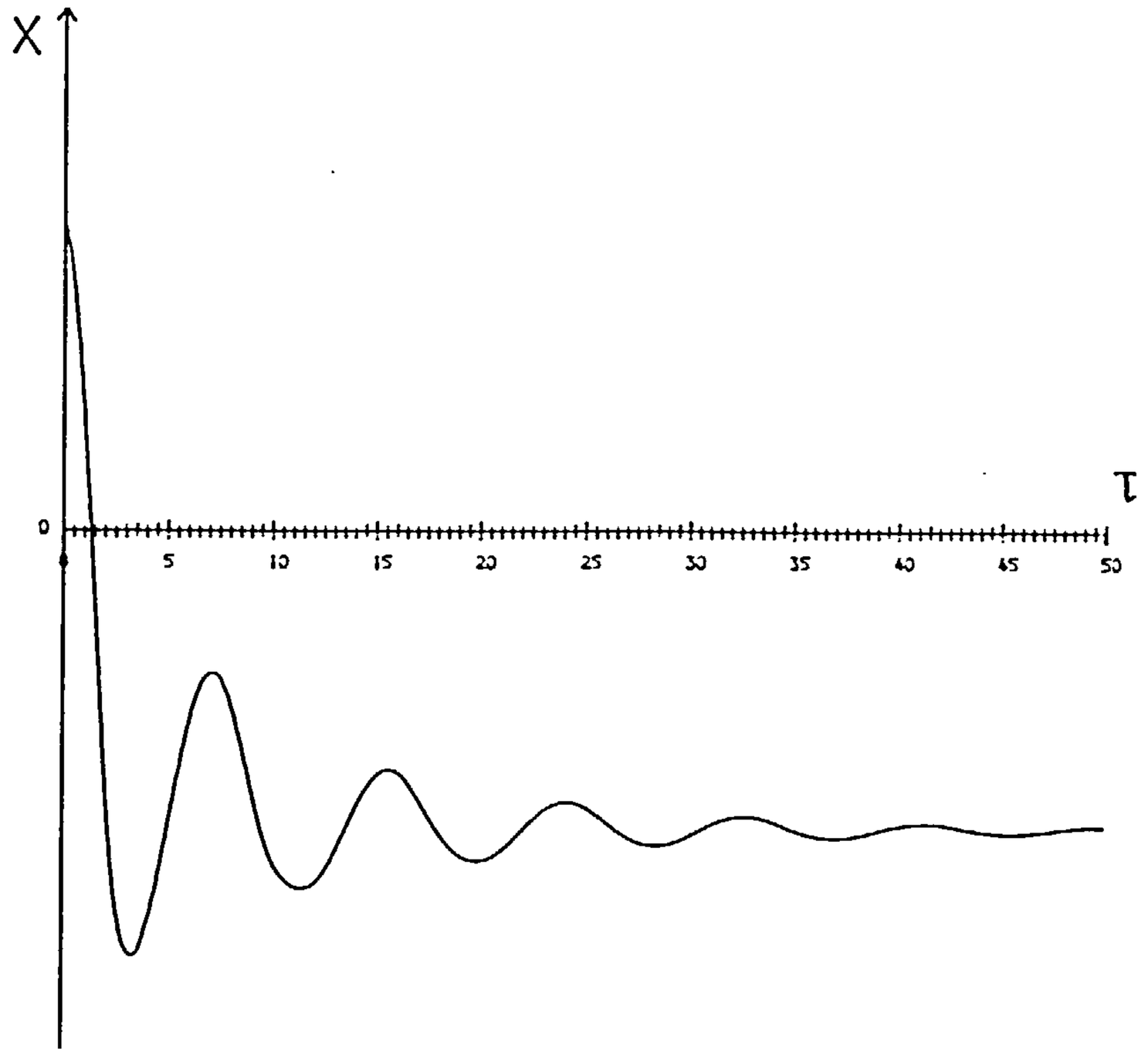

Figure 7.3c

σ=0.06 ϖ=2.92

ϵ_o=0.8 ϕ_o=0.7

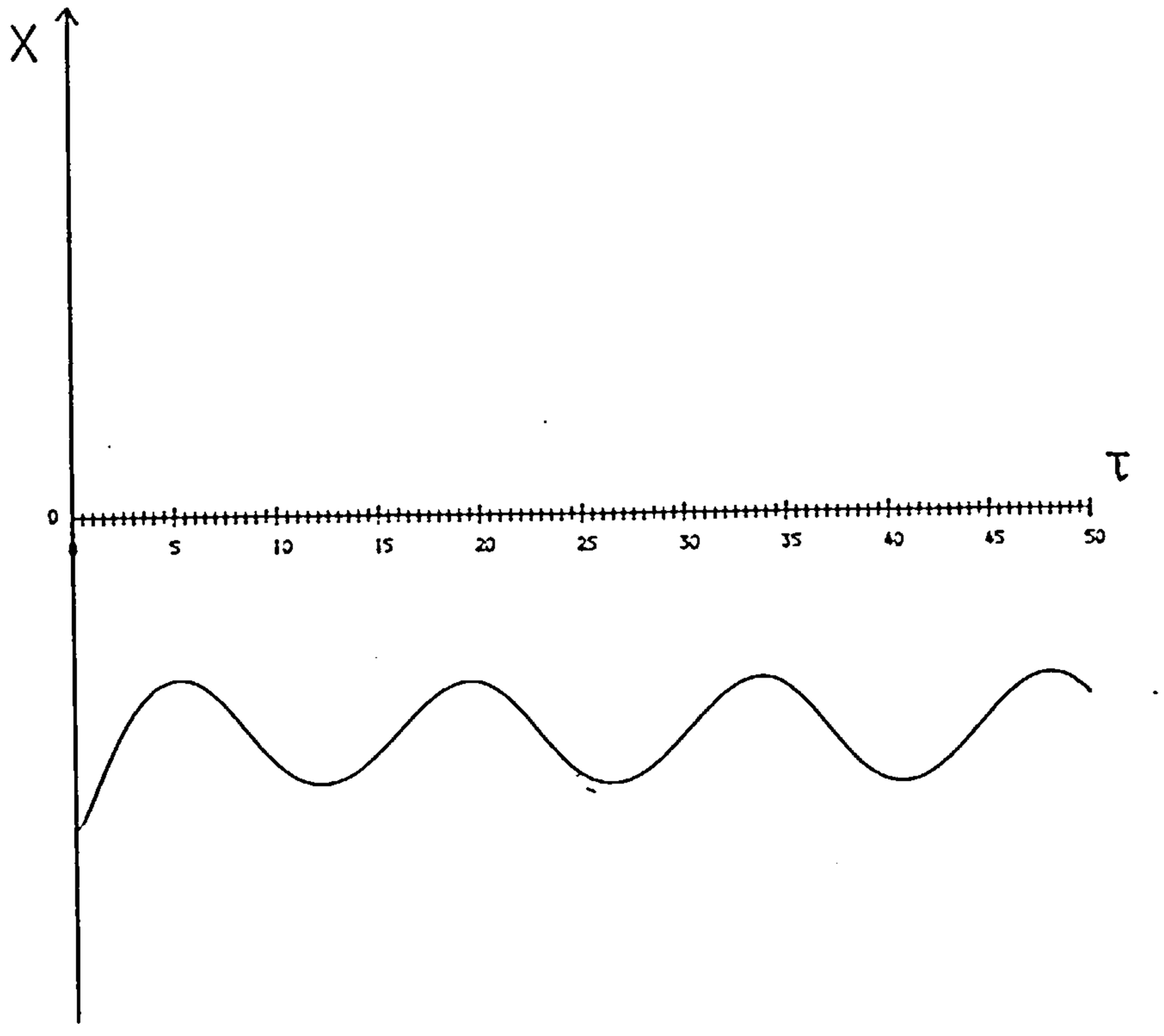

Figure 7.3d

σ=2.0 ω = 2.65

ϵ_o=0.9 ϕ_o= 4.0

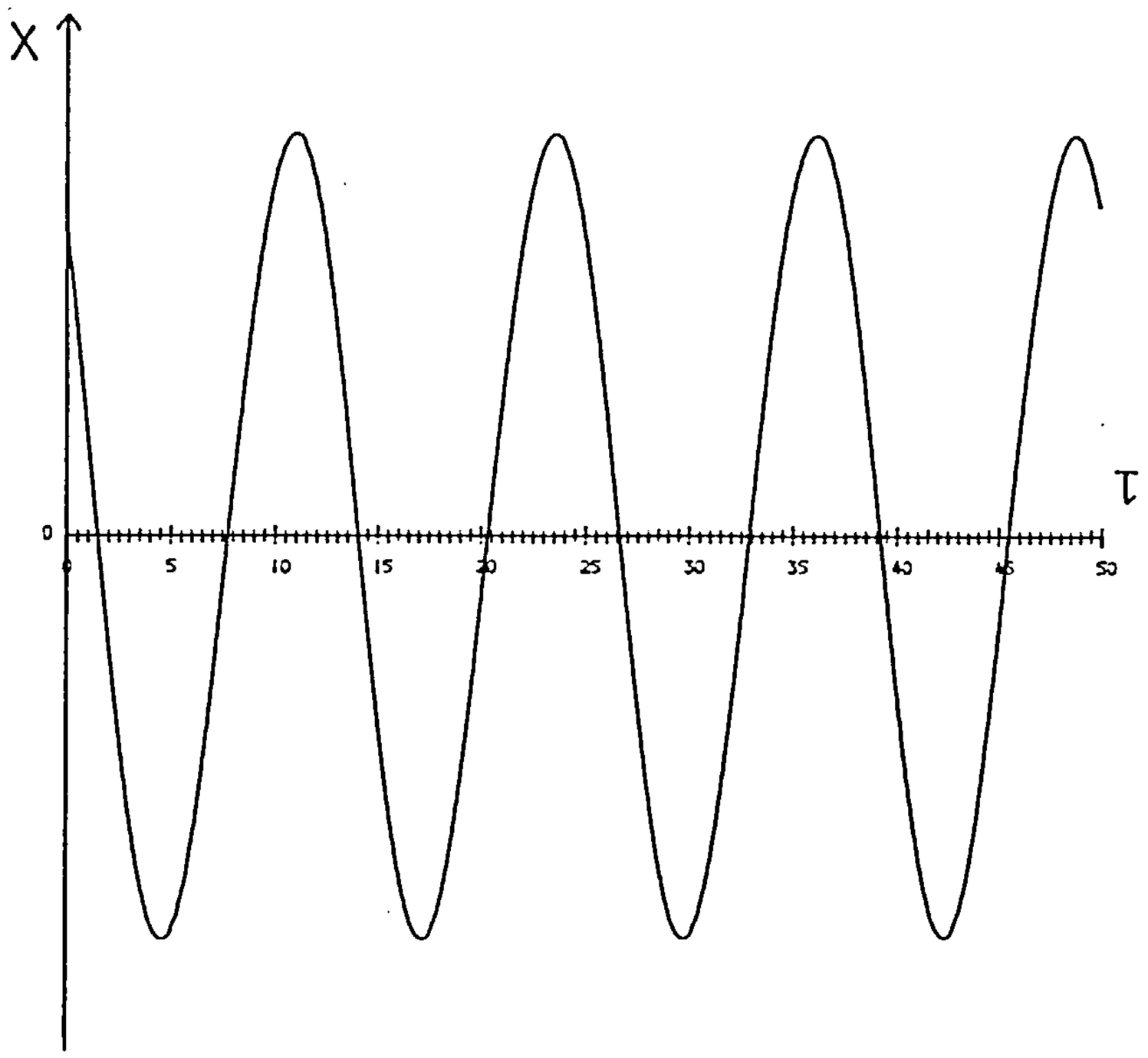

Figure 7.3e

$\sigma=0.06 \quad \varpi=2.92$

$\epsilon_o=0.8 \quad \phi_o=0.0$

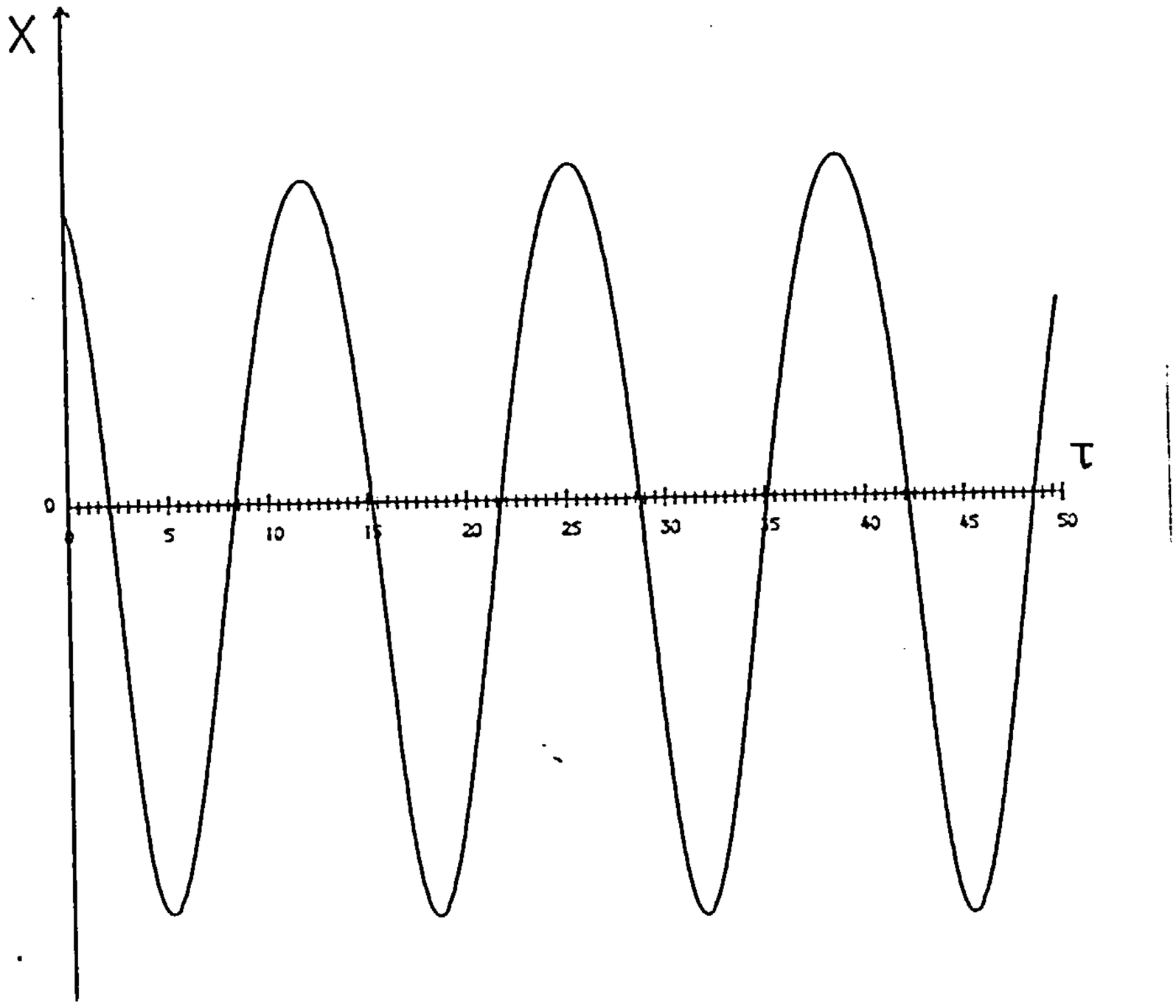

Table 7.1

Results found by numerical integration

$\sigma = 2.0$

$\bar{\omega}_s = 2.76$, $\epsilon_s = 0.06$, $\varphi_s = 1.5$ radians

	$\bar{\omega} < 2.55$	stable equilibrium point
$2.55 < \bar{\omega} < 2.76$		stable equilibrium point or large amplitude limit cycle
$2.76 < \bar{\omega} < 10.0$		large amplitude limit cycle
$10.0 < \bar{\omega}$		completely unstable

$\sigma = 0.06$

$\bar{\omega}_s = 2.81$, $\epsilon_s = 0.63$, $\varphi_s = 0.77$ radians

	$\bar{\omega} < 2.76$	stable equilibrium point
$2.76 < \bar{\omega} < 2.81$		stable equilibrium point or large amplitude limit cycle
$2.81 < \bar{\omega} < 2.96$		small whirl orbit or large amplitude limit cycle
$2.96 < \bar{\omega} < 5.0$		large amplitude limit cycle
$5.0 < \bar{\omega}$		completely unstable

ϵ_s and φ_s, however, a large amplitude (growing with $\bar{\omega}$), stable limit cycle can be observed (Figures 7.1d and 7.1e). For $\bar{\omega}>\bar{\omega}_s$, even for ϵ_0 and φ_0 close to ϵ_s and φ_s, the system is completely unstable, as far as small amplitude oscillations are concerned. There is, however, evidence of large amplitude orbits, growing with $\bar{\omega}$, well into the linearly unstable region (Figures 7.1f, 7.1g, 7.1h, 7.1i).

Figure 7.2 shows the behaviour for a system operating with σ=0.06, crossing the stability borderline in the supercritical region, at $\bar{\omega}_s$=2.81. For $\bar{\omega}<<\bar{\omega}_s$ the system is stable for all values of ϵ_0 and φ_0 (Figures 7.2a and 7.2b). For $\bar{\omega}$ close to $\bar{\omega}_s$ the solution depends on the initial conditions. If the starting position is close to the equilibrium point, the system is stable for $\bar{\omega}<\bar{\omega}_s$ and has a small amplitude limit cycle for $\bar{\omega}>\bar{\omega}_s$, whose amplitude is proportional to $\sqrt{|\bar{\omega}-\bar{\omega}_s|}$ (Figures 7.2d, 7.2f and 7.2h). If the initial position is away from the equilibrium point, a stable, large amplitude limit cycle exists for $\bar{\omega}$ just above and below $\bar{\omega}_s$ (Figures 7.2c, 7.2e and 7.2g). When $\bar{\omega}$ reaches a value of 2.96, the smaller orbit ceases to exist and all solutions grow to the large amplitude solution (Figure 7.2i). This large amplitude orbit continues to grow with $\bar{\omega}$ (Figures 7.2j and 7.2k) until the system becomes completely unstable well into the linearly unstable region.

Figure 7.3 shows the variation of the journal centre location in the X-direction for certain values of σ, $\bar{\omega}$, ϵ_0 and φ_0 as τ increases. Figures 7.3a and 7.3b correspond to Figures 7.1a and 7.2a; they show the quickly decaying oscillations as the system moves towards its equilibrium point. Figure 7.3c corresponds to Figures 7.2f and shows that the period of small stable limit cycles in the supercritical region is approximately equal to 4π. This is in agreement with the half frequency whirl observed experimentally (see Chapter 1) and predicted analytically. Interestingly, the large amplitude orbits surounding both the sub and supercritical solutions are also of half

frequency (Figures 7.3d and 7.3e, which correspond to Figures 7.1d and 7.2g).

Numerical integration is in essence, supplementary to the analytical techniques, since it cannot provide information about the system's general behaviour. It merely provides a solution for a given set of parameter values. A numerical study of a complex system such as (4.6) is a very time consuming operation, since, for a given value of σ it is necessary to integrate the equations for a large number of rotor speeds and initial positions to be certain of identifying the full range of behaviour. Numerical integration does, however, confirm the subcritical and supercritical regions predicted by the earlier analysis. In both cases the small bifurcated orbits are surrounded by stable large amplitude limit cycles; these additional orbits will be discussed further in the next section.

7.2 Discussion of the results obtained by the use of nonlinear techniques

The main features of the methods used in this chapter are set out in Table 7.2. A major achievement of this part of the research has been the consistency of the results obtained by the application of four different techniques to the equations 4.6. In particular, it has been shown that it is possible to achieve agreement between the method of averaging and the method of multiple scales by the correct choice of small parameter. Although the two methods as employed here are essentially different representations of the same technique, this was previously unclear in their application to the journal bearing problem (Myers (1981)).

Now that the consistency of the analytical techniques has been demonstrated, it is clearly of little value to continue to work through all three in the future analysis of other cavitation models. Hopf bifurcation provides a

Table 7.2

Summary of the nonlinear techniques

Bifurcation Theory

Description i) Rigorous mathematical technique ii) Existence theorem which establishes the existence of small amplitude whirl orbits for rotor speeds close to the threshold speed iii) Direction of bifurcation determined algebraically iv) Amplitude = $k\sqrt{|\bar{\omega}-\bar{\omega}_s|}$ as $\bar{\omega}\rightarrow\bar{\omega}_s$.
Advantages i) Mathematical rigour ii) Theory provides detailed information about the structure of periodic solutions close to the threshold speed
Disadvantages i) Algebraic formula is tedious to apply ii) Theory is valid only close to the threshold speed.

Multiple Scaling/Method of Averaging

Description i) Singular perturbation technique ii) Series solution based on physical insight iii) Evolution from equilibrium position is described by an amplitude growth equation iv) The direction of bifurcation is determined by the sign of terms in the amplitude equation v) Consistent with bifurcation theory.
Advantages i) Method is conceptually straightforward ii) Stability of solutions is easily deduced from the amplitude equation
Disadvantages i) Method is tedious to apply ii) Theory is valid only for rotor speeds close to the threshold speed.

Numerical Integration

Description i) Straightforward step-by-step integration of the equations of motion on a digital computer.
Advantages i) Pictorial representation of the journal motion ii) Valuable for confirming theoretical solutions iii) It can be used for any bearing model iv) Valid away from the threshold speed.
Disadvantages i) Expensive in computer time ii) Errors may accumulate significantly over many time steps iii) It does not identify the important regions of parameter space.

rigorous proof of the existence of small amplitude oscillations and an indication of the correct line of approach to be adopted in the scaling/averaging procedure. However, the latter solutions give a more explicit expression for orbit amplitudes (c.f. solutions (5.18) and (6.16) with (3.4)), as well as an indication of the system's evolution to limit cycles. It was necessary to choose between these two methods for the analysis of further boundary conditions in Chapter 8. The method of multiple scales was chosen, since the corresponding algebra is rather less tedious.

It is possible to combine the analytical and numerical results to obtain an overall picture of rotor behaviour at speeds close to the threshold. This is shown in Figure 7.4. The appearance of large amplitude oscillations is rather surprising for this particular rotor configuration; larger orbits are normally associated with oil whip (see Introduction and Chapter 1), which is a resonance effect peculiar to flexible shafts. Figures 7.3d and 7.3e show that these orbits are of half frequency. Oil whip, on the other hand, occurs at full frequency since it takes place when the rotor speed is equal to twice the first critical speed in bending of the shaft. It is not possible at this stage to speculate as to whether these larger limit cycles represent a real effect or are a feature of the numerical scheme used. It is interesting, however, that Myers (1981), in his numerical study of the long bearing oscillating half film model, found evidence of large amplitude orbits in a subcritical region, but not in the corresponding supercritical region.

A defect of the purely analytical approach is that it gives no indication as to how far along the operation line the solutions remain accurate. Figures 7.1 and 7.2 show that they become invalid as soon as $\bar{\omega}$ strays far from its threshold value. It is, however, necessary to resort to trial and error when integrating the equations numerically to find where this breakdown takes place.

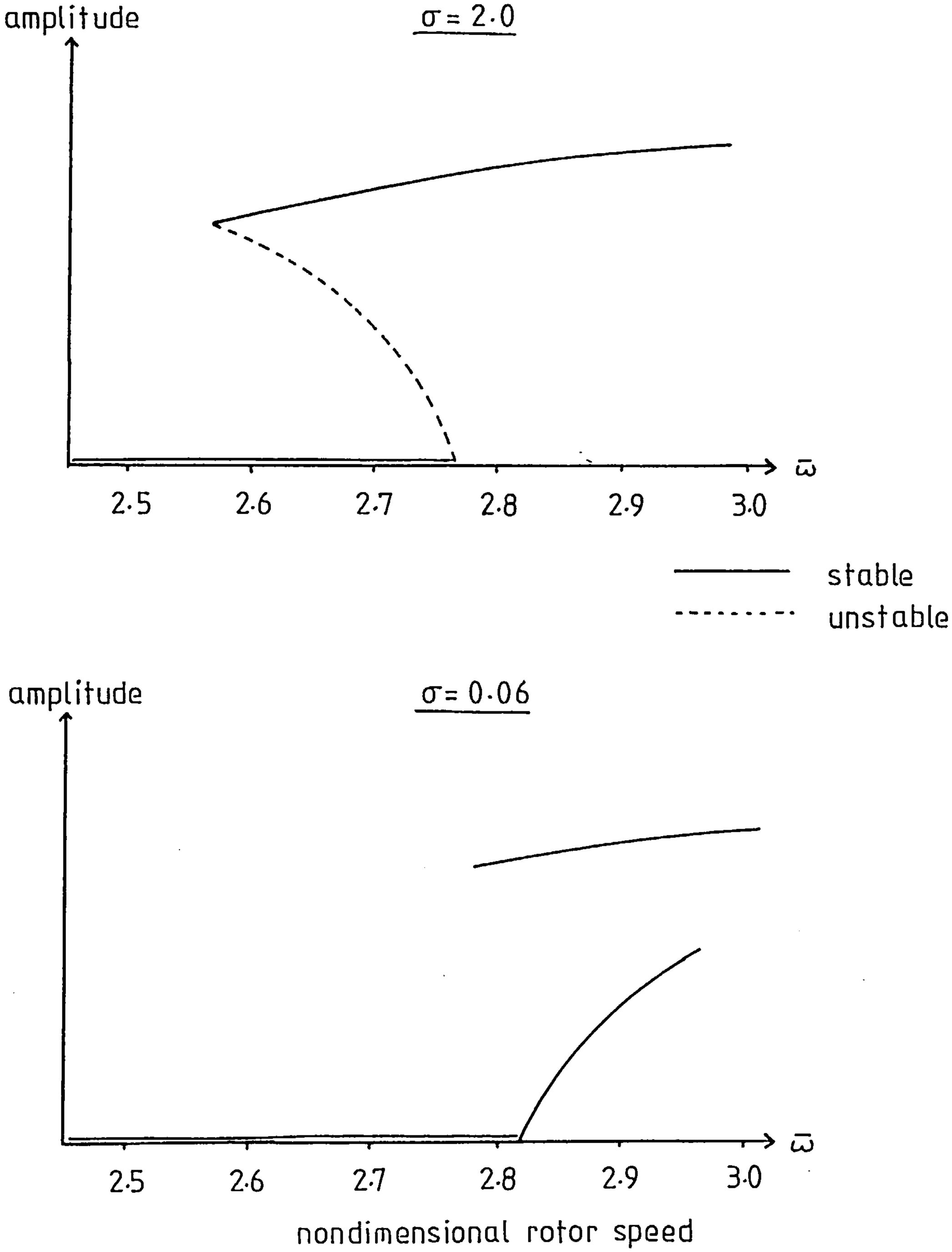

Figure 7.4 System behaviour close to the threshold speed

An examination of the graph of $\sqrt{|\eta_{2r}/\eta_{3r}|}$ plotted against ϵ_s shows that infinite amplitudes are predicted at the borderline between the two regions at ϵ_s=0.141 (Figure 7.5). This singularity arises because af the small number of terms considered in the series expansions for ΔX and ΔY (5.4). The crudeness of these approximations is especially marked close to the subcritical/supercritical exchange, where $\eta_{3r} \to 0$. In order to achieve a smooth transition it would be necessary to consider the problem up to $O(\mu^4)$, or in the case of bifurcation theory, to calculate $\delta''(0)$. This would require an unacceptably large amount of computation, since it involves the calculation of the fourth order derivatives of $\bar{F}_X$ and $\bar{F}_Y$.

The 'describing function' method presents a possible way round this problem (the author is grateful to Dr. D. Taylor of Cornell University for bringing this technique to his attention, Taylor (1981)). This method averages the effective contribution from the nonlinear terms over one cycle; this leads to an expression in terms of the amplitude, which can replace the nonlinear terms in the equations of motion. An outline of the method of solution for the simple nonlinear oscillator considered in Chapter 3 is as follows.

(1) For the system:

$$\ddot{x} + \dot{x}(\gamma x^2 - \nu) + \omega_0^2 x = 0 \qquad (3.11)$$

assume a solution of the form:

$$x = A\sin\omega_0\tau \quad ; \quad \dot{x} = A\omega_0\cos\omega_0\tau$$

(2) Approximate the nonlinear solution by seeking the first term B, in its Fourier series expansion.

$$x^2\dot{x} = A^3\omega_0\sin^2\omega_0\tau\ \cos\omega_0\tau = BA\omega_0\cos\omega_0\tau$$
$$= B\dot{x}$$

(3) Replace the nonlinear part of (3.11) with Bx'. Since B is an algebraic

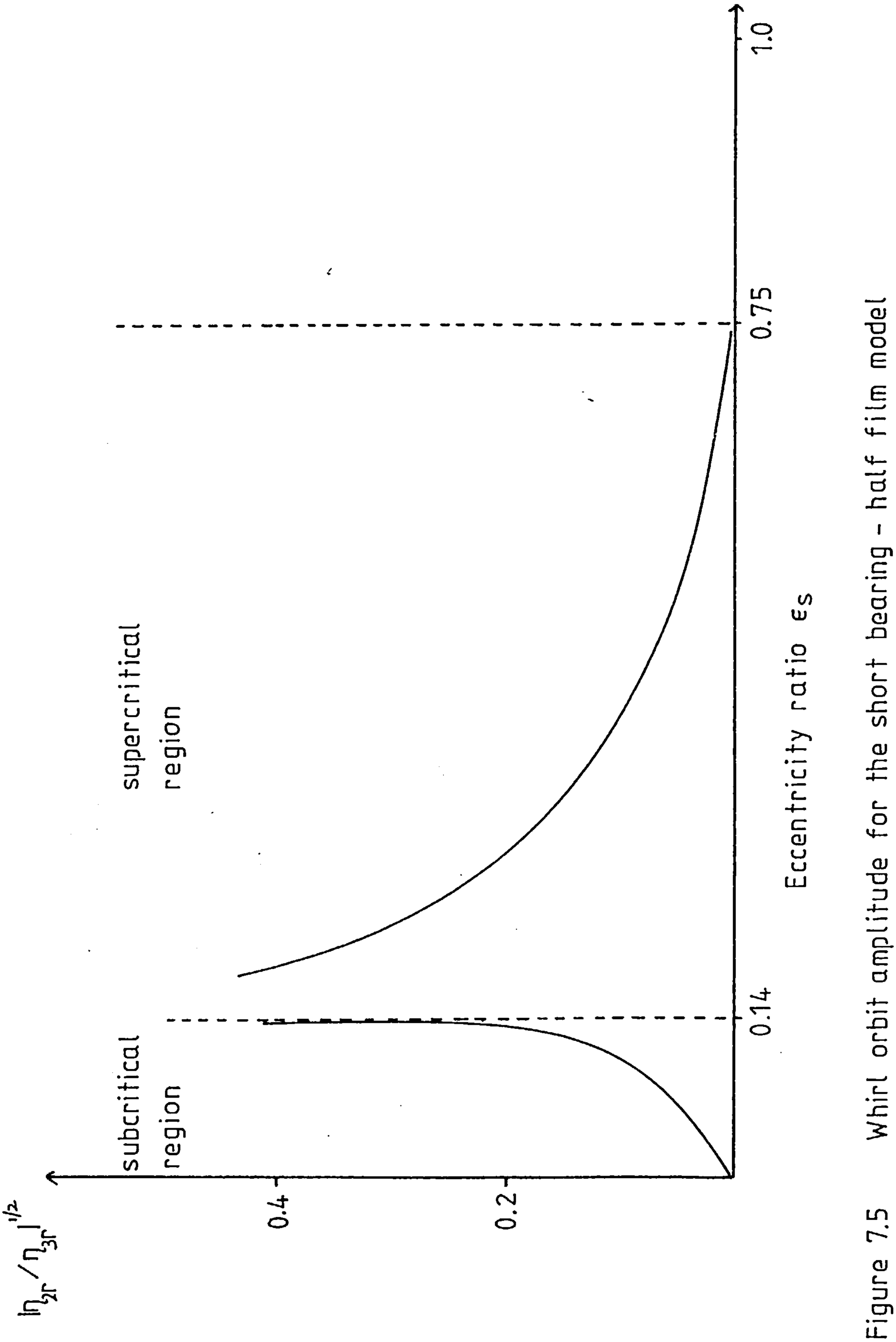

Figure 7.5 Whirl orbit amplitude for the short bearing - half film model

expression of the amplitude a, a condition for periodicity can be found.

(4) The stability of the nonlinear periodic solutions can be found by examining the direction of the 'effective' damping.

This procedure yields exactly the same results as those found by the other analytical methods introduced in Chapter 3. The describing function technique is much easier to apply, however, since it does not require transformations for x, or the calculation of higher derivatives. This facility of application is particularly important for more complex nonlinear damping terms. In the case where (see equation (3.8)):

$$L(x) = 1^2 - (1-d)x^2$$

the solution is analogous to that for the journal bearing. A supercritical solution exists for d<1, a subcritical solution exists for d>1 and infinite amplitude solutions are predicted at d=1. This third case can be avoided by refining the damping force to include an additional term:

$$L(x) = 1^2 - (1-d)x^2 - \beta x^4$$

It is possible to apply bifurcation or scaling/averaging techniques to this refined system, although the process is rather tedious. In contrast, the describing function method is both simple to apply and spectacularly successful. It is only necessary to perform an additional integral in the 'effective damping' calculation. The inclusion of this refinement smooths out the discontinuity at d=1 and introduces a second large amplitude oscillation in the subcritical region. It is felt that this approach might well improve the understanding of nonlinear phenomena in journal bearings, particularly with respect to: (i) large amplitude orbits (ii) behaviour away from the stability borderline.

Both the analytical and numerical techniques employed in this chapter have

been consistent in splitting the (ϵ_s,$\bar{\omega}$) parameter space into two regions. Unfortunately, no satisfactory physical explanation for this has been found. Intuitively, one might expect the system to become more stable at greater values of ϵ_s, since the linear theory states that the system is always stable above ϵ_s=0.756. This intuition is partly borne out by the nonlinear results; Figure 7.5 shows the amplitude of oscillations monotonically decreasing with increasing ϵ_s in the supercritical region. However, this does not explain why the system should suddenly become supercritical when ϵ_s reaches a value of 0.141.

7.3 Conclusions to Chapters 3-7

(1) The three analytical techniques are consistent in their predictions about nonlinear behaviour. In particular, provided that the correct small parameter has been identified, the methods of multiple scales and the method of averaging produce identical results.

(2) The method of multiple scales/method of averaging approach has the advantage of providing a more explicit form for the orbit amplitudes and an indication of the evolution to the limit cycles.

(3) For the short bearing half film model, the (ϵ_s,$\bar{\omega}$) parameter space is split into two regions:

(i) $\epsilon_s \leqslant 0.14$: subcritical bifurcation takes place.

(ii) $0.15 \leqslant \epsilon_s \leqslant 0.75$: supercritical bifurcation takes place.

(4) The validity of the analytical solutions is restricted to values of $\bar{\omega}$ close to $\bar{\omega}_s$.

(5) A numerical integration of the equations of motion confirms the accuracy of the analytical results. There are, however, additional large amplitude solutions to the equations of motion, which cannot be predicted by the analytical methods adopted here.

CHAPTER 8

THE EFFECT OF DIFFERENT CAVITATION BOUNDARY CONDITIONS ON THE NONLINEAR BEHAVIOUR OF THE JOURNAL BEARING

Although the effects of different cavitation boundary conditions on the linear stability of the plain cylindrical journal bearing are well documented (see Chapter 1), there is very little published work examining their influence away from the stability borderline. The intention of this chapter is to attempt to fill this vacuum partially by applying the method of multiple scales to the equations of motion arising from several cavitation models. The rotor configuration is that described at the beginning of Chapter 4, hence the equations of motion remain as in (4.6).

8.1 Description of the computer program NOSCAL

The major disincentive for detailed investigation of equations (4.6) is the complexity of the force terms $\bar{F}_X$ and $\bar{F}_Y$; all three methods described in the previous chapter require the calculation of 68 derivatives up to third order for each value of ϵ_S. However, the format of the equations of motion is unaffected by the choice of boundary conditions (with the obvious exception that the Modified Sommerfeld Number S_m is replaced by the Sommerfeld Number S for long bearing approximations) and in all cases, the forces acting on the journal remain functions of X,Y,X',Y' and S or S_m. The application of the method of multiple scaling therefore remains the same for any cavitation model, it is as described in Section 5.1 and summarised in Table 8.1 below.

Table 8.1

For a given ϵ_S

(1) Calculate $a_1 \ldots a_{34}, b_1 \ldots b_{34}$

Calculate $da_1/d\bar{\omega} \ldots db_4/d\bar{\omega}$

(2) Find the threshold speed $\bar{\omega}_S$

Find $\bar{\Omega}_S$, S or S_m and σ at the threshold

(3) Calculate η_{2r} and η_{3r}

A Fortran computer program has been written to perform the application for any set of boundary conditions. This will be referred to as NOSCAL . Since it is clearly out of the question to perform Stage 1 analytically for the more complex boundary conditions, the program calculates the required values numerically. This program is common to all cavitation models, the forces $\bar{F}_X$ and $\bar{F}_Y$ are supplied through a subroutine.

Calculation of the derivatives

The right hand side of the equations of motion (4.6) can now be written in the form:

$$f(x_1, x_2, x_3, x_4) \tag{8.1}$$

The equilibrium values of $x_1 \ldots x_4$ are:

$$x_1 = x_{1S} \; ; \; x_2 = x_{2S} \; ; \; x_3 = x_{3S} \; ; \; x_4 = x_{4S}$$

It is possible to perturb these independent variables about their equilibrium values to obtain:

$$x_1 = x_{1S} + m_1 \; ; \; x_2 = x_{2S} + m_2 \; ; \; x_3 = x_{3S} + m_3 \; ; \; x_4 = x_{4S} + m_4$$

If (8.1) is expanded in a Taylor series about the steady state position, it is possible to derive the following expressions:

$$\frac{\partial f}{\partial x_i} \simeq \frac{f(m_i) - f(-m_i)}{2m_i} \tag{8.2}$$

$$\frac{\partial^2 f}{\partial x_i^2} \simeq \frac{f(m_i) + f(-m_i) - 2f(0)}{m_i^2} \tag{8.3}$$

$$\frac{\partial^3 f}{\partial x_i^3} \simeq \frac{f(2m_i) - f(-2m_i) - 2(f(m_i) - f(-m_i))}{2m_i^3} \tag{8.4}$$

$$\frac{\partial^2 f}{\partial x_i \partial x_j} \simeq \frac{f(m_i,m_j) + f(m_i,m_j) - f(-m_i,m_j) + f(-m_i,-m_j)}{4m_i m_j} \quad \ldots\ldots (8.5)$$

$$\frac{\partial^3 f}{\partial x_i \partial x_j^2} \simeq \frac{f(m_i,m_j) + f(m_i,-m_j) - f(-m_i,m_j) - f(-m_i,-m_j)}{2m_i m_j^2}$$

$$+ 2\left(\frac{f(-m_i) - f(m_i)}{2m_i m_j^2}\right) \quad \ldots\ldots (8.6)$$

$$\frac{\partial^3 f}{\partial x_i \partial x_j \partial x_k} \simeq \frac{f(m_i,m_j,m_k) - f(m_i,-m_j,m_k) - f(-m_i,m_j,m_k) + f(-m_i,-m_j,m_k)}{8m_i m_j m_k}$$

$$+ \frac{f(m_i,-m_j,m_k) - f(m_i,m_j,-m_k) + f(-m_i,m_j,-m_k) - f(-m_i,-m_j,-m_k)}{8m_i m_j m_k} \quad \ldots\ldots (8.7)$$

where:

$$f(m_i) = f(x_{is}+m_i, x_{js}, x_{ks}, x_{ls})$$

$$f(m_i,m_j) = f(x_{is}+m_i, x_{js}+m_j, x_{ks}, x_{ls})$$

$$f(m_i,m_j,m_k) = f(x_{is}+m_i, x_{js}+m_j, x_{ks}+m_k, x_{ls})$$

$$f(0) = f(x_{1s}, x_{2s}, x_{3s}, x_{4s})$$

Expressions (8.2)-(8.7) can be used to calculate the derivatives $a_1 \ldots b_{34}$; a similar expression to (8.2) can be used to find $da_1/d\bar{\omega}$ etc.

In order to check the program and to determine the most effective values for the m_i, NOSCAL was run for the short bearing half film model and the results obtained were compared with those found analytically and listed in Table 6.1. The program was run on the Leeds University Amdahl V7 computer, which operates at three levels of accuracy: Single Precision (approximately 6 decimal digits), Double Precision (approx. 15 decimal digits), Quadruple

Precision (approx. 33 decimal digits). Since NOSCAL involves the inherently inaccurate numerical calculation of derivatives, it was felt that the maximum possible accuracy should be sought. It was therefore run under both Double and Quadruple Precision. At the Double Precision level, the following values of m_i were chosen after a process of trial and error:

$m_i = m_j = 10^{-5}$ for the calculation of $\frac{df}{dx_i}$, $\frac{d^2f}{dx_i^2}$ and $\frac{d^2f}{dx_i dx_j}$

$m_i = 10^{-4}$ for the calculation of $\frac{d^3f}{dx_i^3}$

$m_i = m_j = m_k = 5\times10^{-5}$ for the calculation of $\frac{d^3f}{dx_i dx_j^2}$ and $\frac{d^3f}{dx_i dx_j dx_k}$

These increments gave the most accurate results for the derivatives; it was not possible to reduce the step size at this precision level due to the onset of rounding errors. NOSCAL calculated η_{2r} and η_{3r} correct to three significant figures for $\epsilon_s > 0.18$, however their sign was calculated correctly for $\epsilon_s > 0.02$. To improve the results obtained at low eccentricity, NOSCAL was run again under Quadruple Precision with increments reduced by a factor of 10^{-4}. In this case η_{2r} and η_{3r} were calculated correctly to within three significant figures for all values of ϵ_s.

As a further check, NOSCAL was also run for the long bearing, oscillating half film model; the results were compared with those obtained analytically by Myers (1981). It was found that accuracy to within four significant figures could be obtained by the use of Double Precision. The problem of accuracy was kept in mind whilst running NOSCAL for other boundary conditions; surprisingly, it was found that the short bearing half film model was unique in requiring the highest level of precision.

8.2 Results and discussion

In addition to the short bearing half film model, NOSCAL was run for four other sets of boundary conditions:- (1) long bearing, oscillating half film (2) long bearing, static half film (3) long bearing, half Sommerfeld film (4) long bearing, Reynolds film. The derivation of the hydrodynamic forces for these models is described in Chapter 2 where the full nonlinear expressions for models (1) and (2) can be found. The full nonlinear forces for models (3) and (4) are not given since they are particularly complex and shed little light on the results that follow (they can be found in Myers (1981)). The results are shown in Tables 8.2-8.5 and Figures 8.1-8.4, which are analogous to Table 5.1. and Figure 4.6.

With the exception of the static half film boundary conditions, the models are consistent in their prediction of two major features of the nonlinear behaviour, i.e. subcritical bifurcation at low eccenticities and supercritical bifurcation at medium eccentricities. The extent of the subcritical region varies between $0 \leqslant \epsilon_s \leqslant 0.09$ and $0 \leqslant \epsilon_s \leqslant 0.21$; the end of the supercritical region varies between $0.64 \leqslant \epsilon_s \leqslant 0.75$. For higher values of ϵ_s, the results are inconclusive. Whereas the short bearing half film model predicts supercritical behaviour up to the point where the system becomes completely unstable, both the long bearing half Sommerfeld film and the long bearing oscillating half film models show a third, subcritical region in a small band just before complete stability is attained. Whilst preserving this additional supercritical region, the long bearing Reynolds' film has a fourth, supercritical region in the interval $0.806 \leqslant \epsilon_s \leqslant 0.815$.

There is very little correlation between linear and nonlinear behaviour; for example, the oscillating half film and half Sommerfeld film models have a very different stability borderline (see Figure 2.14), whereas their

Table 8.2

Results obtained by the method of multiple scales for the long bearing operating with an oscillating half film

ϵ_s	S	$\bar{\omega}_s$	$\bar{\Omega}_s$	σ	$\pm\eta_{2r}$	η_{3r}	amp
0.01	10.61	0.94	1.15	11.26	0.04	-522.8	0.01
0.05	2.12	0.95	1.15	2.24	0.19	-87.02	0.05
0.10	1.06	0.95	1.14	1.11	0.36	-22.24	0.13
0.14	0.76	0.96	1.13	0.79	0.47	- 2.66	0.17
0.15	0.70	0.96	1.13	0.73	0.47	0.41	1.03
0.20	0.53	0.98	1.11	0.54	0.58	9.64	0.25
0.30	0.35	0.98	1.11	0.34	0.64	13.53	0.20
0.40	0.25	1.10	1.02	0.23	0.59	11.35	0.20
0.50	0.19	1.21	0.96	0.16	0.49	8.01	0.21
0.60	0.15	1.37	0.88	0.11	0.37	4.71	0.22
0.70	0.11	1.75	0.72	0.07	0.23	1.42	0.27
0.74	0.10	2.31	0.55	0.04	0.14	0.09	0.75
0.75	0.10	2.31	0.55	0.04	0.14	-0.22	0.43
0.79	0.08	6.43	0.20	0.01	0.02	-0.54	0.19

$$amp = \sqrt{(\eta_{2r}/\eta_{3r})}$$

Table 8.3

Results obtained by the method of multiple scales for the long bearing operating with a static half film

ϵ_s	S	$\bar{\omega}_s$	$\bar{\Omega}_s$	σ	$\pm\eta_{2r}$	η_{3r}	amp
0.01	10.61	1.72	0.50	6.17	0.01	0.002	2.78
0.10	1.06	1.76	0.49	0.61	0.11	0.13	0.92
0.20	0.53	1.90	0.46	0.28	0.13	0.22	0.78
0.30	0.35	2.19	0.41	0.16	0.10	0.15	0.83
0.40	0.25	2.87	0.32	0.09	0.06	0.11	0.73
0.50	0.19	8.21	0.12	0.02	0.01	0.08	0.29
0.51	0.19	18.19	0.05	0.01	0.001	0.003	0.18

$$\text{amp} = \sqrt{(\eta_{2r}/\eta_{3r})}$$

Table 8.4

Results obtained by the method of multiple scales for the long bearing operating with a half Sommerfeld film

ϵ_s	S	$\bar{\omega}_s$	$\bar{\Omega}_s$	σ	$\pm\eta_{2r}$	η_{3r}	amp
0.01	10.61	13.47	0.59	0.79	0.02	-650.9	0.01
0.09	1.18	4.54	0.59	0.26	0.05	-0.36	0.37
0.10	1.06	4.31	0.58	0.17	0.07	0.19	0.33
0.20	0.53	3.16	0.58	0.17	0.07	0.19	0.20
0.30	0.35	2.73	0.56	0.13	0.09	0.15	0.25
0.40	0.25	2.56	0.53	0.09	0.10	0.99	0.31
0.50	0.19	2.54	0.50	0.08	0.10	0.53	0.43
0.60	0.15	2.66	0.46	0.06	0.08	0.12	0.83
0.64	0.14	2.77	0.44	0.05	0.07	0.02	1.88
0.65	0.13	2.80	0.43	0.05	0.07	-0.01	2.53
0.70	0.11	3.05	0.39	0.04	0.06	-0.15	0.62
0.80	0.08	5.44	0.22	0.01	0.01	-0.14	0.29
0.81	0.08	6.76	0.18	0.01	0.01	-0.08	0.28

$$\text{amp} = \sqrt{(\eta_{2r}/\eta_{3r})}$$

Table 8.5

Results obtained by the method of multiple scales for the long bearing operating with a film satisfying Reynolds' boundary conditions

ϵ_s	S	$\bar{\omega}_s$	$\bar{\Omega}_s$	σ	$\pm\eta_{2r}$	η_{3r}	amp
0.01	7.38	9.84	0.59	0.75	0.01	-1639.	0.00
0.10	0.76	3.40	0.57	0.22	0.05	-10.7	0.07
0.20	0.39	2.68	0.55	0.15	0.07	-0.44	0.17
0.21	0.37	2.65	0.55	0.14	0.08	-0.19	0.64
0.22	0.35	2.61	0.55	0.14	0.08	0.03	1.72
0.30	0.26	2.46	0.53	0.11	0.09	0.80	0.34
0.40	0.19	2.41	0.50	0.08	0.09	0.81	0.34
0.50	0.15	2.45	0.48	0.06	0.09	0.53	0.41
0.60	0.12	2.58	0.45	0.05	0.07	0.20	0.60
0.66	0.11	2.76	0.42	0.04	0.06	0.01	3.36
0.67	0.10	2.80	0.41	0.04	0.06	-0.03	1.52
0.70	0.28	2.97	0.39	0.03	0.05	-0.11	0.45
0.80	0.07	6.41	0.18	0.01	0.01	-0.05	0.35
0.81	0.06	10.54	0.11	0.01	0.002	0.03	0.23

$$\text{amp} = \sqrt{(\eta_{2r}/\eta_{3r})}$$

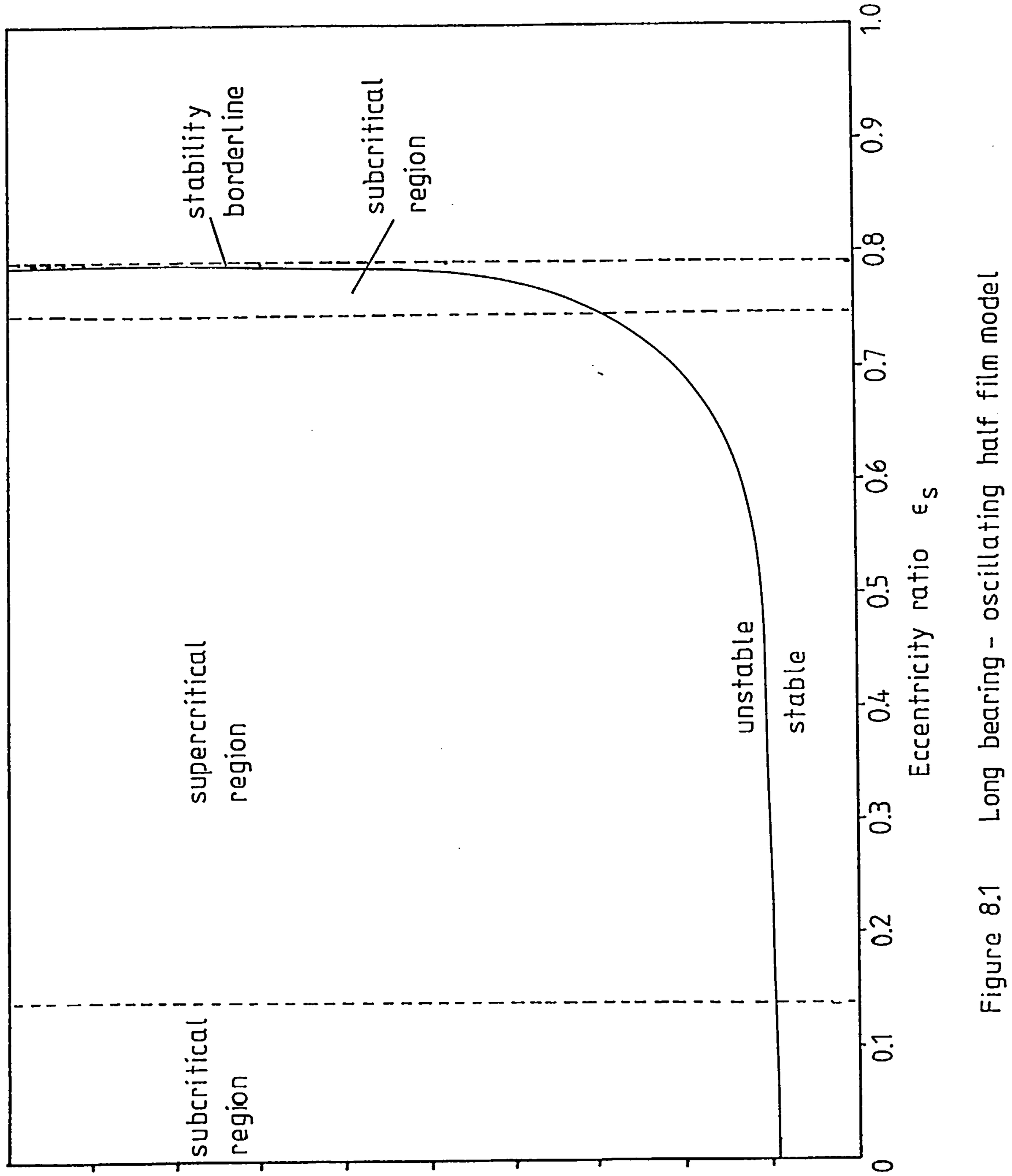
Long bearing - oscillating half film model
Eccentricity ratio ϵ_s
0.2
0.3
0.4
0.5
0.6
0.7
0.8
0.9
1.0
unstable
stable
supercritical region
subcritical region
stability borderline
supercritical region
subcritical region
Nondimensional rotor speed Ω
10
9
8
7
6
5
4
3
2
1
0
0.1

Figure 8.1

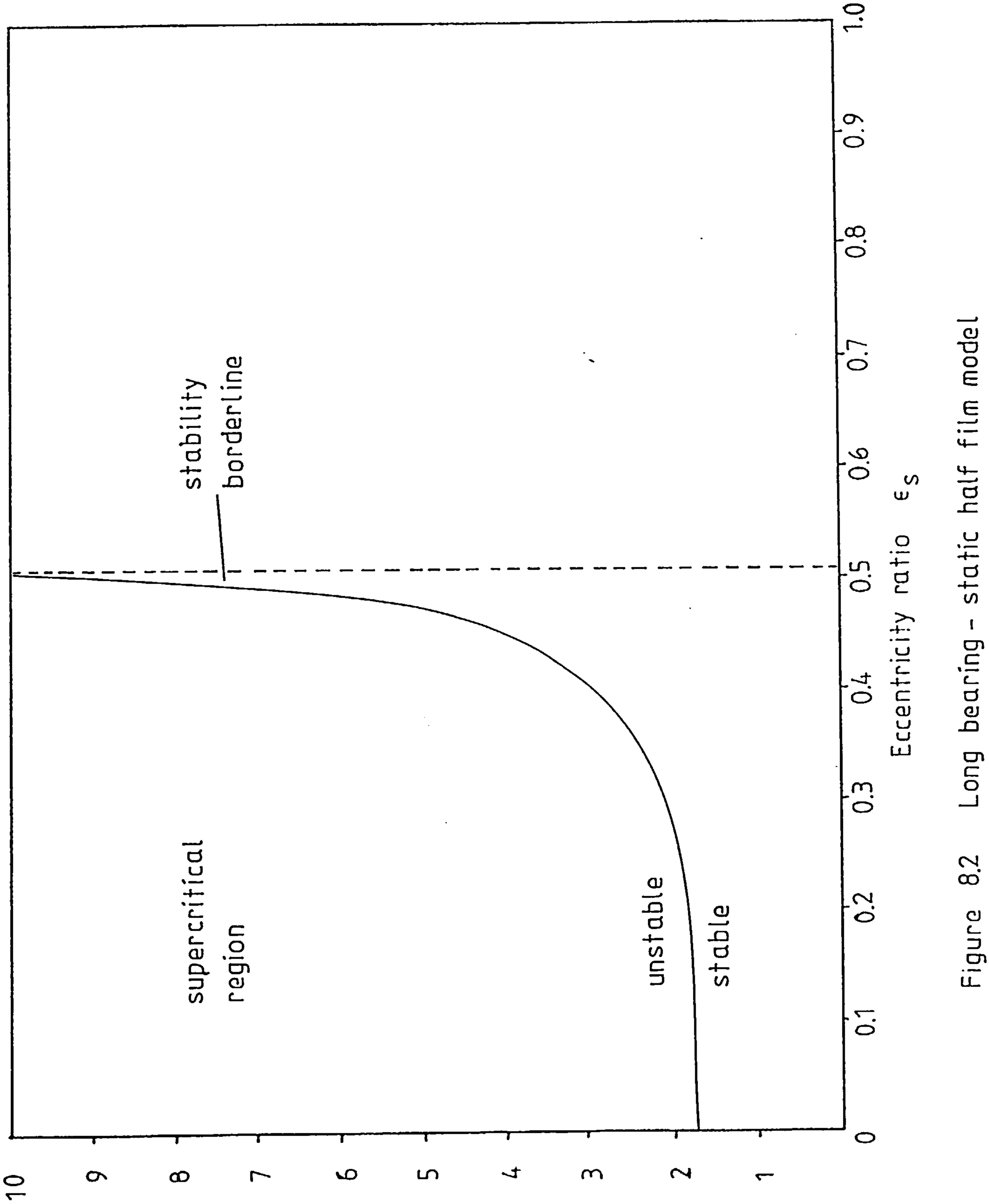

Figure 8.2 Long bearing - static half film model

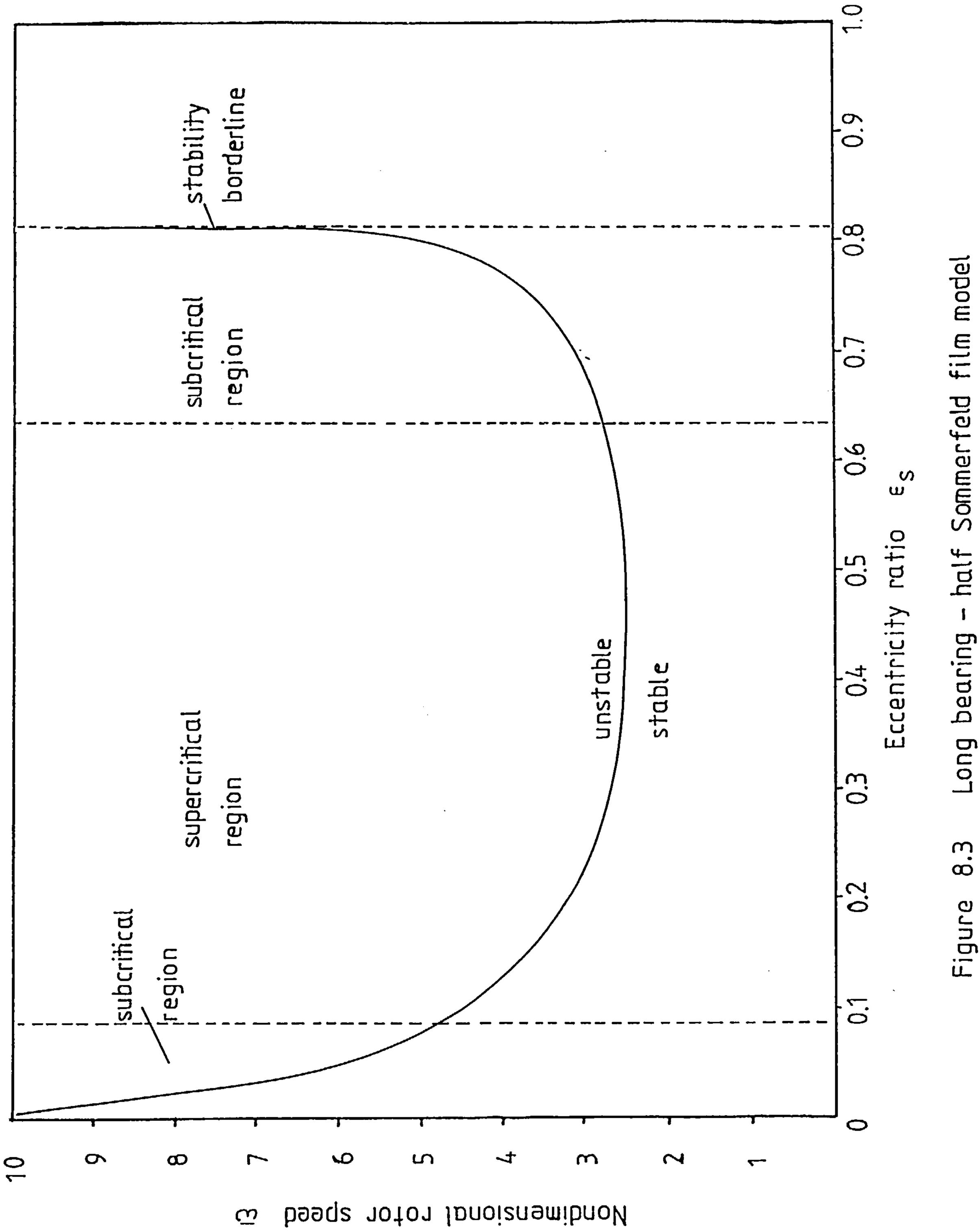
1.0
0.9
0.8
0.7
0.6
0.5
0.4
0.3
0.2
0.1
0
Eccentricity ratio ε_s
Long bearing – half of Sommerfeld film model
stability borderline
subcritical region
supercritical region
unstable
stable
subcritical region
10
9
8
7
6
5
4
3
2
1
Nondimensional rotor speed $\bar{\omega}$

Figure 8.3

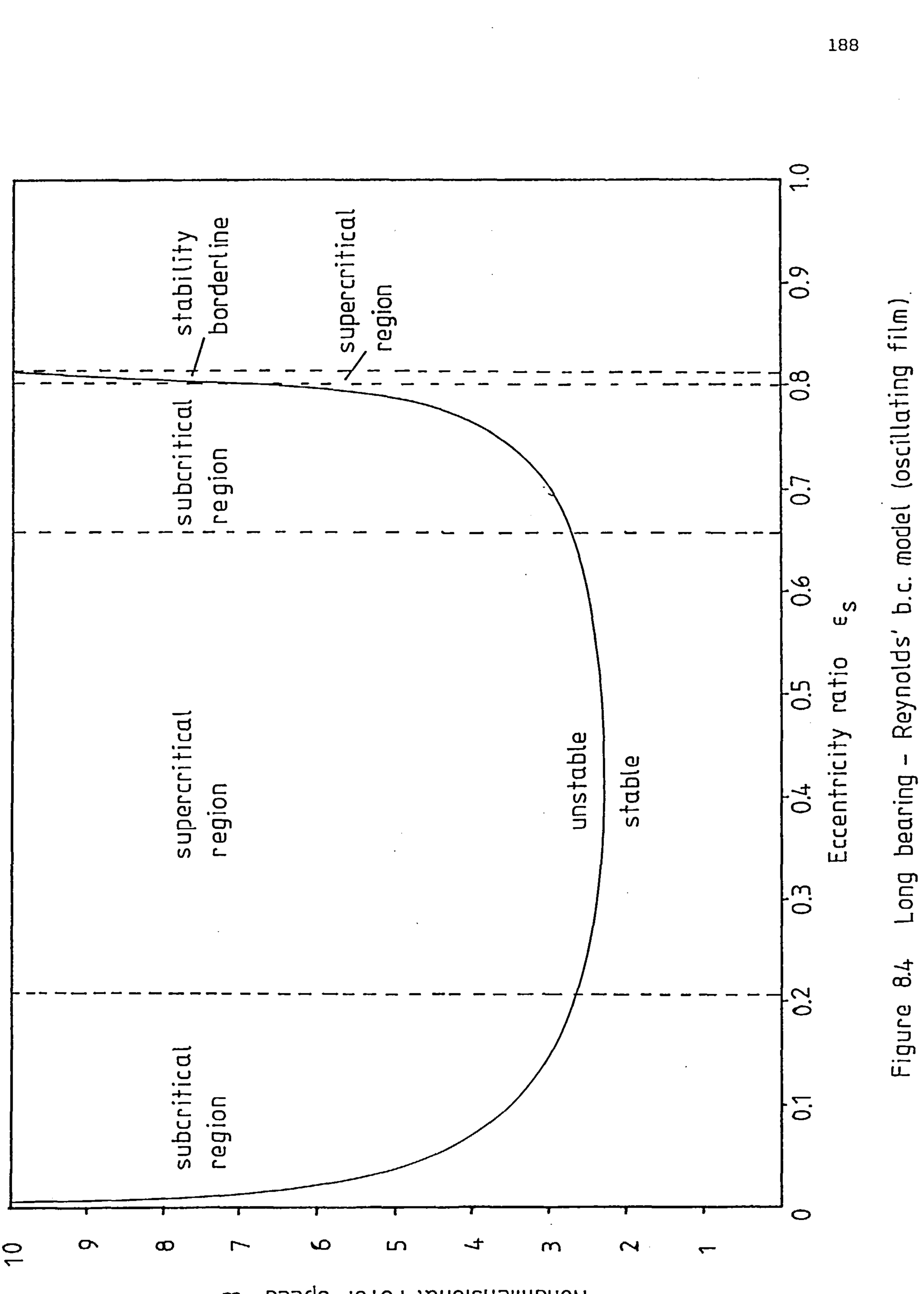

Figure 8.4 Long bearing - Reynolds' b.c. model (oscillating film)

nonlinear behaviour is very similar. The rather anomalous prediction of linear stability at zero eccentricity for two of the models (in particular Reynolds' boundary conditions are not designed to be realistic for low eccentricities) does not affect the consistency of the nonlinear results at low values of ϵ_s.

The value of $\sqrt{|\eta_{2r}/\eta_{3r}|}$ gives a measure of the amplitude of the orbits. As observed in Chapter 5, η_{2r} corresponds to the linear growth rate, i.e. the rate at which the root is crossing the imaginary axis. η_{3r} is inversely proportional to the magnitude of the cubic terms required to balance the linear terms in the amplitude equation (5.16). Consequently (and logically) the smaller the nonlinear content of the forces relative to their linear element, then the larger the predicted orbits. Tables 8.2 and 8.3 show that another discrepancy between the two long bearing half film models, despite the very small difference in oil film behaviour, is that the predicted limit cycle amplitudes for the static half film model are much greater than those for the oscillating half film model.

In the previous chapter, the concept of an operation line was introduced to demonstrate the behaviour of the system as the rotor speed $\bar{\omega}$ increases. It might well be possible, under a particular set of boundary conditions, for the operation line to cross the stability borderline twice, as shown in Figure 8.5. This situation might well lead to hysteresis, since the region in which the stability borderline was crossed would depend on whether the rotor speed was being increased or decreased. In the notional example shown above, the following situation might occur. Increasing the rotor speed from $\bar{\omega}_1$ would lead to the stability borderline being crossed in the supercritical region at A, giving rise to stable orbits persisting until the system becomes linearly stable at B. Decreasing the roor speed from $\bar{\omega}_2$ would lead to unstable limit cycles as the system approached B, followed by completely

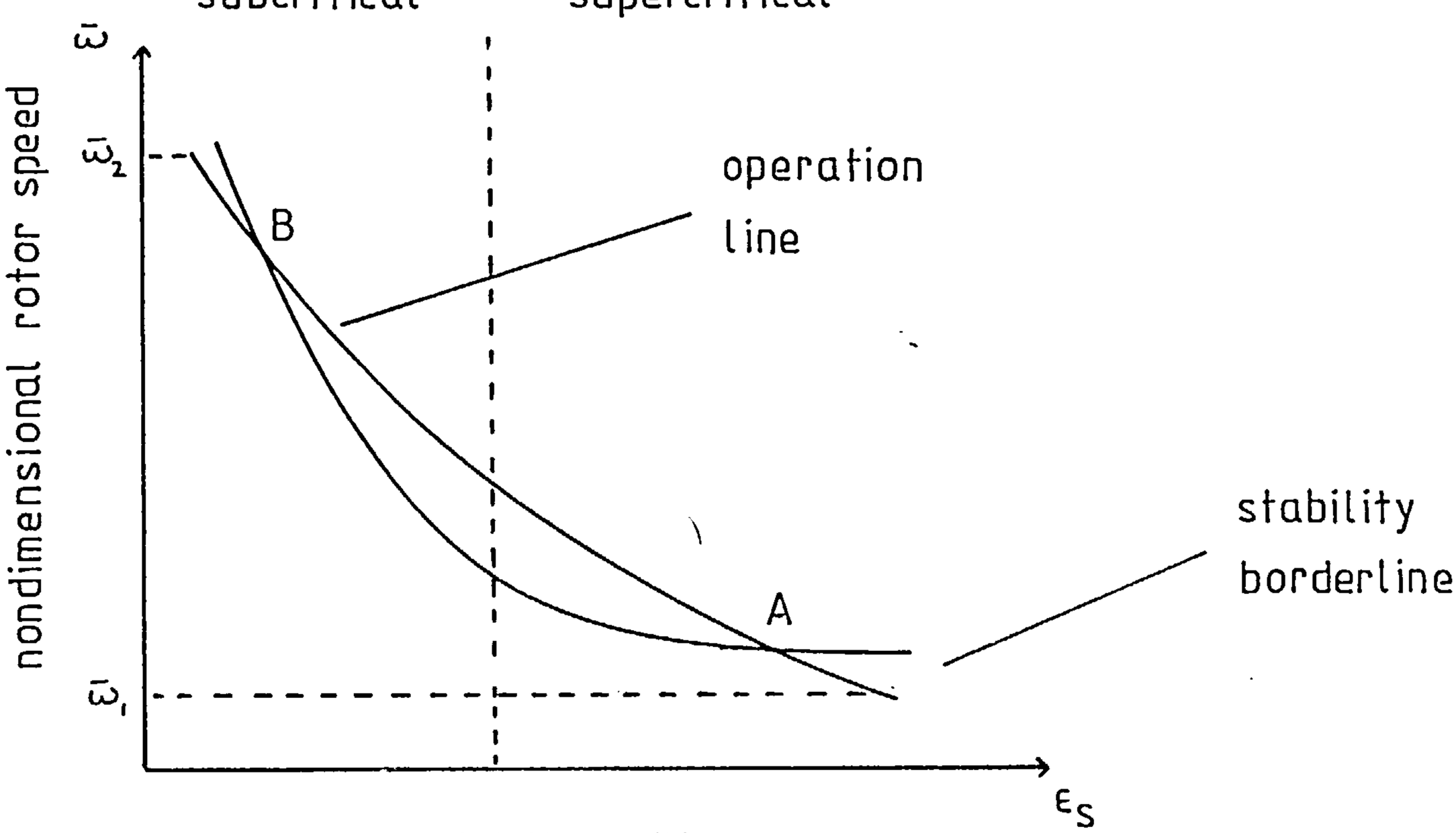

Figure 8.5 A situation in which hysteresis might occur

unstable behaviour beyond B, persisting until the system returns to the linearly stable region at A. There is evidence of hysteresis observed in experimental investigations e.g. Hori (1959); however, the example described above is a purely notional one, none of the boundary conditions examined by the author displayed the two-cross feature of Figure 8.5. The failure of the boundary conditions to produce the two-cross characteristic is clearly a shortcoming, since hysteresis is an observed effect. Any future attempts to model the fluid film behaviour should therefore incorporate this feature.

This chapter represents the first attempt to determine the nonlinear behaviour of a journal bearing operating under a variety of boundary conditions. Although the results are somewhat inconclusive, the author feels that they constitute a significant step forward. The larger questions arising from the results given in this chapter and chapters 4-7 are:-

(1) What are the reasons for the number and position of the different regions for each model?

(2) Why should the models differ?

Unfortunately, throughout the course of this research it has not been possible to provide satisfactory answers to these questions. One might expect the short bearing results to be the most realistic, since they show the stability of both the linear and nonlinear behaviour improving with increasing ϵ_s. However, this is not the case with the more sophisticated Reynolds' and half Sommerfeld film models with their subcritical regions just prior to complete stability. It is rather surprising that the crudest physical model (long bearing, oscillating half film) gives results which are very similar to most sophisticated model (Reynolds' film). The broad similarity between these two models and the half Sommerfeld model, compared with the completely different behaviour shown by the static half film model, suggests that it is film movement rather than film extent which governs the nonlinear characterisitics.

8.3 Conclusions

(1) With one exception, the cavitation models are consistent in predicting two features within the system behaviour:- (i) subcritical bifurcation at low eccentricities (ii) supercritical bifurcation at medium eccentricities.

(2) The predicted system behaviour for $\epsilon > 0.65$ is imprecise and highly model-dependent.

(3) There is little or no correlation between linear and nonlinear behaviour.

(4) Oil film movement rather than oil film extent appears to govern the nonlinear characteristics.

CHAPTER 9

CONCLUSIONS AND SUGGESTIONS FOR FURTHER WORK

9.1 Conclusions

1. The boundary conditions concerning film rupture and reformation play a crucial role in determining the linear stability characteristics of the journal bearing operating with a rigid shaft. These characteristics are particularly sensitive to the behaviour of the oil film during a small vibration of the rotor.

2. A journal bearing which has a flexible shaft becomes unstable at a lower shaft rotational speed than an identical bearing operating with a rigid shaft. However, shaft flexibility has no qualitative effect upon the onset of instability; in particular, the value of the eccentricity ratio above which the bearing is always stable remains the same.

3. The fluid film boundary conditions influence the quantitative change in the stability borderline obtained with a consideration of shaft flexibility (via the critical frequency). Therefore, to predict accurately the behaviour of a journal bearing operating with a flexible shaft, it is necessary to model the oil film behaviour correctly.

4. Although shaft flexibilty is important in determining the speed at which a journal bearing becomes unstable, its effect on oil film instability is likely to be small. If the shaft is flexible enough to cause a substantial reduction in this speed, any oil whirl encountered will be swamped by resonant whip.

5. Hopf bifurcation, the method of multiple scales and the method of averaging produce identical results if correctly applied to the journal bearing problem. The techniques are complementary in that Hopf bifurcation can provide an indication of the appropriate expansion forms to be adopted in

the scaling/averaging approach.

6. The nonlinear analytical techniques show that a short bearing, operating with a half film, manifests two types of nonlinear behaviour close to the stability borderline:

(i) Supercritical bifurcation: small stable whirl orbits exist at speeds just above the speed at which the system becomes unstable. Below the threshold speed, the system regresses to the equilibrium point.

(ii) Subcritical bifurcation: small unstable whirl orbits exist at speeds just below the threshold speed. No small limit cycles exist above the threshold speed.

The $(\epsilon_s, \bar{\omega})$ parameter space is split into two regions:-

(i) $\epsilon_s \leqslant 0.14$: subcritical, (ii) $0.15 \leqslant \epsilon_s \leqslant 0.75$: supercritical.

7. A numerical integration of the equations of motion confirms the results found by analytical methods for the short bearing. This approach also shows that, since the limit cycles are close to 'half frequency', they fulfill the necessary criteria for oil whirl. However, the existence of small, stable whirl orbits is confined to a very narrow speed range. In both the subcritical and supercritical cases, numerical integration shows that large amplitude limit cycles (also of half frequency) surround the small orbits above and below the threshold speed.

8. The application of the method of multiple scaling to other cavitation models for the long bearing shows that the number and position of the nonlinear regions is highly model-dependent. As in the case of the linear stability borderline, subtle changes in the boundary conditions can lead to dramatic differences in behaviour. The models are, however, consistent in their prediction of two particular features in the $(\epsilon_s, \bar{\omega})$ parameter space:

(i) subcritical behaviour in the range $0 \leqslant \epsilon_s \leqslant 0.09$, (ii) supercritical behaviour in the range $0.21 \leqslant \epsilon_s \leqslant 0.64$ (with the exception of the long bearing, operating with a static half film).

9.2 Suggestions for further work

1. Two important questions have remained unanswered throughout this research.

   (i) What is the physical explanation for the differences in the predicted behaviour (both linear and nonlinear) for the different boundary conditions?

   (ii) What accounts for the number and position of the regions of nonlinear behaviour in $(\epsilon_s, \bar{\omega})$ parameter space?

No satisfactory answers have been found to these questions. A tentative attempt to answer the first question might be that since the long bearing, operating with a static half film, appears to stand out from the other models, then film behaviour, rather than film extent, is the most important feature governing oil whirl. There is clearly a need to provide answers to the above questions , since a full understanding of oil whirl is unlikely to be achieved until the effects of different fluid film boundary conditions are appreciated. A straightforward, although tedious, approach to this problem would be to complete a numerical integration of the other boundary conditions like that the one described in Section 7.1. Unfortunately, since the journal bearing equations of motion are so complex, it is not possible to get a 'feel' for the type of nonlinear behaviour they are likely to predict. Therefore, a study of a simple second order system displaying similar features might well be fruitful.

2. The nonlinear analytical techniques used in this thesis have three major deficiencies: (i) they are tedious to apply, (ii) they cannot predict the

existence of large amplitude orbits, (iii) they are restricted in their validity to speeds close to the threshold speed. This final point is particularly important, since it might well be possible for a small stable limit cycle to exist well away from the stability borderline. Further nonlinear studies should concentrate on the development of analytical methods to overcome these difficulties; the describing function technique appears to be an excellent starting point.

3. The majority of analytical work on journal bearings has been hampered by its restriction to simple and often unrealistic physical models. The main reason for this being that the equations of motion are highly complex for even the simplest cases. Indeed, however sophisticated the mathematical techniques adopted, if the models to which they are applied are inaccurate, the results obtained will be erroneous. For a bearing model to represent the physics accurately, it should incorporate shaft flexibility and mass unbalance, as well as realistic cavitation boundary conditions. Noncircular bearing geometries present another problem that arises in engineering applications. It is clearly beyond the scope of the methods described in Chapters 4, 5 and 6 to handle the equations of motion that would result from the inclusion of these effects, but it is envisaged that the method of multiple scales might be used to introduce the additional effects individually.

4. This thesis has been exclusively concerned with a <u>mathematical</u> study of journal bearing dynamic instability. There is, however, a great deal of experimental work to be done in two particular areas in this field:

(i) An investigation into lubricant cavitation and in particular the determination of the behaviour of the oil film during a vibration of the shaft. The importance of lubricant behaviour to oil whirl has been demonstrated; if the techniques described here are to be used

effectively, they should be applied to realistic cavitation models.

(ii) An investigation to determine the onset and dimensions of oil whirl in a simple journal bearing system. It is clearly important to validate the theoretical predictions experimentally, particularly in the light of recent scepticism amongst some engineers about the existence of small, stable limit cycles.

9.3 Some observations

A mathematical study of journal bearing dynamics is a particularly difficult one to undertake, due to the number and diversity of the subjects that need to be mastered before any progress can be made. The major obstacle is that the study is concerned with both mathematics and engineering. Journal bearings are complex machine elements which are not easy to understand. Moreover, the mathematical techniques used study the physical models need to be studied carefully and often require some understanding of pure mathematics, e.g. Hopf bifurcation. The physics of the cavitation conditions provides another difficulty. A further problem arises from the fact that there is a vast amount of literature and very little of it is of interest to mathematicians.

It is very easy, therefore, to become obsessed with one aspect of the problem to the detriment of one's understanding of the problem as a whole, particularly because the equations resulting from the models are so complicated that the mathematics is very difficult to apply. The time spent checking algebra can run into weeks.

It must be stressed that to produce results in this field, it is necessary to understand both the working of the journal bearing and the theory of

nonlinear ordinary differential equations. The author would suggest that any future research student should spend the first six to nine months studying these two subjects independently, in order to equip himself with a thorough understanding of both before tackling the problem as a whole.

References

AKERS, A., MICHAELSON, S. and CAMERON, A. (1971). Stability contours for a whirling finite journal bearing. Trans. A.S.M.E., J. Lub. Tech.

ALLAIRE, P.E. (1980). Journal bearing design for high speed turbomachinery. A.S.M.E. International conference on bearing design.

BADGLEY, R.H. and BOOKER J.F. (1969). Turborotor instability: effect of initial transients on plane motion. Trans. A.S.M.E., J. Lubr. Tech., Vol. 91, p625.

BANNISTER, R.H. (1980). The effect of unbalance on stability and its influence on non-synchronous whirling. I. Mech. Eng., Paper C310/80.

BATCHELOR, G.K. (1967). An introduction to fluid dynamics. Cambridge Univ. Press.

BIRKHOFF, G. and HAYS, D.F. (1963). Free boundaries in partial lubrication. J. Maths. Phys., Vol. 42, p126.

BRETHERTON, F.P. (1960). The motion of long bubbles in tubes. J. Fluid Mech., Vol. 10, p66.

BOGOLIUBOV N.N.and MITROPOLSKI, Y.A. (1961). Asymptotic methods in the theory of nonlinear oscillations. Gordon and Breach Science Publishers, New York.

CAMERON, A. (1970). Basic lubrication theory. Longman.

COHEN, D.S. (1972). Nonlinear problems in the physical sciences and biology. Proc. Bottelle summer Inst., Seattle, p15.

COLE, J.D. (1968). Perturbation methods in applied mathematics. Blaisdell Publishing Co., Mass., U.S.A.

COYNE, J.C. and ELROD, H.G. (1970). Conditions for the rupture of a lubricating film, Part I: Theoretical Model. Trans. A.S.M.E., J. Lubr. Tech., Vol. 92, p451.

COYNE, J.C. and ELROD, H.G. (1971). Conditions for the rupture of a lubricating film, Part II: New boundary conditions for Reynolds' equation. Trans. A.S.M.E., J. Lubr. Tech., Vol. 93, p156.

DOWSON, D. (1957). Cavitation in lubricating films supporting small loads. Proc. Inst. Mech. Eng. Conf. Lubr. and Wear, p93.

DOWSON, D. and TAYLOR, C.M. (1979). Cavitation in bearings. Ann. Rev. Fluid. Mech., Vol 11, p35.

FLOBERG, L. (1975). Cavitation boundary conditions with regard to the number of streamers and tensile strength of the liquid. First Leeds-Lyon Symp. Cavit. Relat. Phenom. Lubr., p31. London New York Mech. Eng. Publ. Ltd.

FRIEDRICHS, K.O. (1965). Advanced ordinary differential equations. Gordon and Breach, New York.

GANTMACHER, F.R. (1959). The theory of matrices 2. New York. Chelsea.

GUMBEL, L.K.R. (1921). Vergleich der Ergebrusse der rectinerischen Behandling der Legerschmierangsproblem mit neueren Veisuchsergebrussen. Monatsbl. Berliner Berz. Ver. Dtsch. Ing., p125.

HAGG, A.C. and WARNER, P.C. (1953). Oil whip of flexible rotors. Trans. A.S.M.E. Vol. 75, no. 7, p1339.

HAHN, E.J. (1975). The excitability of flexible rotors in short sleeve bearings. Trans. A.S.M.E. J. Lub. Tech., p105.

HALL, G. and WATT, J.M. (1976). Modern numerical methods for ordinary differential equations. Clarendon press, Oxford.

HARRISON, W.J. (1919). The hydrodynamical theory of the lubrication of a cylindrical bearing under variable load, and of a pivot bearing. Trans. Edinburgh. Phil. Soc., Vol. 22, p373.

HASSARD, B.D., KAZARINOFF, N.D. and WAN, Y.H. (1981). Theory and applications of Hopf bifurcation. London Math. Soc. Lecture Note Series, No. 41, Cambridge Univ. Press, New York.

HORI, Y. (1959). A theory of oil whip. Trans. A.S.M.E. J. Appl. Mech., Vol. 81, p189.

HOLMES, R. (1960). The vibration of rigid shaft on short sleeve bearings. J. Mech. Eng. Sci., Vol. 2, No. 4, p337.

HOLMES, R. (1963). Oil-whirl characteristics of a rigid rotor in 360° journal bearings. Proc. Inst. Mech. Eng., Vol. 177, No. 11, p291.

HOLMES, R. (1970). Nonlinear performance of turbine bearings. J. Mech. Eng. Science. Vol. 12, No. 6, p377.

HOPKINS, M.R. (1957). Viscous flow between two rotating cylinders and a sheet moving between them. Brit. J. Appl. Phys. Vol. 8, p442.

HUGGINS, N.J. (1964). Non-linear modes of vibration of a rigid rotor in short journal bearings. Proc. Inst. Mech. Eng. Conf. Lubr. and Wear, Paper 18, London.

HUMMEL, C. (1926). Kritische Drehzahlen als Folge der Nachgiebigkeit des Schmiermittels im Lager, VDI-Forschungsheft 287.

JENNINGS, U.D. (1960). An investigation of oil bearing whirl by electronic-analog computer techniques. Ph.D. thesis, Cornell Univ., U.S.A.

KERVORKIAN, J. (1966). The two variable expansion procedure for the approximate solution of certain nonlinear differential equations. Lecture in Appl. Math., No. 7, Space Math., Part III, Amer. Math. Soc.

KIRK, R.G. and GUNTER, E.J. (1975). Short bearing analysis applied to rotor dynamics Part 1: Theory. Trans. A.S.M.E. J. Lub. Tech., Paper 75-Lub-30.

KIRK, R.G. and GUNTER, E.J. (1975). Short bearing analysis applied to rotor dynamics Part II: Results of journal bearing response. Trans. A.S.M.E. J. Lub. Tech., Paper 75-Lub-31.

KRYLOV, N.M. and BOGOLIUBOV, N.N. (1947). Inroduction to non-linear mechanics. Annals of Maths. Study, No. 11, Princeton University Press.

LUND, J.W. (1966). Self-excited, stationary whirl orbits of a journal in a sleeve bearing. Ph.D. thesis, Rensselaer Polytechnic Inst., U.S.A.

LUND, J.W. and SAIBEL, E. (1967). Oil whip whirl orbits of a rotor in sleeve bearings. Trans. A.S.M.E. J. Eng. Ind., Vol. 89, p813.

LUND, J.W. and THOMSEN, K.K. (1978). A calculation method and data for the dynamic coefficients of oil lubricated journal bearings. Topics in Fluid Film Bearing and Rotor Bearing System Design and Optimisation, A.S.M.E.

LUND, J.W. and TONNESEN, J. (1978). Some experiments on instability of rotors supported in fluid film bearings. Trans. A.S.M.E. J. Mech. Design. Vol. 100, p147.

LUND, J.W. and NIELSEN, H.B. (1980). Instability threshold of an unbalanced rigid rotor in short journal bearings. I. Mech. E. C263/80.

LUNDHOLM, G. (1969). The circumferential groove journal bearing considering cavitation and dynamic stability. Acta. Poly. Scandinavica, Mech. Eng. Ser., No. 42, Stockholm.

LUNDHOLM, G. (1971). The axial groove journal bearing considering cavitation and dynamic stability. Acta. Poly. Scandinavica, Mech. Eng. Ser., No. 58, Stockholm.

LUNDHOLM, G. (1973). On whirl frequencies and stability borderlines for journal bearings. Trans of Machine Elements Division, Lund Univ., Sweden.

McKAY, J.T. (1981). Fluid flow and whirl orbits in a whirling rotor bearing. Ph.D. thesis, Leeds Univ.

MARSDEN, J.E. and McCRACKEN, M. (1976). The Hopf bifurcation and its applications. Appl. Math. Sciences, Vol. 19, Springer-Verlag, New York.

MITCHELL, J.R., HOLMES, R. and BYRNE, J. (1965-6). Oil whirl of a rigid rotor in 360° journal bearings: further characteristics. Proc. Inst. Mech. Eng., Vol. 180, p593.

MORRISON, J.A. (1966). Comparison of the modified method of averaging and the two variable expansion procedure. S.I.A.M. Review 8, p66.

MYERS, C.J. (1981). Linear and nonlinear vibrational characteristics of oil lubricated journal bearings. Ph.D. thesis, Leeds Univ.

NAYFEH, A. (1972). Perturbation Methods. . Wiley-Interscience. New York.

NEWKIRK, B.L. (1924). Shaft Whipping. Gen. Elect. Review. p169.

NEWKIRK, B.L. (1930). Whirling of balanced shafts. Third. Intern. Cong. of Appl. Mech., Sweden.

NEWKIRK, B.L. (1956). Varieties of shaft disturbances due to fluid films in Journal bearings. Trans. A.S.M.E., Vol. 78, p985.

NEWKIRK, B.L. (1957). Journal bearing instability. Inst. Mech. Eng.- A.S.M.E. Conf. Lubr. and Wear, London, Rev. paper, session 1, No. 2.

NEWKIRK, B.L. and GROBEL, L.P. (1934). Oil-film whirl - A non-whirling bearing. Trans. A.S.M.E., Vol. 56, p607.

NEWKIRK, B.L. and LEWIS, J.F. (1956). Oil-film whirl - An investigation of disturbances due to oil films in journal bearings. Trans. A.S.M.E., Vol. 78, p21.

NEWKIRK, B.L. and TAYLOR, H.D. (1925). Shaft whipping due to oil action in journal bearings. Gen. Elect. Review, p559.

OCVIRK, F.W. (1952). Short bearing approximation for full journal bearings. NASA TN 2808.

PAN, C.H.T. (1980). An improved short bearing analysis for the submerged operation of plain journal bearings and squeeze film dampers. A.S.M.E.-A.S.L.E. Lub. Conf., Paper 79-Lub-33.

PAN, C.H.T. and IBRAHIM R.A., (1980). Cavitation in a short bearing with pressurised lubricant supply. A.S.M.E.-A.S.L.E. Conf., Paper 80-C2/Lub-47.

PINKUS, O. (1956). Experimental investigation of resonant whip. Trans. A.S.M.E., Vol. 78, p975.

PINKUS, O. and STERNLICHT, B. (1961). Theory of hydrodynamic lubrication. McGraw-Hill Book Co., New York.

POORE, A.B. (1976). On the theory and application of Hopf-Friedrichs bifurcation theory. Arch. Rat. Mech. and Anal., Vol. 60, p371.

PORITSKY, H. (1953). Contribution to the theory of oil whip. Trans. A.S.M.E., Vol. 75, p1153.

REDDI M.M.and TRUMPLER P.R. (1962). Stability of the high-speed journal bearing under steady load. Trans. A.S.M.E., J. Eng. Ind., Vol. 84, p351.

REYNOLDS, O. (1886). On the theory of lubrication and its application to Beauchamp Towers' experiments, including an experimental determination of the viscosity of olive oil. Phil. Trans. R. Soc., London, Ser. A, Vol. 177, p157.

ROBERTSON, D. (1933). Whirling of a journal in a sleeve bearing. Phil. Mag. Ser. 7, Vol. 15, p113.

SAVAGE, M.D. (1977). Cavitation in lubrication. Pt. I. On boundary conditions and cavity fluid interfaces. Pt. II. Analysis of wavy interfaces. J. Fluid. Mech., Vol. 80, p743.

SMITH, D.M. (1963). Dynamic characteristics of turbine journal bearings. Proc. Inst. Mech. Eng. Conf. Lubr. and Wear, p72.

SMITH, D.M. (1970). Journal bearings in turbomachinery. Chapman and Hull Ltd.

SOMEYA, T. (1963-4). Stability of a balanced shaft running in cylindrical journal bearings. Proc. Inst. Mech. Eng. Vol. 178, Part 3N, p196.

SOMMERFELD, A. (1904). Zur hydrodynamischen Theorie der Schmiermittehreibung. Zeitschrift Math. Phys., Vol. 50, p97.

STERNLICHT, B. (1962). Stability and dynamics of rotors supported on fluid film bearings. A.S.M.E. paper 62-WA-190.

STODOLA, A. (1925). Kritische Wellenstorung Infolge der Nachgiebigkeit des Oelpolsters im Lager. Schweizerische Bauzeitung, Vol. 85, p265.

TAYLOR, D.L. (1981). Nonlinear stability and response of car trailer combinations. Trans. S.A.E., 800152.

TAYLOR, G.I. (1963). Cavitation of a viscous fluid in narrow passages. J. Fluid. Mech., Vol. 16, p595.

TONDL, A. (1965). Some problems of rotor dynamics. Publishing House of the Czechoslovak Academy of Sciences, Prague.

TOLLE, G.C. and MUSTER, D. (1969). An analytic solution for whirl in a finite journal bearing with a continuous lubricating film. Trans. A.S.M.E., J. Eng. Ind., Vol. 91, p1189.

TOWER, B. (1883). Experiments on the friction of a collar bearing. Proc. Inst. Mech. Eng. 1, p173.

WARNER, P.C. (1963). Static and dynamic properties of partial journal bearings. Trans. A.S.M.E., J. Basic Eng., Vol. 85, p247.

WOODCOCK, J.S. and HOLMES, R. (1969-70). The determination and application of the dynamic properties of a turborotor bearing oil film. Proc. Inst. Mech. Eng., Vol. 184, Part 3L.

Appendix 1 Details of the linearisation of equations 2.10-2.13

The following relationships can be obtained from (2.10) and (2.11):

$$\delta = \frac{\nu}{\nu}_1 \ddot{x} + x + \nu_1 \sin\varphi_s \quad ; \quad \dot{\delta} = \frac{\nu}{\nu}_1 \dot{x} + \dot{x} \tag{A1.1}$$

$$\epsilon_s \gamma = \frac{\nu}{\nu}_1 \ddot{y} + y + \nu_1 \cos\varphi_s \quad ; \quad \epsilon_s \dot{\gamma} = \frac{\nu}{\nu}_1 \dot{y} + \dot{y} \tag{A1.2}$$

The substitution of (2.14) and (2.15) along with (A1.1) and (A1.2) into (2.12) and (2.13) leads to:

$$\dddot{x}(SD_r\nu_1) + \ddot{x}(1+SB_r\nu_1) + \dot{x}(SD_r\nu) + x(SB_r\nu)$$

$$- \frac{\dddot{y}}{\epsilon_s}(SC_r\nu_1) + \frac{\ddot{y}}{\epsilon_s}(SE_r\nu_1 - SA_t\nu_1) - \frac{\dot{y}}{\epsilon_s}(SC_r\nu) + \frac{y}{\epsilon_s}(SE_r\nu - SA_t\nu)$$

$$+ \text{constant terms} = 0$$

$$\dddot{x}(SD_t\nu_1) + \ddot{x}(SB_t\nu_1) + \dot{x}(SD_t\nu) + x(SB_t\nu)$$

$$- \frac{\dddot{y}}{\epsilon_s}(SC_t\nu_1) - \frac{\ddot{y}}{\epsilon_s}(1+SE_t\nu_1 - SA_r\nu_1) - \frac{\dot{y}}{\epsilon_s}(SC_t\nu) - \frac{y}{\epsilon_s}(SE_t\nu - SA_r\nu)$$

$$+ \text{constant terms} = 0$$

where:

$$a_1 = SD_r \; ; \; a_2 = SB_r \; ; \; a_3 = \frac{SC_r}{\epsilon_s} \; ; \; a_4 = \frac{SA_t}{\epsilon_s} \; ; \; a_5 = \frac{SE_r}{\epsilon_s}$$

$$b_1 = SD_t \; ; \; b_2 = SB_t \; ; \; b_3 = SC_t \; ; \; b_4 = SA_r \; ; \; b_5 = \frac{SE_t}{\epsilon_s}$$

In equation (2.17) we have:

$$A_0 = B_0\nu_1^2$$

$$A_1 = B_1\nu_1^2 + B_1'\nu_1$$

$$A_2 = 2B_0\nu\nu_1 + B_2'\nu_1^2 + B_2''\nu_1 + 1$$

$$A_3 = 2B_1\nu_1\nu + B_1'\nu$$

$$A_4 = 2B_2'\nu_1\nu + B_2''\nu + B_0\nu^2$$

$$A_5 = B_1\nu^2$$

$$A_6 = B_2'\nu^2$$

B_0, B_1 etc. are all functions of ϵ_s which can easily be found for any cavitation model by considering the characteristic equation.

To obtain relationships (2.24) and (2.25), first note that at the stablity threshold:

$$\nu = \kappa_1(\kappa_2 + \nu_1) \qquad \text{(A1.3)}$$

where:

$$\kappa_1 = \frac{B_1^2 - B_1B_1'B_2'' + B_1'^2B_2'}{B_0B_1'^2} \qquad \kappa_2 = \frac{B_1'}{B_1}$$

The solution of (2.23) can be written in the form:

$$\bar{\Omega}_s^2 = \frac{2B_1\nu\nu_1 + B_1'\nu}{2B_1\nu_1^2 + 2B_1'\nu_1} \pm \frac{\left\{4B_1^2\nu^2\nu_1^2 + B_1'^2\nu^2 + 4B_1B_1'\nu^2\nu_1 - 4B_1^2\nu^2\nu_1^2 - 4B_1B_1'\nu_1\nu^2\right\}}{2B_1\nu_1^2 + 2B_1'\nu_1}$$

$$\rightarrow \bar{\Omega}_s^2 = \frac{\nu}{\nu_1} \qquad \text{or} \qquad \frac{B_1\nu}{B_1\nu_1 + B_1'}$$

Consider the second result, substuting (A2.3) for ν in the numerator yields:

$$\nu = \kappa_1(\kappa_2 + \nu_1)$$

$$\rightarrow \bar{\Omega}_s^2 = \frac{B_1\kappa_1(\nu_1 + B_1'/B_1)}{B_1\nu_1 + B_1'}$$

$$\rightarrow \bar{\Omega}_s^2 = \kappa_1$$

Appendix 2 The Sommerfeld substitution

In order to evaluate integrals of the type:

$$I = \int_{\theta_1}^{\theta_2} \frac{\cos^n\theta \, \sin^m\theta \, d\theta}{(1 + \epsilon\cos\theta)^3} \qquad n,m = 1,2,...$$

the following substitution can be used:

$$1 - \epsilon\cos\psi = \frac{1 - \epsilon^2}{1 + \epsilon\cos\theta}$$

This is known as the Sommerfeld substitution and ψ as the Sommerfeld angle (which coincides with θ at 0, π, 2π). Some typical examples are given below (ψ_1 and ψ_2 correspond to θ_1 and θ_2):

$$\int_{\theta}^{\theta_2} \frac{d\theta}{(1+\epsilon\cos\theta)^3} = \frac{1}{4(1-\epsilon^2)^{5/2}}\Big\{\epsilon^2(\sin2\psi_2-\sin2\psi_1) - 8\epsilon(\sin\psi_2-\sin\psi_1) + 2(2+\epsilon^2)(\psi_2-\psi_1)\Big\}$$

$$\int_{\theta_1}^{\theta_2} \frac{\sin\theta d\theta}{(1+\epsilon\cos\theta)^3} = \frac{1}{4(1-\epsilon^2)^2}\Big\{\epsilon(\cos2\psi_2-\cos2\psi_1)-4(\cos\psi_2-\cos\psi_1)\Big\}$$

$$\int_{\theta_1}^{\theta_2} \frac{\cos\theta d\theta}{(1+\epsilon\cos\theta)^3} = \frac{1}{4(1-\epsilon^2)^{5/2}}\Big\{4(1+\epsilon^2)(\sin\psi_2-\sin\psi_1)-6\epsilon(\psi_2-\psi_1) - \epsilon(\sin2\psi_2-\sin2\psi_1)\Big\}$$

Appendix 3 Force integrals for the short bearing half film model

$$I_1 = -2\int_{\theta_1}^{\theta_1+\pi} \frac{\cos\theta \sin\theta \, d\theta}{(1+\epsilon\cos\theta)^3} = \pm \frac{4\epsilon\cos^2\theta_0}{(1-\epsilon^2\cos^2\theta_0)}$$

$$I_2 = -2\int_{\theta_1}^{\theta_1+\pi} \frac{\cos^2\theta d\theta}{(1+\epsilon\cos\theta)^3} = \frac{\pi(1+2\epsilon^2)}{(1-\epsilon^2)^{5/2}} \pm J_2$$

$$I_3 = -2\int_{\theta_1}^{\theta_1+\pi} \frac{\sin^2\theta d\theta}{(1+\epsilon\cos\theta)^3} = \frac{2}{(1-\epsilon^2)^{3/2}}\left\{ \frac{\pi}{2} \pm J_3 \right\}$$

where:

$$J_2 = \frac{2(1+2\epsilon^2)}{(1-\epsilon^2)^{5/2}} \tan^{-1}\left\{ \frac{u(a^2-1)}{a(1+u^2)} \right\}$$

$$- \frac{u}{(1-\epsilon^2)^2}\left\{ \frac{(3-5a^2)u^2+(5-3a^2)a^2}{(u^2+a^2)} + \frac{(3-5a^2)+(5-3a^2)a^2u^2}{(1+a^2u^2)} \right\}$$

$$J_3 = \tan^{-1}\left\{ \frac{u(a^2-1)}{a(1+u^2)} \right\} - \frac{au(u^2-a^2)}{(u^2+a^2)^2} - \frac{au(1-a\,u\,)}{(1+a^2u^2)^2}$$

$$\cos\theta_0 = \frac{\epsilon|1-2\varphi'|}{\sqrt{(\epsilon^2(1-2\varphi')^2 + (2\epsilon')^2)}}$$

$$u = \tan(\theta_0/2) \quad ; \quad a = \left[\frac{1+\epsilon}{1-\epsilon}\right]^{1/2}$$

In the case of I_1 the sign is taken to be positive if the sign of $1-2\varphi'$ is positive and vice versa. In the cases of I_2 and I_3 the sign is taken to be positive if the sign of ϵ' is positive and vice versa.

Appendix 4 Transformation of the coordinate systems

The relationship between the cartesian (X,Y) coordinate system and the polar (ϵ,φ) system is defined by (4.4) to be:

$$X = \epsilon\cos\varphi \quad ; \quad Y = \epsilon\sin\varphi$$

$$\epsilon^2 = X^2 + Y^2 \quad ; \quad \cos\varphi = \frac{X}{\epsilon} \quad ; \quad \sin\varphi = \frac{Y}{\epsilon}$$

Differentiate with respect to τ, to obtain:

$$\dot{X} = \dot{\epsilon}\cos\gamma + \epsilon\dot{\varphi}\sin\varphi \quad ; \quad \dot{Y} = \dot{\epsilon}\sin\varphi + \epsilon\dot{\varphi}\cos\varphi \qquad \text{(A4.1)}$$

$$\dot{\epsilon} = \dot{X}\cos\varphi + \dot{Y}\sin\varphi \quad ; \quad \epsilon\dot{\varphi} = \dot{Y}\cos\varphi + \dot{X}\sin\varphi \qquad \text{(A4.2)}$$

The force components are defined by equations (4.5). In order to derive $\partial F_X/\partial x$ etc., the relationship between the force derivatives is required, these can be established by the use of (4.4) and (A4.1), (A4.2). For example:

$$\frac{\partial F_x}{\partial X} = \frac{\partial F_x}{\partial \epsilon}\frac{\partial \epsilon}{\partial X} + \frac{\partial F_x}{\partial \varphi}\frac{\partial \varphi}{\partial X} + \frac{\partial F_x}{\partial \dot{\epsilon}}\frac{\partial \dot{\epsilon}}{\partial X} + \frac{\partial F_x}{\partial \dot{\varphi}}\frac{\partial \dot{\varphi}}{\partial X}$$

where:

$$\frac{\partial \epsilon}{\partial X} = \cos\varphi \quad ; \quad \frac{\partial \varphi}{\partial X} = -\frac{1}{\epsilon}\sin\varphi \quad ; \quad \frac{\partial \dot{\epsilon}}{\partial X} = \frac{\partial \dot{\varphi}}{\partial X} = 0$$

Full details of these transformations can be found in Lund (1966).

Appendix 5 The calculation of $d\bar{\alpha}/d\omega$ and $d\bar{\Omega}/d\omega$

The characteristic (4.9) can be written the form:

$$\bar{\lambda}^4 + \frac{1}{\bar{\omega}^4} A(\epsilon_s)\bar{\lambda}^3 + \frac{1}{\bar{\omega}^2}\left(B(\epsilon_s) + \frac{1}{\bar{\omega}^2} C(\epsilon_s)\right)\bar{\lambda}^2$$

$$+ \frac{1}{\bar{\omega}^4} D(\epsilon_s)\bar{\lambda} + \frac{1}{\bar{\omega}^4} E(\epsilon_s) = 0 \qquad \text{(A5.1)}$$

where:

$$A = B_{XX} + B_{YY}$$

$$B = K_{XX} + K_{YY}$$

$$C = B_{XX}B_{YY} - B_{XY}B_{YX}$$

$$D = B_{XX}K_{YY} + B_{YY}K_{XX} - B_{XY}K_{YX} - B_{YX}K_{XY}$$

$$E = K_{XX}K_{YY} - K_{XY}K_{YX}$$

using relationships (4.16) and (4.14) and retaining first order terms only, (A5.1) can be written as follows:

$$\left\{4(i\bar{\Omega}_s)^3 - \frac{3}{\bar{\omega}^2} A\bar{\Omega}_s^2 + \frac{2}{\bar{\omega}^2} i\left(B + \frac{C}{\bar{\omega}^2}\right) + \frac{D}{\bar{\omega}^4}\right\} \delta\bar{\lambda}$$

$$+ \left\{\left(\frac{1}{\bar{\omega}^2}\frac{da}{d\epsilon}\frac{d\epsilon}{d\omega} - \frac{4D}{\bar{\omega}^5}\right)(i\bar{\Omega}_s)^3 - \left\{\left(\frac{1}{\bar{\omega}^2}\frac{dB}{de} + \frac{1}{\bar{\omega}^4}\frac{dC}{d\epsilon}\right)\frac{d\epsilon}{d\omega} - \frac{2B}{\bar{\omega}^3} - 4C\right\}\bar{\Omega}_s^2\right.$$

$$\left. + i\left(\frac{1}{\bar{\omega}^4}\frac{dD}{d\epsilon}\frac{d\epsilon}{d\omega} - \frac{4D}{\bar{\omega}^5}\right)\bar{\Omega}_s + \left(\frac{1}{\bar{\omega}^4}\frac{dE}{d\epsilon}\frac{d\epsilon}{d\omega} - \frac{4E}{\bar{\omega}^5}\right)\right\} \delta\bar{\omega} = 0$$

It is now possible to determine the value of $d\bar{\lambda}/d\bar{\omega}$ at the stability threshold; $d\bar{\alpha}/d\bar{\omega}$ and $d\bar{\Omega}/d\bar{\omega}$ can then be found by separating real and imaginary parts.